NASA
Technical
Paper
2068

October 1982

An Experimental and Theoretical Investigation of Thick Wings at Various Sweep Angles In and Out of Ground Effect

John W. Paulson, Jr.,
and Scott O. Kjelgaard

NASA

NASA Technical Paper 2068

1982

An Experimental and Theoretical Investigation of Thick Wings at Various Sweep Angles In and Out of Ground Effect

John W. Paulson, Jr.,
and Scott O. Kjelgaard
Langley Research Center
Hampton, Virginia

National Aeronautics
and Space Administration

Scientific and Technical Information Branch

SUMMARY

An analysis of the effects of sweep and aspect ratio on the longitudinal aerodynamics of a wing in and out of ground effect has been made. Experimental data were obtained in the Langley 4- by 7-Meter Tunnel for a wing with various sweep angles, aspect ratios, and flap deflections both in and out of ground effect. Theoretical predictions of the out-of-ground-effect lift coefficients and flap effectiveness and the in-ground-effect lift coefficients are compared with the experimental results.

As expected, the lift-curve slope and flap effectiveness are reduced when the aspect ratio is reduced or the sweep angle is increased both in and out of ground effect. In ground effect, the lift and flap effectiveness are increased above a wing height-to-span ratio of 0.15. However, with flap deflections less than or equal to 10° and an angle of attack near 0°, lift is markedly decreased at very low heights above the ground plane. This trend is not predicted by planar theoretical models but is predicted by a surface-panel method where thickness effects are included.

INTRODUCTION

In the early 1970's, a very large airplane was proposed to transport oil from the North Shore of Alaska to the continental United States. This airplane was designed to carry the payload of oil inside the wing itself. It was proposed that by distributing the payload across the wing span the aerodynamic loads on the wing would be largely balanced by the payload and structural weight as depicted in figure 1. Thus, the wing-root bending moments would be considerably reduced (see fig. 2), and the structural-weight fraction of the airplane would be improved because the weight of the massive spar structure required on conventional airplanes would be reduced. Along with the proposed improvements in structural-weight fraction, it appeared that because the payload was to be carried in the wing, the fuselage could be eliminated; thus, the aerodynamic efficiency of the airplane would be improved because of the more favorable ratio of wetted area to wing area. This early design led to the span-distributed-load airplane or spanloader concept of the middle 1970's. These airplanes were designed, again, to carry the payload in the wing, but the payload of conventional consumables (instead of oil) was to be carried in standard 2.4- by 2.4-m containers. Several companies designed such airplanes, and the Langley Air Cargo Work Group had the responsibility of monitoring the company designs and analyzing the concept. (See refs. 1 to 9.) Another large span airplane to be used to ferry and air-launch the space shuttle orbiters was proposed during this time and was reported in reference 10.

One of the major operating-problem areas for these large airplanes was seen as the landing. Due to the long wing span and sweep angle of the airplane, conventional landing techniques such as rotating to higher angles of attack for flaring at touchdown or decrabbing and dropping a wing for crosswind operations, do not appear to be feasible. Therefore, alternate techniques must be developed for landing, such as not increasing the angle of attack at landing but allowing for ground effect to reduce the rate of descent as lift increases near the ground, and developing the method of landing while in crabbing flight, like the B-52 strategic bomber, for crosswind operations. However, this is an area that was not addressed in a previous wind-tunnel

investigation in the Langley High-Speed 7- by 10-Foot Tunnel (ref. 11) or in theoretical studies in the contractor reports (refs. 1 and 3 to 5).

A survey of NASA wind-tunnel reports indicated three applicable reports. (See refs. 12 to 14.) These, however, covered only unswept wings with either a high aspect ratio (AR = 10 in ref. 12) or a very low aspect ratio (AR = 1 in refs. 13 and 14). Information did not exist at intermediate ranges of wing aspect ratio (AR = 2 to 8) with varying sweep angles (Λ = 0° to 45°) either in or out of ground effect. It appeared that there was an opportunity to generate both a data base and an understanding of ground effects for very large span configurations where airplane wing height-to-span ratios h/b can be small. When planning the present investigation, the first step involved a determination of the appropriate range of wing heights or h/b for the test program. For example, conventional transport-type airplanes generally have a minimum h/b at wheel touchdown of about 0.1. This minimum occurs because the landing gear must be long enough to allow rotation of the airplane to take-off and landing attitudes. However, because the spanloader airplane will not rotate but will take off and land in a flat attitude, and because there is a reasonable limit to the maximum length of the landing gear, these airplanes will have extremely low minimum ratios of h/b of about 0.01 to 0.02. (See fig. 3.) This very low h/b might lead to some aerodynamic interaction between the wing lower surface and the runway that is not generally seen at more conventional heights.

An investigation of the longitudinal aerodynamics for this class of vehicle both in and out of ground effect was conducted with both a research model in the Langley 4- by 7-Meter Tunnel (formerly V/STOL Tunnel) and analytical-computer models. An initial data report of this wind-tunnel investigation was given in reference 15. The wind-tunnel model had an NACA 0018 airfoil section with a 25-percent-chord plain trailing-edge flap. The sweep of the model could be varied from 0° to 45°, and the aspect ratio could be varied from 2 to 8. These various configurations were analyzed with computer studies to predict the basic aerodynamics both in and out of ground effect before wind-tunnel testing began. These same configurations were then tested in the wind tunnel to correlate the effects of sweep, aspect ratio, and ground height on the longitudinal aerodynamics of the wing in and out of ground effect. These data were obtained at a dynamic pressure of 1.44 kPa or a Mach number of 0.14. (See ref. 15.) The range of angle of attack was from -7.2° to 18.7° and the range of wing height-to-span ratio was from 0.016 to greater than 2.0.

SYMBOLS

All data have been reduced to standard coefficient form and are presented in the stability axis system. Where there are differences, the symbols enclosed in parentheses are added to help correlate with the tabulated printouts in reference 15 and their usual notation precedes them.

AR		aspect ratio
b		wing span, m
C_D	(CD)	drag coefficient, $D/q_\infty S$
C_L	(CL)	lift coefficient, $L/q_\infty S$
C_{L_α}		lift-curve slope measured over the linear portion of the lift curve, $\partial C_L/\partial\alpha$, deg^{-1}

$C_{L_{\delta_f}}$		flap effectiveness measured between $\delta_f = 0°$ and $5°$, $\partial C_L/\partial\delta_f$, deg^{-1}
C_m	(CM)	pitching-moment coefficient, (Pitching moment)/$q_\infty S\bar{c}$
C_p		pressure coefficient
c		chord length, m
$\bar{c}$	(CBAR)	wing mean aerodynamic chord, m
D		drag, N
h	(H)	distance from ground in z-direction to lower surface of wing at $0.25\bar{c}$, m
h/b	(H/B)	ratio of height of wing above ground to wing span
jth		arbitrary (panel)
kth		arbitrary (horseshoe vortex)
L		lift, N
$\hat{n}$		unit normal vector
q_∞	(Q)	free-stream dynamic pressure, kPa (KPA)
S		wing area, m^2
t		wing maximum thickness, m
$t/\bar{c}$		thickness-to-chord ratio
$\vec{V}_\infty$		free-stream velocity vector, m/sec
x		dimension on longitudinal axis
x/c		nondimensional distance along wing chord line from leading edge
x_{mc}		distance from nose of centerbody to moment reference center, found to be the theoretical center of pressure of configuration, m
Δx		length of panel in vortex-lattice modeling
z		direction on vertical axis
α	(ALPHA)	angle of attack, deg
Γ		horseshoe-vortex circulation strength
γ		vorticity strength in surface-panel modeling

δ	deflection of flap or elevon, measured perpendicular to hinge line (positive trailing edge down), deg
Λ	leading-edge sweep, deg
σ	source strength in surface-panel modeling

Subscripts:

e	elevon
f	flap
s	streamwise

Abbreviations:

IGE	in ground effect
OGE	out of ground effect
VTOL	vertical take off and landing

MODEL DESCRIPTION

The spanloader model tested in the Langley 4- by 7-Meter Tunnel (formerly the V/STOL Tunnel) was a conceptual tailless configuration with an untwisted, NACA 0018 airfoil, constant chord wing with a centerbody (sized to accommodate the balance). Figures 4 and 5 are photographs of the model installed in the tunnel.

A sketch of the model configurations is presented in figure 6. The four leading-edge sweeps of 0°, 15°, 30°, and 45° are designated as configurations I, II, III, and IV, respectively, and were obtained by using different root sections. Appropriate tip sections were added to maintain streamwise tips. Various aspect ratios were obtained by the addition or subtraction of wing sections to the spanwise segmented wing. For each leading-edge sweep angle, the configuration with the highest aspect ratio is referred to as configuration A and with the lowest as configuration D. Table I gives the geometric characteristics for each of the 16 configurations.

Figure 7 shows the available aspect ratios plotted against the available sweep angles for the model. The points are faired to connect the configuration points marked A, B, C, and D. It can be seen that, for this model, sweep cannot be varied at a constant aspect ratio. The dashed line indicates that sweep can almost be varied at a constant aspect ratio of 4; however, the aspect ratio actually varies from 4.25 to 3.92, or about 8 percent. This model construction constraint presents some problems in direct comparisons between configurations, because the wing area and thickness ratio also change when sweep is varied.

The trailing edge of the wing was divided into several simple flap elements which equal 25 percent of the wing chord in length from pivot to trailing edge. These elements were defined as flaps on configuration D and as a combination of flaps and elevons on configurations A, B, and C. Figure 6 shows the definition of flap and elevons for configuration A. Note that for the 30° and 45° sweep configurations, the two outboard trailing-edge elements plus the small trailing-edge element on the wing

tip are defined as elevons in figure 6(b). This elevon definition is maintained on configurations B and C by removing an inboard section of the wing to change configuration aspect ratio, while retaining the outboard and tip sections. Thus, the elevon span remains constant while the flap span is reduced.

After a review of the solution for the flow separation on the spanloader model tested in reference 11, vortex generators were placed on the wing upper surface at $x/c = 0.55$ on the full span for all model configurations. These vortex generators were designed with a toe out of 15° from free stream. Drawings of the vortex-generator geometry for the left wing are given in figure 8; and figure 9 is a photograph showing the installation on the $\Lambda = 30°$ configuration. Note that the right-hand vortex generators are simply mirror images of those on the left.

Transition strips of No. 80 abrasive grains, 0.3175 cm in width, were placed 2.54 cm aft of the leading edge on the upper- and lower-wing surfaces in accordance with reference 16. Forces and moments were measured by an internally mounted six-component strain-gage balance, and angle of attack was measured with an internally mounted accelerometer. All pitching-moment data are referred to the moment reference locations shown in table I. These data correspond to the aerodynamic center of pressure of each configuration as predicted by the vortex-lattice theory of reference 17. All axial-force data were corrected for the base-pressure drag of the centerbody. Because of the relatively small model size and low lift coefficients generated, wall effects were minimal. Therefore, no jet-boundary corrections have been applied to these data.

Tests performed on each model configuration included an angle-of-attack sweep, out of ground effect at $\alpha = -7.2°$ to 18.7°, and height sweeps at $\alpha = -1.2°$, 0.8°, and 2.8° in ground effect. Approximate values of h/b for the in-ground-effect sweep were 0.02, 0.03, 0.05, 0.10, 0.25, 0.35, 0.50, and 1.00.

In many cases, ground-effect testing is conducted in the presence of a moving-belt ground plane to represent more accurately the interaction between the airplane and the ground without the interference of a thick boundary layer on the wind-tunnel floor. However, the use of the moving belt for this test would have limited the Mach number to about 0.09 which would have reduced the Reynolds number for some configurations below 1×10^6. It was felt that the data obtained at such low Reynolds numbers could be questionable. The criteria of reference 18 indicated that the combination of low lift coefficients and the range of h/b to be used on most of the present group of model configurations would provide test conditions which did not require the use of the moving-belt ground plane. The tunnel-floor boundary-layer thickness was reduced to approximately 4 to 5 cm with a displacement thickness of approximately 1 cm (see ref. 19) at the model location by the boundary-layer removal system located at the leading edge of the test section. This meant that some of the configurations with a lower aspect ratio would be in the upper portion of the boundary layer at the lower h/b setting. However, since most configurations met the requirement of reference 18 and were out of the floor boundary layer, the test was conducted at higher Mach numbers without the moving belt so that Reynolds numbers would be in the range from 1.3 to 1.8×10^6.

PRESENTATION OF RESULTS

The complete tabulated results of the data obtained in this wind-tunnel investigation are given in reference 15. Pertinent coefficient data, along with panel geometries and comparisons of theoretical and experimental results, are presented in this report as follows:

DISCUSSION

EXPERIMENTAL RESULTS

Longitudinal Aerodynamics Out of Ground Effect

Effect of aspect ratio.- The effect of aspect ratio on the longitudinal aerodynamic characteristics of configurations I to IV with several flap deflections is presented in figures 10 to 13. The effect of aspect ratio on experimental lift-curve slope (measured on the linear portion of the lift curve) is presented in figure 14, and, as expected, C_{L_α} is reduced as aspect ratio decreases and leading-edge sweep

is held constant. For example, in configuration I-A (AR = 8), C_{L_α} = 0.084 per degree and this is reduced in configuration I-C (AR = 4) to 0.067 per degree. It can also be seen that the effect of aspect ratio on C_{L_α} is reduced as sweep angle is increased. That is, for a given decrease (or increase) in aspect ratio, the change observed in C_{L_α} is smaller at higher sweep angles than at 0° sweep.

There is also, at first look, a possible anomaly in the data for the configurations with lowest aspect ratio when the flaps are deflected. The lift-curve slopes appear to be correct, but the angle of attack for zero lift is lower for configuration D than for configurations A, B, and C. (See figs. 10(b), 10(c), and 10(d).) This trend is present because configuration D has full-span flaps; whereas, configurations A, B, and C have elevons (as discussed in the model description) which are not deflected, and thus, are only partial-span flaps. This trend is also apparent in the nose-down increment in the pitching-moment data and in the large increment in minimum C_D for configuration D.

There are also fairly large increases in minimum C_D as the aspect ratio decreases for all configurations when $\delta_f = 0°$. (For example, see fig. 10(a), 11(a), 12(a), or 13(a).) This trend is a function of aspect ratio because as the wing span (and, hence, the reference area) decreases the drag from the centerbody, which is constant, becomes proportionally larger relative to the wing drag, thus increasing minimum C_D. An opposite effect would be seen as sweep angle is increased. Because the wing area is increased for a given aspect ratio (as the root and tip sections are added), the constant centerbody drag would contribute a smaller drag coefficient and minimum C_D would be decreased. Aside from the minimum C_D shifts due to centerbody effects, the drag polars show the expected trends of decreased span efficiency as aspect ratio is decreased.

Effect of flap deflection.- The effects of flap deflection on the longitudinal aerodynamic data of configurations I to IV are presented in figures 15 to 18. The data in figure 15 are for flap deflections of 0°, 10°, 20°, and 30°. It can be seen that the increments in C_L and C_m are greatly reduced at $\delta_f = 30°$ although minimum C_D increases at that flap setting. This is typical of the trends seen when a plain flap separates at large deflection angles. This was noticed early during the wind-tunnel tests, and the $\delta_f = 30°$ deflection was replaced by $\delta_f = 5°$ on subsequent configurations to avoid flap separation. In general, these data show the expected trend of decreasing the effects of the flaps as flap deflections are increased, thus showing the increasing flow separation on a simple flap as deflection is increased. The flow separation is also evident in the increasing increments in minimum C_D as flap deflections are increased, particularly for $\delta_f > 20°$. Finally, the effect of the flaps is generally reduced as sweep is increased or aspect ratio is decreased. These trends are consistent with the effects of sweep and aspect ratio on C_{L_α}. Along with this trend, it is seen that the negative pitching-moment increment for a given δ_f is greatly reduced as the sweep angle is increased.

Elevon Trim

The effects on the longitudinal aerodynamics caused by the outboard flap elements as elevons are presented in figures 19 to 22. As discussed in the section "Model Description," the elevons are simple flap elements which are deflected both positively and negatively in order to generate longitudinal pitch-control moments

similar to those of a horizontal tail. It can be seen in figures 19 to 22 that the elevons can maintain trim for neutral stability on all longitudinal configurations with flaps deflected 10° over the entire angle-of-attack range tested except on configurations I-A and I-B ($\Lambda = 0°$, AR = 8, and AR = 6). In these two straight-wing configurations, because the moment arms for the flaps and elevons are the same (see fig. 6(a)), the moment generated by the larger flap area cannot be balanced by the moments from the smaller elevons. Configuration I-C can be trimmed by the elevons because the elevons as defined are larger than the flap. On all other configurations, the favorable moment arm available for the elevons, due to the wing sweeps, is dominant and trim can be easily obtained over the complete angle-of-attack range tested. Also, as expected, positive elevon deflections (which become a full-span trailing-edge flap) produce increases in C_L and C_D. Negative elevon deflections produce decreases in C_L and increases in C_D. The changes in the drag polar and minimum C_D are typical of those caused by simple control deflections.

Longitudinal Aerodynamics in Ground Effect

Effect of aspect ratio.- The effects of aspect ratio on the longitudinal aerodynamic characteristics of configurations I to IV in ground effect are presented for $\alpha = 2.78°$ in figures 23 to 26 and for $\alpha = 0.78°$ in figures 27 to 30. As previously shown by the out-of-ground-effect data, the effect of decreased aspect ratio in ground effect is to also reduce C_{L_α}, or as shown in these figures, to reduce C_L at a constant angle of attack. Also, the trend of increasing C_D with decreasing aspect ratio, due to proportionally higher centerbody drag relative to the wing, is again present in these data.

Effect of flap deflection.- The effects of flap deflection on the longitudinal aerodynamics of configurations I to IV in ground effect are presented for $\alpha = 2.78°$ in figures 31 to 34 and for $\alpha = 0.78°$ in figures 35 to 38. As previously shown in the out-of-ground-effect data, the effect of flap deflection is decreased with increased flap deflection because of flow separation. Also, flap effectiveness is reduced with increasing sweep angle. However, the effect of flap deflection is approximately constant as the ground plane is approached at $\alpha = 2.78°$. However, at $\alpha = 0.78°$, the effect of flap deflection seems to increase as the ground plane is approached.

Ground Effect

As a conclusion to the discussion of experimental results, a comment should be made about ground effects. It should be noted that when $\alpha = 2.78°$ (see fig. 23, for example) the minimum h/b is increasing as the aspect ratio is decreased. This result is because the geometry of the sting support system limits the minimum h that can be obtained; and, thus, as wing span decreases, minimum h/b must increase. However, when $\alpha = 0.78°$, the model lower-surface limits h; and thus, a generally constant minimum h/b can be maintained by lowering the model as aspect ratio decreases. The data of figures 23 to 26 ($\alpha = 2.78°$) generally indicate expected ground effects in that C_L is increased, C_D is decreased, and, for these data only, slight nose-up changes in pitching moment are observed. However, as shown in figures 27 to 30, there are some interesting trends in the data at $\alpha = 0.78°$. These data show that C_L increases down to $h/b \approx 0.1$ as would be expected; and then, for the data with low or zero flap setting, C_L decreases at the very low h/b. Also, for these cases, C_D increases at low h/b and rather substantial nose-up

pitching moments are indicated. These effects, which are due to accelerated flow beneath the wing, will be discussed in greater detail in the following section of this report.

These lift losses and drag increases are of particular interest because it has been proposed that these spanloader airplanes would land at about $\alpha = 0°$ and, instead of cushioning a landing, these effects would lead to rather hard landings. Rather than land with $\delta_f = 0°$, it is more likely that an airplane would land with some larger flap deflection. In this instance, with $\delta_f = 5°$ to $10°$, these effects would be reduced but not eliminated. These effects appear to be eliminated at $\delta_f = 20°$.

THEORETICAL PREDICTIONS OF C_L AND C_{L_α}

Preliminary theoretical predictions of lift-curve slope were made with the method of reference 17. This method is based on the vortex-lattice concept where a planform can be modeled as shown in figure 39. On each panel, a horseshoe vortex is placed with the bound leg at the quarter chord of the panel, and the boundary condition of no flow perpendicular to the panel surface $\left(\vec{V}_\infty \cdot \hat{n} = 0\right)$ is applied at the 0.75c on the panel. (See fig. 40.)

Ground interference effects can be calculated with this method by using an image concept, as shown in figure 41, where a mirror image is placed below the ground plane. This system is then represented as a planar vortex-lattice system. (See fig. 42.) The image system produces a condition of no flow perpendicular to the ground plane (or plane of symmetry), and induces an upwash on the main configuration that simulates the normal ground effects. One possible drawback to this method was the planar modeling of the configuration, especially when very near the ground plane. It appeared that for a wing with $t/\bar{c} = 0.18$, the thickness effects should not be omitted. Another potential problem with this method is that for a high-aspect-ratio wing with sweep, there is a large variation in actual height between the wing apex and the trailing edge of the wing tip which is not accounted for in planar modeling.

Therefore, the configurations were modeled with the Hess method of reference 20 which included thickness effects. Because of the thickness representation used in this model, it was felt that the ground effects calculated by the Hess method could be different from those calculated by the vortex-lattice method (to be discussed in a later section). This method models a configuration as shown in figure 43. Constant source and vorticity panels are then placed on the actual-configuration surface geometry, and the boundary condition $\vec{V}_\infty \cdot \hat{n} = 0$ is applied at the centroid of each panel. (See fig. 44.) With this approach, the nonlifting or thickness solution is given by the source panels, and this is combined with the lifting solution from the vorticity panels to give the final surface pressures which can be integrated to give total forces and moments. This approach was also used to estimate ground effects with an image system. (See fig. 45.)

Lift-Curve Slope Out of Ground Effect

The theoretical calculations of C_{L_α} from both methods for configurations I to IV are given in figure 46 as a function of aspect ratio. Because it is well known that vortex-lattice methods give reasonable results for C_{L_α} and because inputs to

the Hess program are somewhat tedious and the calculations are rather expensive, only three configurations (I-A, II-A, and III-A) were modeled as a check of C_{L_α} with thickness effects included. The predictions in figure 46 indicate the expected trends of reduction in C_{L_α} when sweep is increased or aspect ratio is decreased. These data are cross-plotted in figure 47 to show more clearly the effect of increasing sweep angle at a constant aspect ratio on C_{L_α}. The three values of C_{L_α} for configurations I-A, II-A, and III-A are plotted in figure 46 for comparison of the Hess results with the vortex-lattice results. The results from Hess which include thickness are, as expected, slightly higher than the results from the vortex lattice which do not include thickness.

From these results, it can be seen that the effect of sweep diminishes at the lower aspect ratios. For example, if AR = 5, then $\left(C_{L_\alpha}\right)_{\Lambda=0°} = 0.731$ per degree and $\left(C_{L_\alpha}\right)_{\Lambda=45°} = 0.0562$ per degree for a change of C_{L_α} of 0.0169 per degree. At AR = 3, $\left(C_{L_\alpha}\right)_{\Lambda=0°} = 0.0600$ per degree and $\left(C_{L_\alpha}\right)_{\Lambda=45°} = 0.0500$ per degree for a change of C_{L_α} of 0.0100 per degree.

Effect of Ground Plane on Lift Coefficient

The vortex-lattice results for the ground effect on C_L are presented in figure 48. The results are presented as C_L plotted against h/b for each configuration at a constant sweep angle as aspect ratio is decreased. The typical result of ground-induced upwash, which causes an increase in C_L as the ground is approached, is clearly shown in the figure. The ground effects are generally limited to $h/b < 0.25$ with a decided break in the curve at $h/b \approx 0.10$ where the slope of the curve increases rapidly. This trend is consistent for all configurations, along with the trends associated with increasing Λ and decreasing AR as discussed earlier.

Results from using the Hess method for the ground effect on C_L for configurations I-A, II-A, and III-A are presented in figure 49. Corresponding results from using the vortex-lattice method are also shown for comparison. The striking difference in predicted ground effects for the two methods is apparent. At low h/b, the Hess results predict decreasing C_L as h/b is decreased, rather than the expected increases in C_L shown by the vortex-lattice results. This result had not been seen previously. However, as the following discussion and figure 50 will show, this result is not at all surprising and, in fact, should be expected for these very thick wings at low h/b.

Figure 50 shows a two-dimensional section of the wing and its image of configuration I-A as represented in this method at $\alpha = 1.0°$ and at $h/b = 0.1$ or the break in the C_L curve in figure 49. Also shown in figure 50 is the two-dimensional section of the configuration when $h/b = 0.05$. Notice the similarity of the wing lower surface and the image upper surface to the shape of a venturi tube. It would seem that the flow would accelerate between these two surfaces and reduce the pressures on those surfaces. The pressure distributions show that this venturi effect is exactly what happens in this calculation. The upper-surface pressure is almost unchanged, whereas the lower-surface pressure is markedly decreased; and the minimum pressure is seen to occur at the point of minimum area between the wing and image

(i.e., at maximum $t/\bar{c}$) exactly as in a venturi tube. This lowering of the lower-surface pressure reduces C_L in a manner not unlike the "suck down" seen on some powered-lift VTOL configurations. Thus, for these thick wings, the venturi effect on the lower surface can completely negate the upwash effect of the ground plane and actually reduce C_L rather drastically very near the ground. This result now becomes one of great importance because spanloader airplanes were proposed to operate at these low h/b ratios, and this reduction in lift (if present on the real configuration) would lead to some rather hard landings, instead of the cushioned landings that were anticipated due to favorable ground effect. As will be discussed in a following section and as was mentioned in the discussion of experimental ground effects, this effect is moderate at $\delta_f = 5°$ and $10°$ and is effectively eliminated at $\delta_f = 20°$.

COMPARISON OF THEORY AND EXPERIMENT

Lift-Curve Slope

A comparison of the predicted lift curves and the experimental lift curve for three selected configurations is presented in figure 51. These three configurations (I-A, II-A, and III-A) represent the configurations which were modeled in both the vortex-lattice and Hess methods. The vortex-lattice method appears to give a fairly accurate prediction of the lift curve for configuration I-A, whereas the Hess method tends to overpredict the lift curve. At the higher sweep angles (i.e., $\Lambda = 15°$ and $30°$), both methods underpredict the lift curve of configurations II-A and III-A. This trend is consistent for all configurations as shown in figure 52 where all configurations are modeled in the vortex-lattice method. These predicted lift-curve slopes are compared with the experimental C_{L_α}; and the theory fairly accurately predicts C_{L_α} at $\Lambda = 0°$ and increasingly underpredicts C_{L_α} as sweep is increased to 45°. This trend is thought to be caused by the increased loads generated by the vortex generators as sweep and resulting spanwise flow are increased. This discussion is found in a later section of this paper.

Flap Effectiveness

A comparison of predicted out-of-ground-effect flap effectiveness $C_{L_{\delta_f}}$ and the experimental $C_{L_{\delta_f}}$ is presented in figure 53. The experimental values of $C_{L_{\delta_f}}$ were determined for the 5° flap deflection since $C_{L_{\delta_f}}$ fell off rapidly at $\delta_f = 10°$ and $20°$ because of flow separation on the flap. It should be noted that the theory had streamwise flap deflections where the flap elements are deflected parallel to the free stream. (See fig. 39.) However, the data (because of model constraints) had hinge-line flap deflections where the flap elements are deflected normal to the flap hinge line. (See fig. 6.) Therefore, the $C_{L_{\delta_f}}$ from the data has been adjusted to the equivalent streamwise values. This was done by calculating the effective streamwise deflection of the model flap system by using

$$\delta_{f,s} = \tan^{-1}(\tan \delta_f \cos \Lambda)$$

and then computing

$$C_{L_{\delta_{f,s}}} = C_{L_{\delta_f}} \left(\frac{\delta_f}{\delta_{f,s}} \right)$$

A list of hinge-line and streamwise flap deflections is given in table II.

It can be seen that the predictions of $C_{L_{\delta_f}}$ are quite good for configuration I and are somewhat poorer for the other configurations with configuration III being the worst case. Also, where there is disagreement, the experimental $C_{L_{\delta_f}}$ is generally below that predicted by theory. This result is not surprising because for any simple hinge flap there will be a reduction from potential-flow effectiveness at any deflection. The adverse pressure gradient, because of rapid pressure recovery, aft of the large negative pressures generated by the high curvature at the knee of the flap will, at least, result in a thick boundary layer which will reduce flap effectiveness and will, at most, completely separate the flow on the flap.

Ground Effects

The comparison of predicted and experimental ground effects on the four selected configurations (I-A, I-C, II-A, and III-A) is presented in figure 54. The data are presented as $C_{L,IGE}/C_{L,OGE}$ to nondimensionalize the results as a percentage increase or decrease in lift from that of the configuration out of ground effect. The theoretical results from figure 48 are replotted in the same form $C_{L,IGE}/C_{L,OGE}$ for direct comparisons. The data follow the trend seen in the Hess prediction discussed earlier in that there is a lift increase indicated as the ground plane is approached which becomes a rapid lift loss as $h/b \leq 0.10$. There is scatter in the data, and the magnitude and location (h/b) of the peak in lift increase are not exactly as predicted; however, the overall trend is well established and in direct opposition to the trends predicted by conventional vortex-lattice methods. There does not seem to be a consistent trend to the difference between experimental and theoretical data. That is, the differences do not appear to be a function of sweep or aspect ratio which would indicate a basic problem with the modeling technique. This reduction in lift at low h/b was present for all configurations except those with high flap deflections where the traditional increases in C_L are present.

When the flap is deflected, the flap trailing edge becomes the low point (i.e., nearest the ground plane) on the configuration and interference between the flap and the boundary layer on the ground plane may be effectively blocking the flow. This will tend to produce stagnation conditions under the wing and can then lead to large increases in lift like the wing in-ground-effect (WIG) configuration of reference 21.

Another possibility for the change in ground effect when the flap is deflected is that the area ratio between the maximum thickness point and the trailing-edge flap point is changed. At $\delta_f = 20°$, the minimum area is located at the trailing edge which eliminates the venturi-tube shape under the wing (see fig. 6(c)) and thus, the flow will not accelerate under the wing. At the intermediate flap settings ($\delta_f = 5°$ and 10°), the area at the trailing edge is not the minimum under the wing but is reduced from the $\delta_f = 0°$ area. Thus, the venturi-tube shape is modified, and the

velocities under the wing will be correspondingly modified. As such, the ground effects are reduced but not eliminated at $\delta_f = 5°$ and $10°$. This is verified in figure 55 where $C_{L,IGE}/C_{L,OGE}$ from the Hess theory for configurations I-C and III-B or $\Lambda = 0°$ and $\Lambda = 30°$ with $\delta_f = 10°$ are compared with the experimental results. Again, it can be seen that the theory and experiment agree well and that the lift loss at low h/b is greatly reduced (but not eliminated) from the previous $\delta_f = 0°$ cases.

EFFECT OF VORTEX GENERATORS

As noted in the section "Comparion of Theory and Experiment" for C_{L_α}, the theory tends to underpredict the lift data at sweeps greater than 0° and the error seems to get worse as the sweep angle is increased. In an effort to define and explain this problem, a general discussion of the effect of the vortex generators is presented.

Prior to the wind-tunnel tests, reference 11 was used to determine the need for a set of vortex generators to maintain attached flow on the aft portions of the thick NACA 0018 airfoil section used on this model. The effect of the vortex generators was large. (See fig. 56.) Significant increases in lift and increments in nose-down pitching moment indicate that the aft portion of the wing was indeed separated and was reattached when the vortex generators were in place. It may be pointed out that while this flow was being reattached, a large increment in drag was shown for the vortex generator. It would seem that reattaching the flow in an effort to approach potential flow would result in a drag reduction. However, the physical size of the generators and the drag associated with producing the vortices have outweighed the benefit in drag reduction expected when separated flow is reattached.

The underprediction of the experimental lift-curve slope is another matter. As seen before, C_{L_α} at $\Lambda = 0°$ is predicted accurately and the error seems to increase with increasing sweep angle. It was also noted before that the vortex generators were placed on the wing in such a way that they are toed out a constant 15° relative to the free stream. In retrospect, this would seem to give an increased loading on the vortex generators since the sidewash velocity (spanwise flow) would be increased as sweep angle was increased. Thus, the vortex generators would be at a higher angle of attack and generate more intense vortex flows at higher sweep angles. If these vortices produced suction forces on the wing in a manner similar to a leading-edge vortex (see ref. 22), it might be possible to generate higher than potential-flow lift on the aft portion of the wing. A possible indicator of this is shown in figure 57 where C_L and C_m are plotted against α for four configurations having an aspect ratio of 4 at $\Lambda = 0°$, 15°, 30°, and 45°. The following table lists the theoretical and experimental values of C_{L_α}:

Configuration	AR	Λ, deg	Theoretical C_{L_α}	Experimental C_{L_α}
I-C	4	0	0.0672	0.0664
II-C	4.25	15	.0672	.0683
III-C	3.92	30	.0620	.0698
IV-B	4.1	45	.0549	.0572

The trend is consistent except for configuration II-C which has an aspect ratio of 4.25 rather than 4. If the higher than predicted C_{L_α} is due to excessive aft loading from the vortex generator, then the pitching moments should show increasing nose-down increments. This trend is seen in the C_m data.

Another indication is seen in the stall characteristics of the various configurations. (See fig. 57.) Here, as the wing sweep is increased and the vortex generators produce increased vorticity, the stall break is seen to be delayed to higher angles of attack. When $\Lambda = 45°$, it can be seen that there is no indication of stall up to $\alpha = 19°$. The delay in wing stall shows that the increased vorticity from the vortex generators delays flow separation on the aft portion of the airfoil.

From this discussion, it would appear that the vortex generators are developing excessive vorticity and actually are producing a greater than potential-flow condition on the aft portion of the wing. The penalty paid for this would appear to be the large increment in drag that occurs when the vortex generators are on the configuration as shown in figure 55. A more accurate placement of the vortex generators would seem to be at a constant 15° angle relative to the resultant spanwise flow as the sweep is increased. This would give an approximate constant vorticity which would be equal to that generated on the straight-wing configurations, which seems to be close to potential-flow conditions.

CONCLUSIONS

An analysis of the effects of sweep and aspect ratio on the longitudinal aerodynamics of a wing in and out of ground effect has been made. Experimental data were obtained in the Langley 4- by 7-Meter Tunnel for a wing with various sweep angles, aspect ratios, and flap deflections both in and out of ground effect. Theoretical predictions of the out-of-ground-effect lift coefficients and flap effectiveness and in-ground-effect lift coefficients are compared with experimental results. Some general conclusions concerning the longitudinal aerodynamics of spanloader-type (i.e., wing alone) configurations both in and out of ground effect are presented as follows:

1. As expected, lift-curve slope is decreased when either the aspect ratio is decreased or the sweep angle is held constant or is increased.

2. As expected, flap effectiveness is reduced at higher deflections, because of flow separation, and it is also reduced when aspect ratio is decreased or when sweep angle is increased.

3. Lift-curve slope and flap effectiveness at low angles of attack are both generally increased in ground effect above wing height-to-span ratios h/b of 0.15. However, at higher angles of attack, flap effectiveness is essentially unchanged in ground effect.

4. At low angles of attack and flap deflections of 0°, lift-curve slope is markedly reduced at very low h/b ratios. This appears to be caused by a venturi effect that is formed when the flow is accelerated between the lower surface of the wing and the ground plane, thus reducing the pressures on the underside of the wing. The phenomenon is reduced at flap deflections δ_f of 5° and 10° and is effectively eliminated at $\delta_f = 20°$ where the flap trailing edge is the low point beneath the airfoil.

5. Theory tends to predict the out-of-ground-effect lift-curve slope and flap effectiveness fairly well. The experimental lift curve does seem to be underpredicted by theory at increasing sweep angles. This appears to be the result of the vortex generators producing greater than potential lift on the aft portion of the wing.

6. Theoretical and experimental predictions of lift-curve slope in ground effect differ markedly, depending on whether planar (no thickness) or surface-panel (thickness) modeling techniques are used. The reductions in lift-curve slope at low h/b indicated in the surface-panel modeling when $\delta_f = 0°$ or $10°$ agree with the experimental data.

Langley Research Center
National Aeronautics and Space Administration
Hampton, VA 23665
July 26, 1982

REFERENCES

1. Preliminary Design Dep., Boeing Commercial Airplane Co.: Technical and Economic Assessment of Swept-Wing Span-Distributed Load Concepts for Civil and Military Air Cargo Transports. NASA CR-145229, 1977.

2. Whitener, P. C.: Distributed Load Aircraft Concepts. AIAA Paper 78-100, Jan. 1978.

3. Whitlow, David H.; and Whitener, P. C.: Technical and Economic Assessment of Span-Distributed Loading Cargo Aircraft Concepts. NASA CR-144963, 1976.

4. Johnston, William M.; Muehlbauer, John C.; Eudaily, Roy R.; Farmer, Ben T.; Honrath, John F.; and Thompson, Sterling G.: Technical and Economic Assessment of Span-Distributed Loading Cargo Aircraft Concepts. NASA CR-145034, 1976.

5. Technical and Economic Assessment of Span-Loaded Cargo Aircraft Concepts. NASA CR-144962, 1976.

6. Whitehead, Allen H., Jr.: The Promise of Air Cargo - System Aspects and Vehicle Design. NASA TM X-71981, 1976.

7. Nicks, Oran W.; Whitehead, Allen H., Jr.; and Alford, William J., Jr.: An Outlook for Cargo Aircraft of the Future. NASA TM X-72796, 1975.

8. Whitehead, Allen H., Jr.: Preliminary Analysis of the Span-Distributed-Load Concept for Cargo Aircraft Design. NASA TM X-3319, 1975.

9. Whitehead, Allen H., Jr.: Perspective on the Span-Distributed-Load Concept for Application to Large Cargo Aircraft Design. NASA TM X-3320, 1975.

10. Paulson, John W., Jr.: Aerodynamic Characteristics of a Large Aircraft To Transport Space Shuttle Orbiter or Other External Payloads. NASA TN D-7962, 1975.

11. Rao, Dhanvada M.; and Huffman, Jarrett K.: Wind Tunnel Tests on a Tail-Less Swept Wing Span-Distributed Cargo Aircraft Configuration. NASA TM-78767, 1978.

12. Carter, Arthur W.: Effects of Ground Proximity on the Longitudinal Aerodynamic Characteristics of an Unswept Aspect-Ratio-10 Wing. NASA TN D-5662, 1970.

13. Carter, Arthur W.: Effect of Ground Proximity on the Aerodynamic Characteristics of Aspect-Ratio-1 Airfoils With and Without End Plates. NASA TN D-970, 1961.

14. Schade, Robert O.; and Parlett, Lysle P.: Summary of NASA Research on Aerial Jeeps, Flying Platforms, and Ground-Effect Machines. Paper presented to the National Army Aviation Meeting of the Institute of the Aerospace Sciences (Washington, D.C.), Apr. 12-14, 1961.

15. Kjelgaard, Scott O.; and Paulson, John W., Jr.: Effect of Sweep and Aspect Ratio on the Longitudinal Aerodynamics of a Spanloader Wing In- and Out-of-Ground Effect. NASA TM-80199, 1981. (Supersedes NASA TM-80199, 1980.)

16. Braslow, Albert L.; and Knox, Eugene C.: Simplified Method for Determination of Critical Height of Distributed Roughness Particles for Boundary-Layer Transition at Mach Numbers From 0 to 5. NACA TN 4363, 1958.

17. Tulinius, J.: Unified Subsonic, Transonic, and Supersonic NAR Vortex Lattice. TFD-72-523, Los Angeles Div., North American Rockwell, Apr. 27, 1972.

18. Turner, Thomas R.: Endless-Belt Technique for Ground Simulation. Conference on V/STOL and STOL Aircraft, NASA SP-116, 1966, pp. 435-446.

19. Roper, Alan T.; and Gentry, Garl L., Jr.: Turbulent Boundary Layers Over Nonstationary Plane Boundaries. NASA TM-74091, 1978.

20. Hess, John L.: Calculation of Potential Flow About Arbitrary Three-Dimensional Lifting Bodies. Rep. No. MDC J5679-01 (Contract N00019-71-C-0524), McDonnell Douglas Corp., Oct. 1972. (Available from DTIC as AD 755 480.)

21. Thomas, James L.; Paulson, John W., Jr.; and Margason, Richard J.: Powered Low-Aspect-Ratio Wing in Ground Effect (WIG) Aerodynamic Characteristics. NASA TM-78793, 1979.

22. Polhamus, Edward C.: A Concept of the Vortex Lift of Sharp-Edge Delta Wings Based on a Leading-Edge-Suction Analogy. NASA TN D-3767, 1966.

TABLE I.- GEOMETRIC CHARACTERISTICS OF SPANLOADER CONFIGURATION

Configuration	Λ, deg	AR	b, m	$\bar{c}$, m	S, m^2	x_{mc}, m	$x/\frac{\bar{c}}{4}$, m	$t/\bar{c}$
I-D	0	2	0.80	0.40	3.20	0.35	0.40	0.180
I-C	0	4	1.60	.40	6.40	.38	.40	.180
I-B	0	6	2.40	.40	9.60	.38	.40	.180
I-A	0	8	3.20	.40	12.80	.39	.40	.180
II-D	15	2.38	.99	.41	4.09	.39	.43	.174
II-C	15	4.25	1.76	.41	7.28	.45	.48	.174
II-B	15	6.11	2.53	.41	10.49	.50	.53	.174
II-A	15	7.98	3.31	.41	13.69	.56	.58	.174
III-D	30	2.42	1.12	.46	5.17	.42	.46	.156
III-C	30	3.92	1.81	.46	8.37	.52	.56	.156
III-B	30	5.42	2.51	.46	11.57	.62	.66	.156
III-A	30	6.92	3.20	.46	14.77	.72	.76	.156
IV-D	45	2.1	1.19	.57	6.73	.44	.47	.127
IV-C	45	3.1	1.76	.57	9.93	.58	.61	.127
IV-B	45	4.1	2.32	.57	13.12	.72	.76	.127
IV-A	45	5.1	2.89	.57	16.33	.86	.90	.127

TABLE II.- COMPARISON OF HINGE-LINE AND STREAMWISE FLAP DEFLECTIONS

Sweep angle, Λ, deg	Hinge-line deflection, δ_f, deg	Streamwise deflection, $\delta_{f,s}$, deg
0	0	0
0	5	5
0	10	10
0	20	20
15	0	0
15	5	4.83
15	10	9.67
15	20	19.37
30	0	0
30	5	4.33
30	10	8.68
30	20	17.49
45	0	0
45	5	3.54
45	10	7.11
45	20	14.43

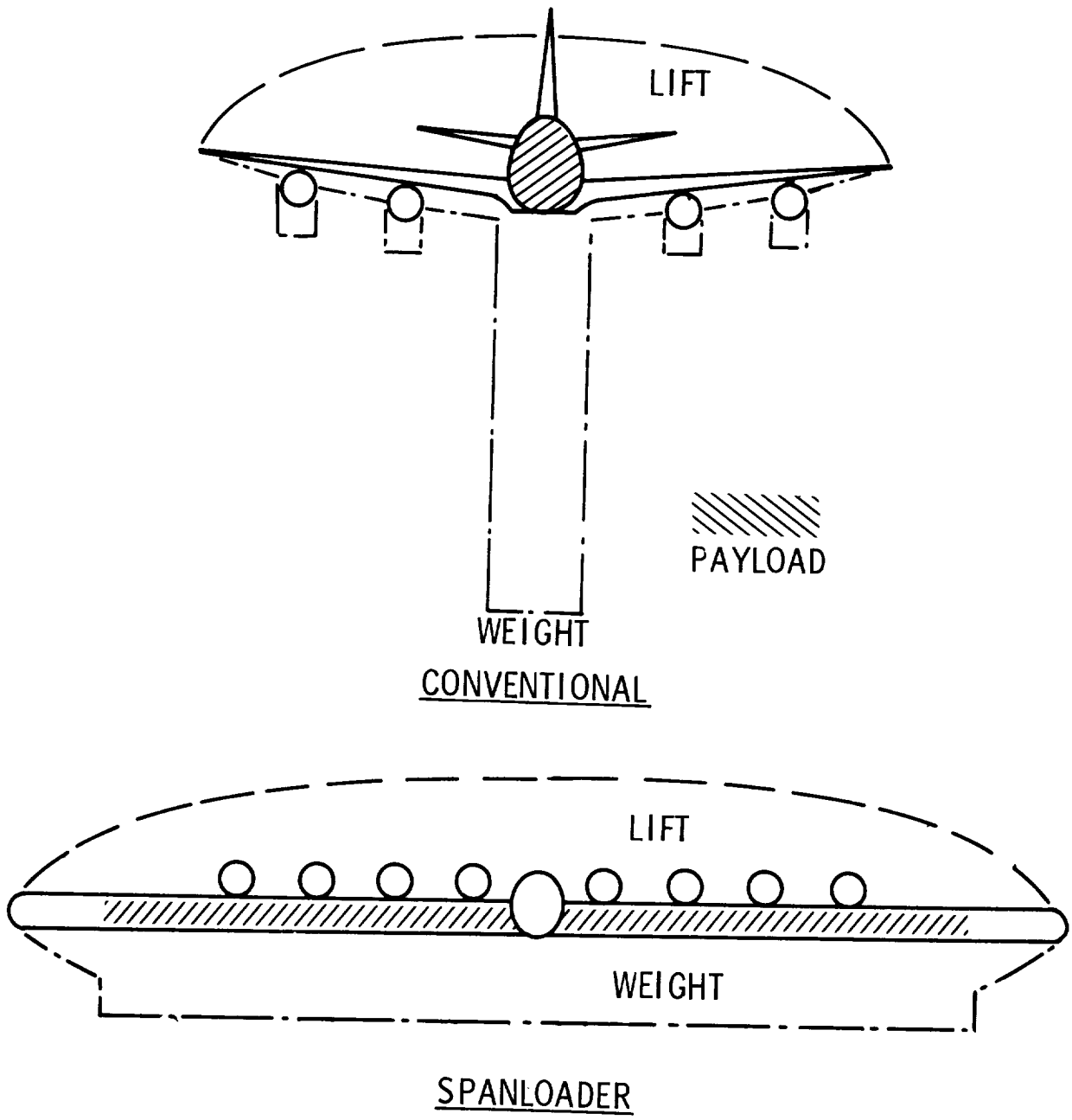

Figure 1.- Spanloading and weight distribution for conventional and spanloader transport airplanes.

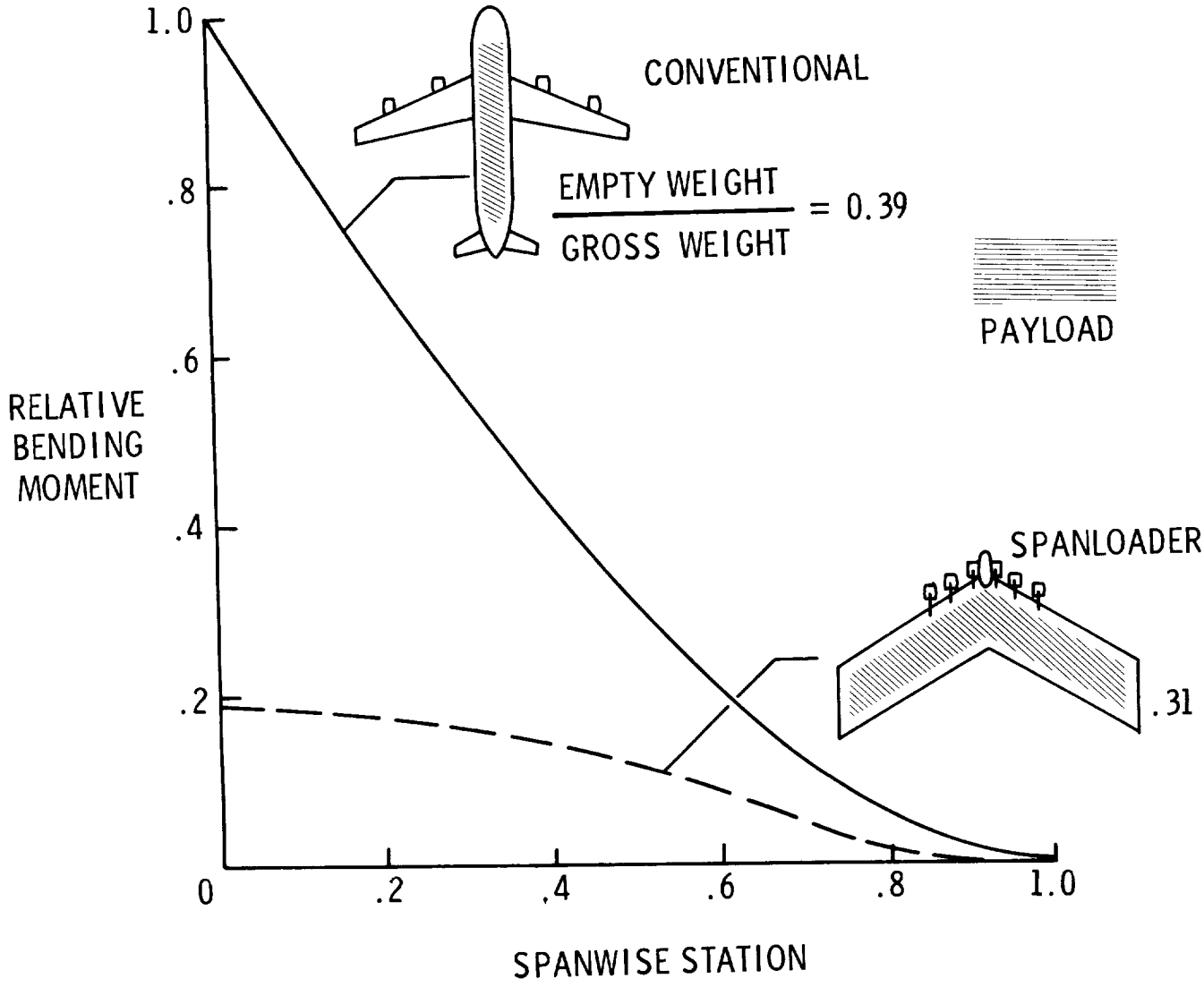

Figure 2.- Comparison of relative wing-root bending moments for conventional and spanloader transport airplanes.

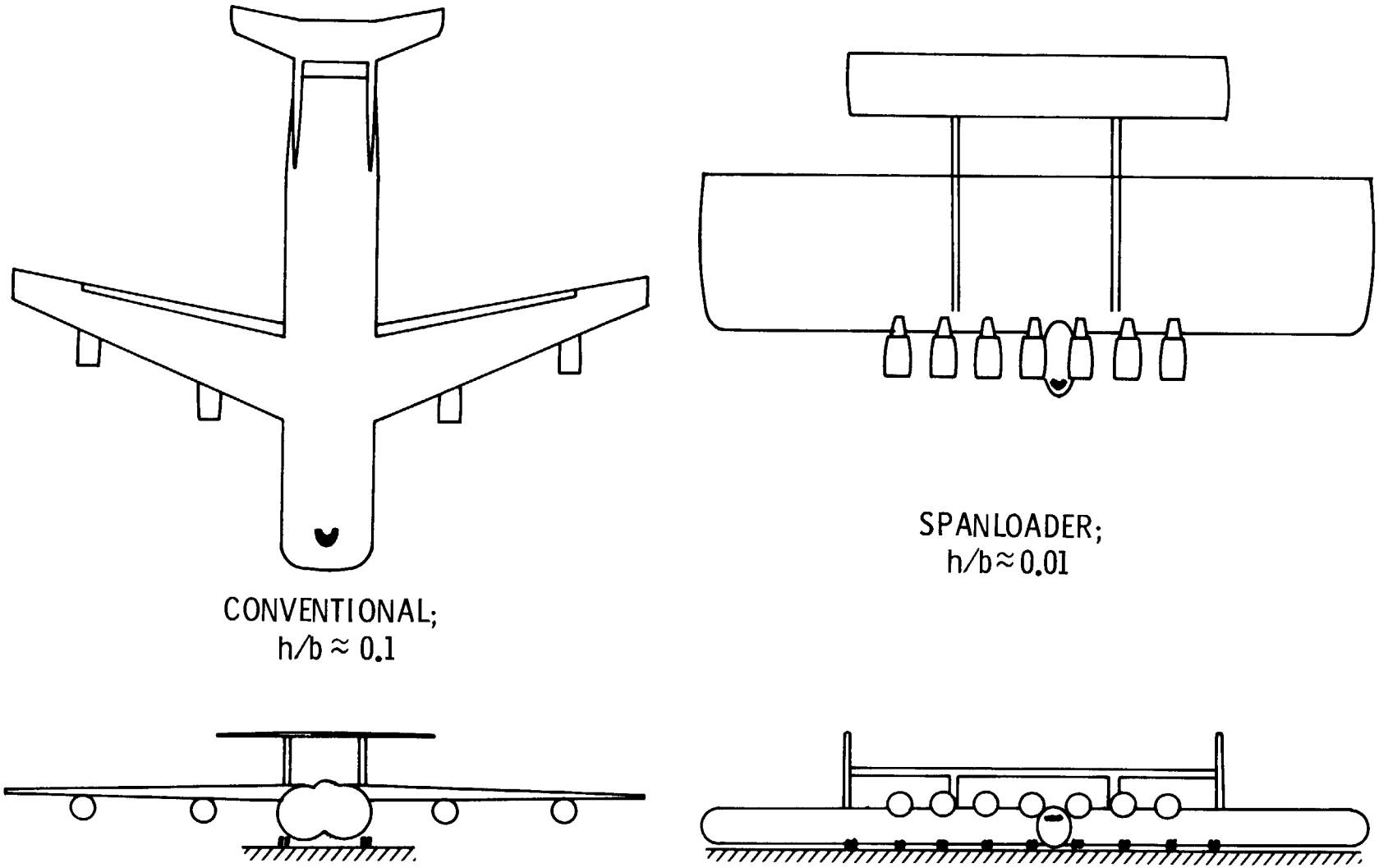

Figure 3.- Comparison of wing height-to-span ratios for conventional and spanloader configurations in landing.

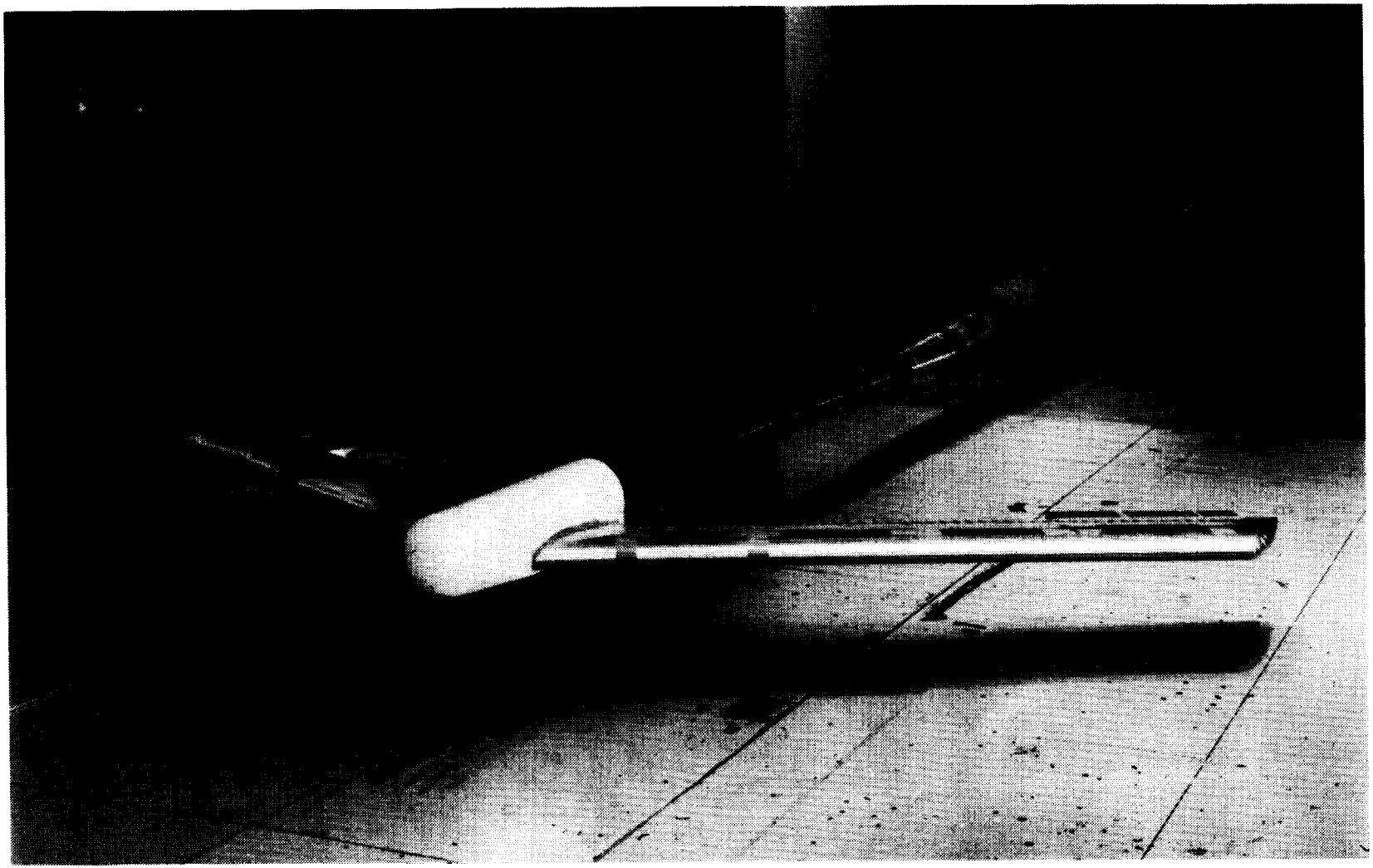

L-79-7518

Figure 4.- Spanloader model in ground effect installed in the Langley 4- by 7-Meter Tunnel.

L-79-7517

Figure 5.- Spanloader model out of ground effect installed in the Langley 4- by 7-Meter Tunnel.

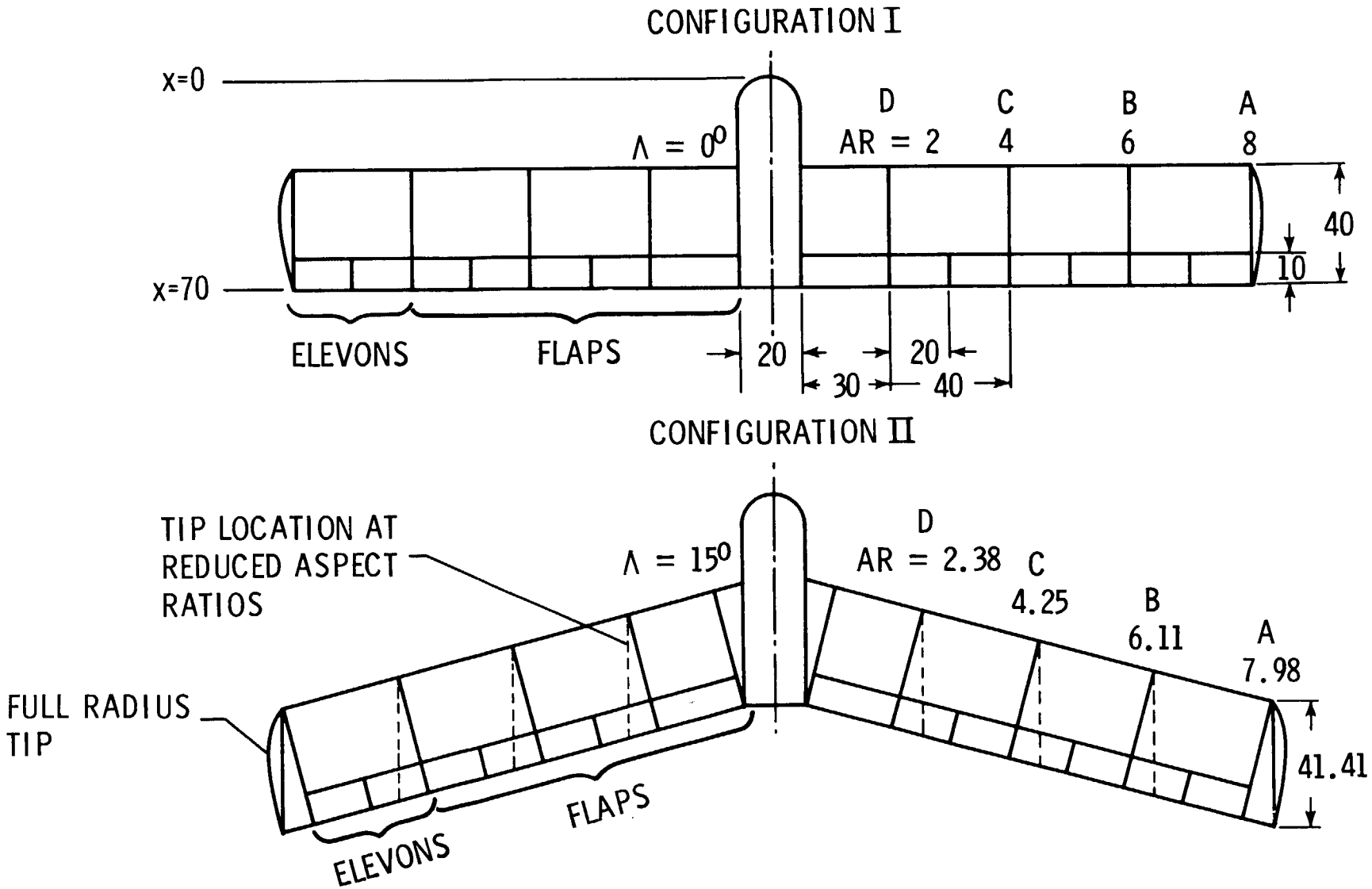

(a) Configurations I and II, Λ = 0° and 15°.

Figure 6.- Geometry of spanloader model. All dimensions are in centimeters unless otherwise noted.

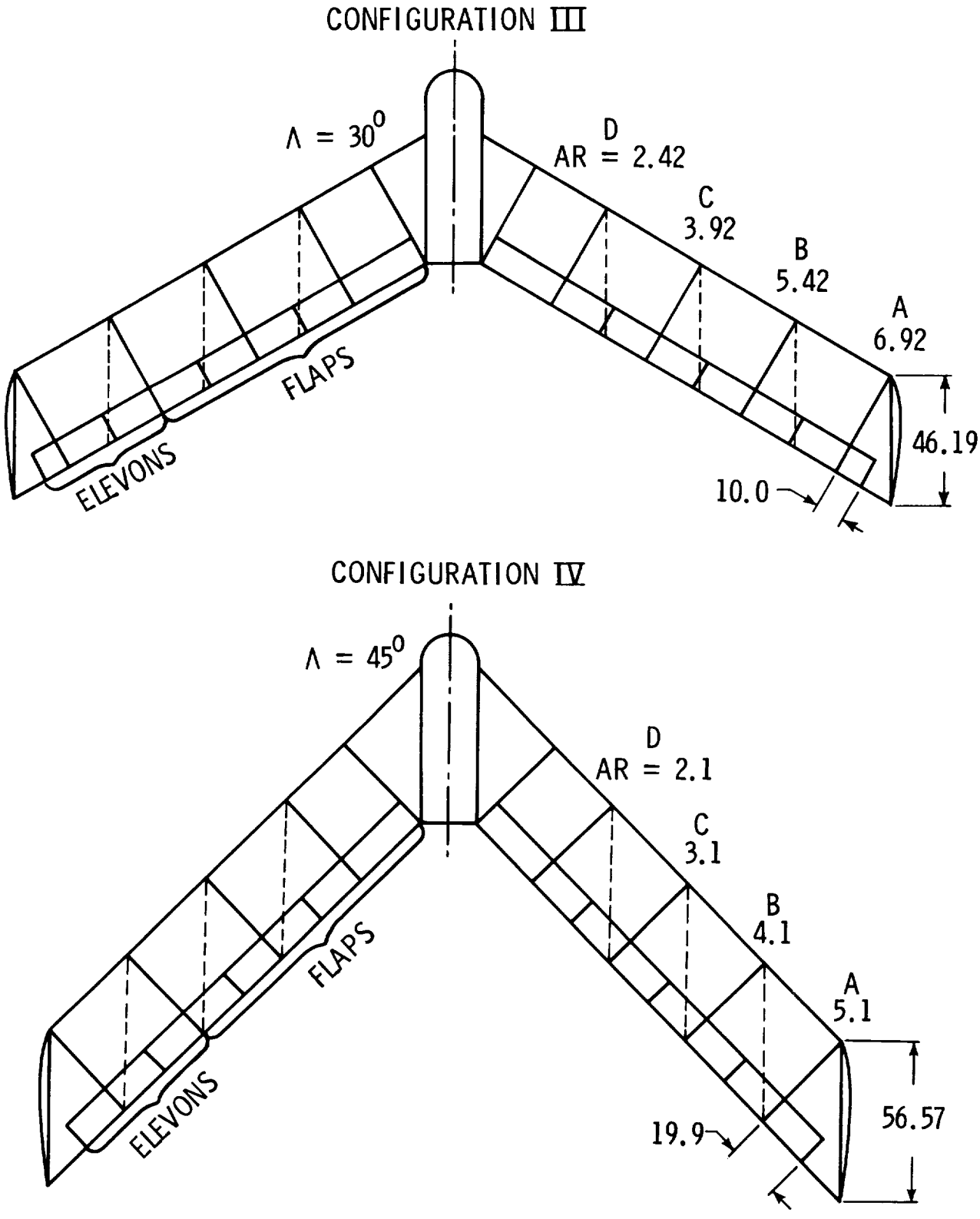

(b) Configurations III and IV. Λ = 30° and 45°.

Figure 6.- Continued.

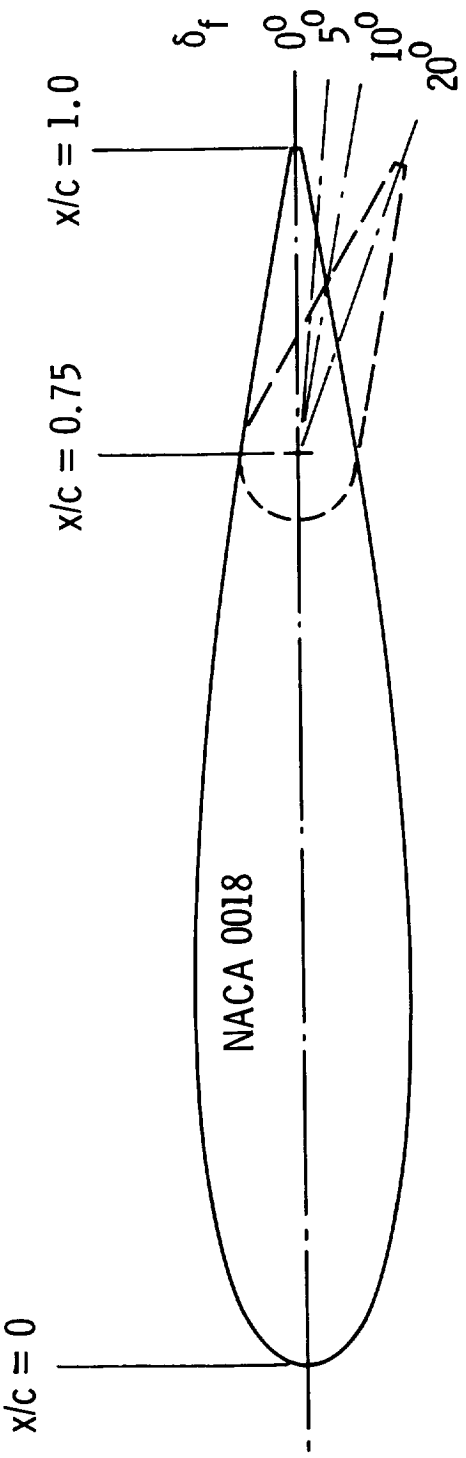

(c) Airfoil section.

Figure 6.- Concluded.

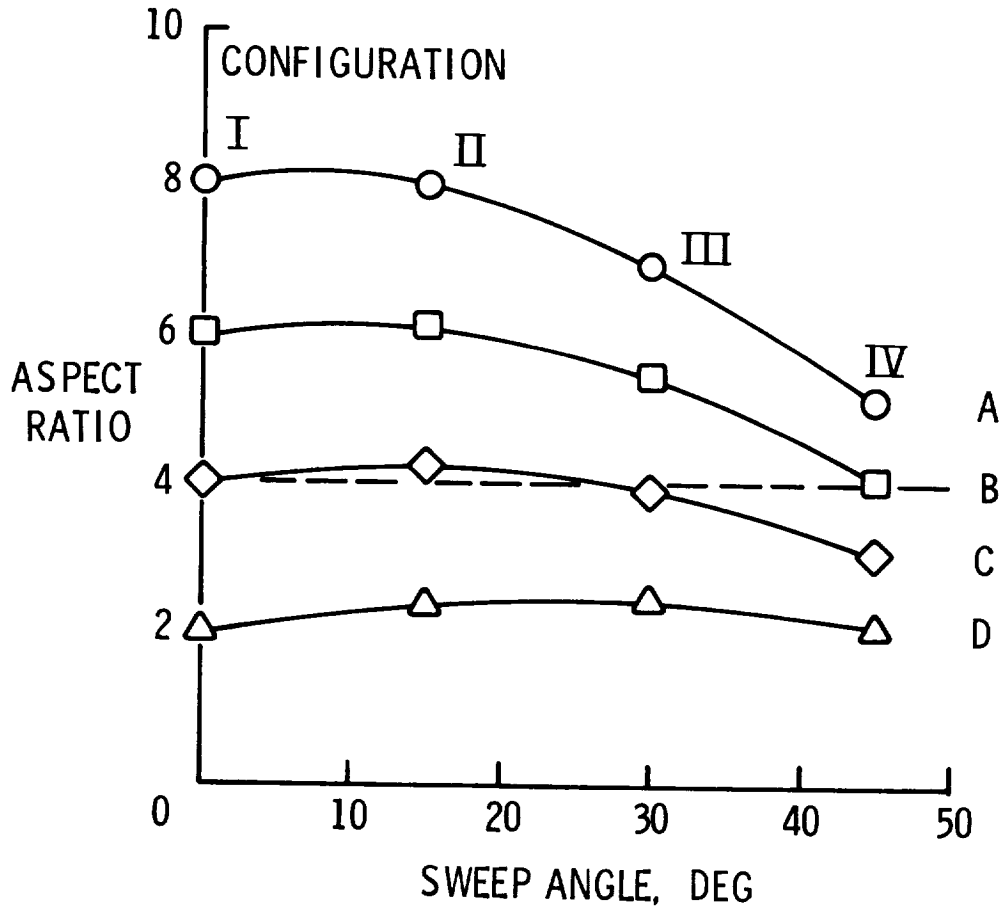

Figure 7.- Plot of aspect ratio against sweep angles available for spanloader model. Dashed line indicates that sweep can almost be varied at a constant ratio of 4.

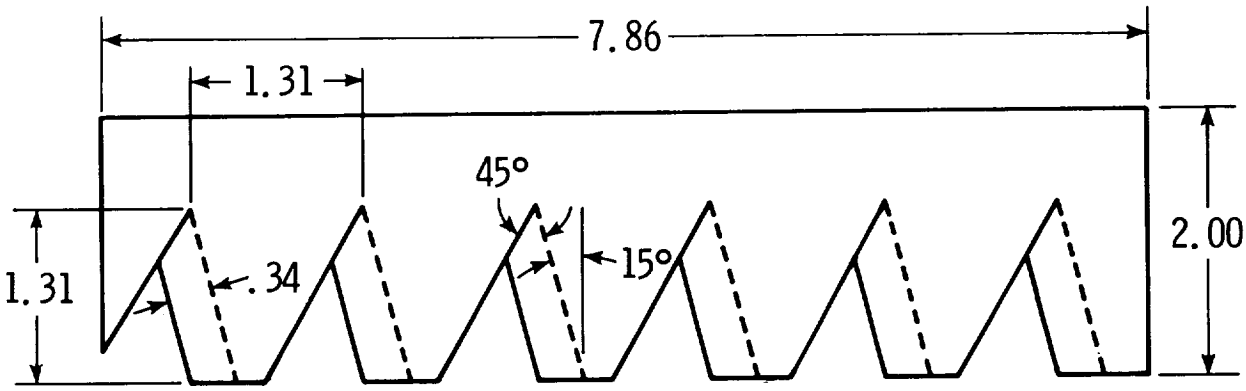

(a) Configurations with Λ = 0° and 30°.

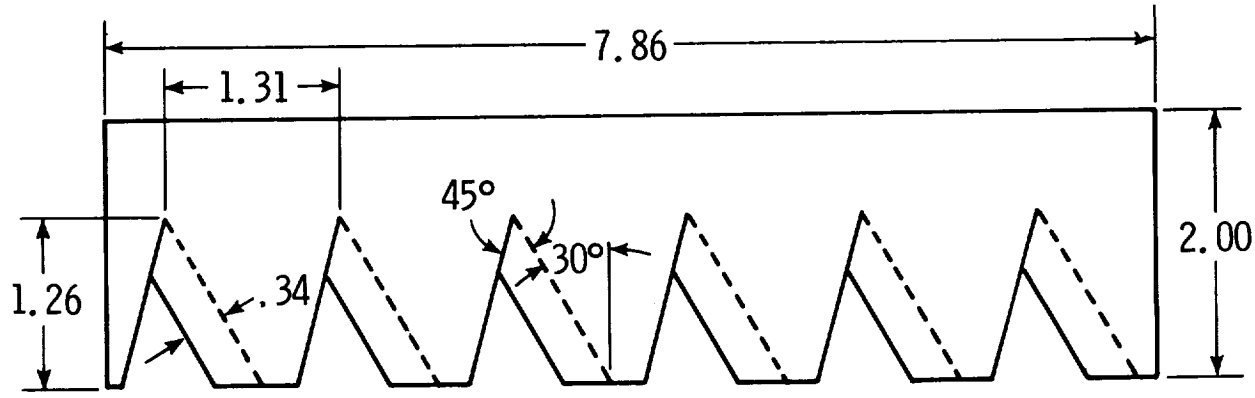

(b) Configurations with Λ = 45°.

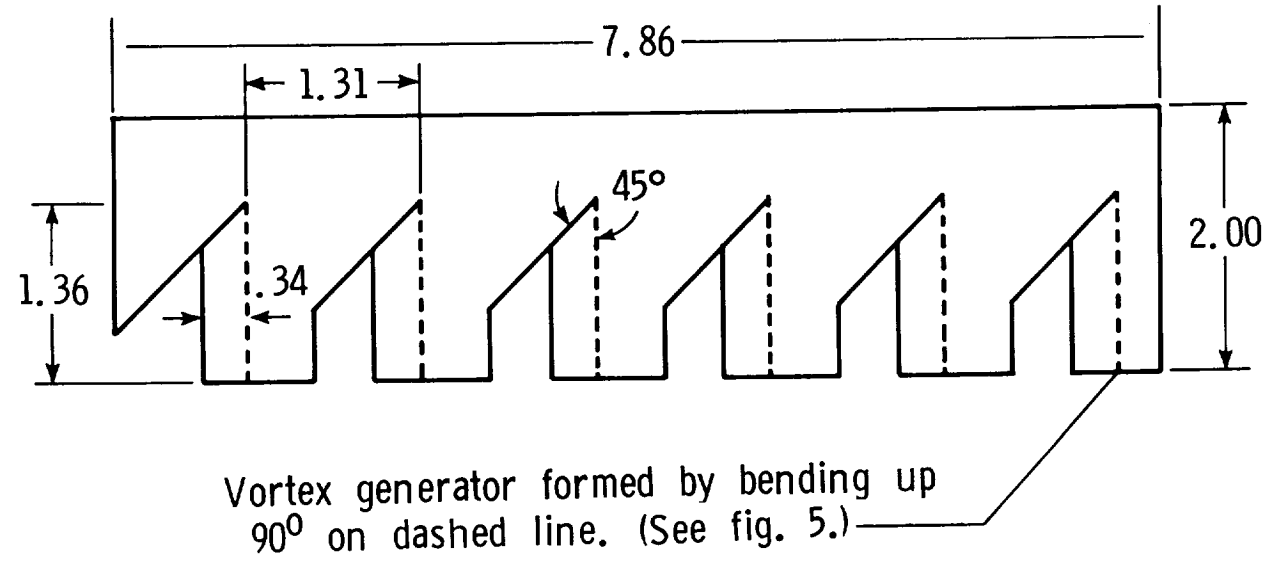

(c) Configurations with Λ = 15°.

Figure 8.- Vortex generator plates. All dimensions in centimeters unless otherwise noted.

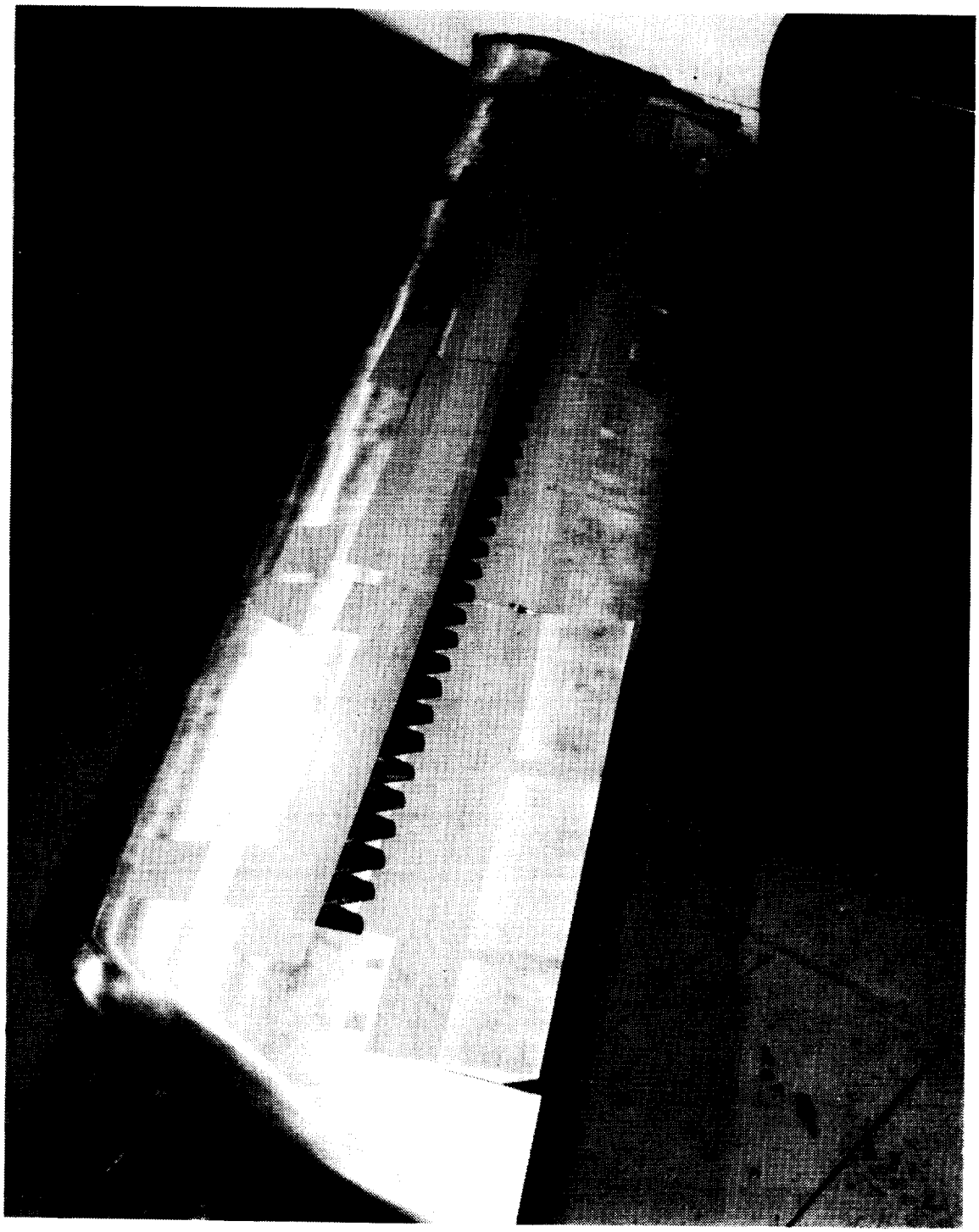

L-79-7515

Figure 9.- Vortex generator installed on configuration III-A.
$\Lambda = 30°$; AR = 6.92.

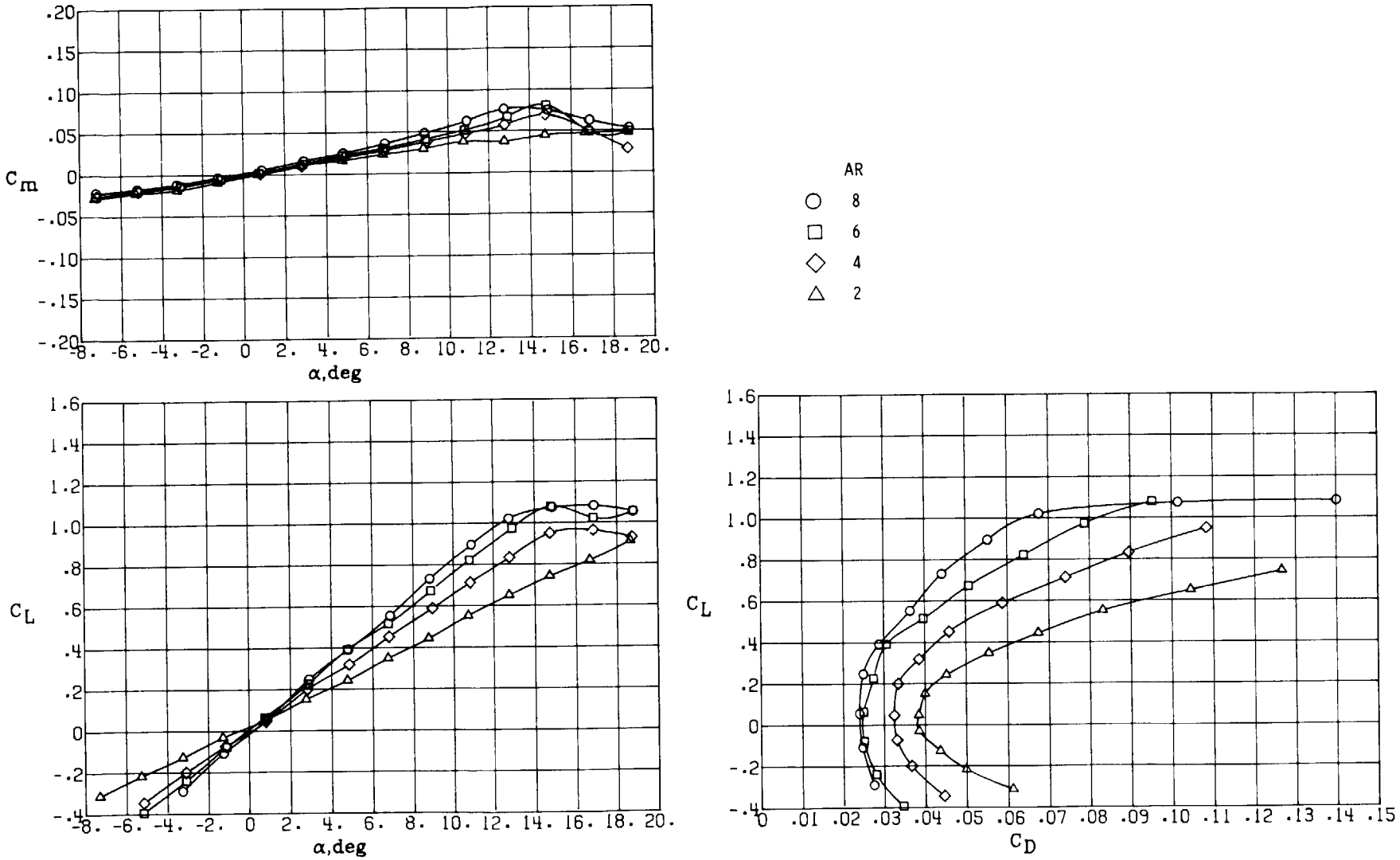

(a) $\delta_f = 0°$.

Figure 10.- Effect of aspect ratio on the longitudinal aerodynamics of configuration I ($\Lambda = 0°$) at several flap deflections. $\delta_e = 0°$.

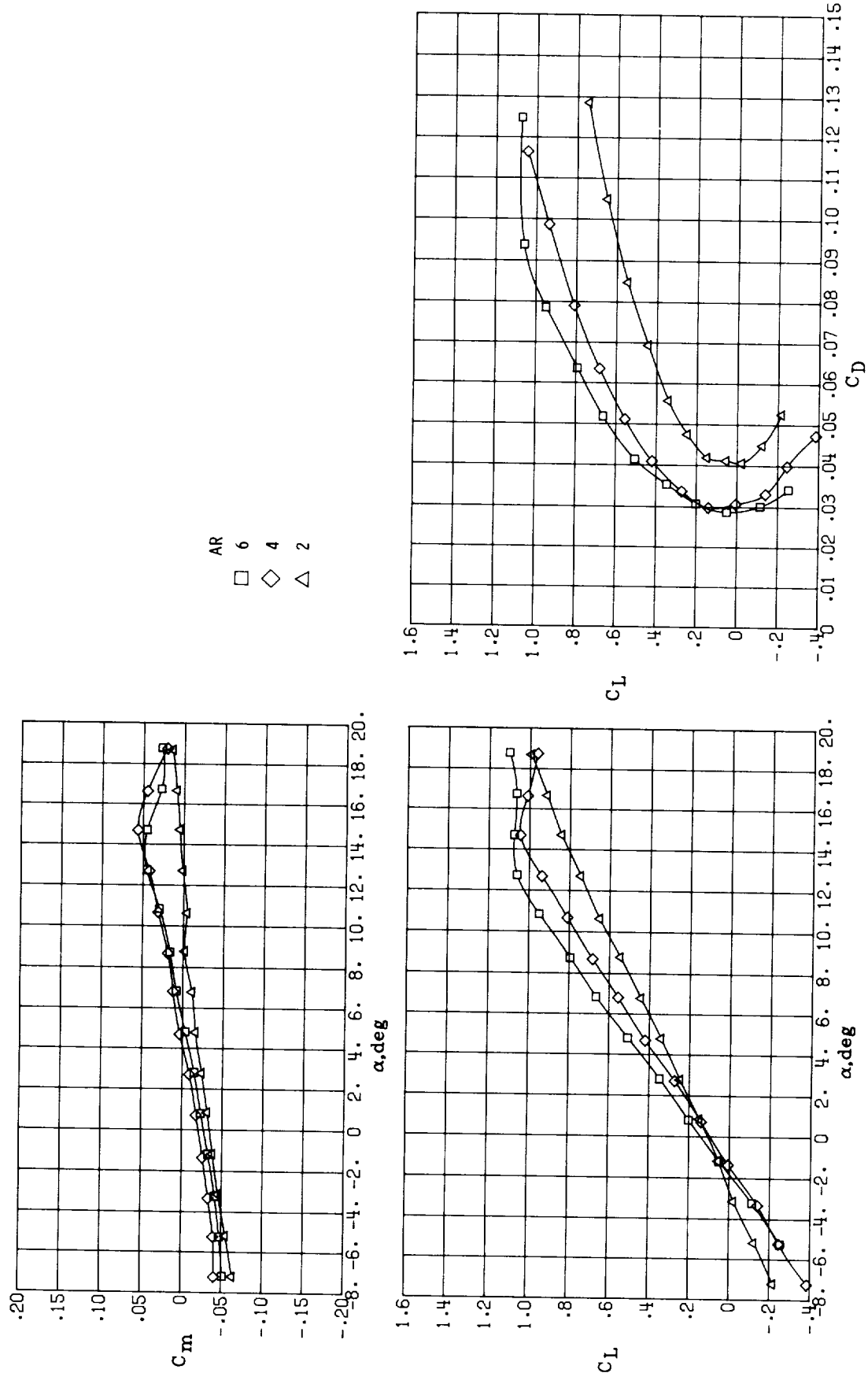

(b) $\delta_f = 5°$.

Figure 10.- Continued.

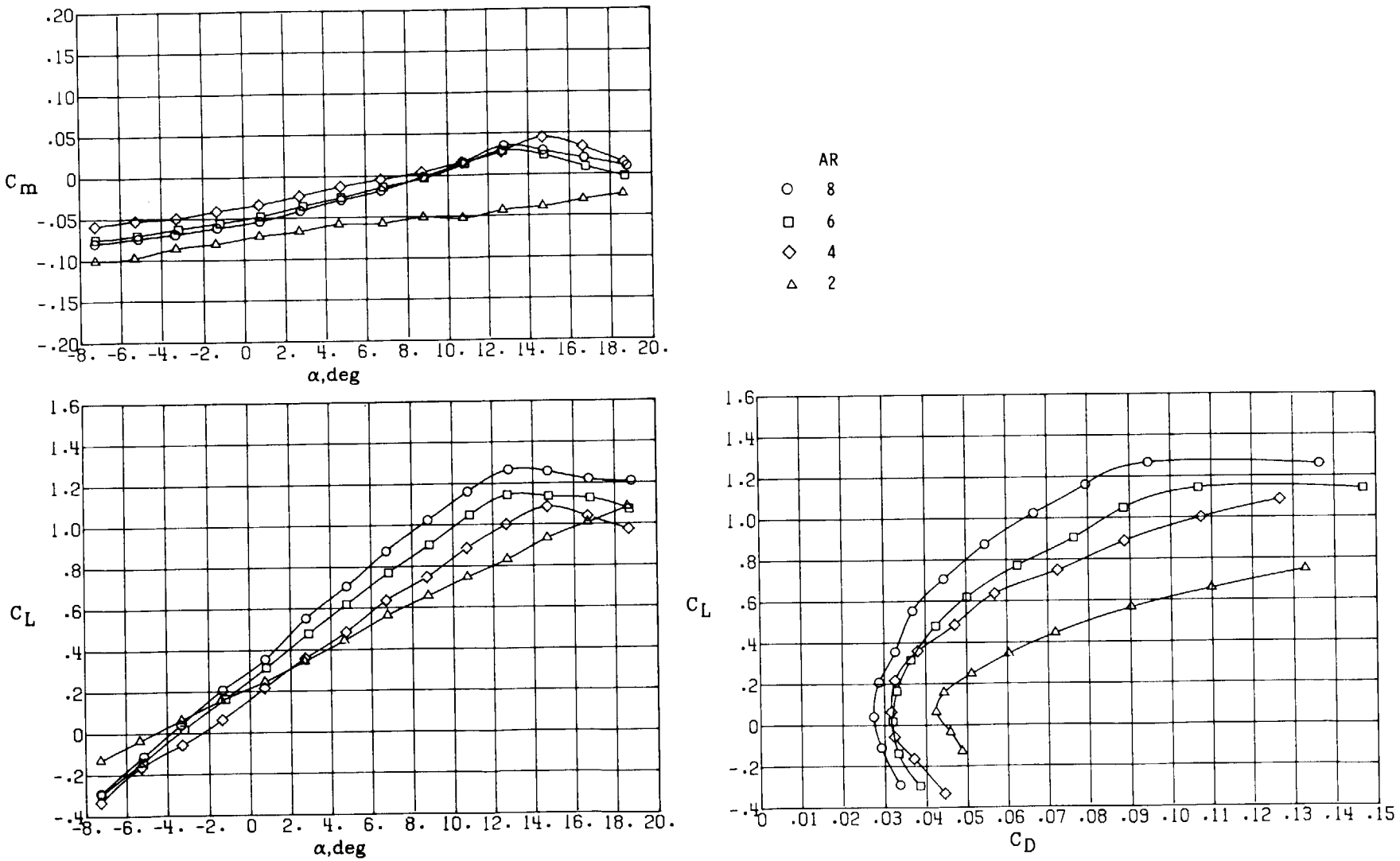

(c) δ_f = 10°.

Figure 10.- Continued.

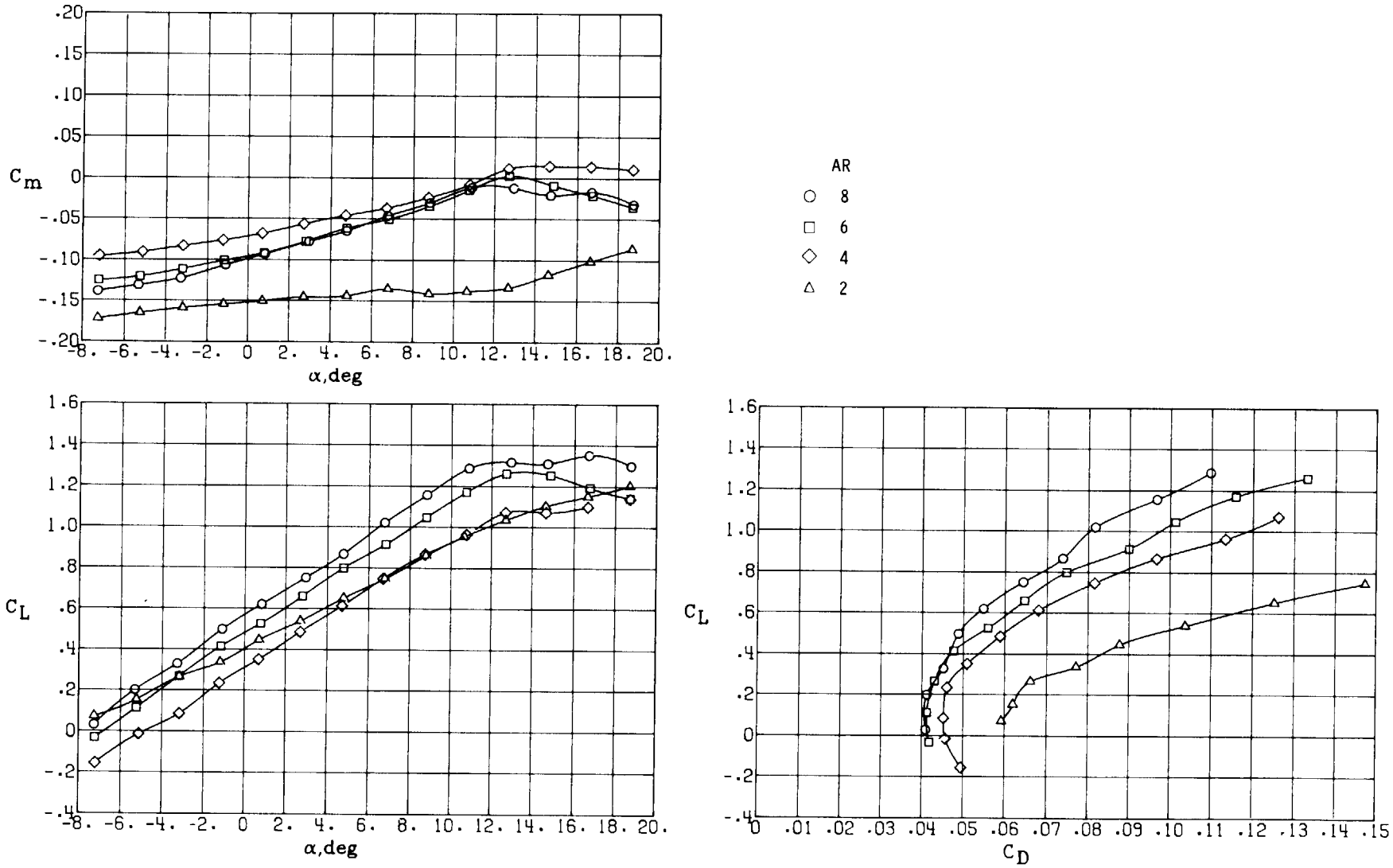

(d) $\delta_f = 20°$.

Figure 10.- Concluded.

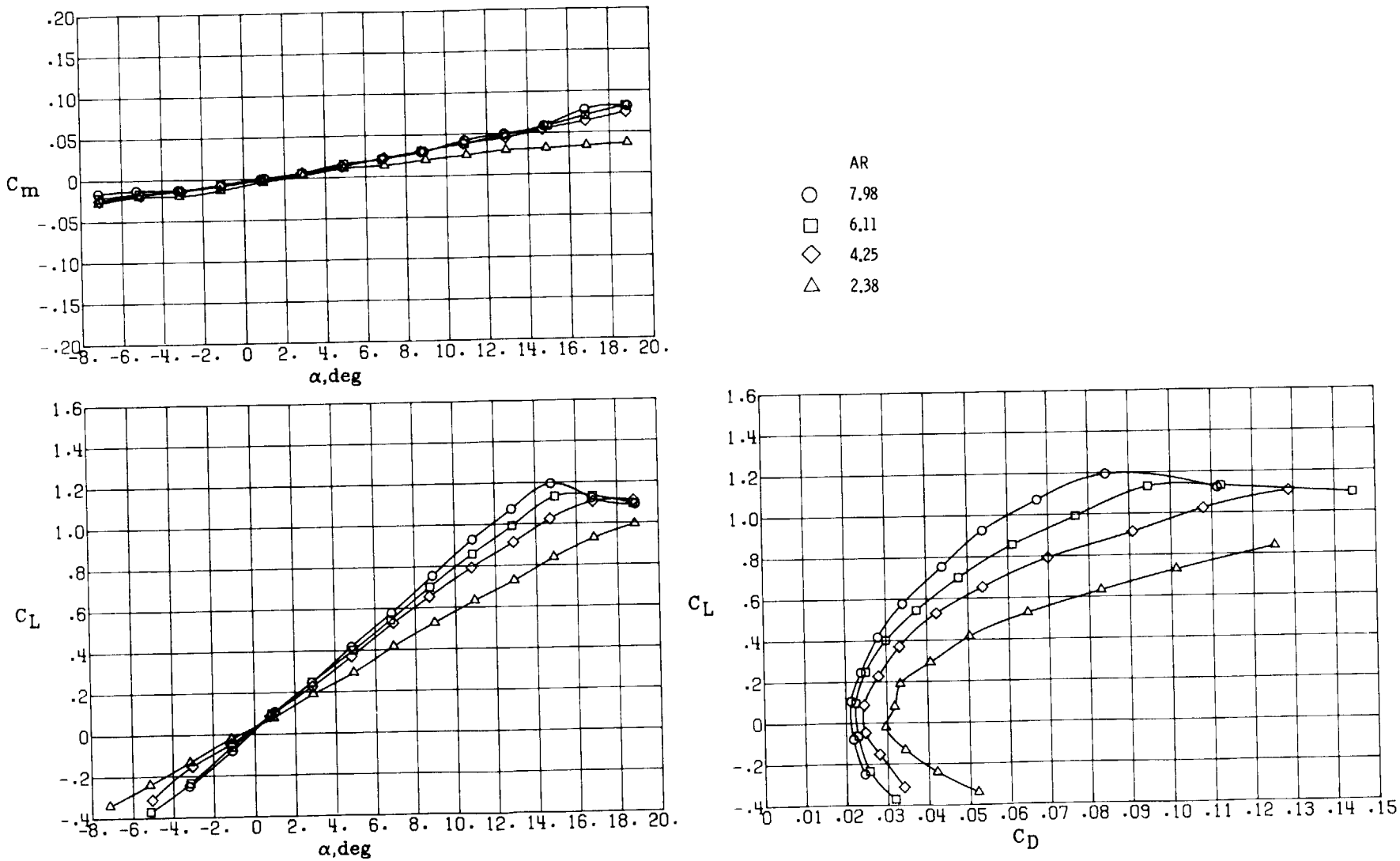

(a) $\delta_f = 0°$.

Figure 11.- Effect of aspect ratio on the longitudinal aerodynamics of configuration II ($\Lambda = 15°$) at several flap deflections. $\delta_e = 0°$.

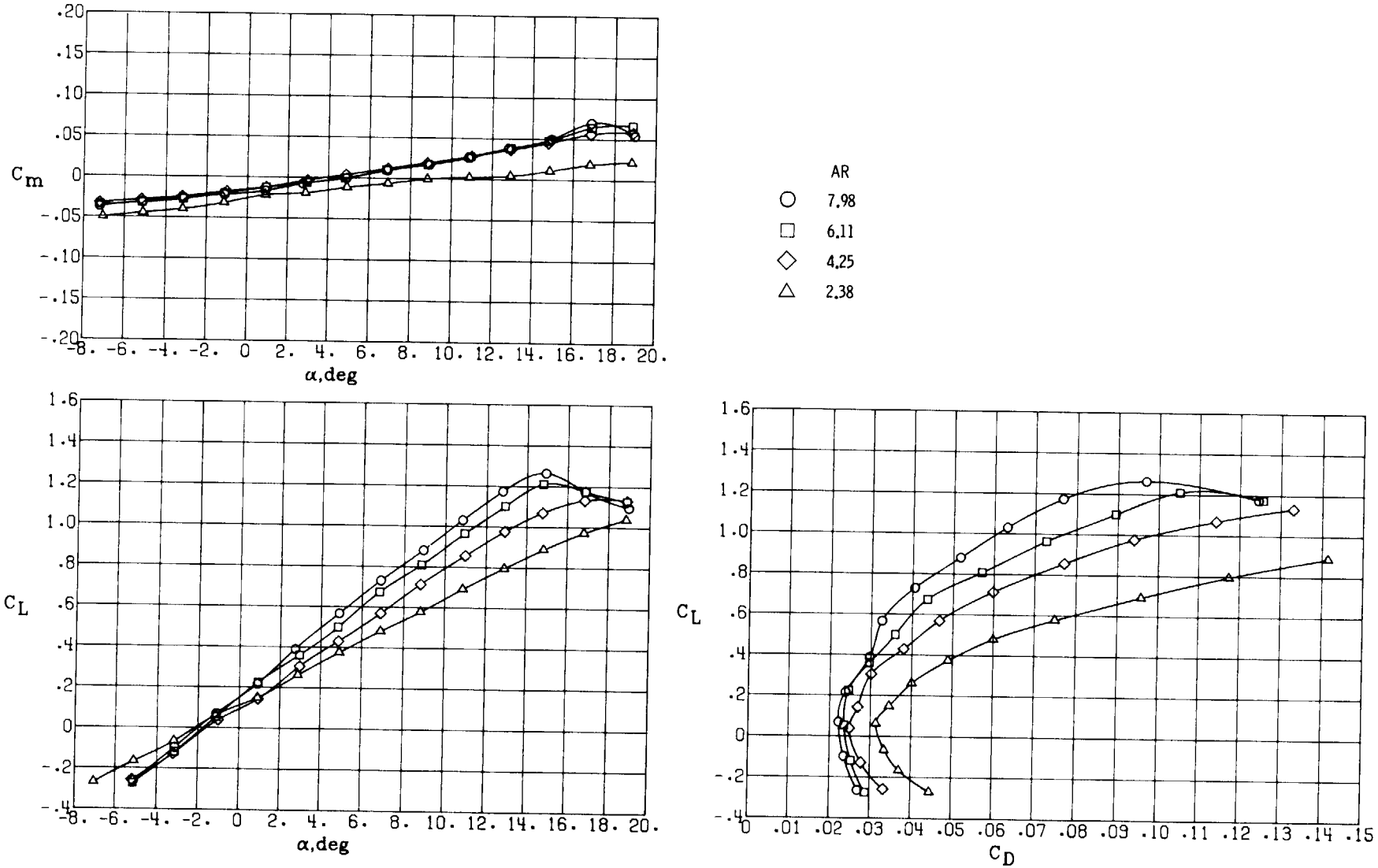

(b) $\delta_f = 5°$.

Figure 11.- Continued.

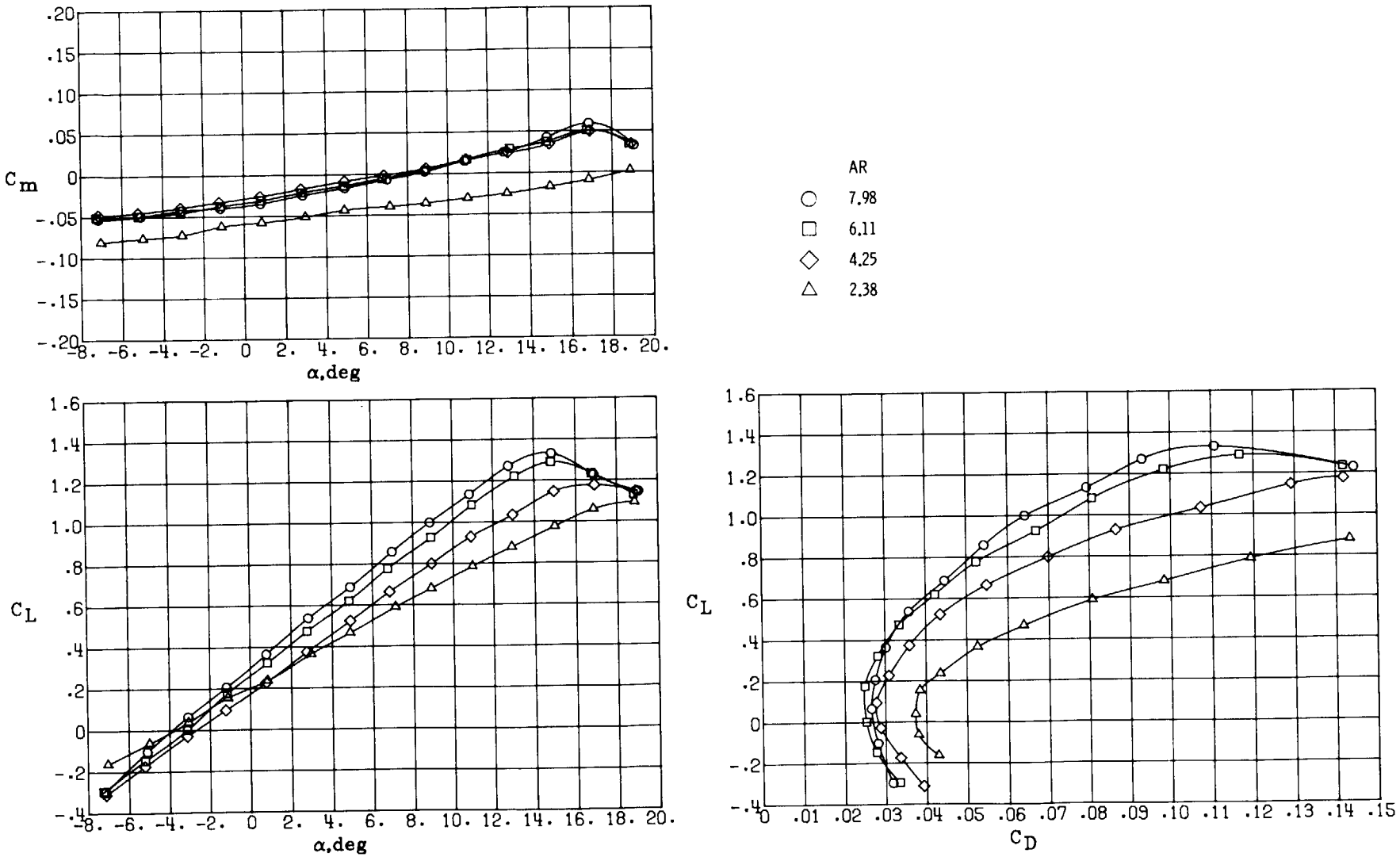

(c) δ_f = 10°.

Figure 11.- Continued.

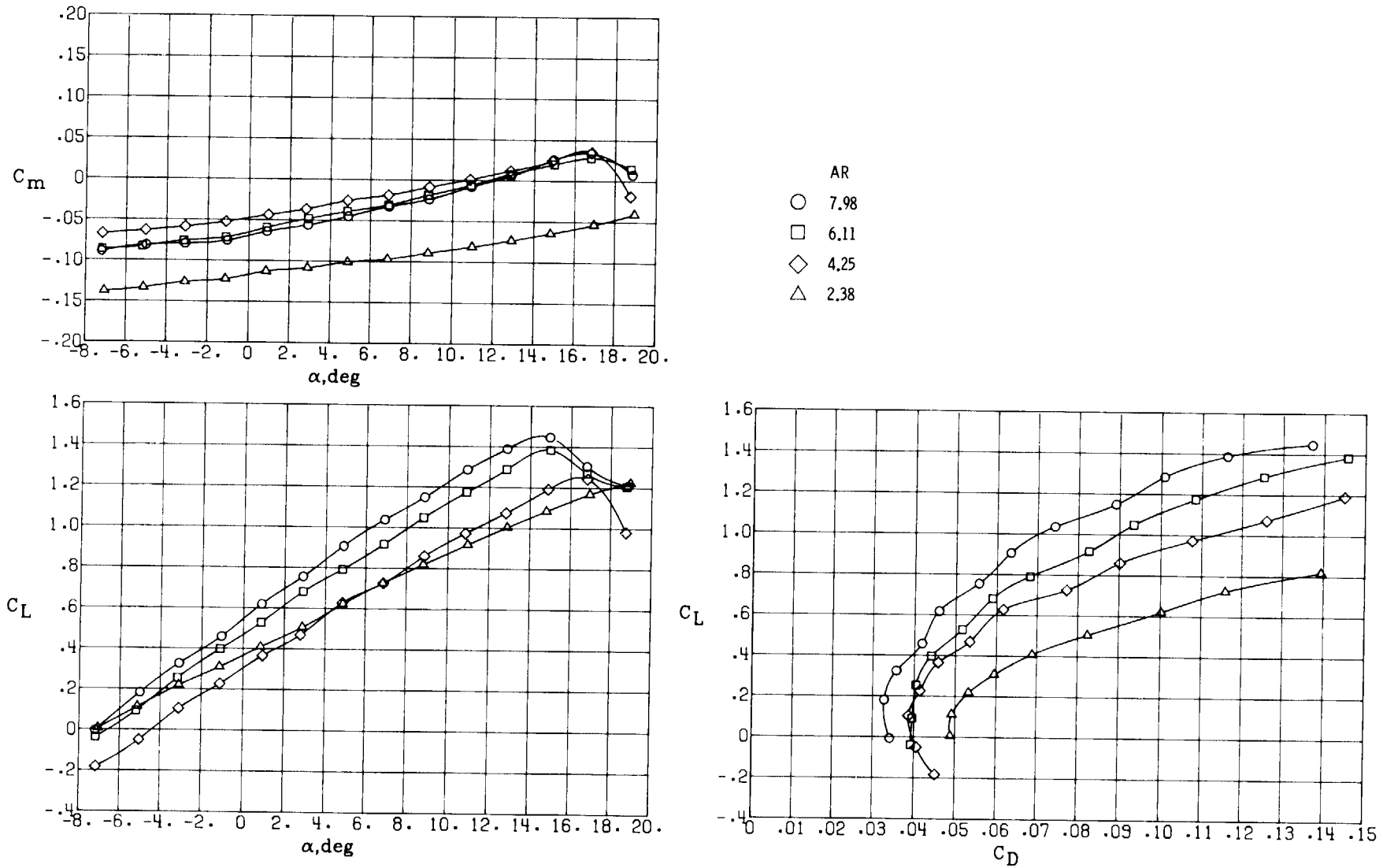

(d) $\delta_f = 20°$.

Figure 11.- Concluded.

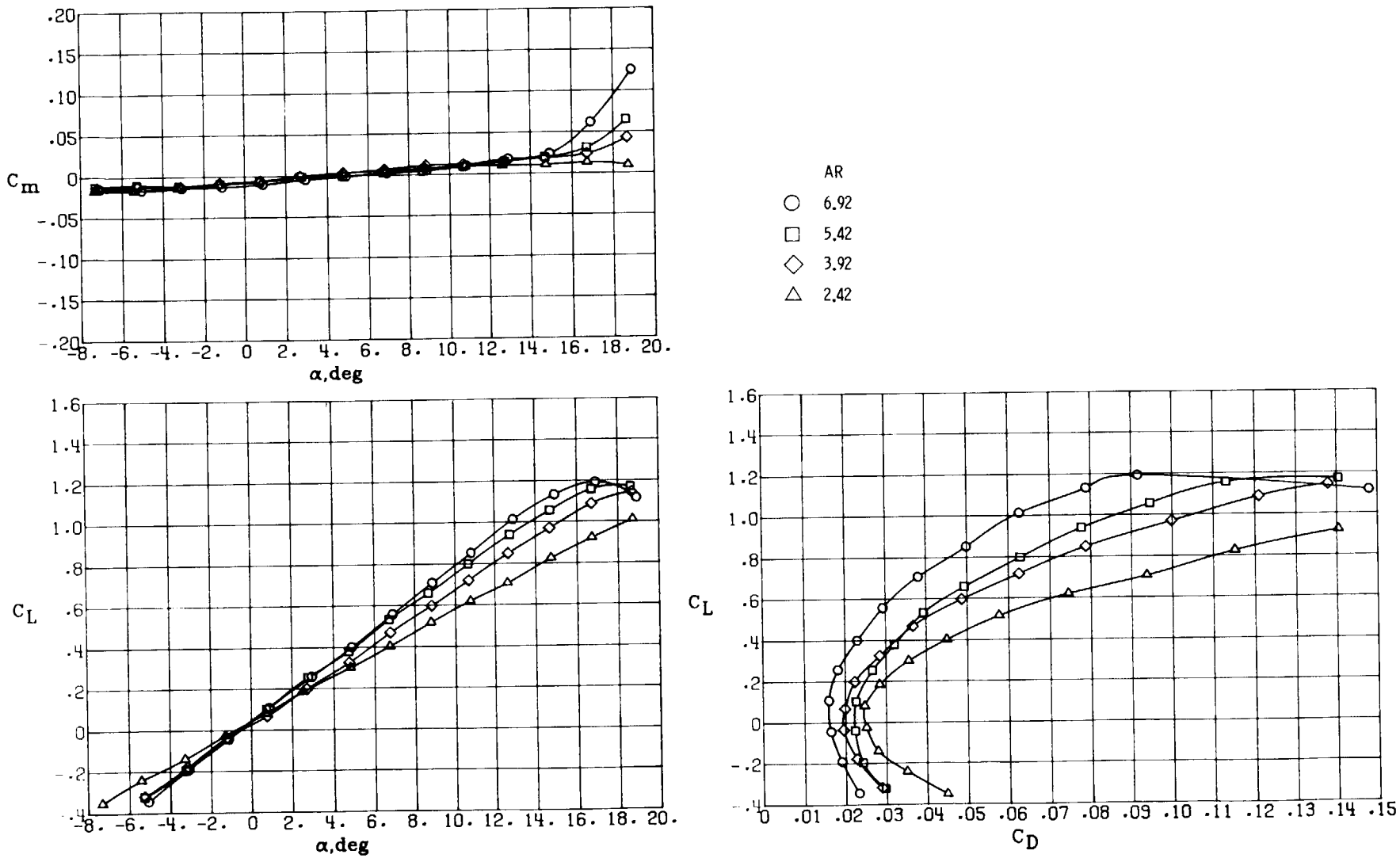

(a) $\delta_f = 0°$.

Figure 12.- Effect of aspect ratio on the longitudinal aerodynamics of configuration III ($\Lambda = 30°$) at several flap deflections. $\delta_e = 0°$.

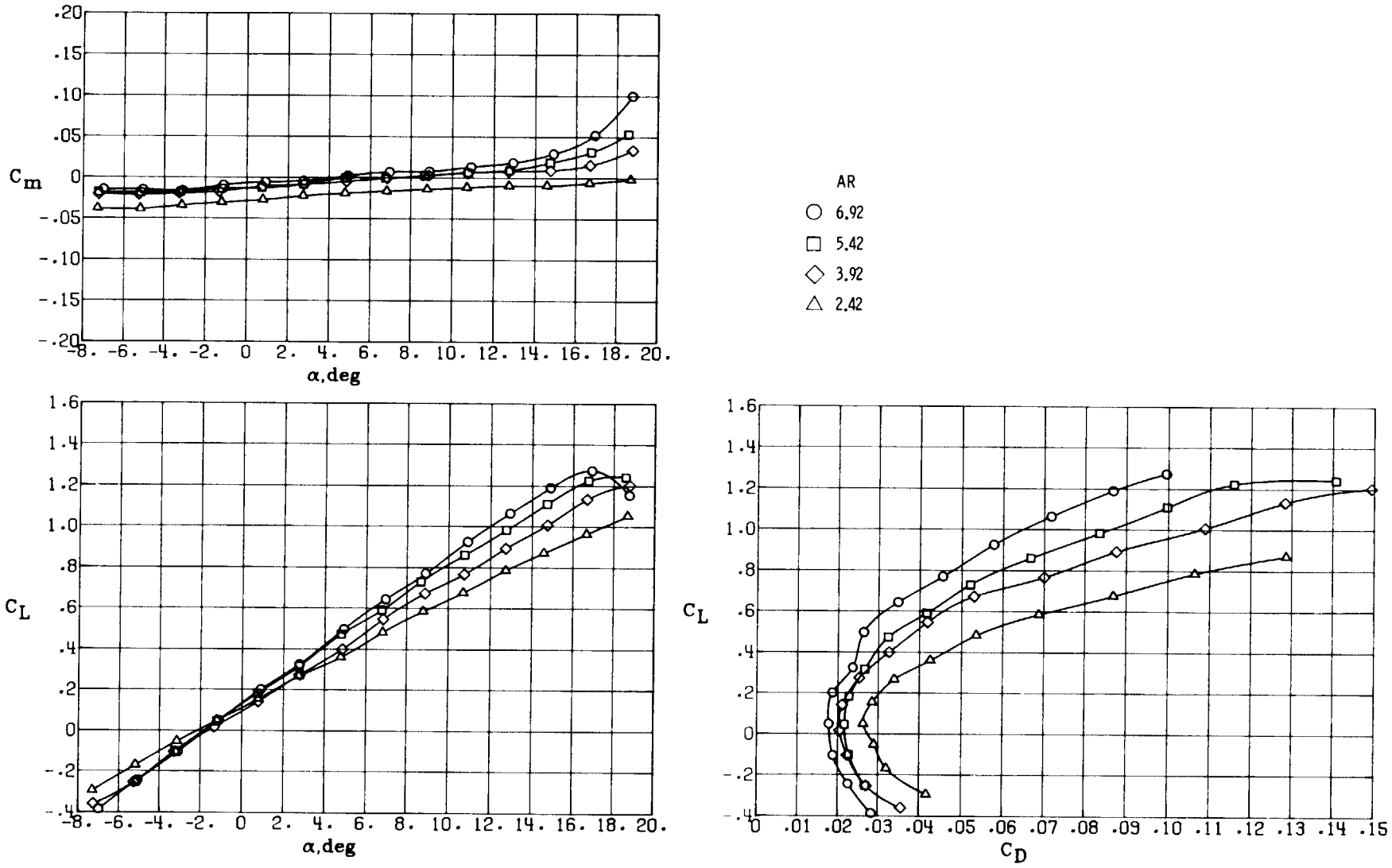

(b) $\delta_f = 5°$.

Figure 12.- Continued.

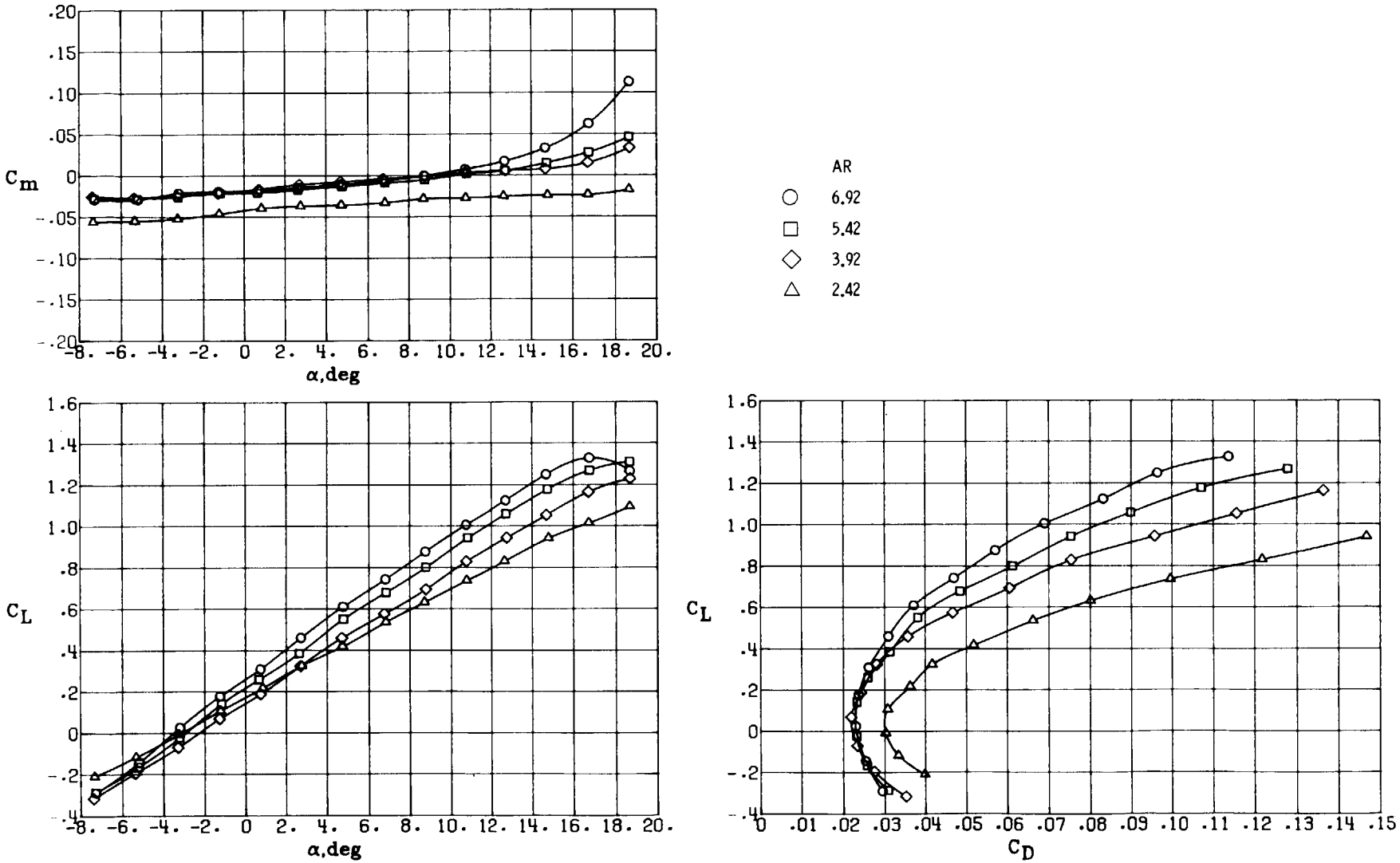

(c) $\delta_f = 10°$.

Figure 12.- Continued.

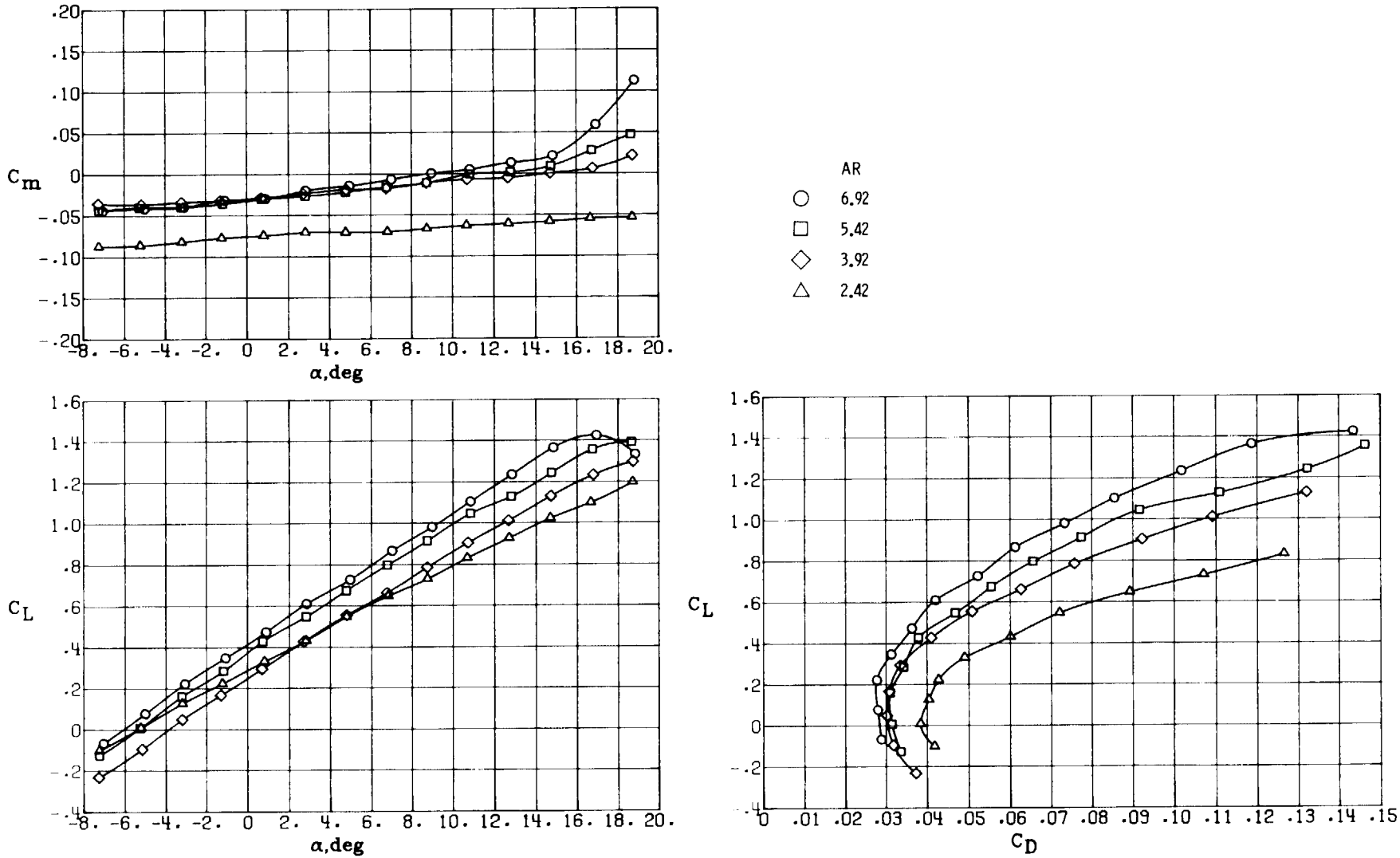

(d) $\delta_f = 20°$.

Figure 12.- Concluded.

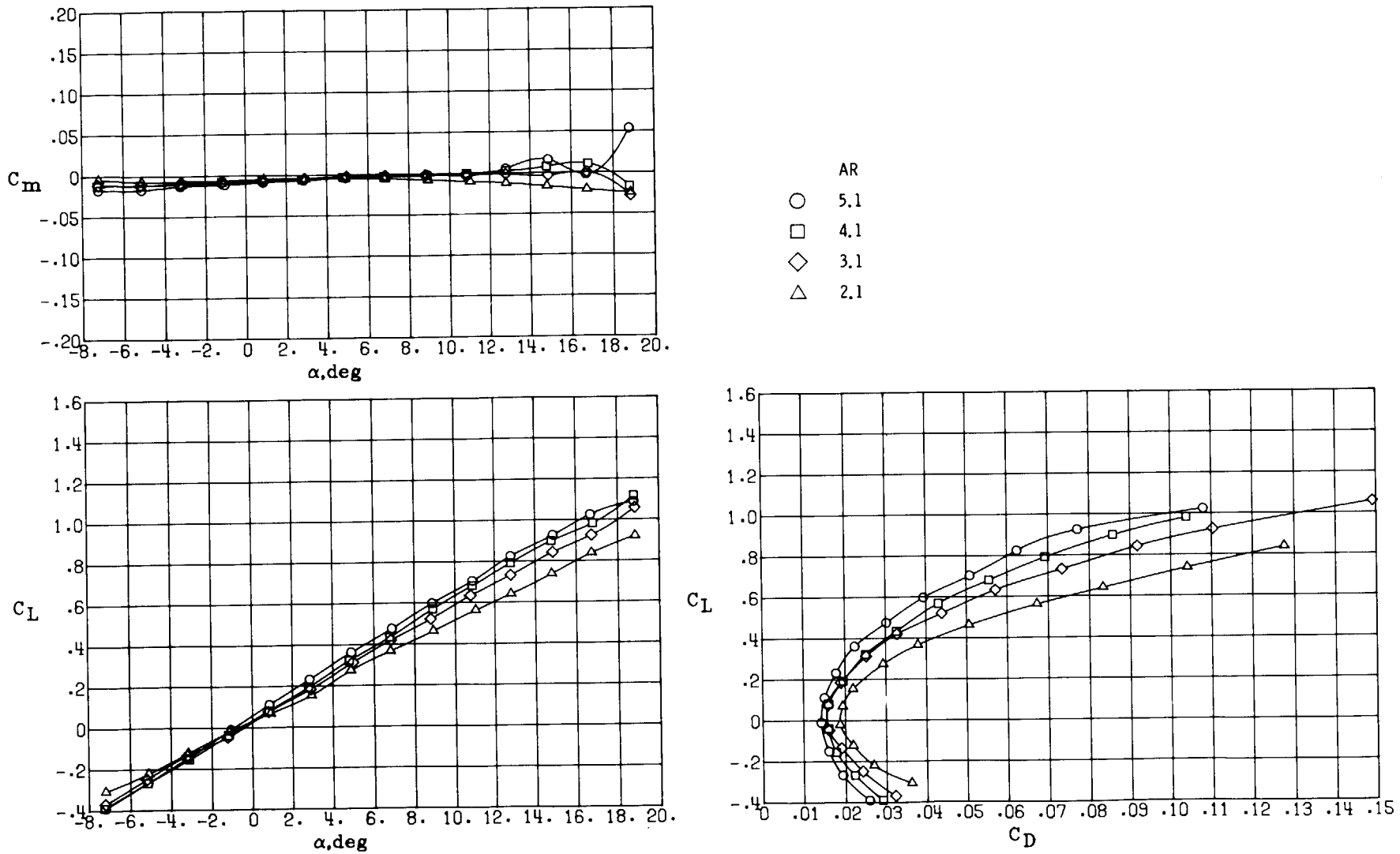

(a) $\delta_f = 0°$.

Figure 13.- Effect of aspect ratio on the longitudinal aerodynamics of configuration IV ($\Lambda = 45°$) at several flap deflections. $\delta_e = 0°$.

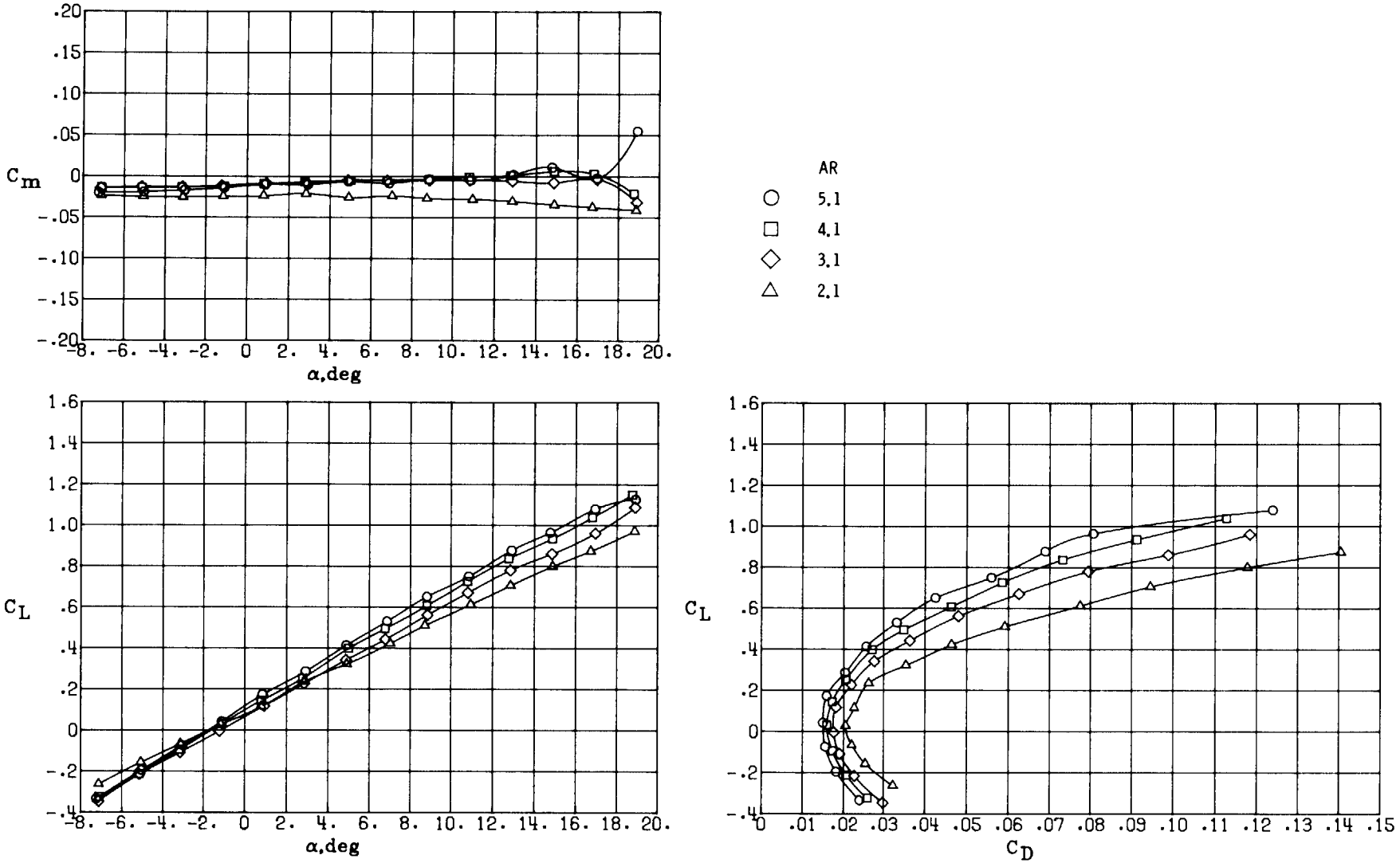

(b) $\delta_f = 5°$.

Figure 13.- Continued.

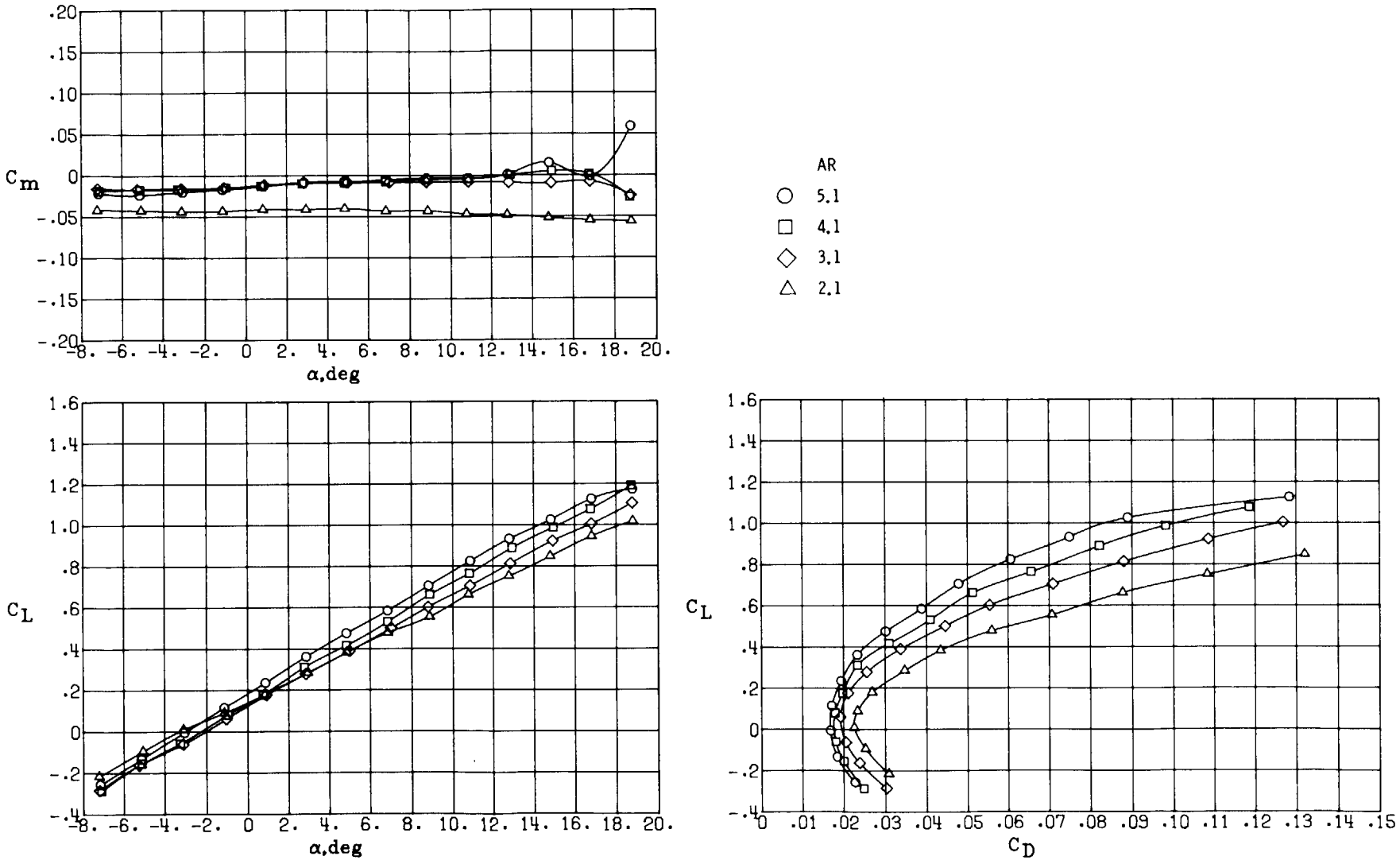

(c) δ_f = 10°.

Figure 13.- Continued.

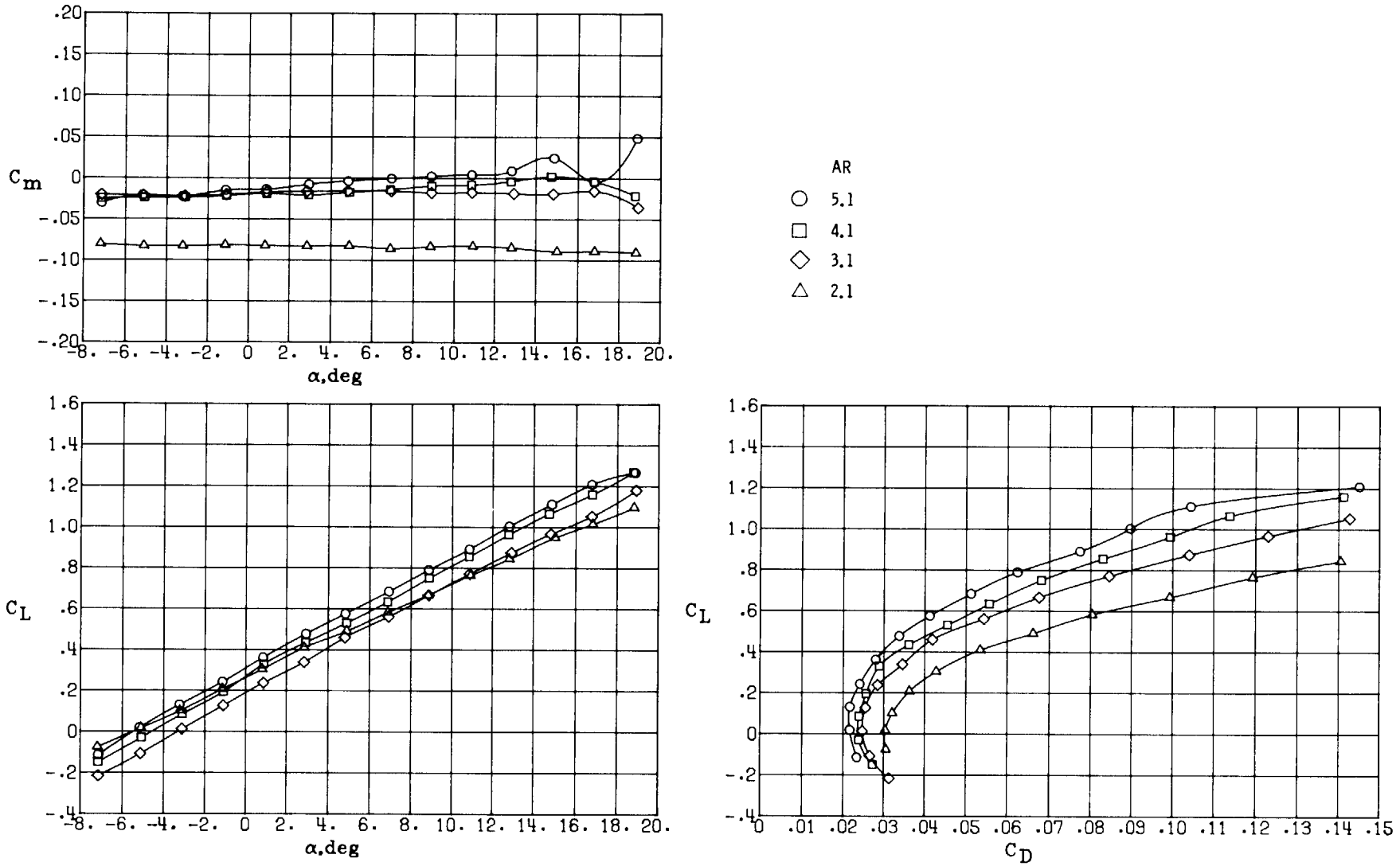

(d) $\delta_f = 20°$.

Figure 13.- Concluded.

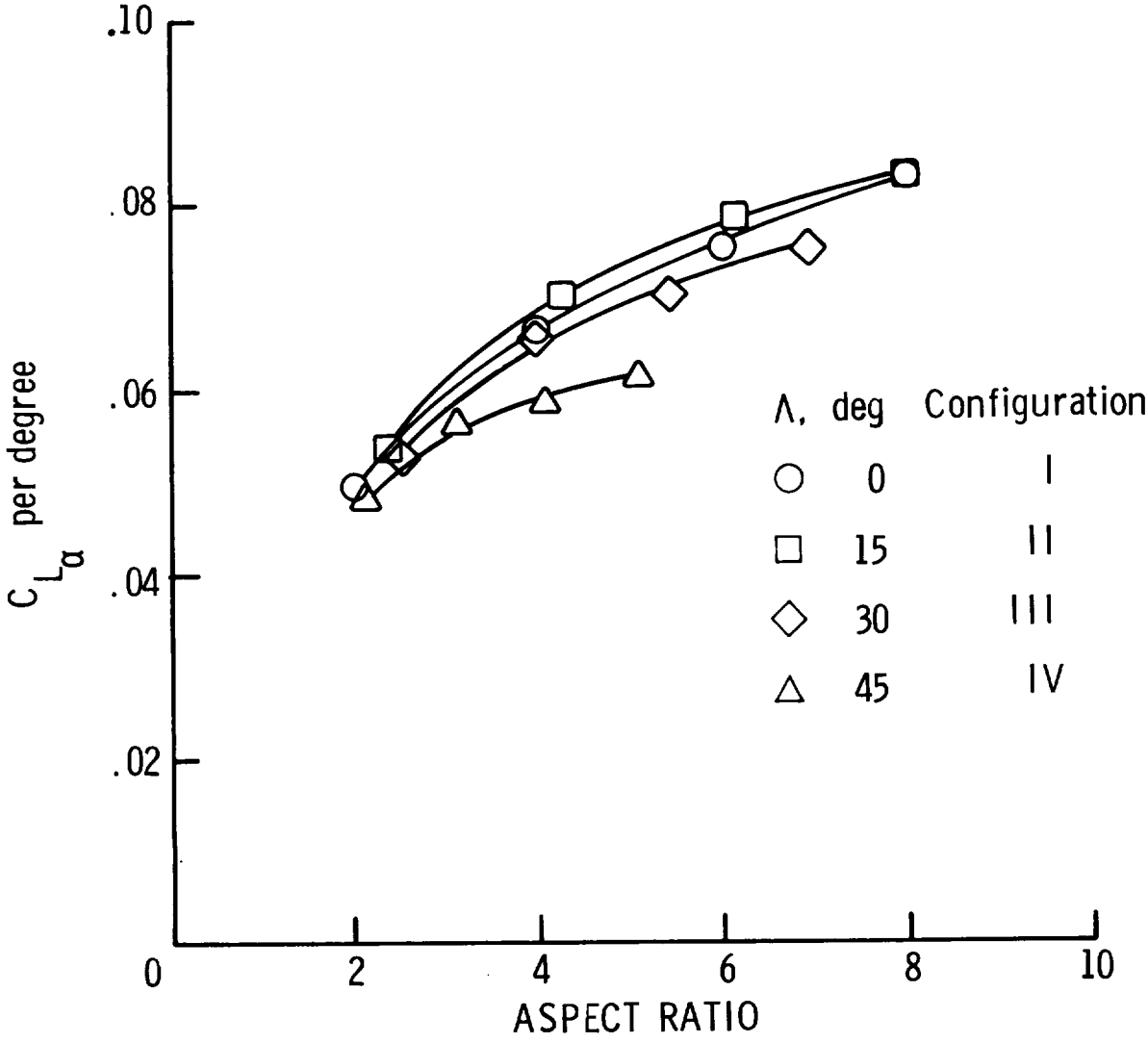

Figure 14.- Lift-curve slope C_{L_α} plotted against aspect ratio for configurations I to IV with $\delta_f = 0°$ and $\delta_e = 0°$.

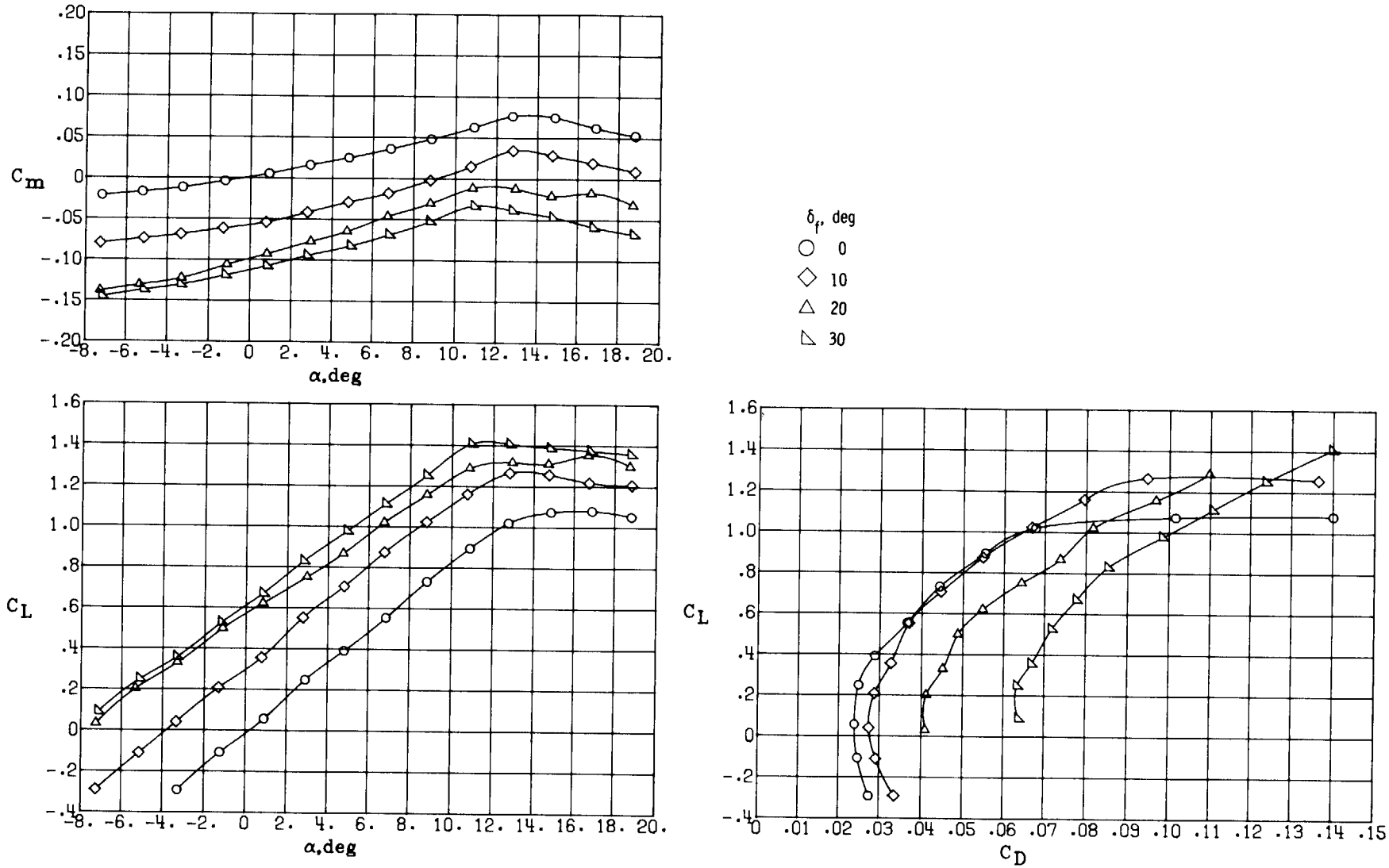

(a) AR = 8.

Figure 15.- Effect of flap deflection on the longitudinal aerodynamics of configuration I (Λ = 0°) at several aspect ratios. δ_e = 0°.

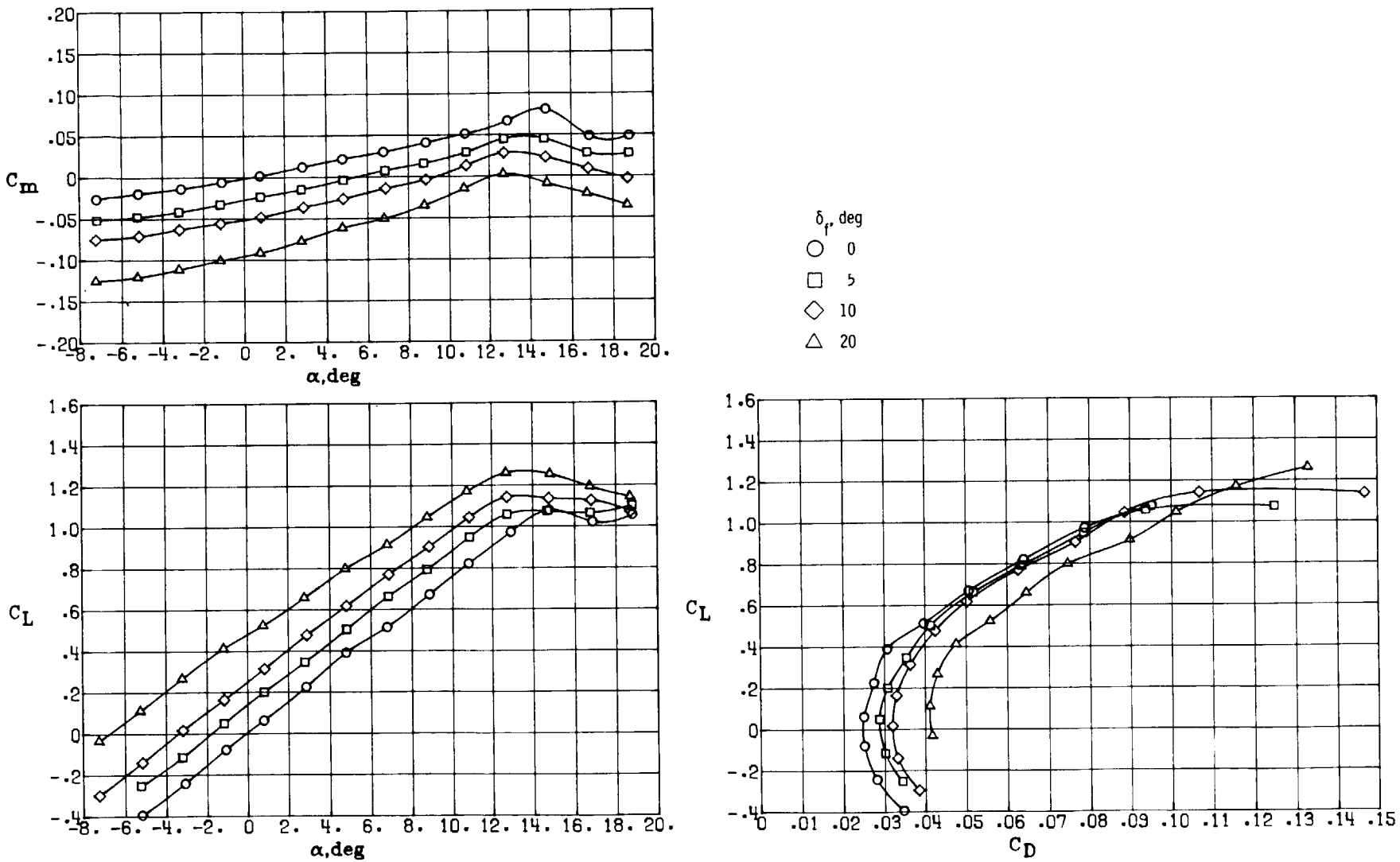

(b) AR = 6.

Figure 15.- Continued.

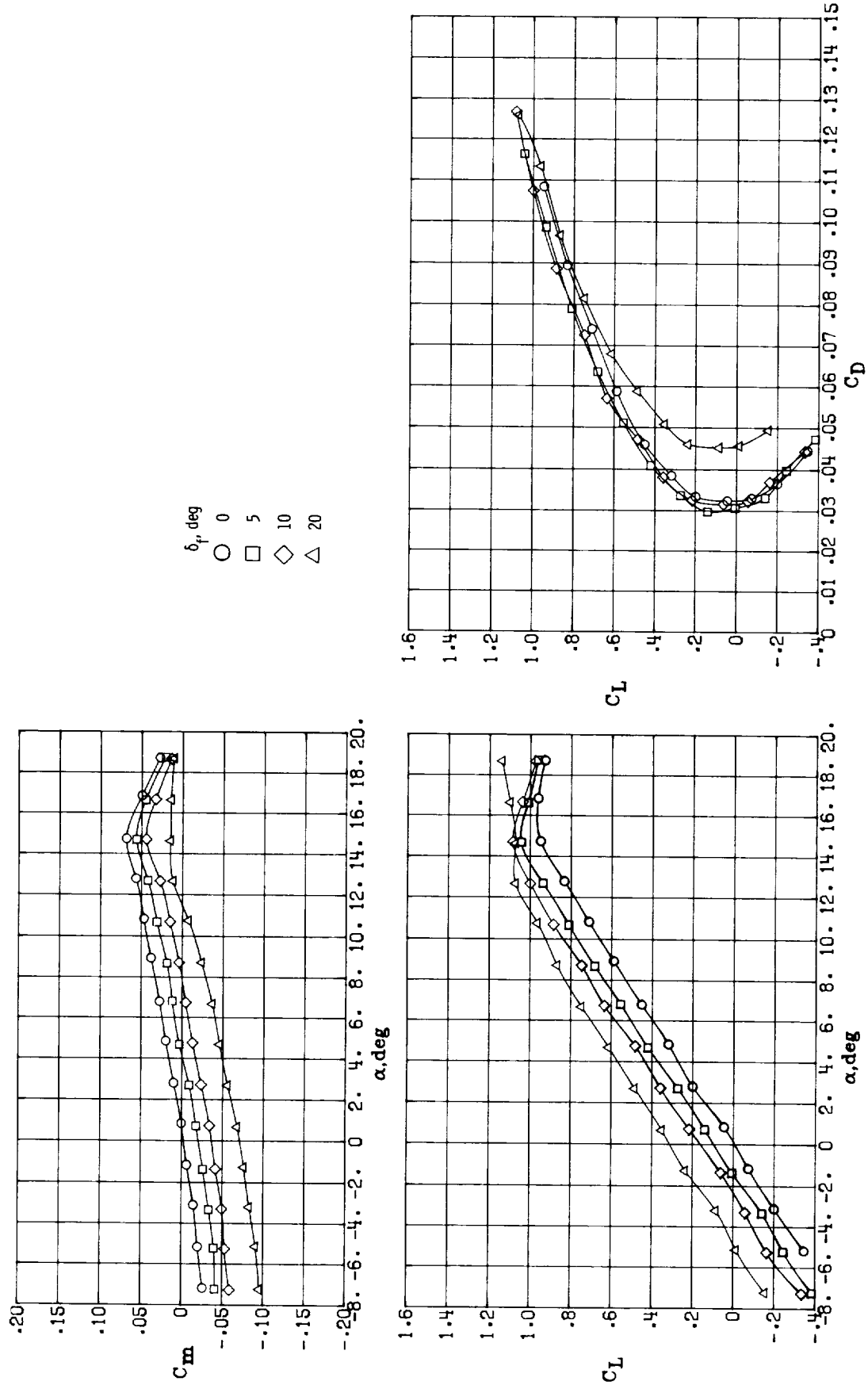

(c) AR = 4.

Figure 15.- Continued.

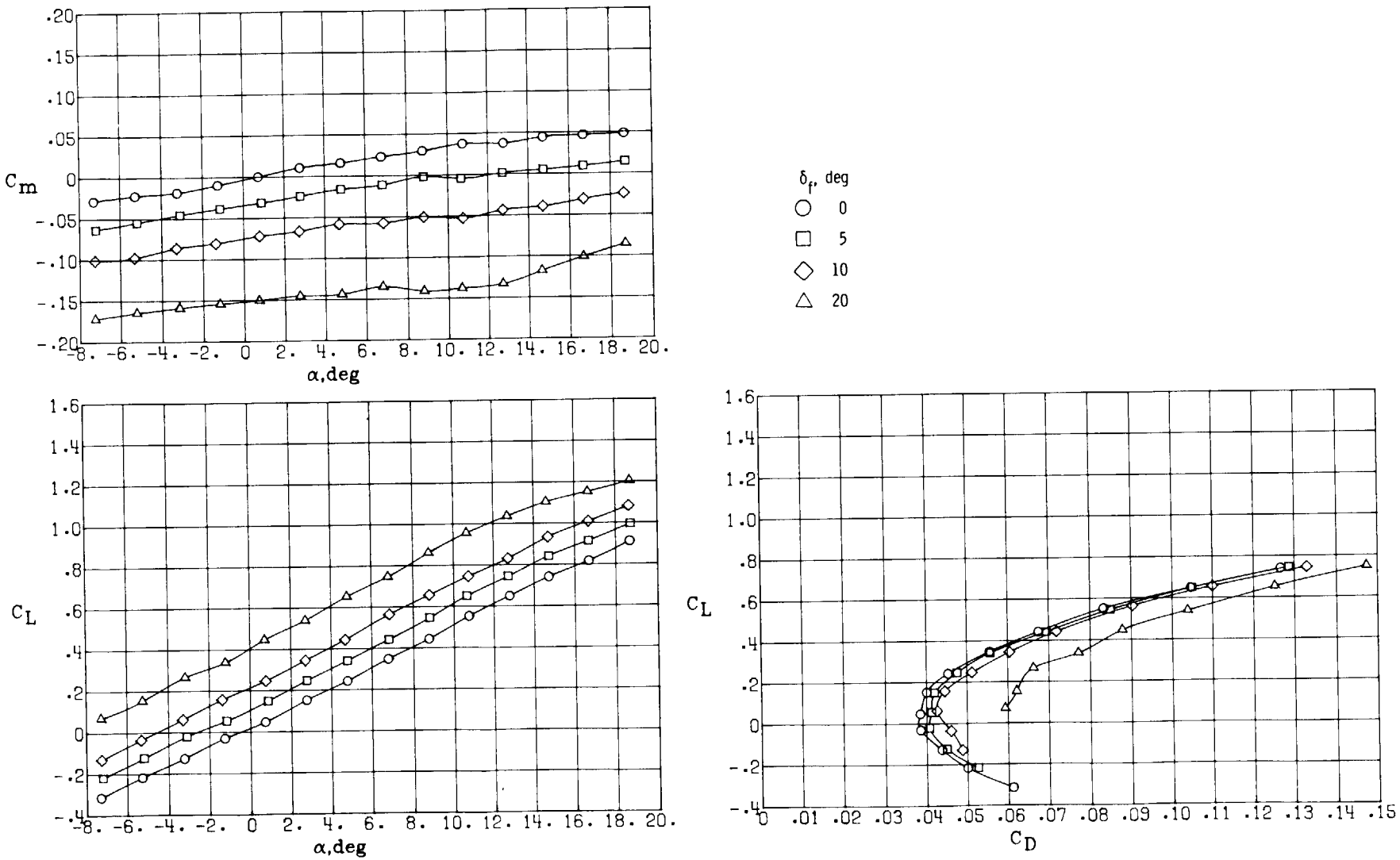

(d) AR = 2.

Figure 15.- Concluded.

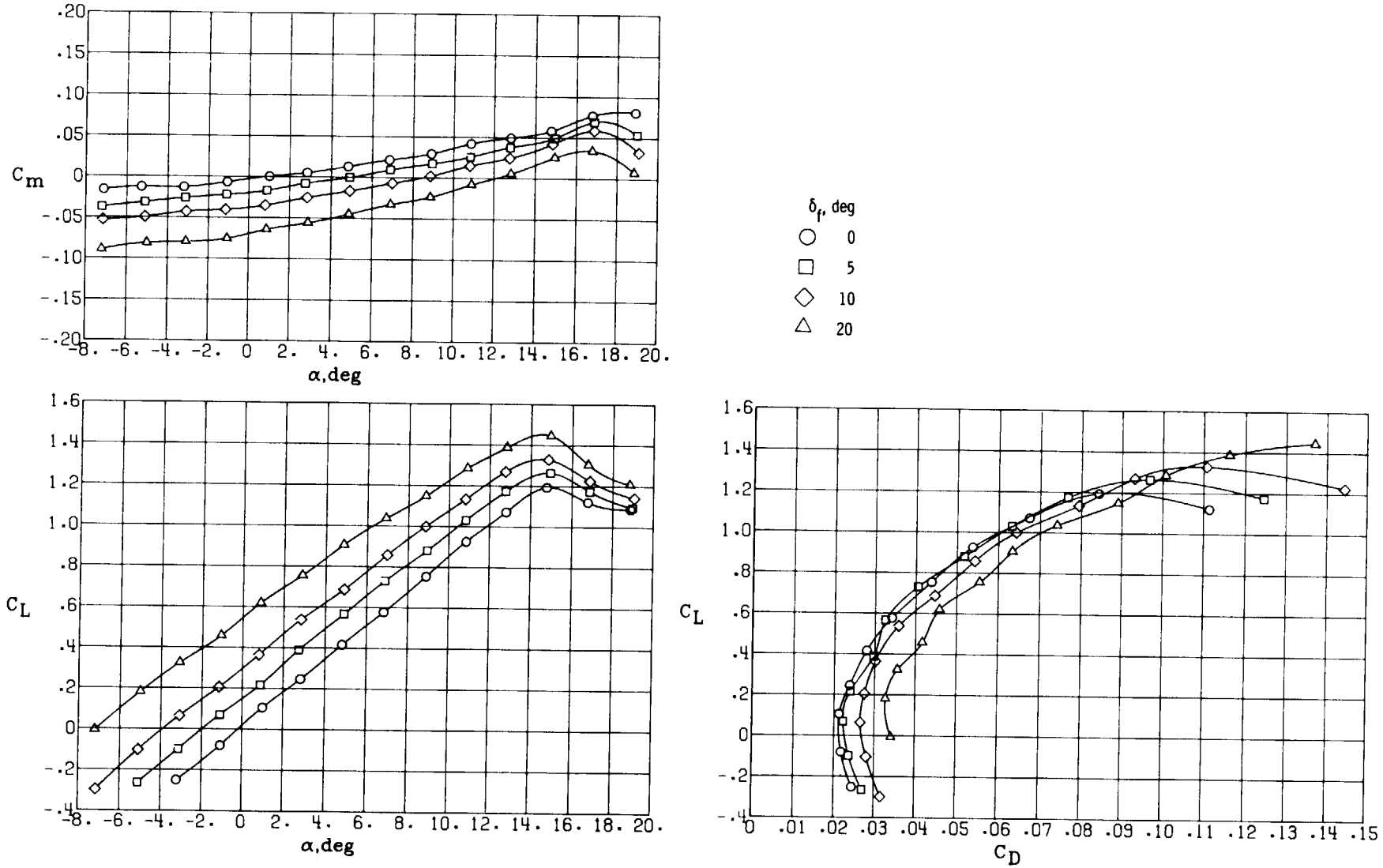

(a) AR = 7.98.

Figure 16.- Effect of flap deflection on the longitudinal aerodynamics of configuration II (Λ = 15°) at several aspect ratios. δ_e = 0°.

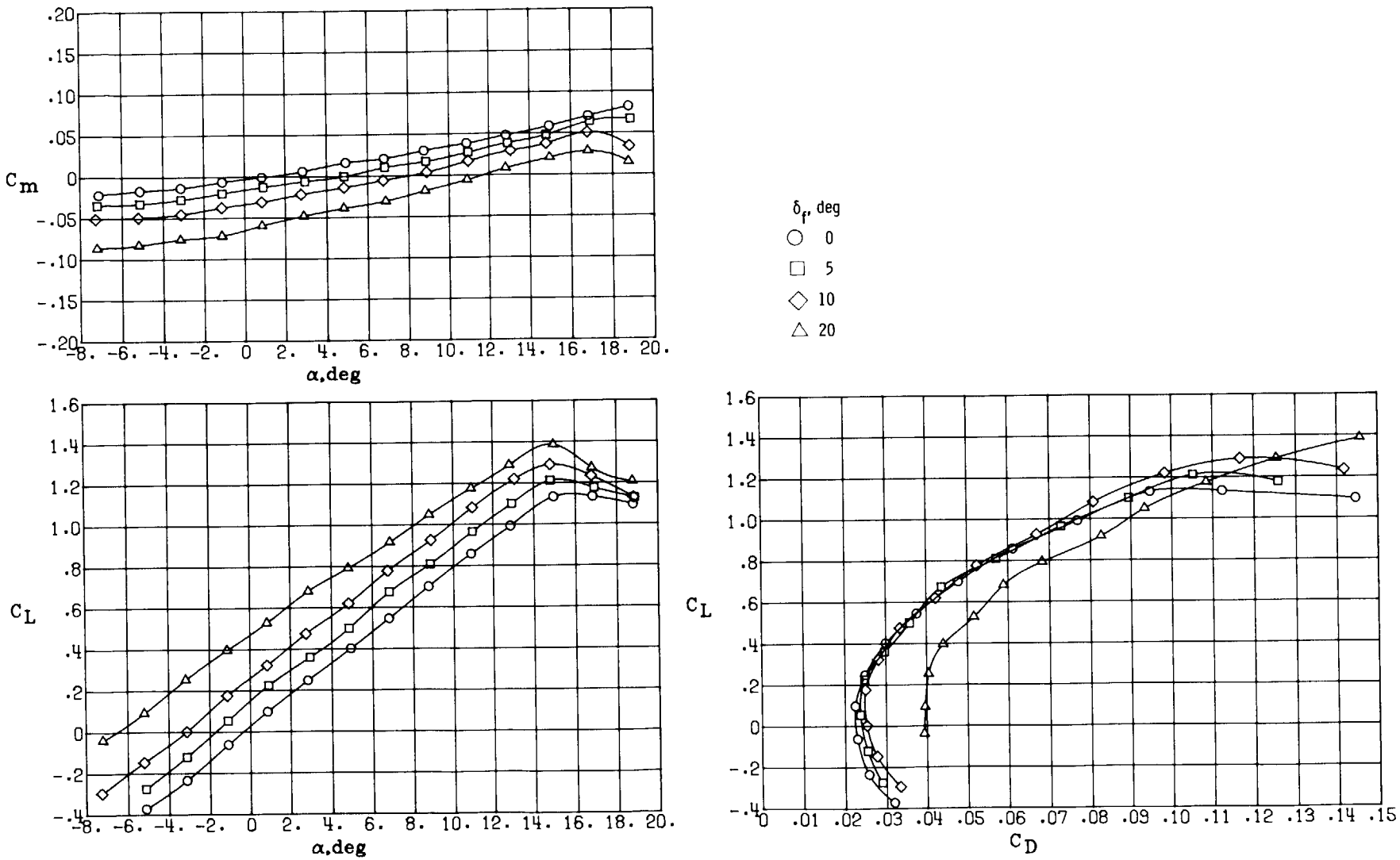

(b) AR = 6.11.

Figure 16.- Continued.

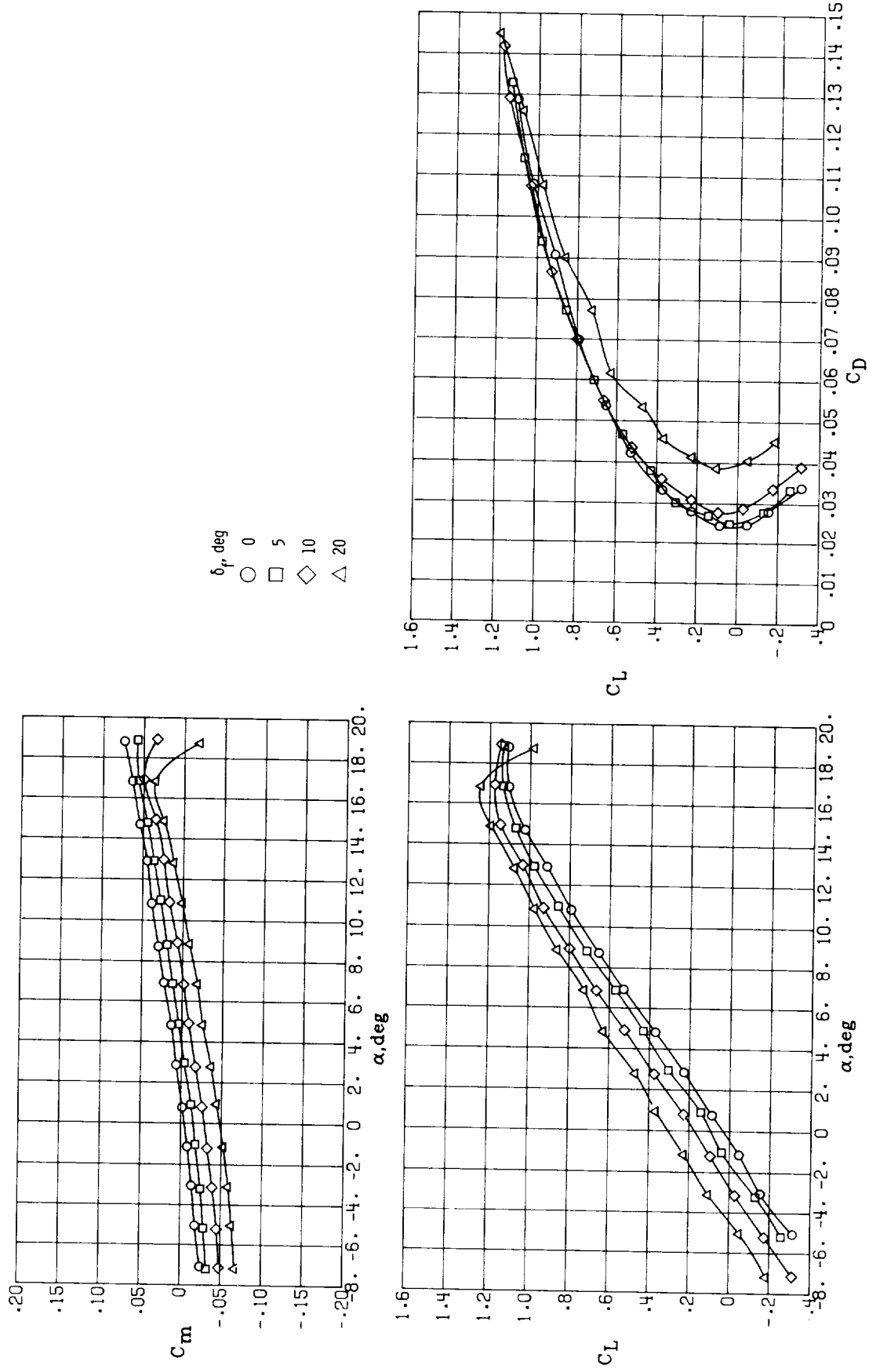

(c) AR = 4.25.

Figure 16.- Continued.

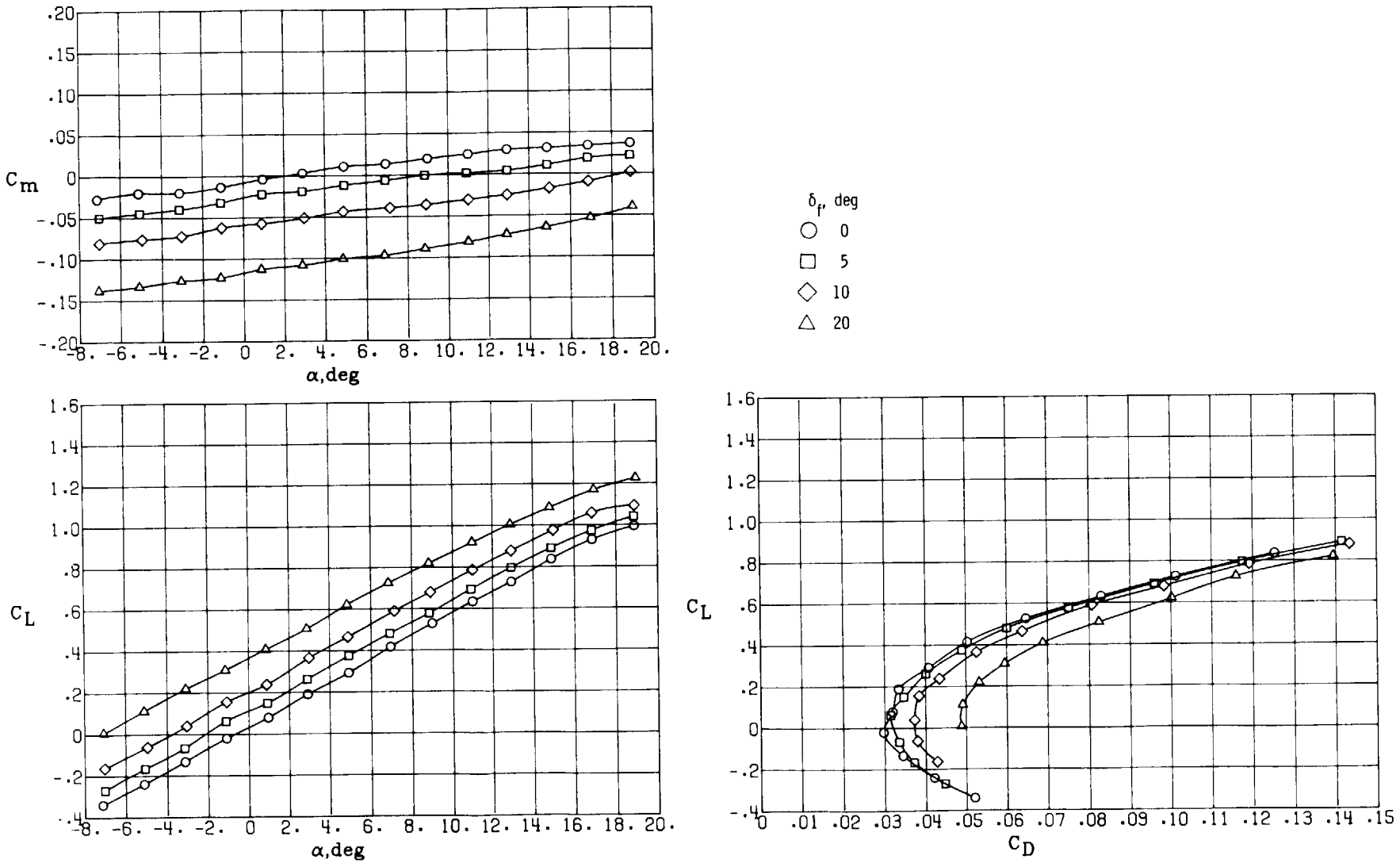

(d) AR = 2.38.

Figure 16.- Concluded.

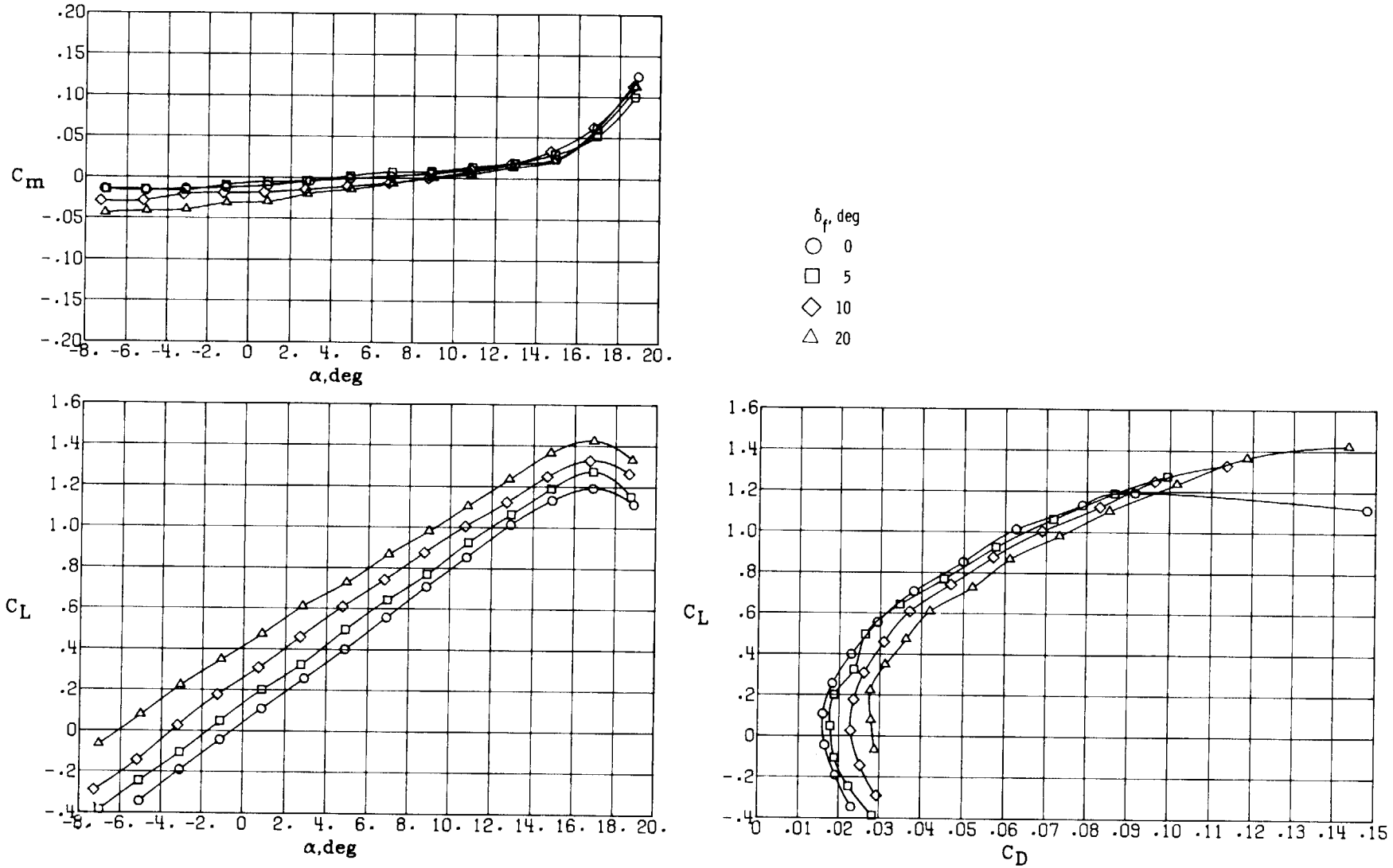

(a) AR = 6.92.

Figure 17.- Effect of flap deflection on the longitudinal aerodynamics of configuration III (Λ = 30°) at several aspect ratios. δ_e = 0°.

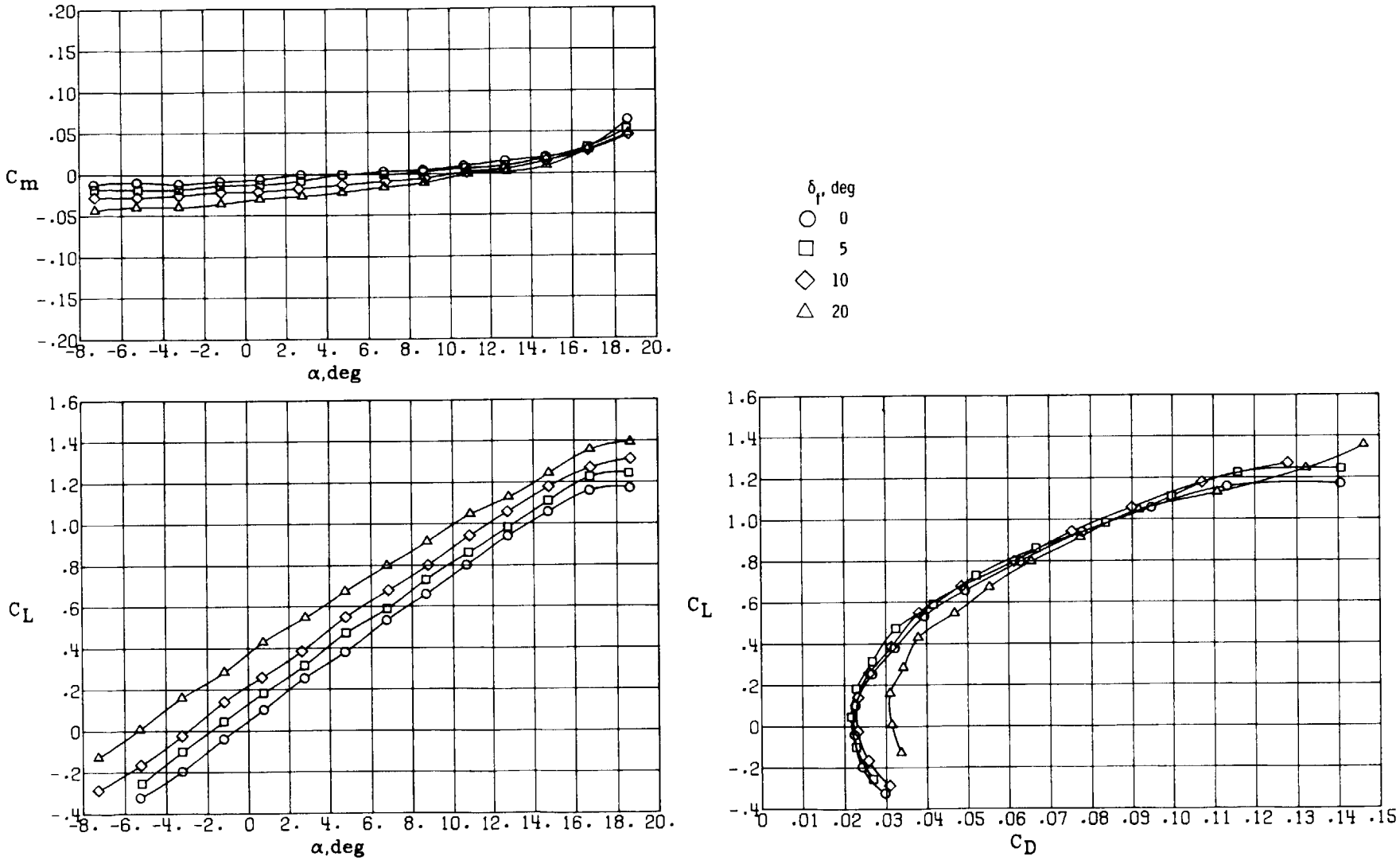

(b) AR = 5.42.

Figure 17.- Continued.

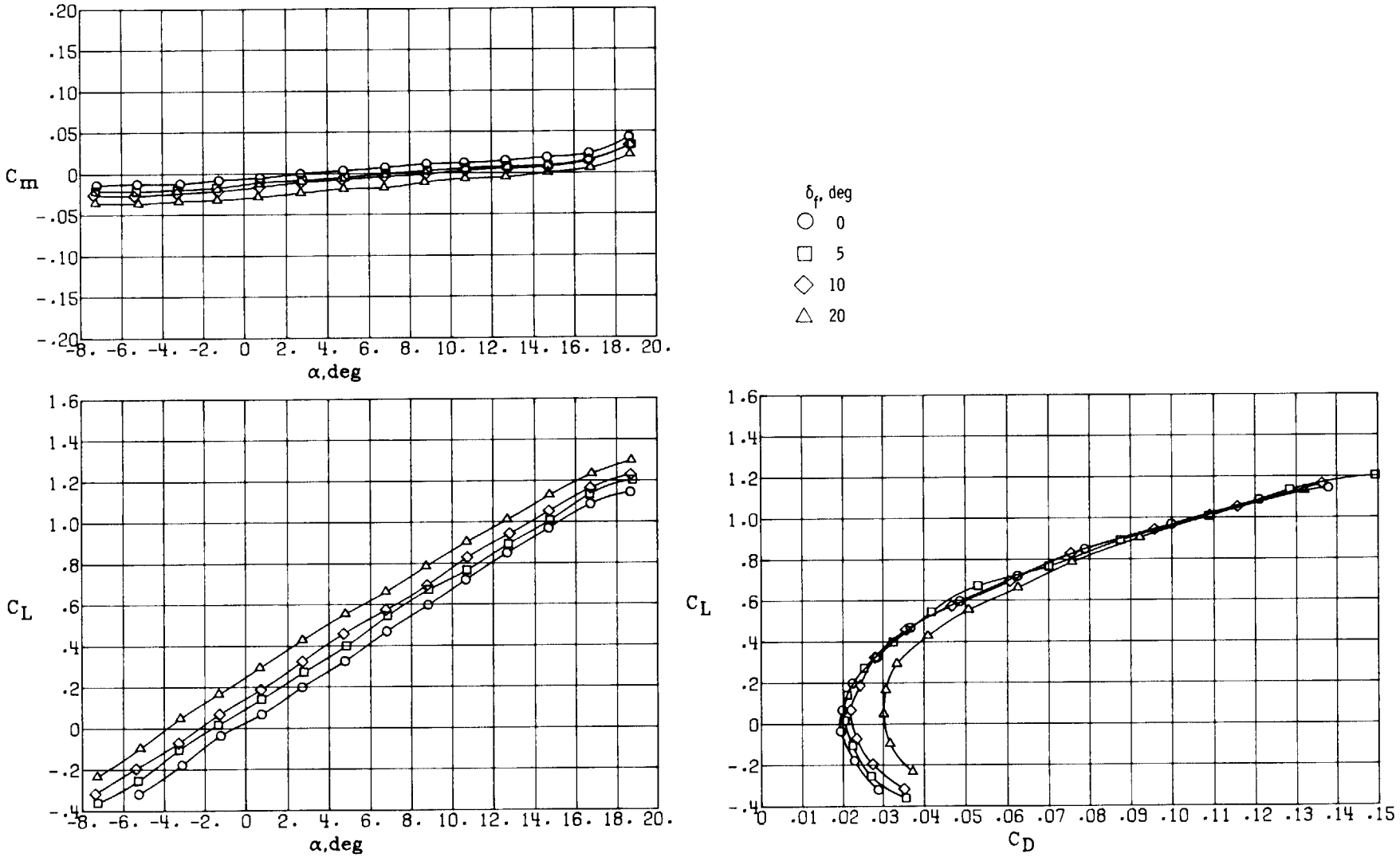

(c) AR = 3.92.

Figure 17.- Continued.

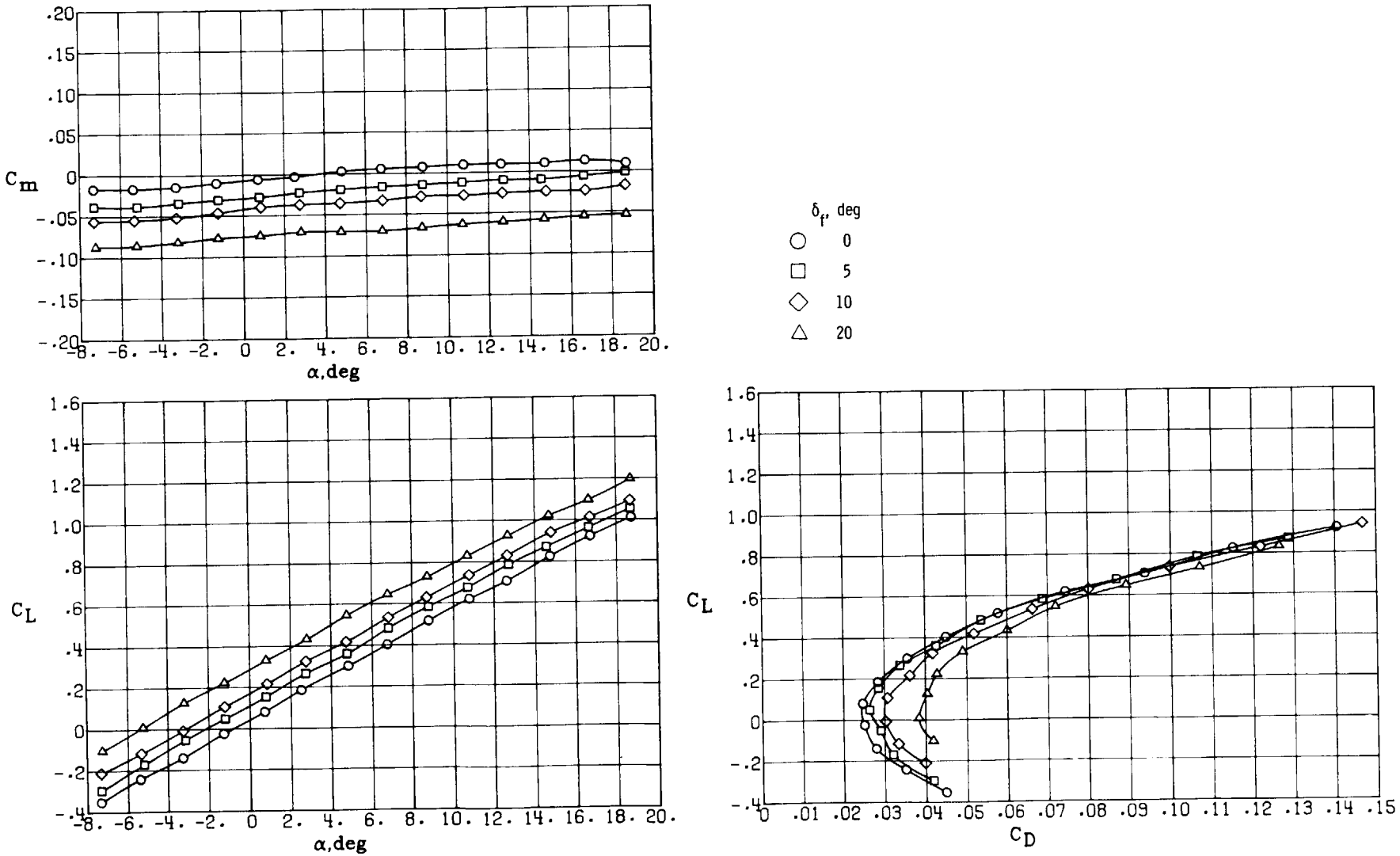

(d) AR = 2.42.

Figure 17.- Concluded.

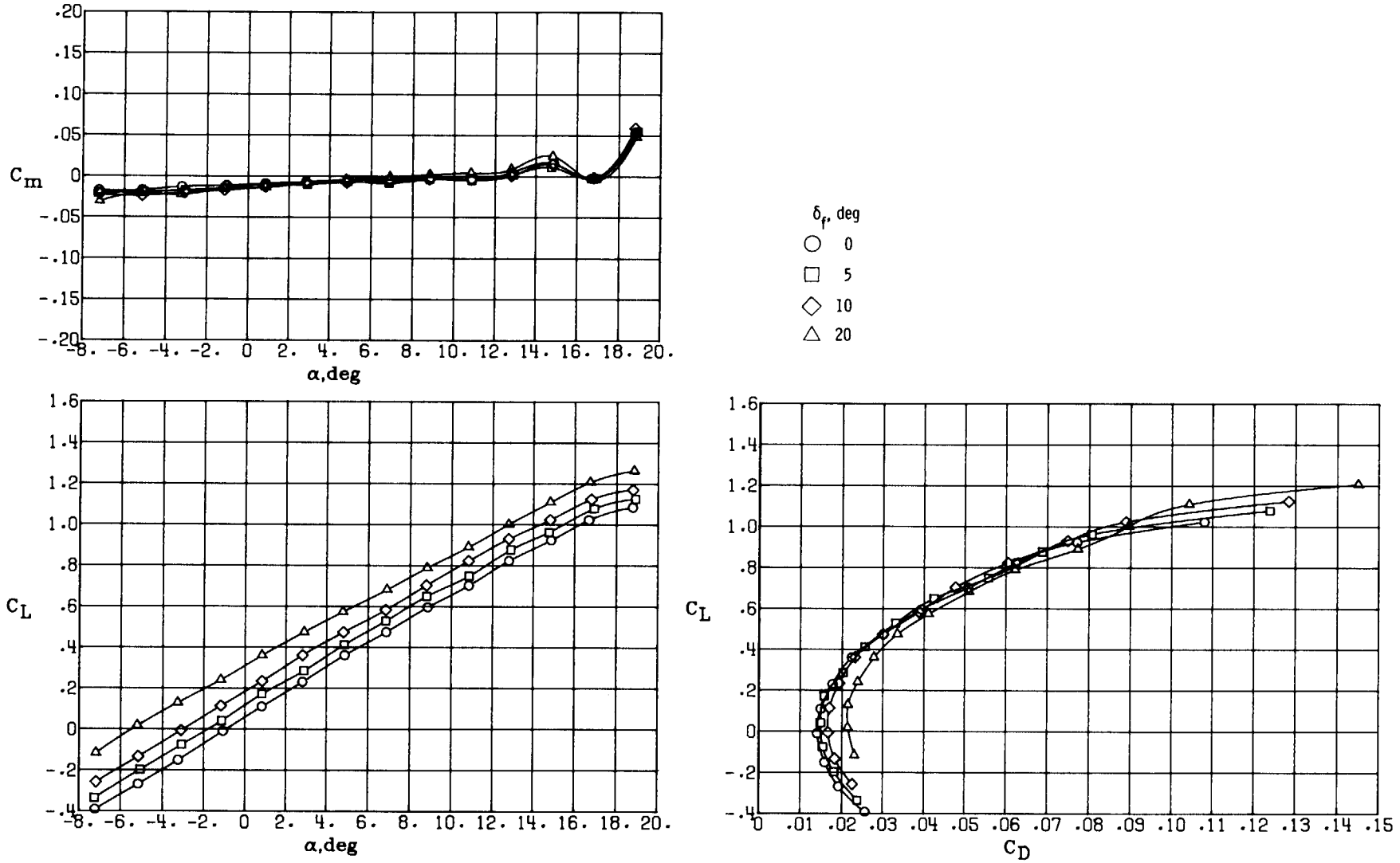

(a) AR = 5.1.

Figure 18.- Effect of flap deflection on the longitudinal aerodynamics of configuration IV (Λ = 45°) at several aspect ratios. δ_e = 0°.

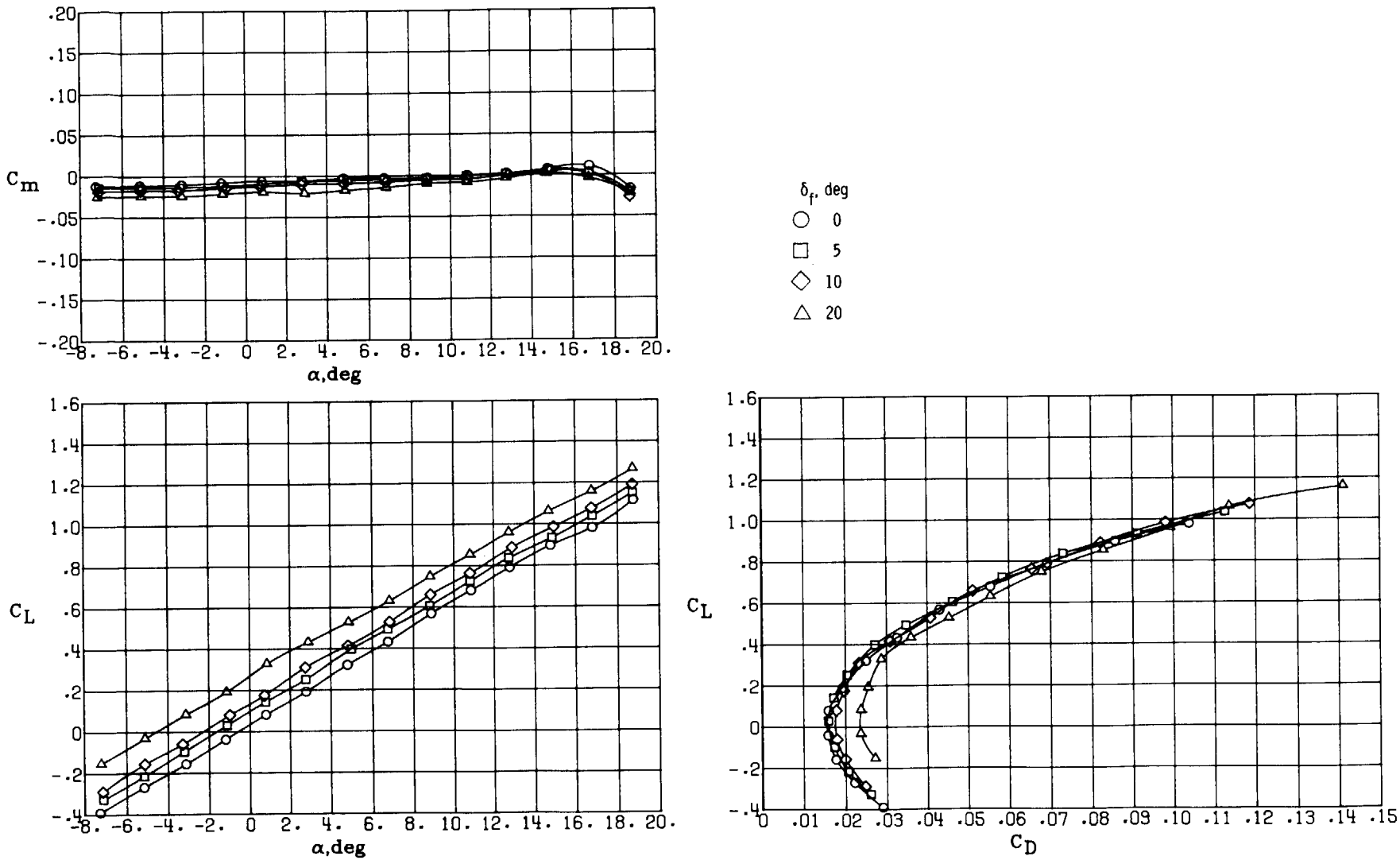

(b) AR = 4.1.

Figure 18.- Continued.

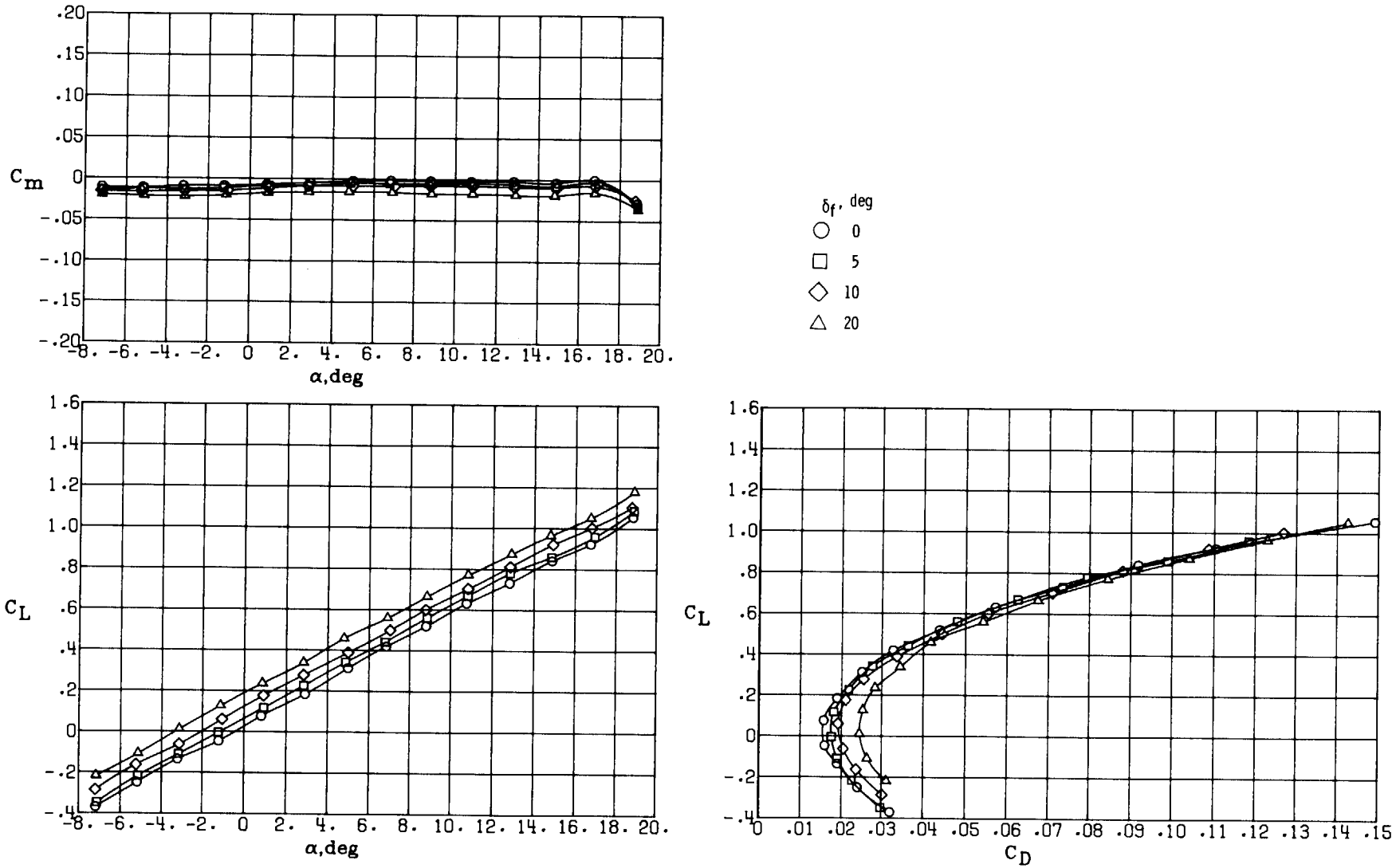

(c) AR = 3.1.

Figure 18.- Continued.

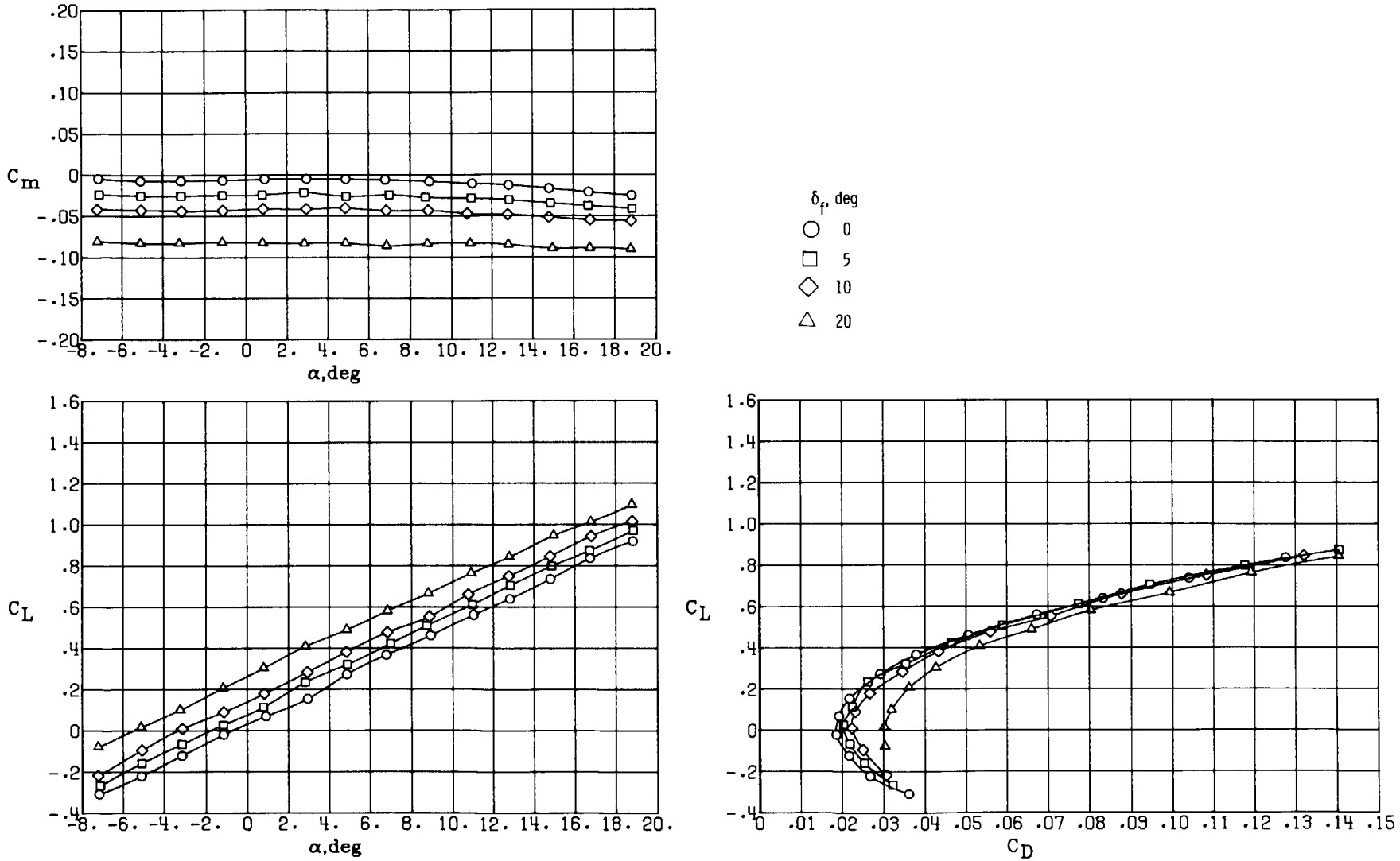

(d) AR = 2.1.

Figure 18.- Concluded.

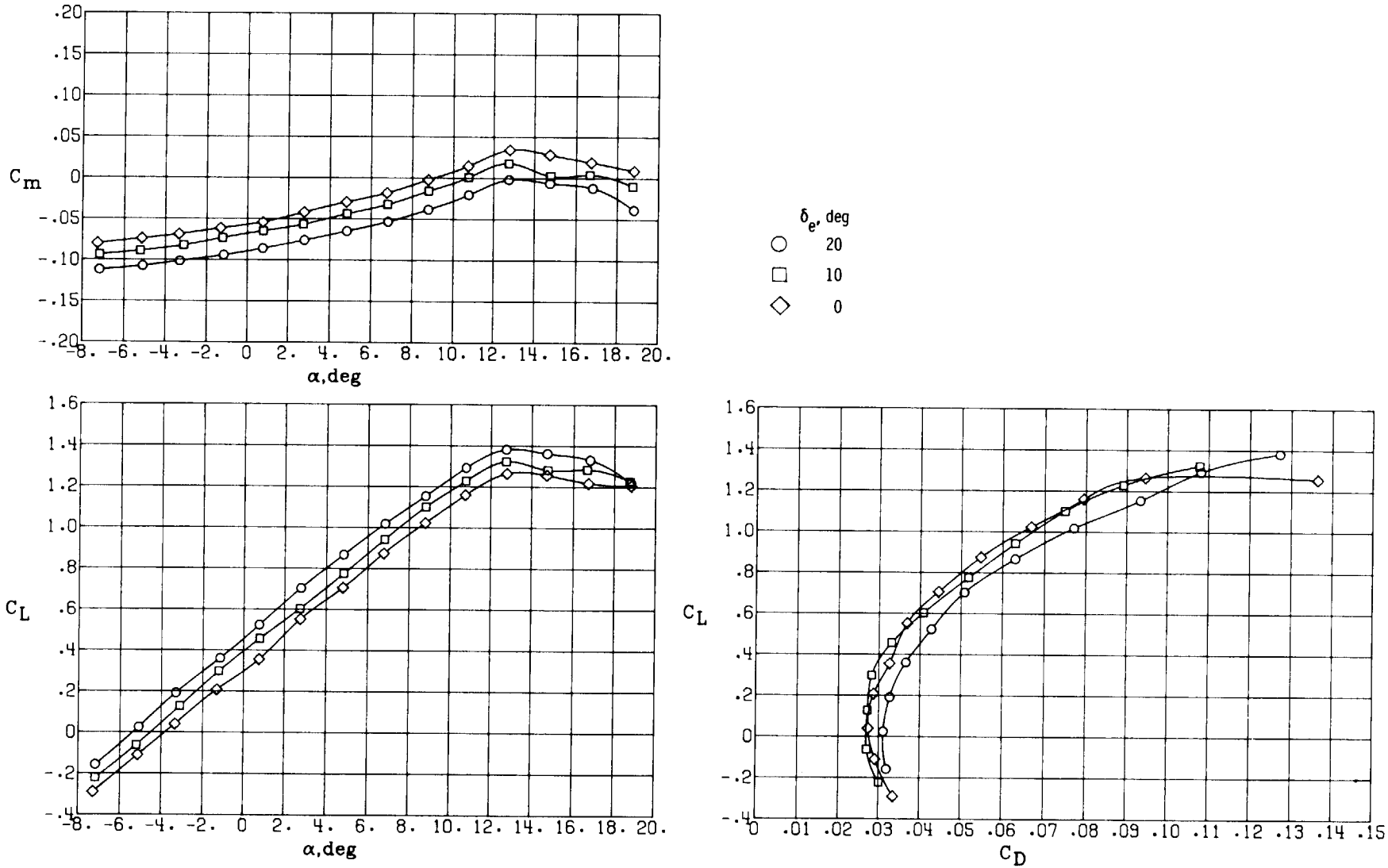

(a) AR = 8.

Figure 19.- Effect of elevon deflection on the longitudinal aerodynamics of configuration I (Λ = 0°) at several aspect ratios. δ_f = 10°.

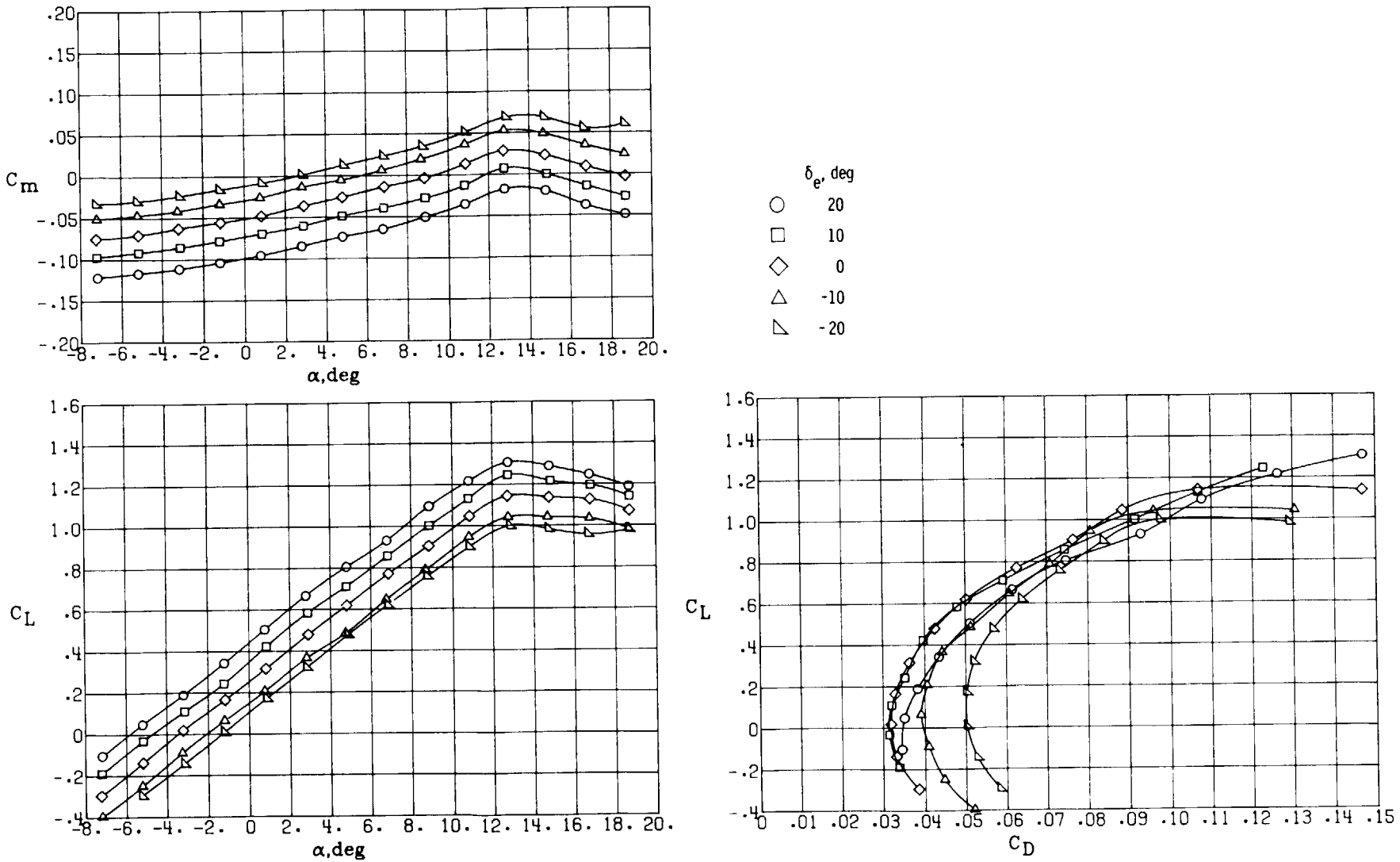

(b) AR = 6.

Figure 19.- Continued.

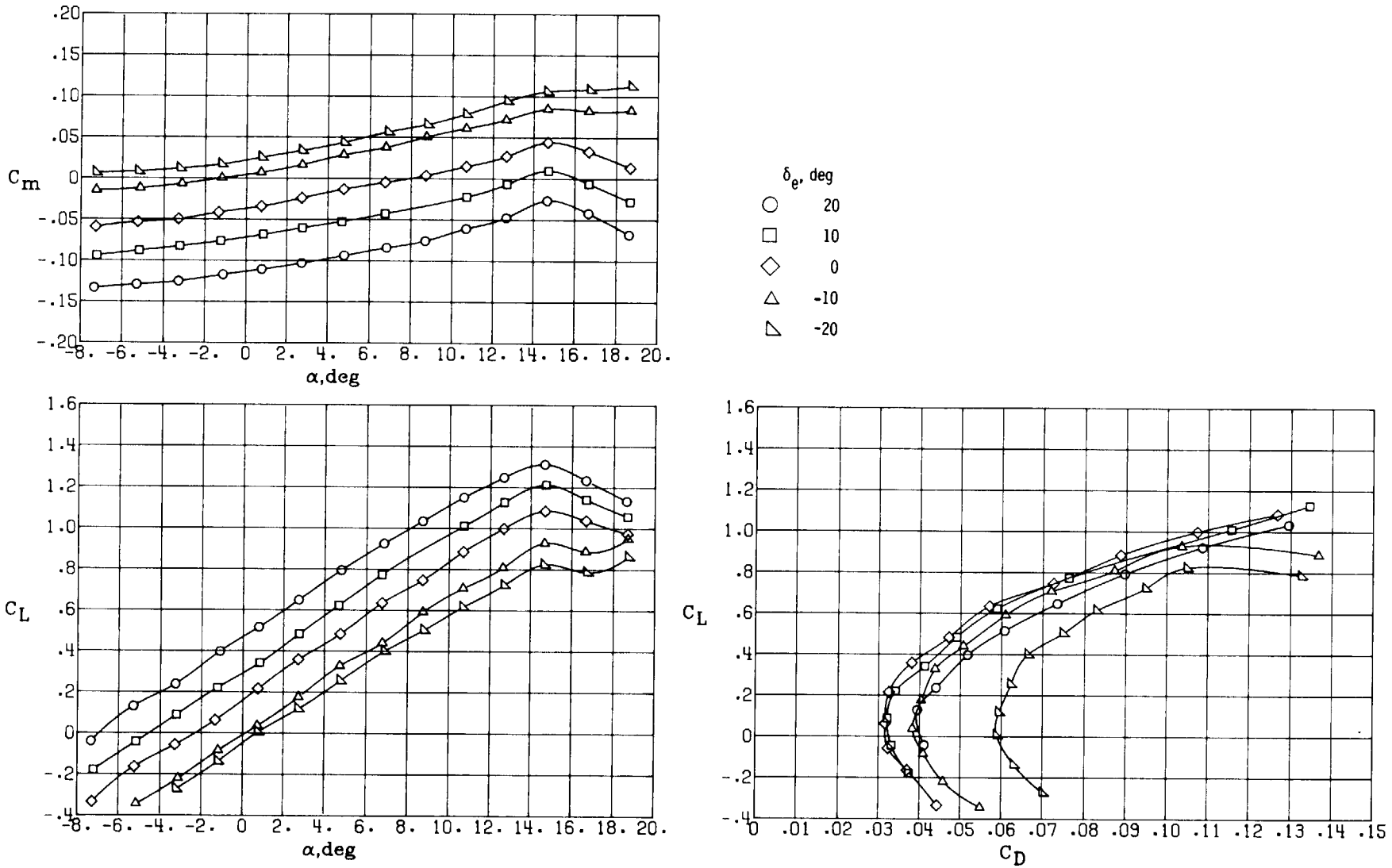

(c) AR = 4.

Figure 19.- Concluded.

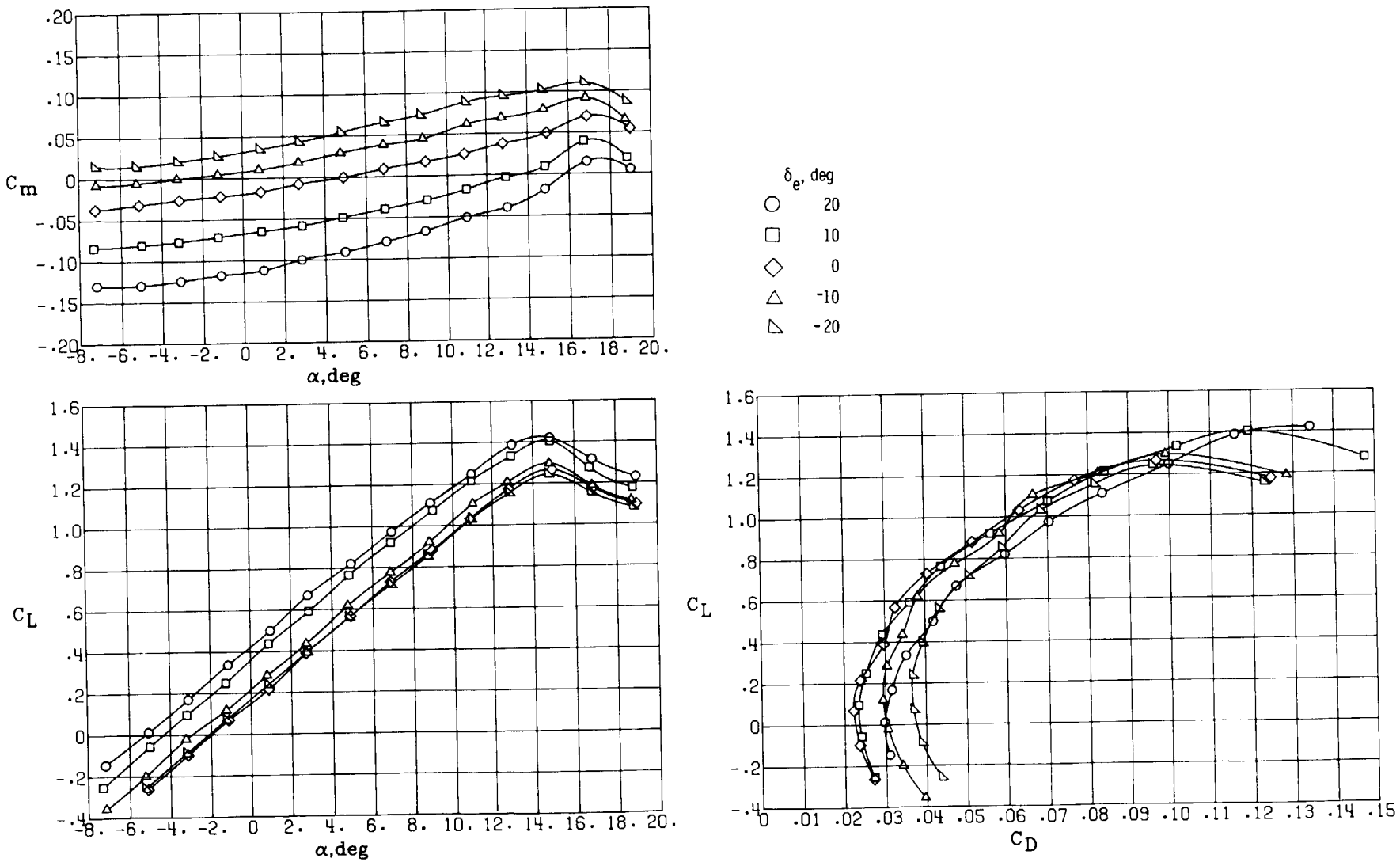

(a) AR = 7.98.

Figure 20.- Effect of elevon deflection on the longitudinal aerodynamics of configuration II (Λ = 15°) at several aspect ratios. δ_f = 10°.

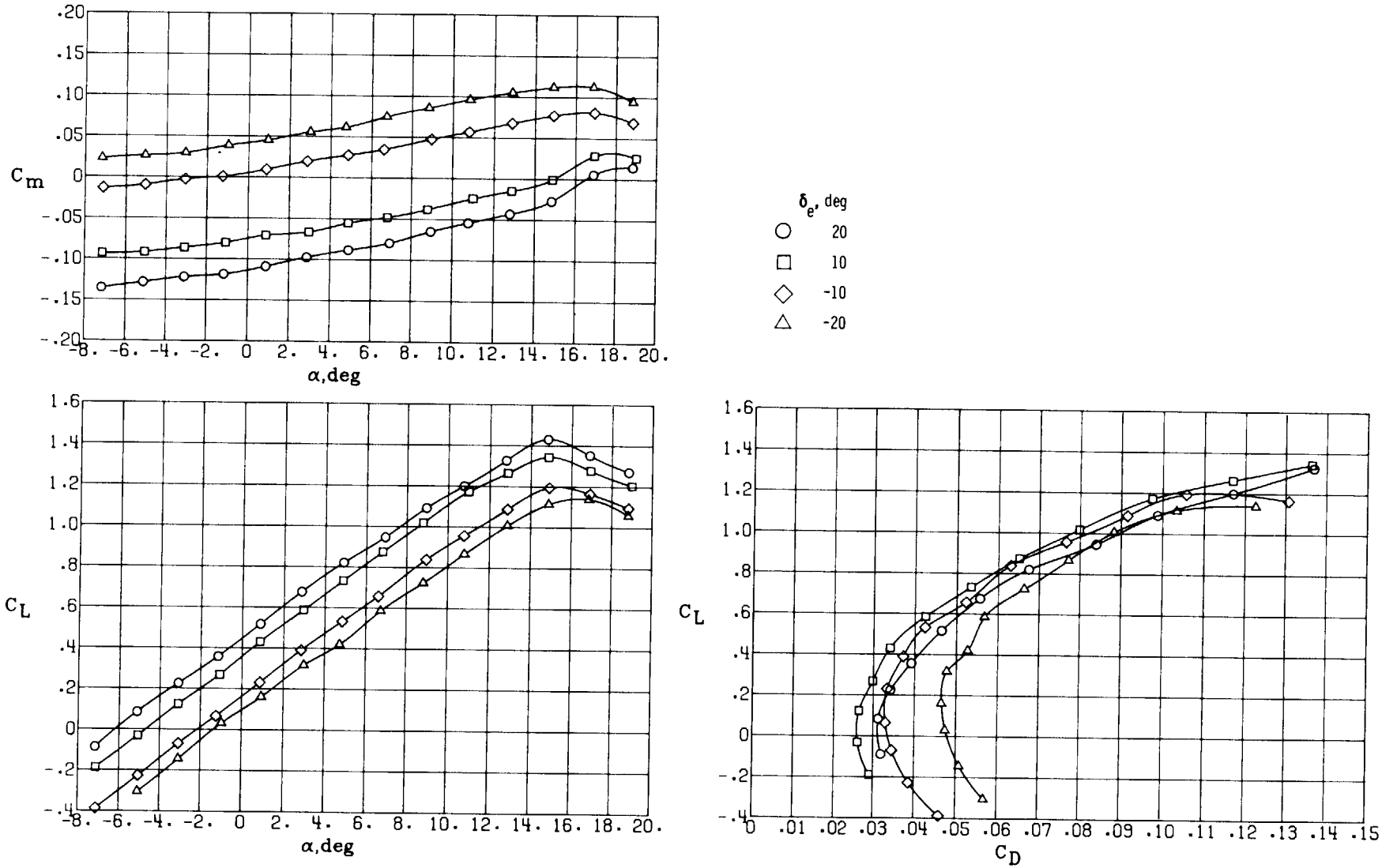

(b) AR = 6.11.

Figure 20.- Continued.

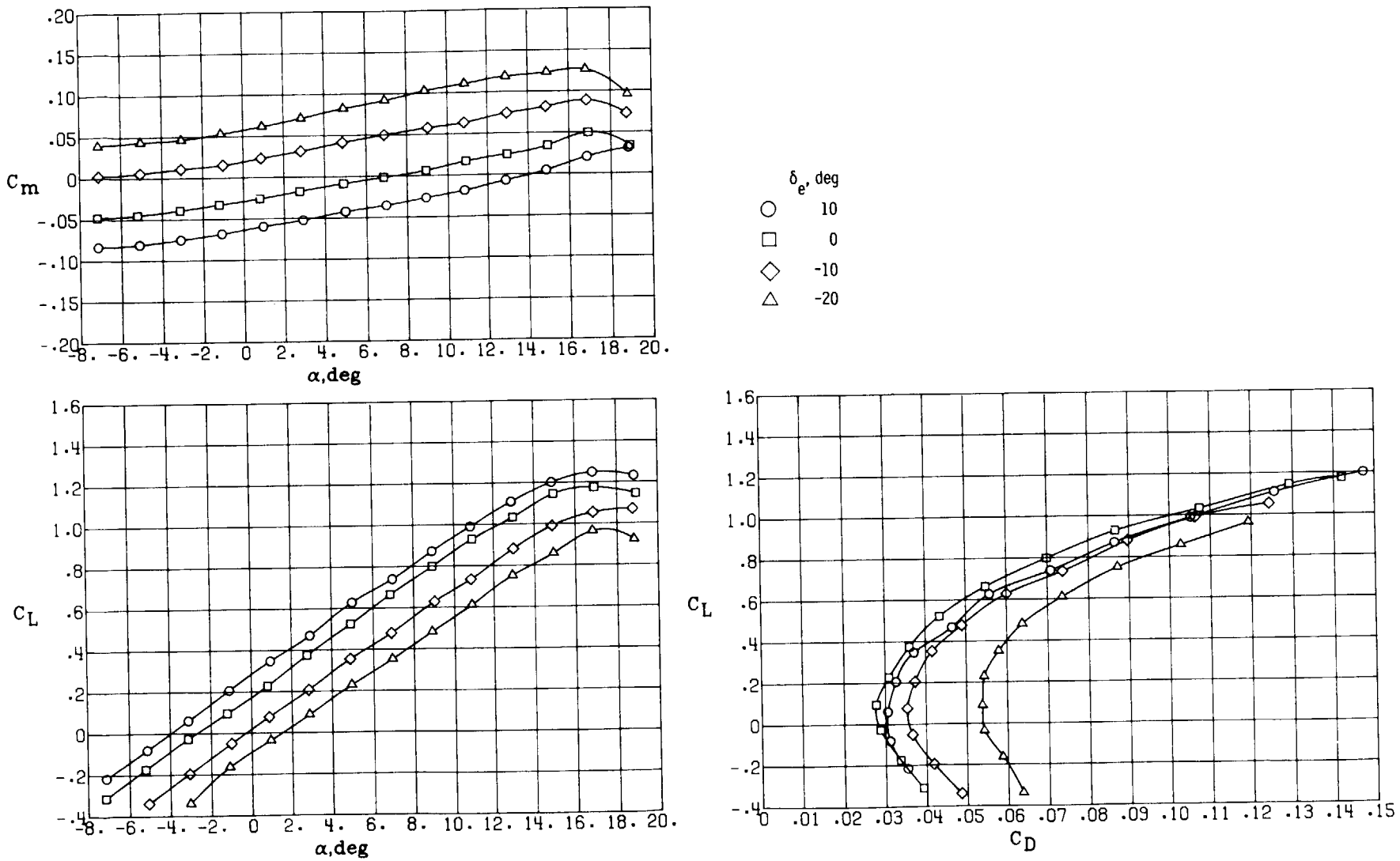

(c) AR = 4.25.

Figure 20.- Concluded.

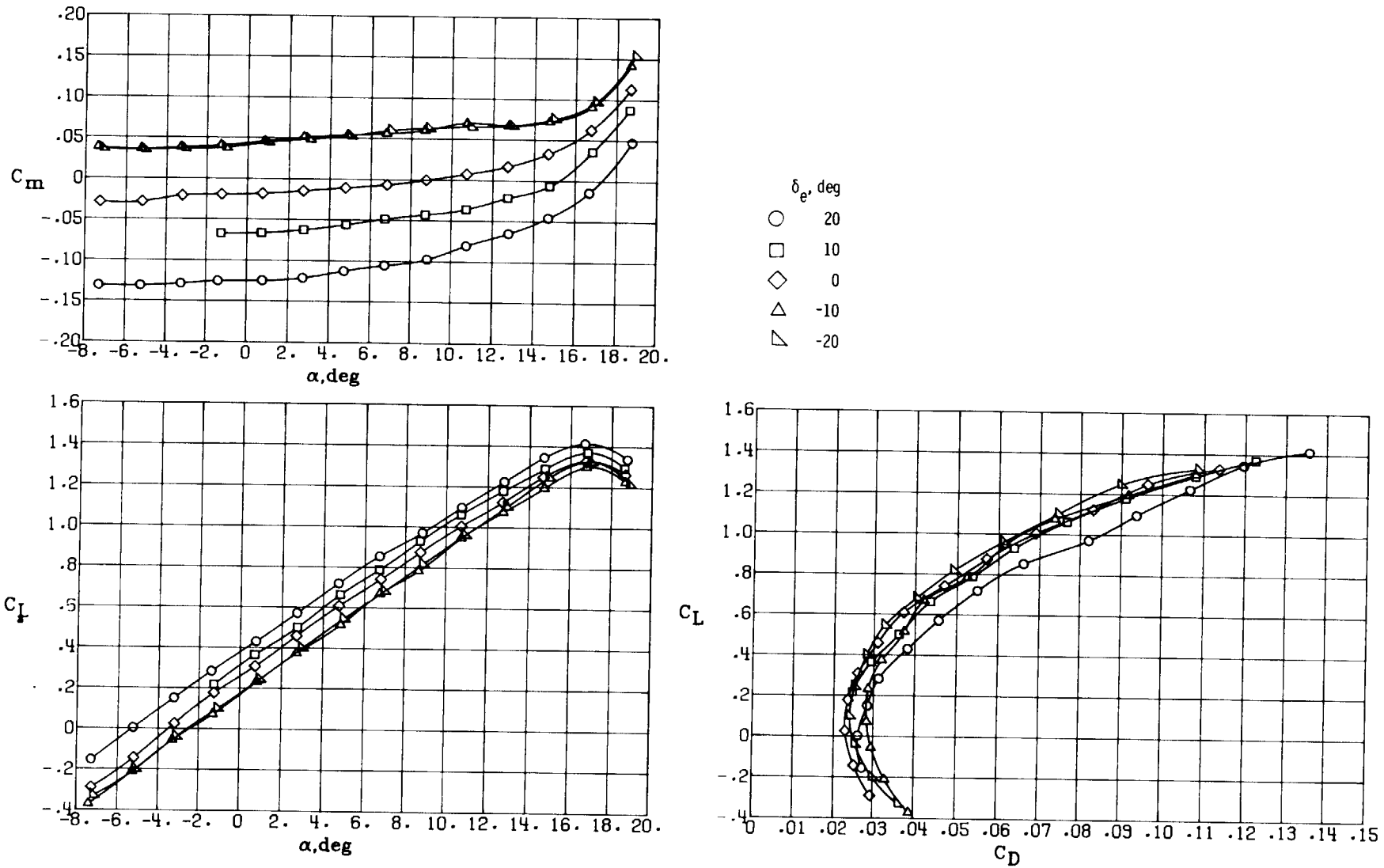

(a) AR = 6.92.

Figure 21.- Effect of elevon deflection on the longitudinal aerodynamics of configuration III ($\Lambda = 30°$) at several aspect ratios. $\delta_f = 10°$.

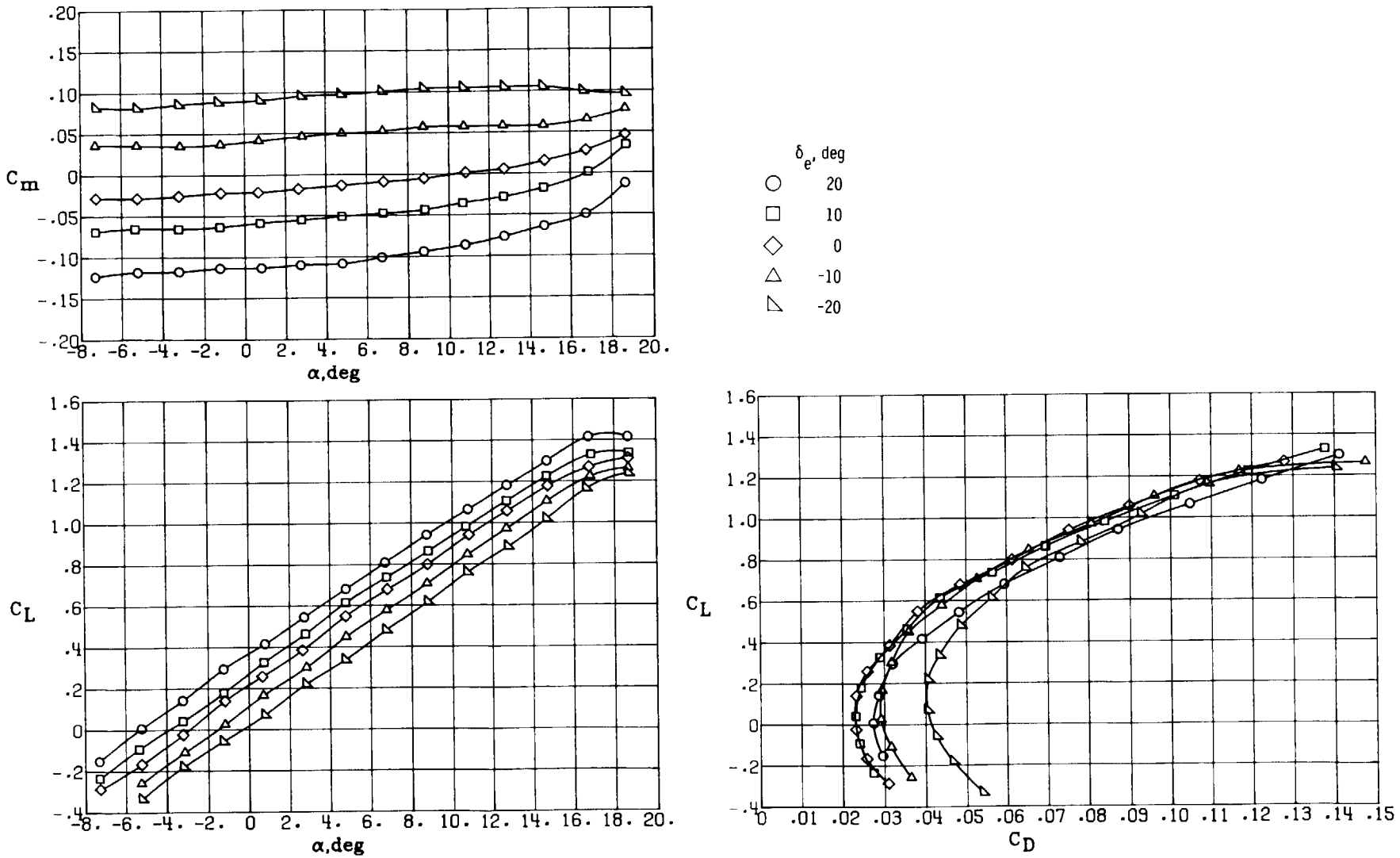

(b) AR = 5.42.

Figure 21.- Continued.

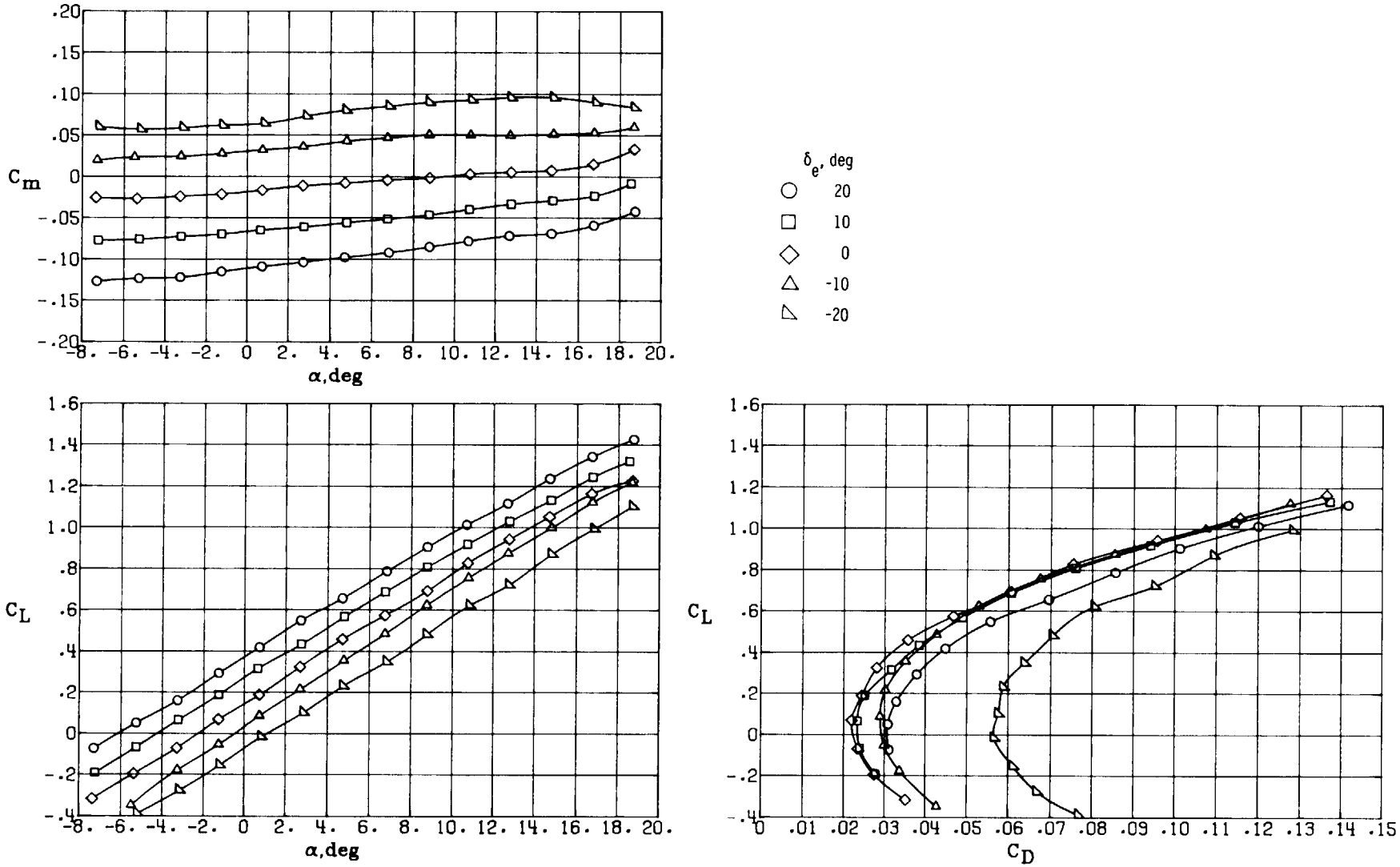

(c) AR = 3.92.

Figure 21.- Concluded.

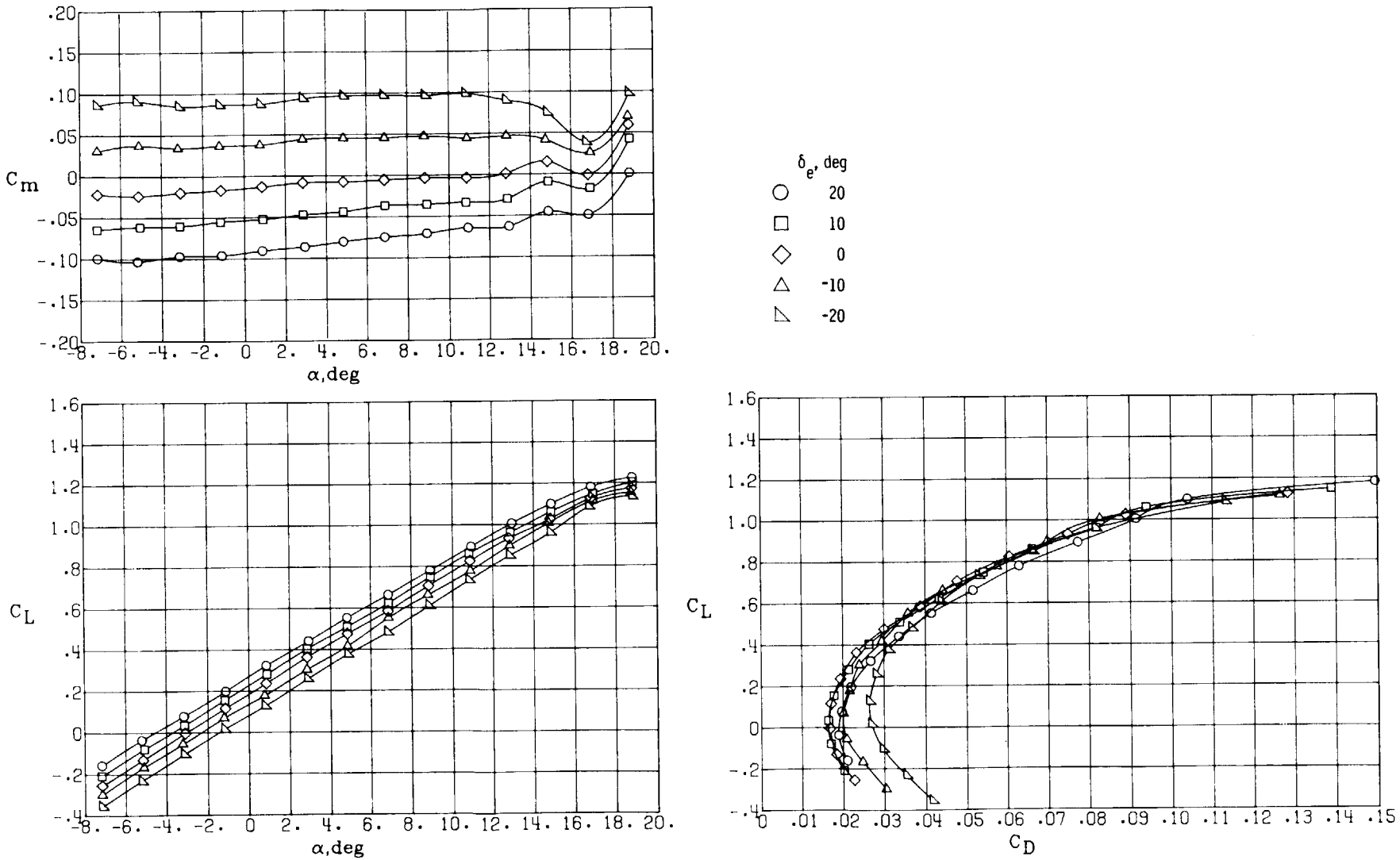

(a) AR = 5.1.

Figure 22.- Effect of elevon deflection on the longitudinal aerodynamics of configuration IV (Λ = 45°) at several aspect ratios. δ_f = 10°.

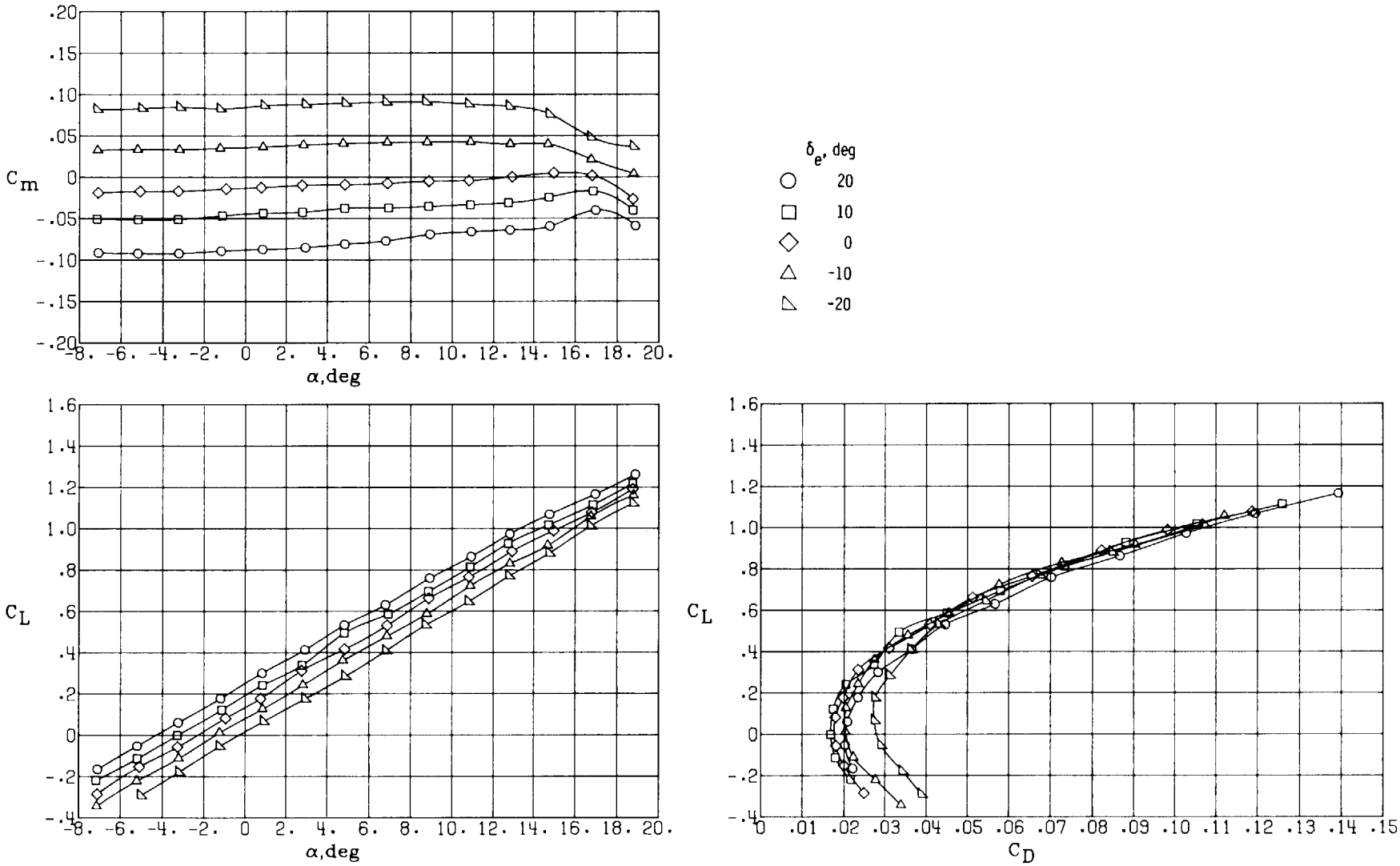

(b) AR = 4.1.

Figure 22.- Continued.

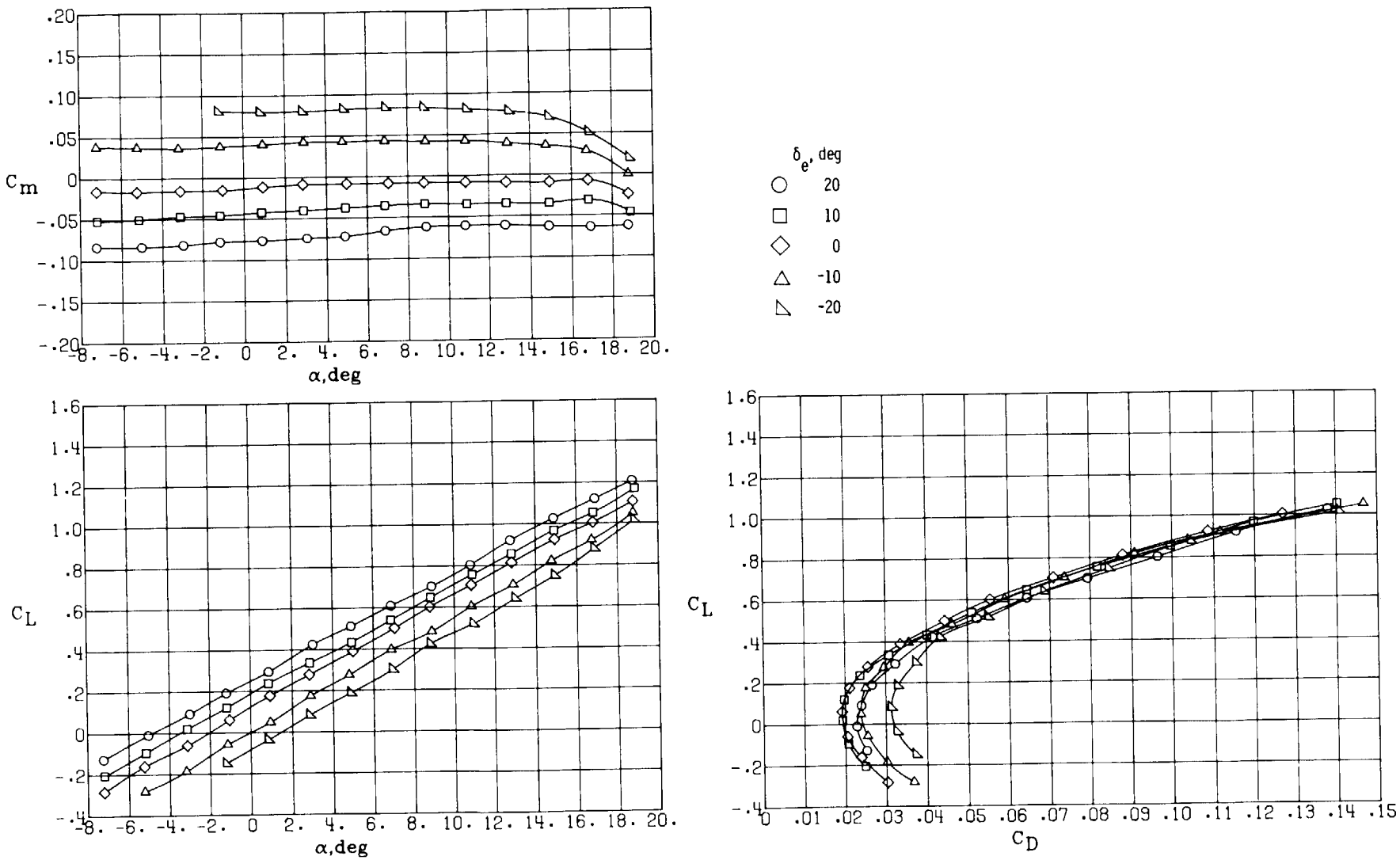

(c) AR = 3.1.

Figure 22.- Concluded.

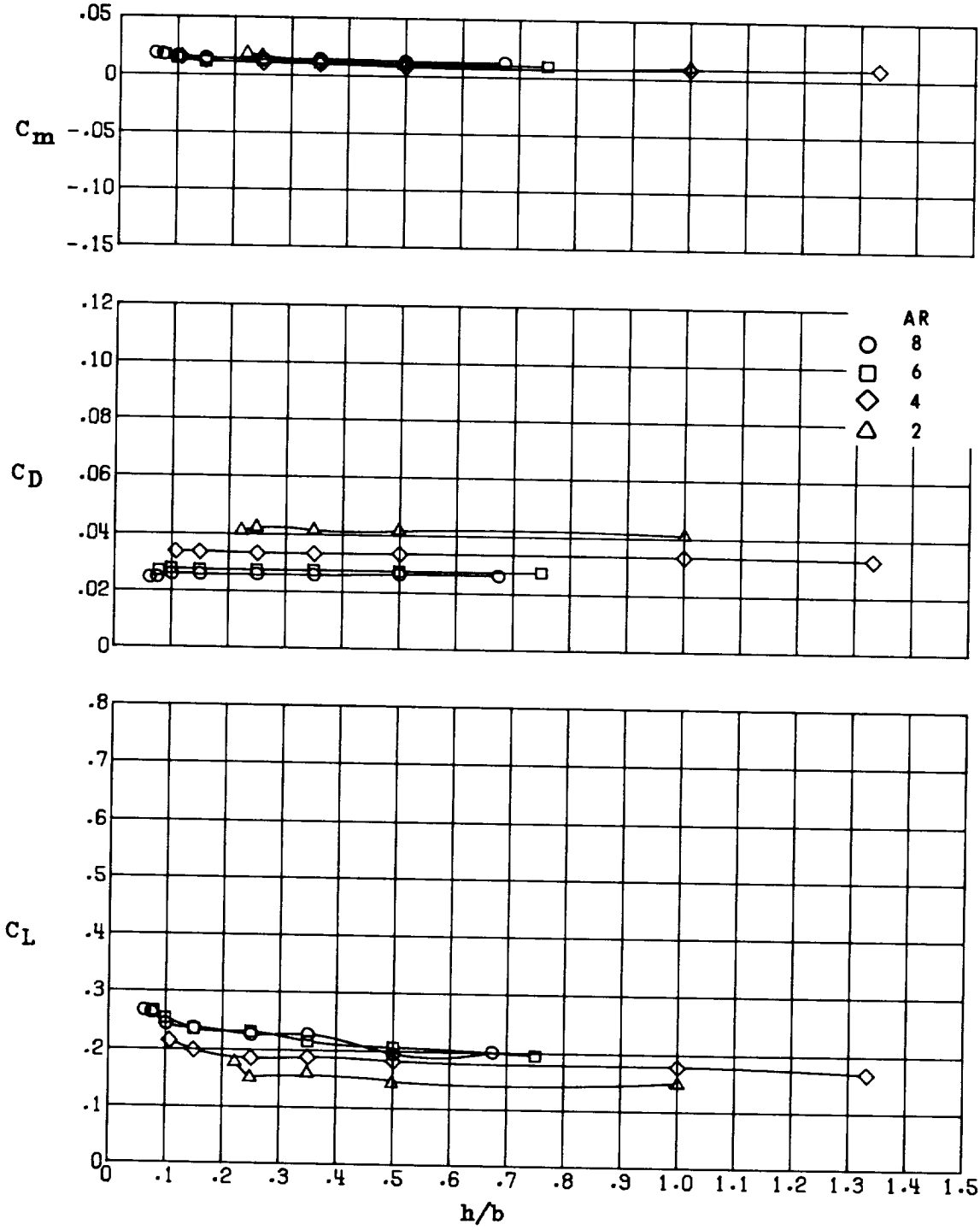

(a) $\delta_f = 0°$.

Figure 23.- Effect of aspect ratio on the longitudinal aerodynamics in ground effect of configuration I ($\Lambda = 0°$) at several flap deflections. $\delta_e = 0°$; $\alpha = 2.78°$.

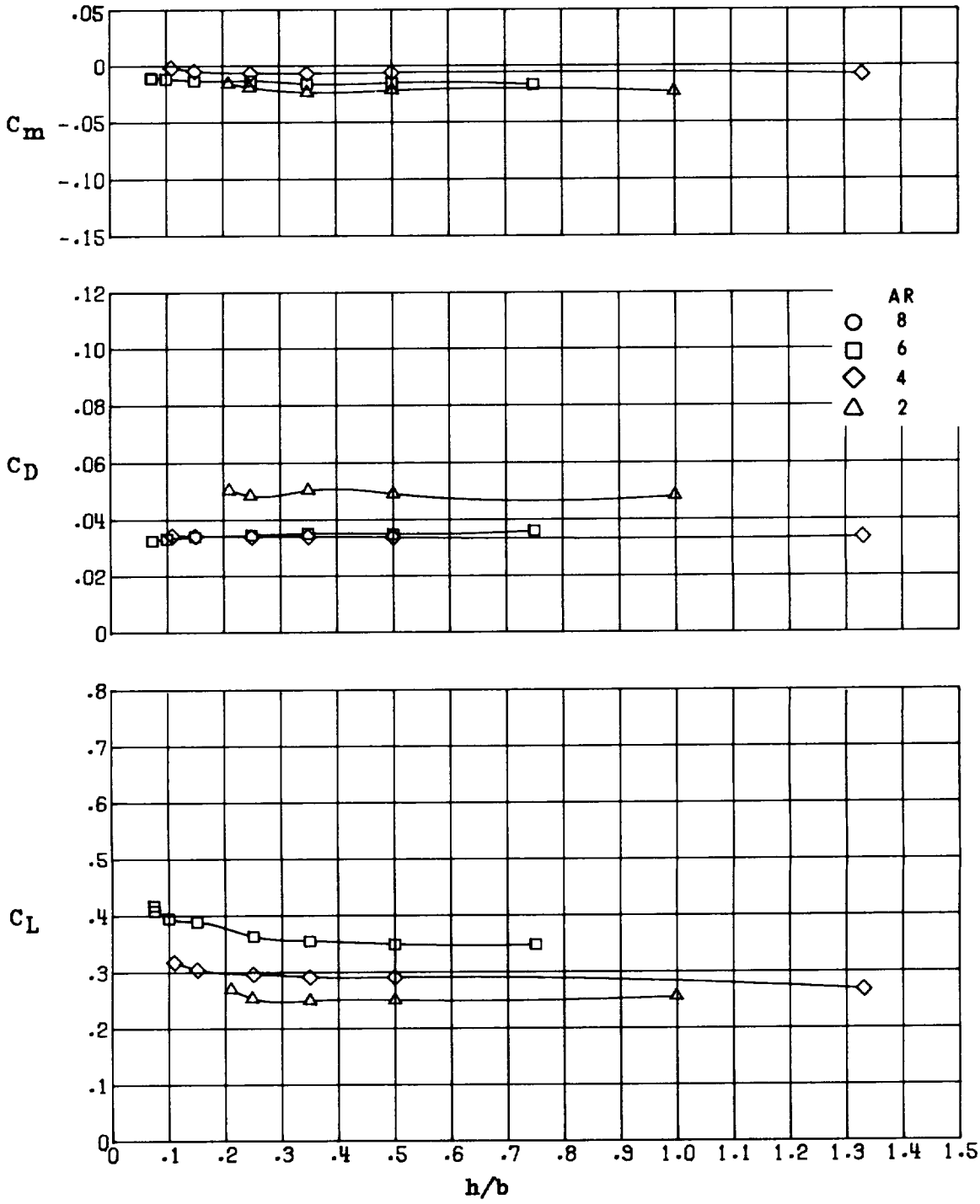

(b) $\delta_f = 5°$.

Figure 23.- Continued.

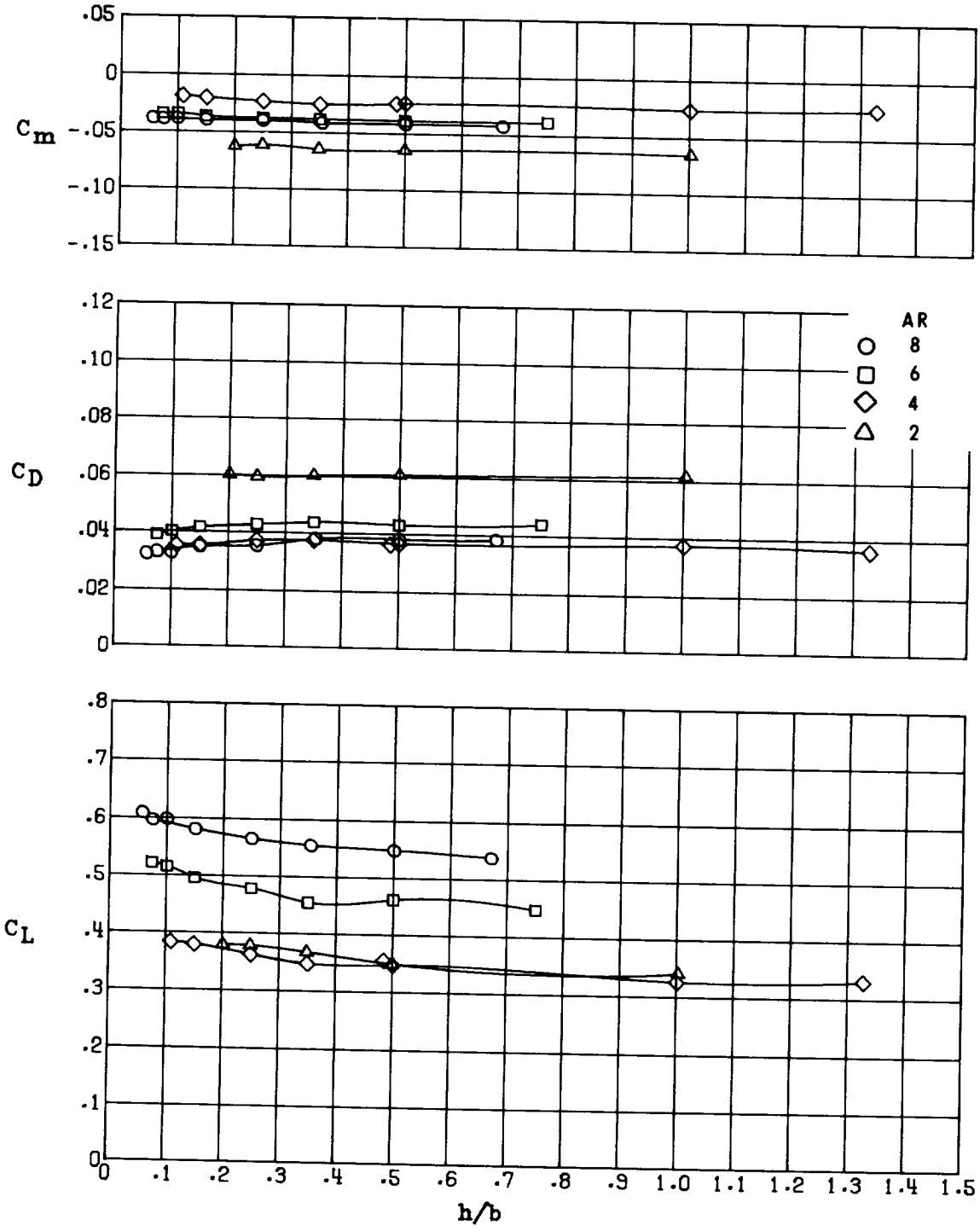

(c) δ_f = 10°.

Figure 23.- Continued.

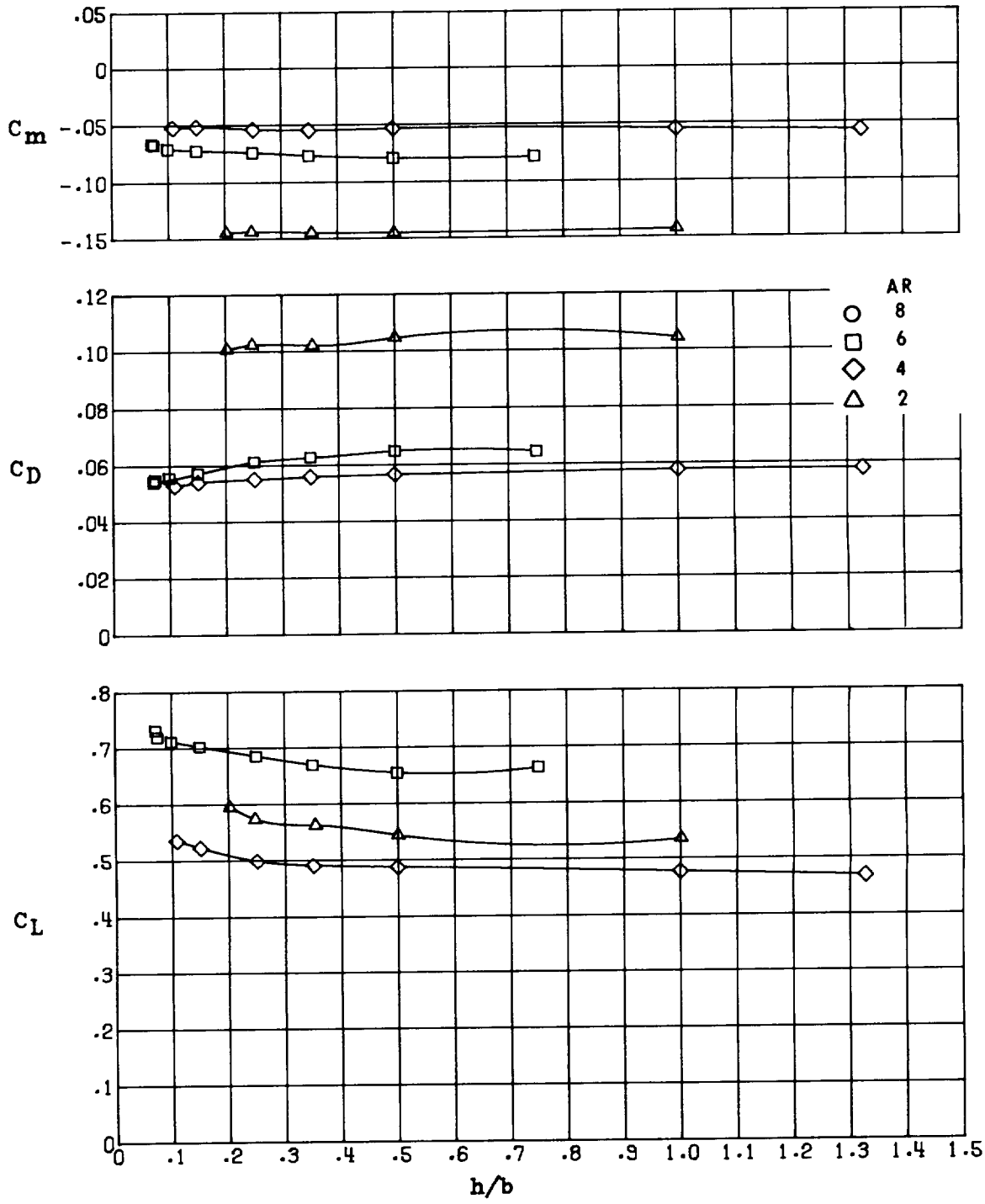

(d) $\delta_f = 20°$.

Figure 23.- Concluded.

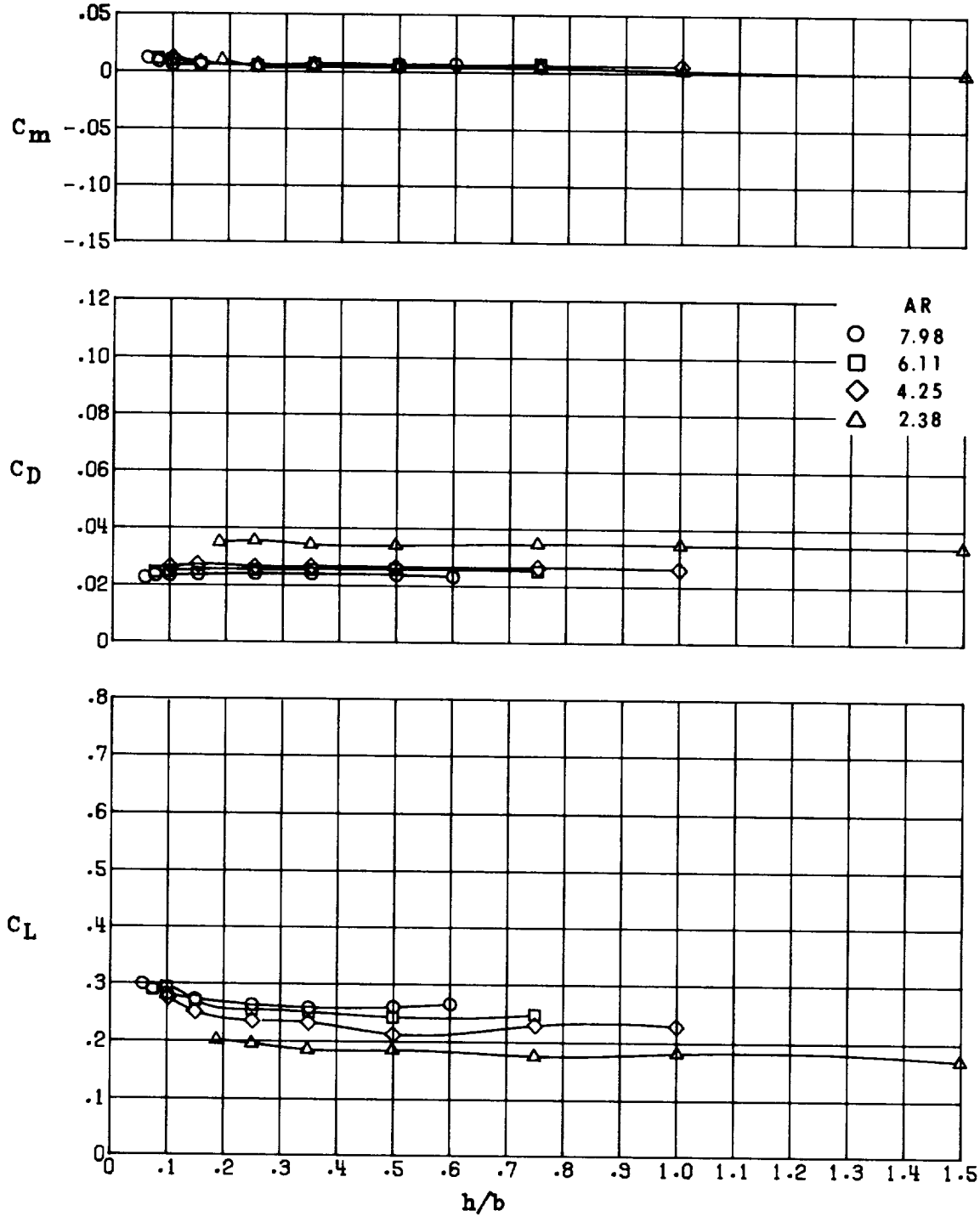

(a) $\delta_f = 0°$.

Figure 24.- Effect of aspect ratio on the longitudinal aerodynamics in ground effect of configuration II ($\Lambda = 15°$) at several flap deflections. $\delta_e = 0°$; $\alpha = 2.78°$.

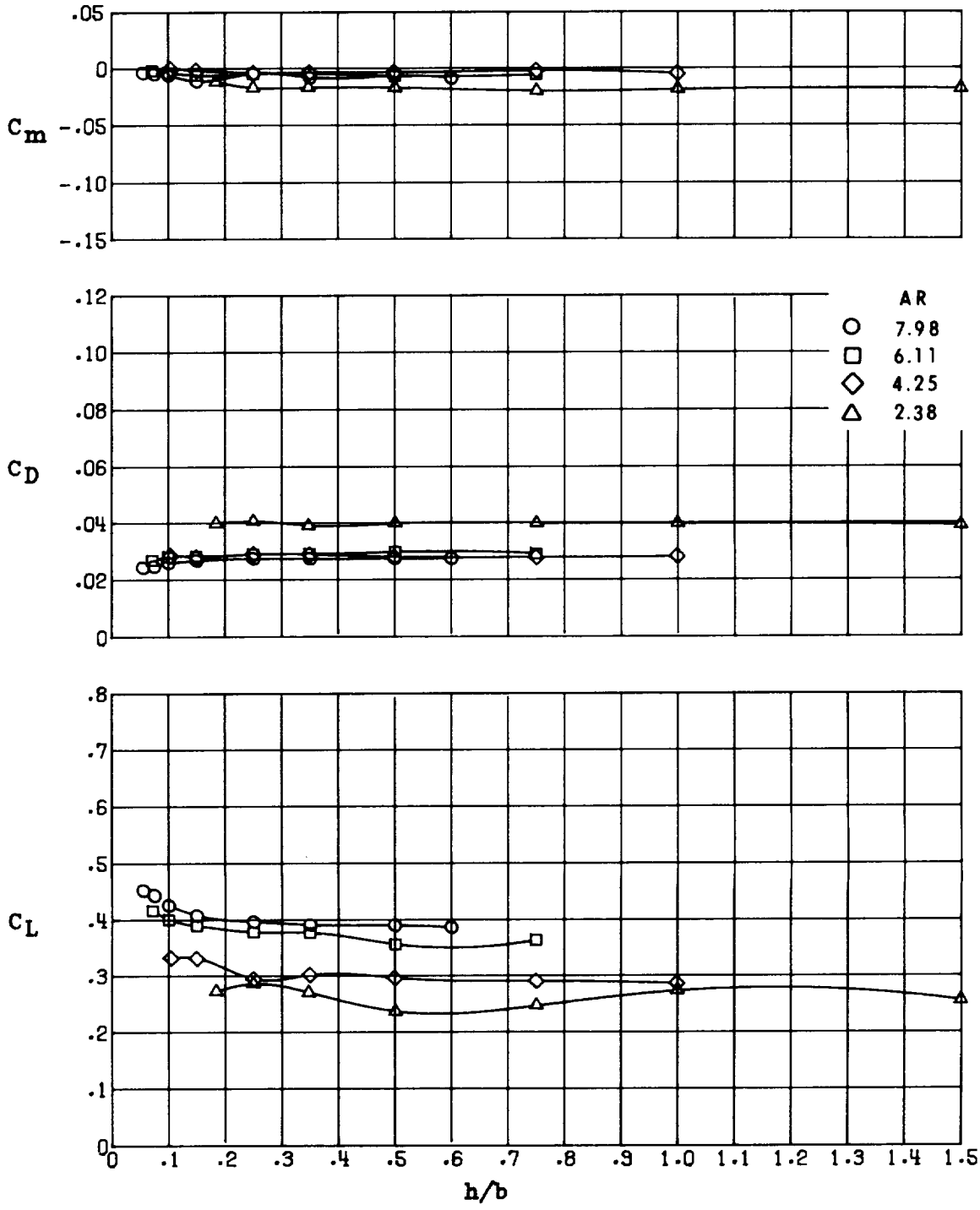

(b) $\delta_f = 5°$.

Figure 24.- Continued.

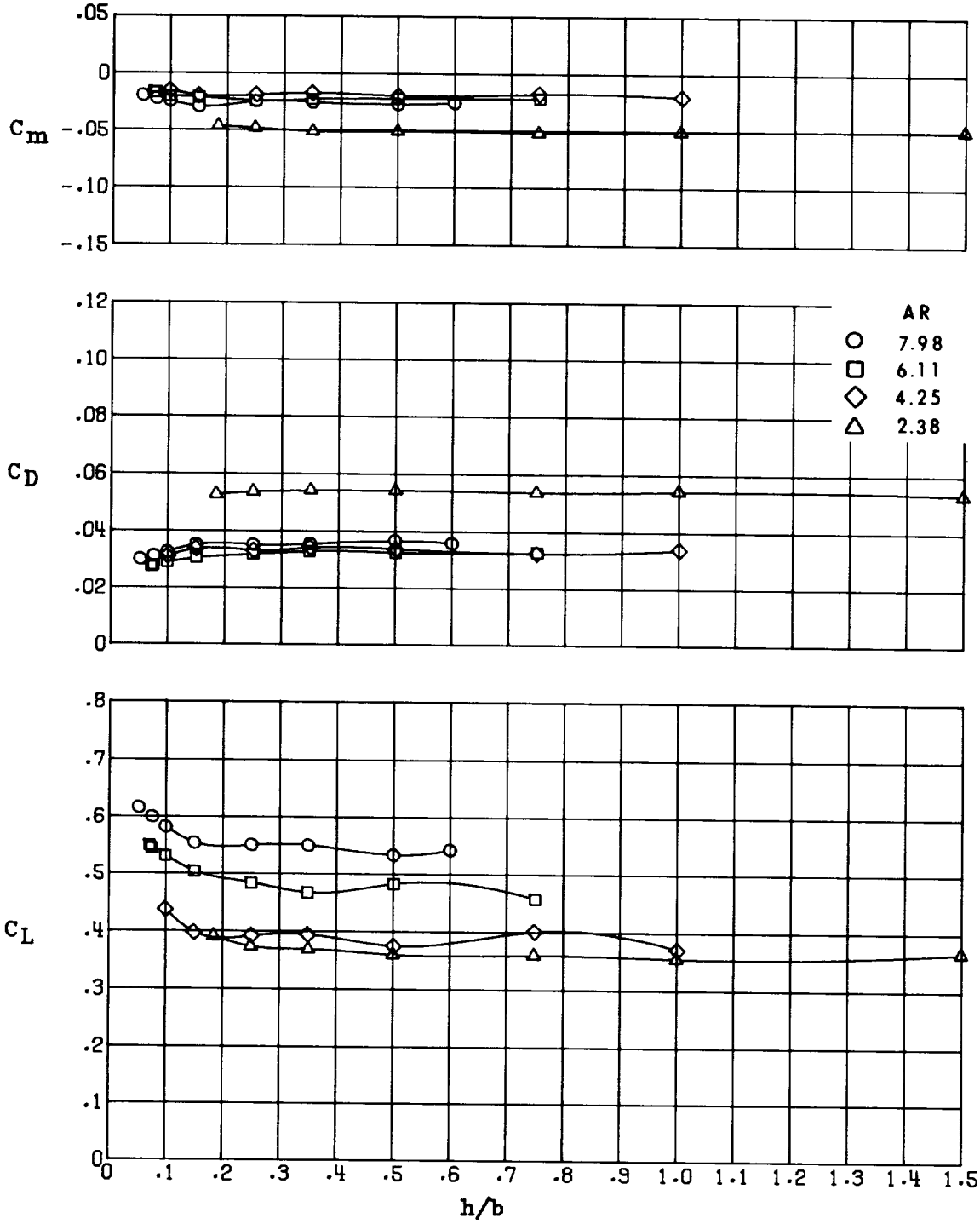

(c) $\delta_f = 10°$.

Figure 24.- Continued.

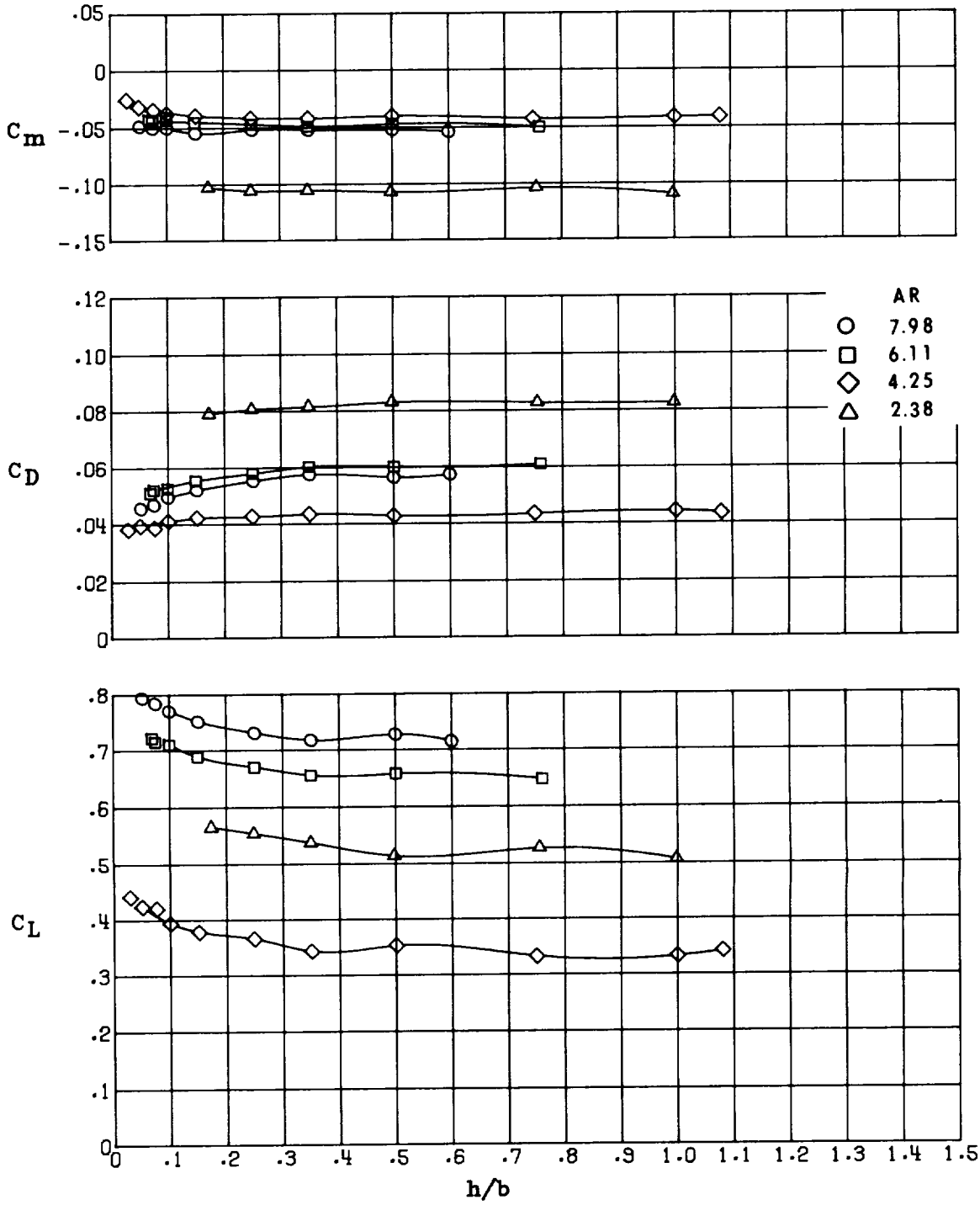

(d) $\delta_f = 20°$.

Figure 24.- Concluded.

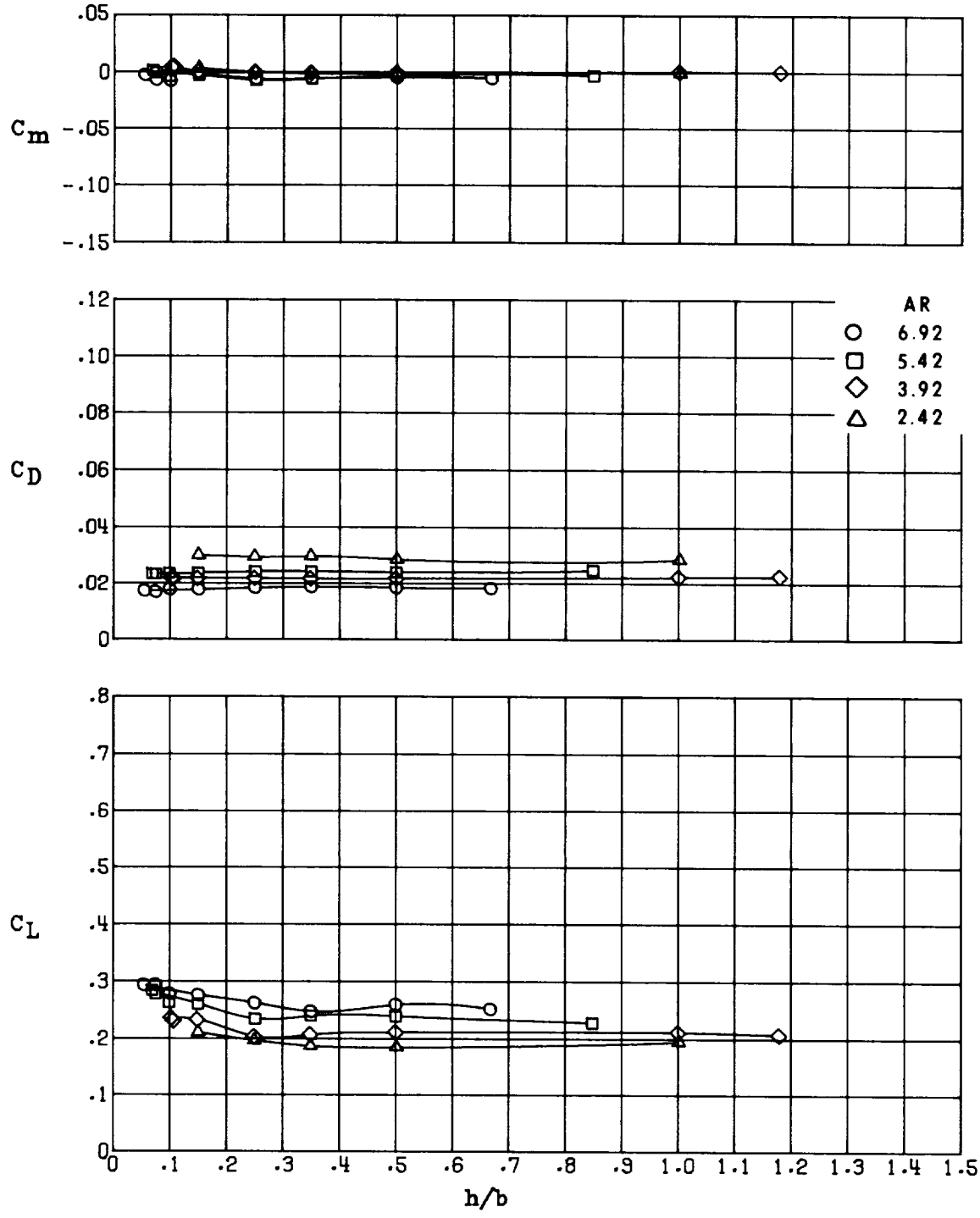

(a) $\delta_f = 0°$.

Figure 25.- Effect of aspect ratio on the longitudinal aerodynamics in ground effect of configuration III ($\Lambda = 30°$) at several flap deflections. $\delta_e = 0°$; $\alpha = 2.78°$.

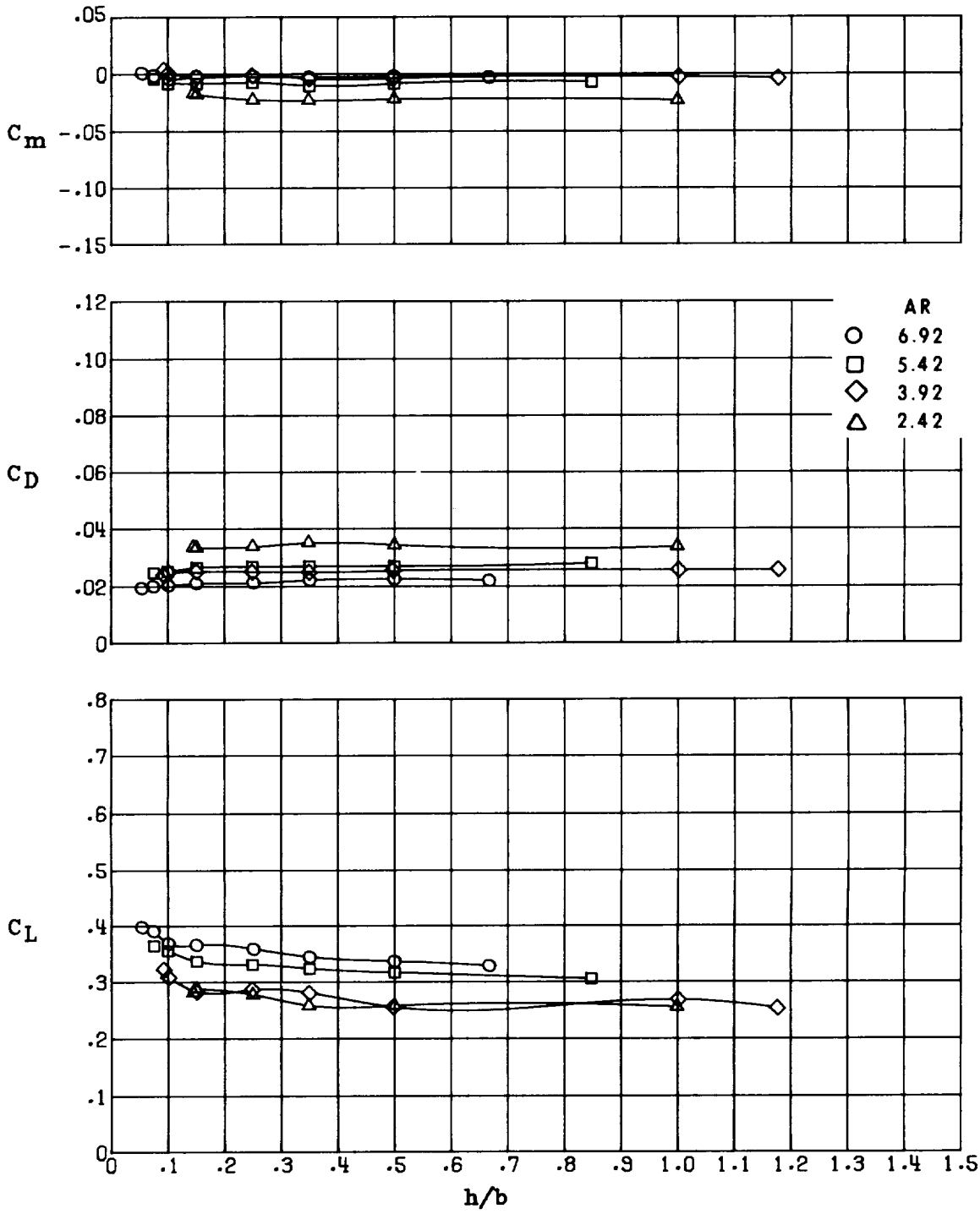

(b) $\delta_f = 5°$.

Figure 25.- Continued.

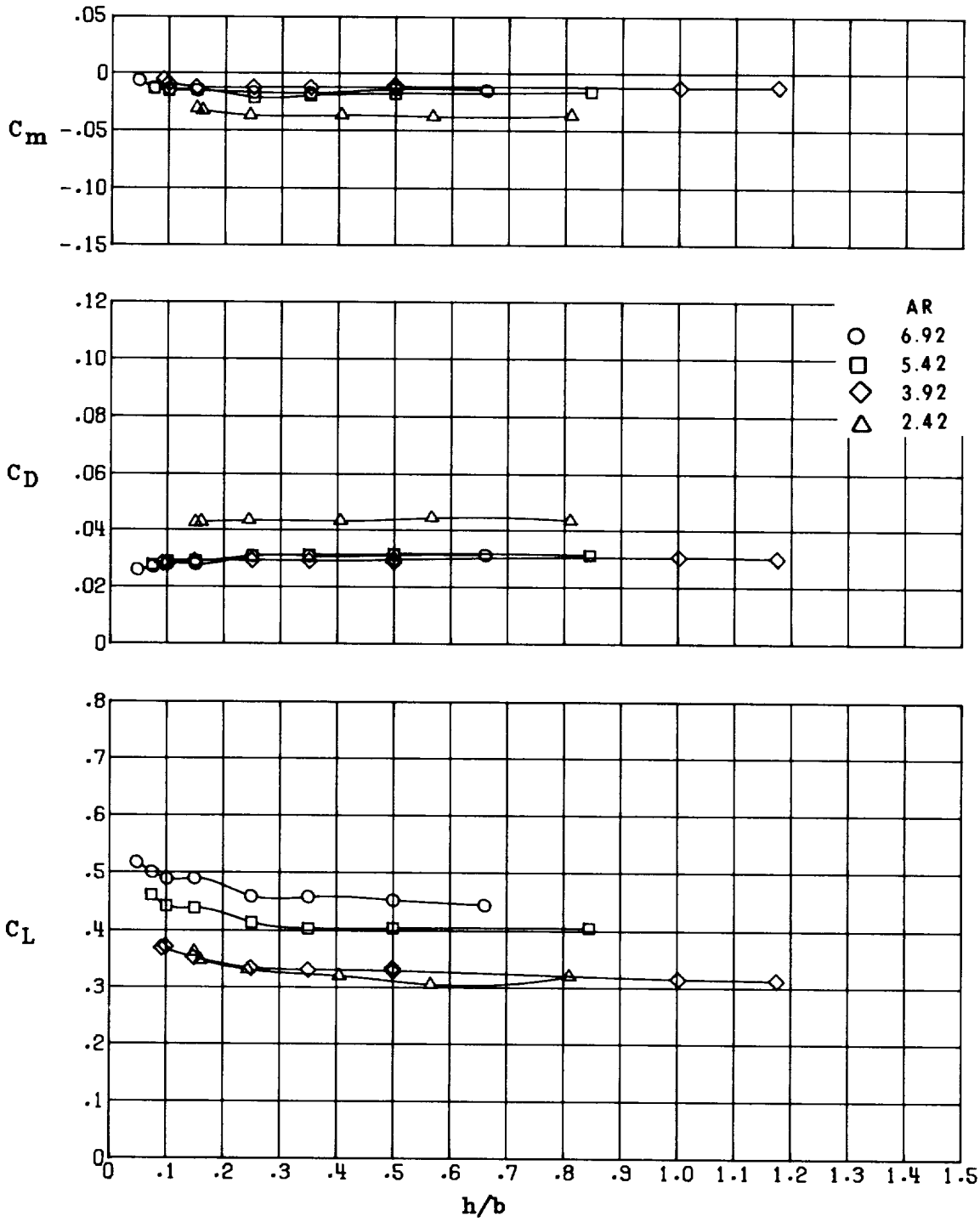

(c) δ_f = 10°.

Figure 25.- Continued.

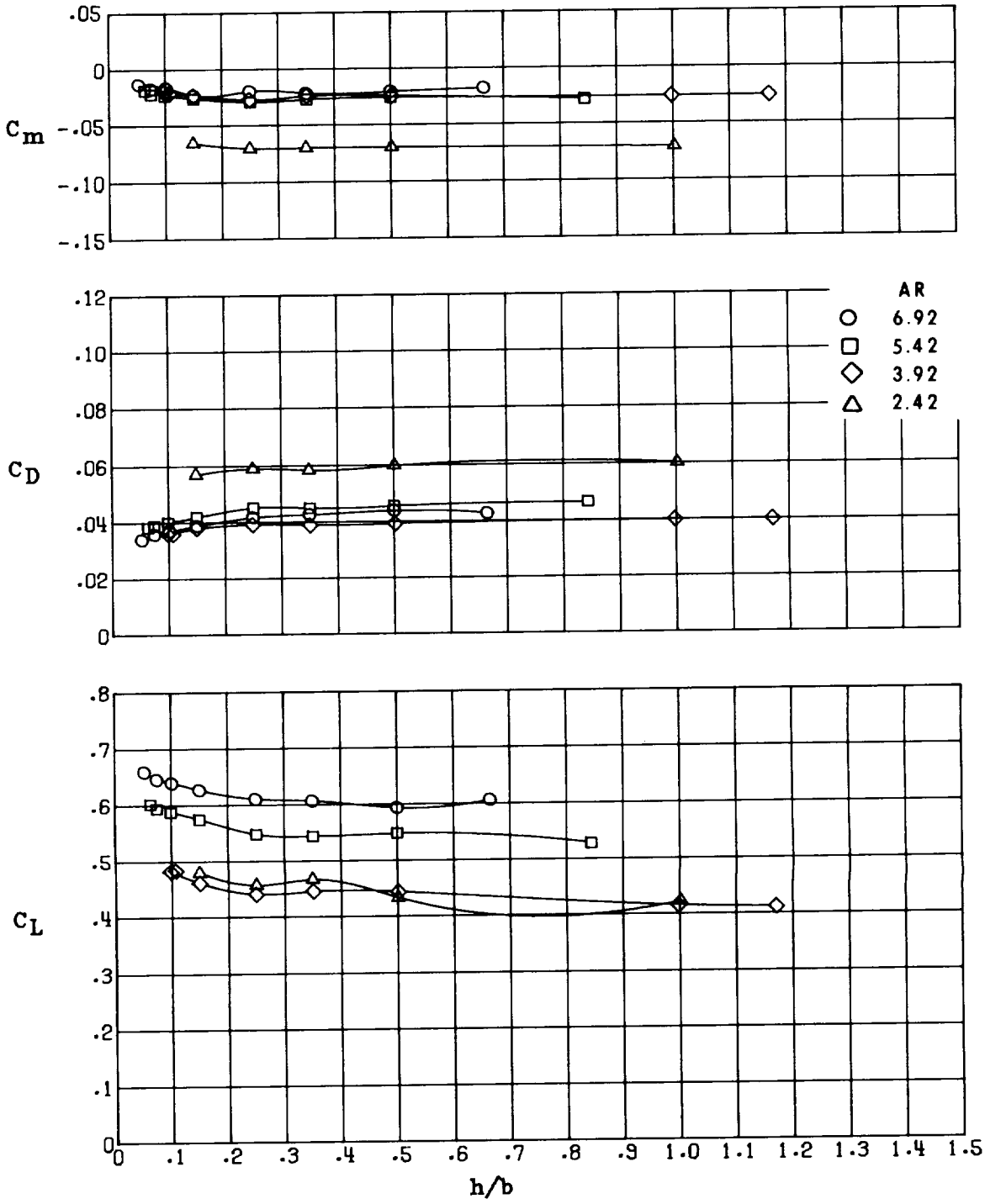

(d) $\delta_f = 20°$.

Figure 25.- Concluded.

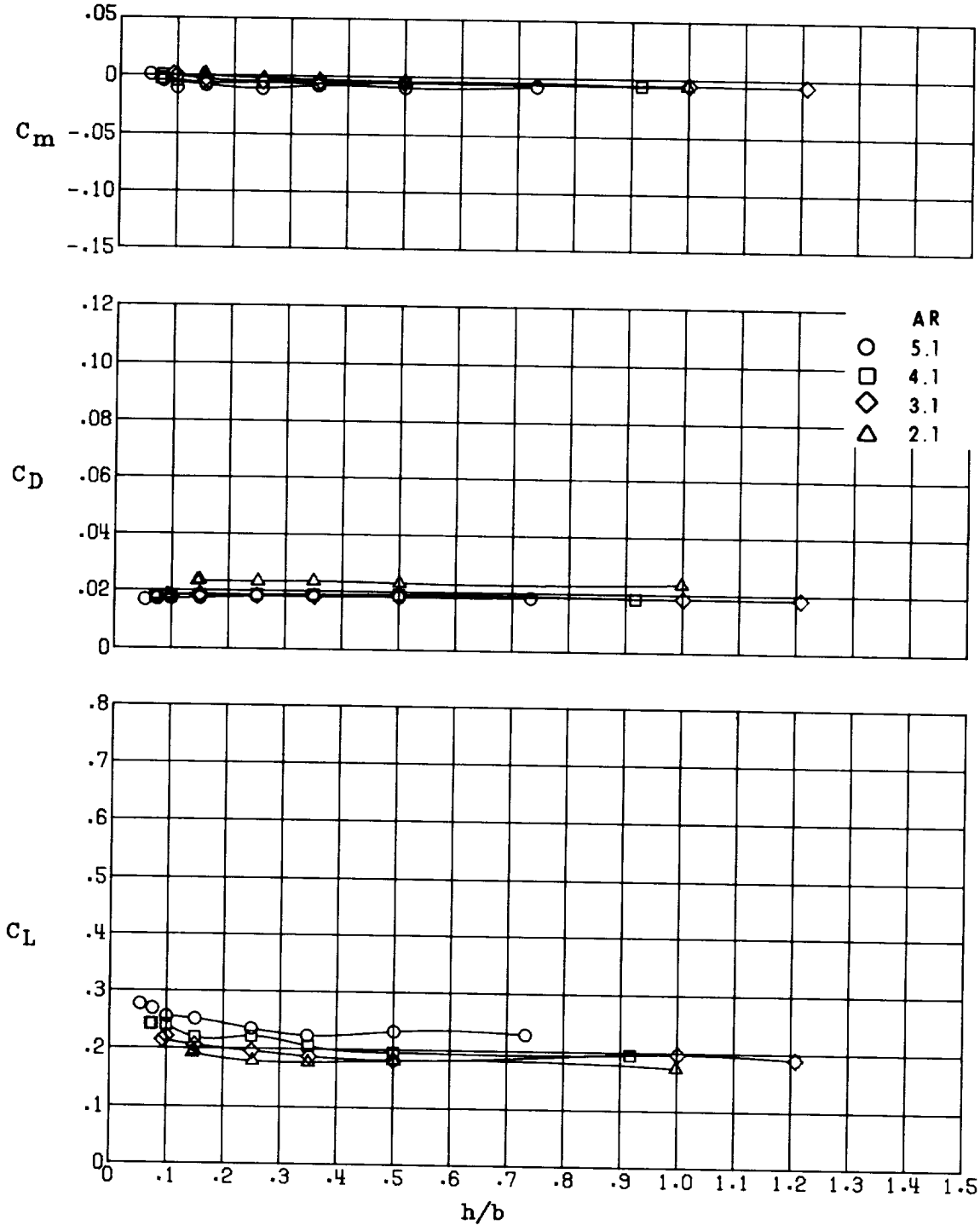

(a) $\delta_f = 0°$.

Figure 26.- Effect of aspect ratio on the longitudinal aerodynamics in ground effect of configuration IV ($\Lambda = 45°$) at several flap deflections. $\delta_e = 0°$; $\alpha = 2.78°$.

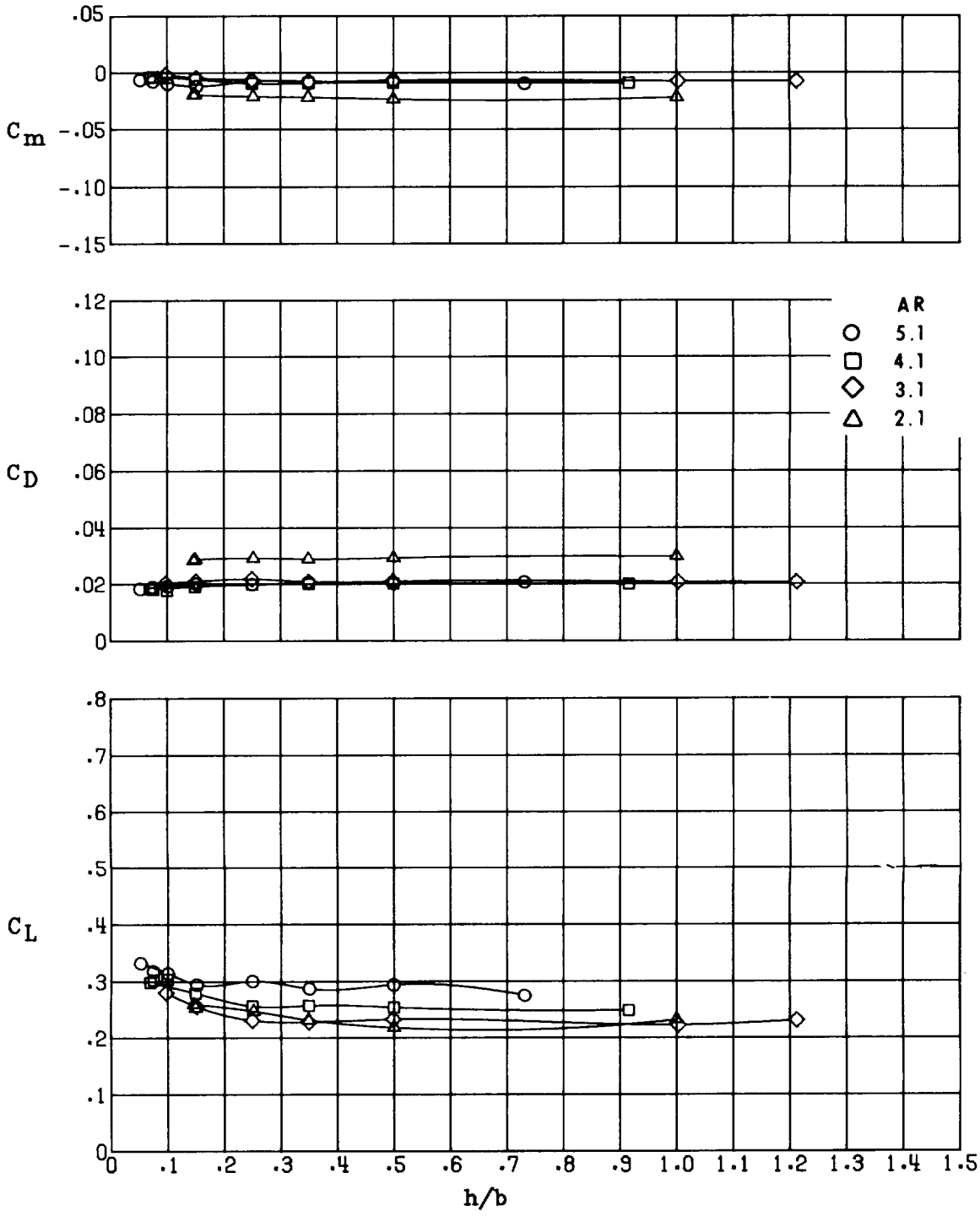

(b) $\delta_f = 5°$.

Figure 26.- Continued.

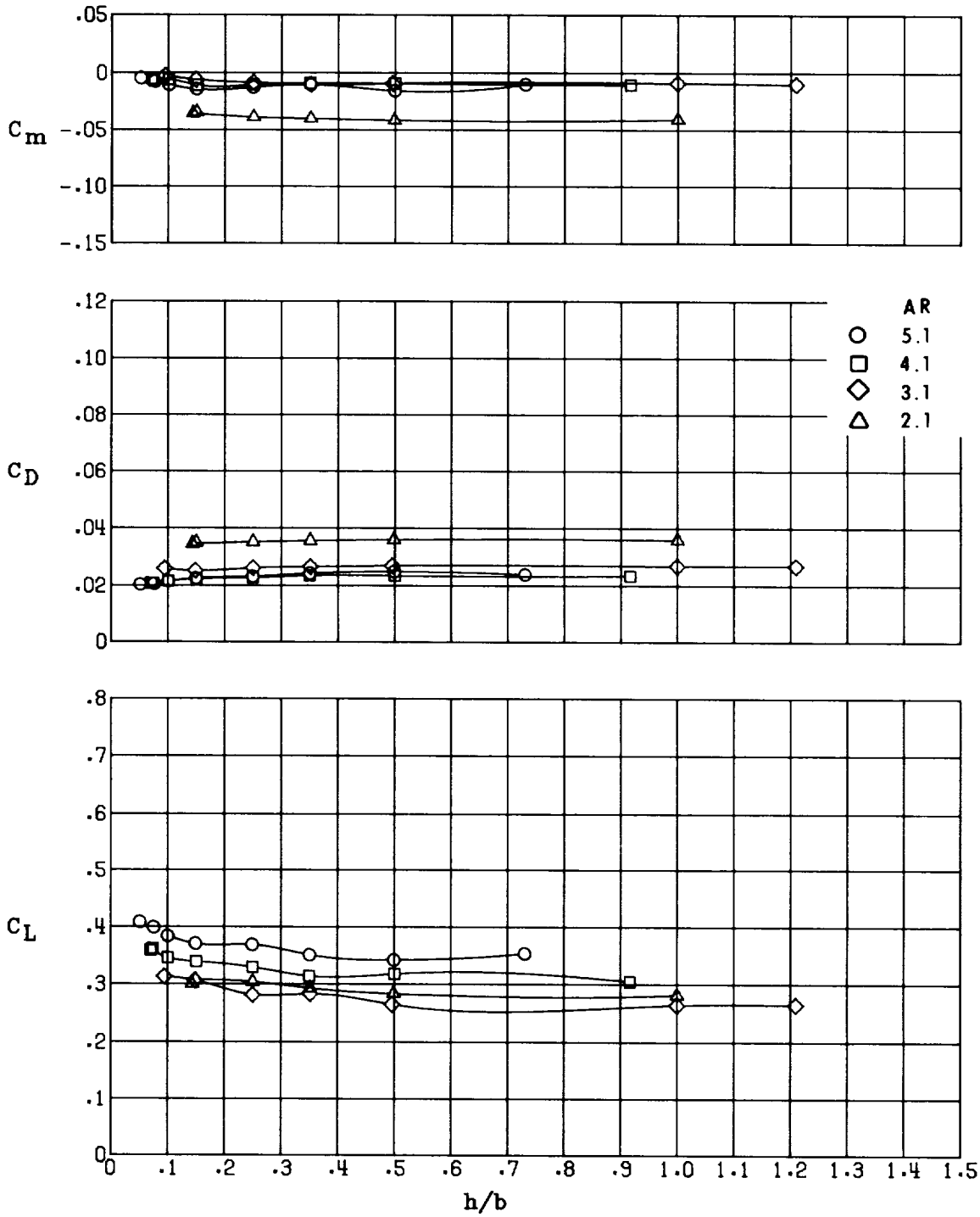

(c) δ_f = 10°.

Figure 26.- Continued.

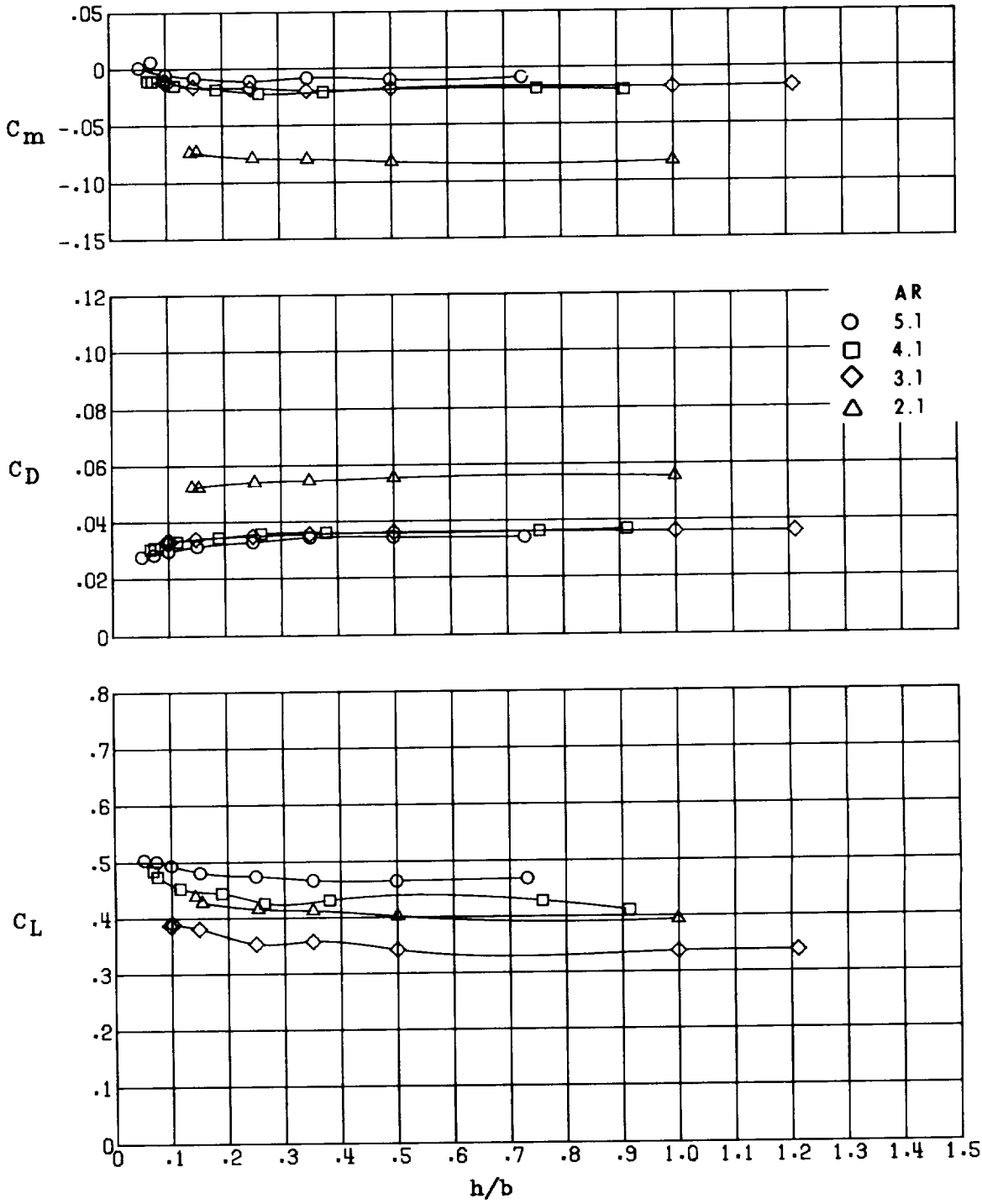

(d) $\delta_f = 20°$.

Figure 26.- Concluded.

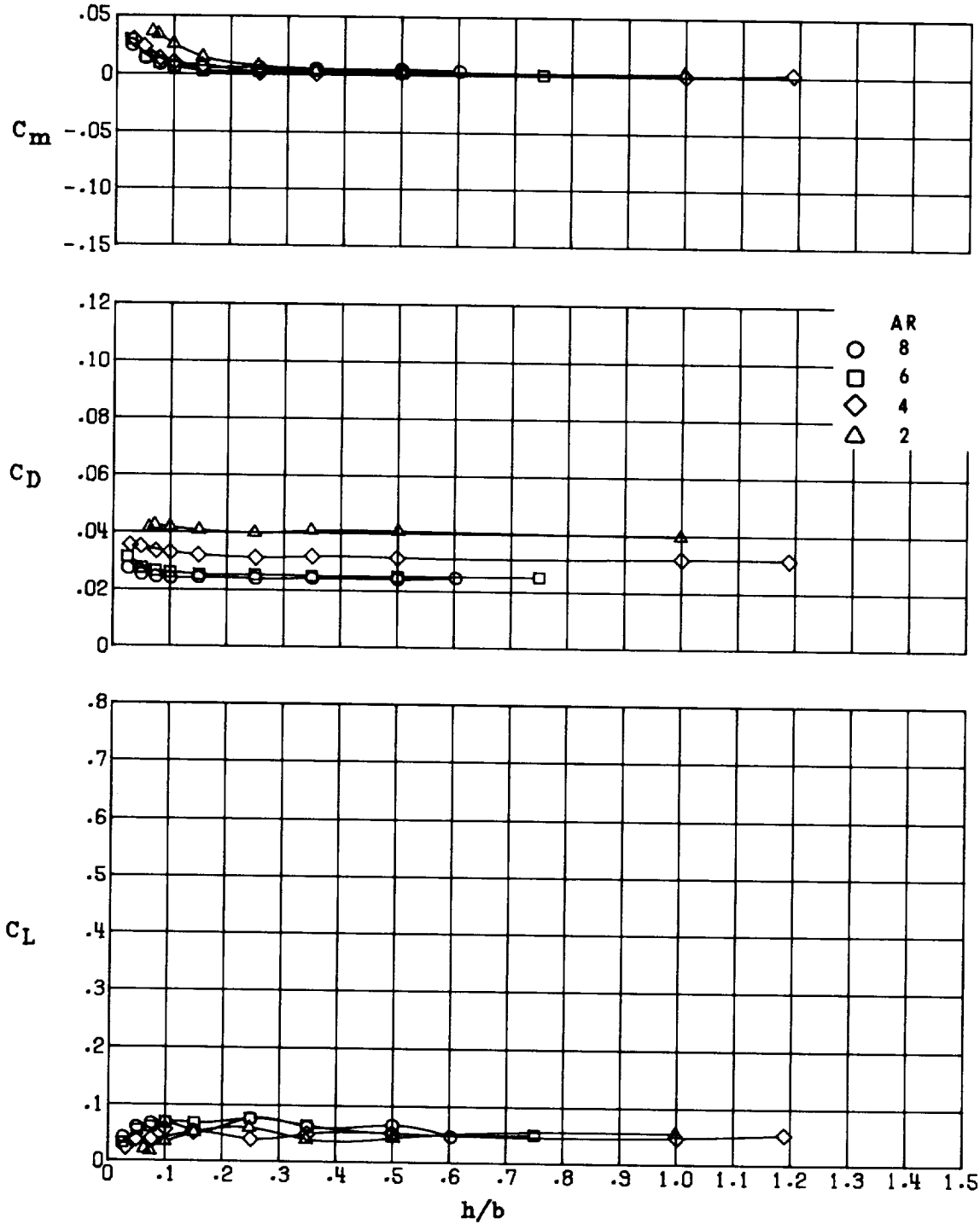

(a) $\delta_f = 0°$.

Figure 27.- Effect of aspect ratio on the longitudinal aerodynamics in ground effect of configuration I ($\Lambda = 0°$) at several flap deflections. $\delta_e = 0°$; $\alpha = 0.78°$.

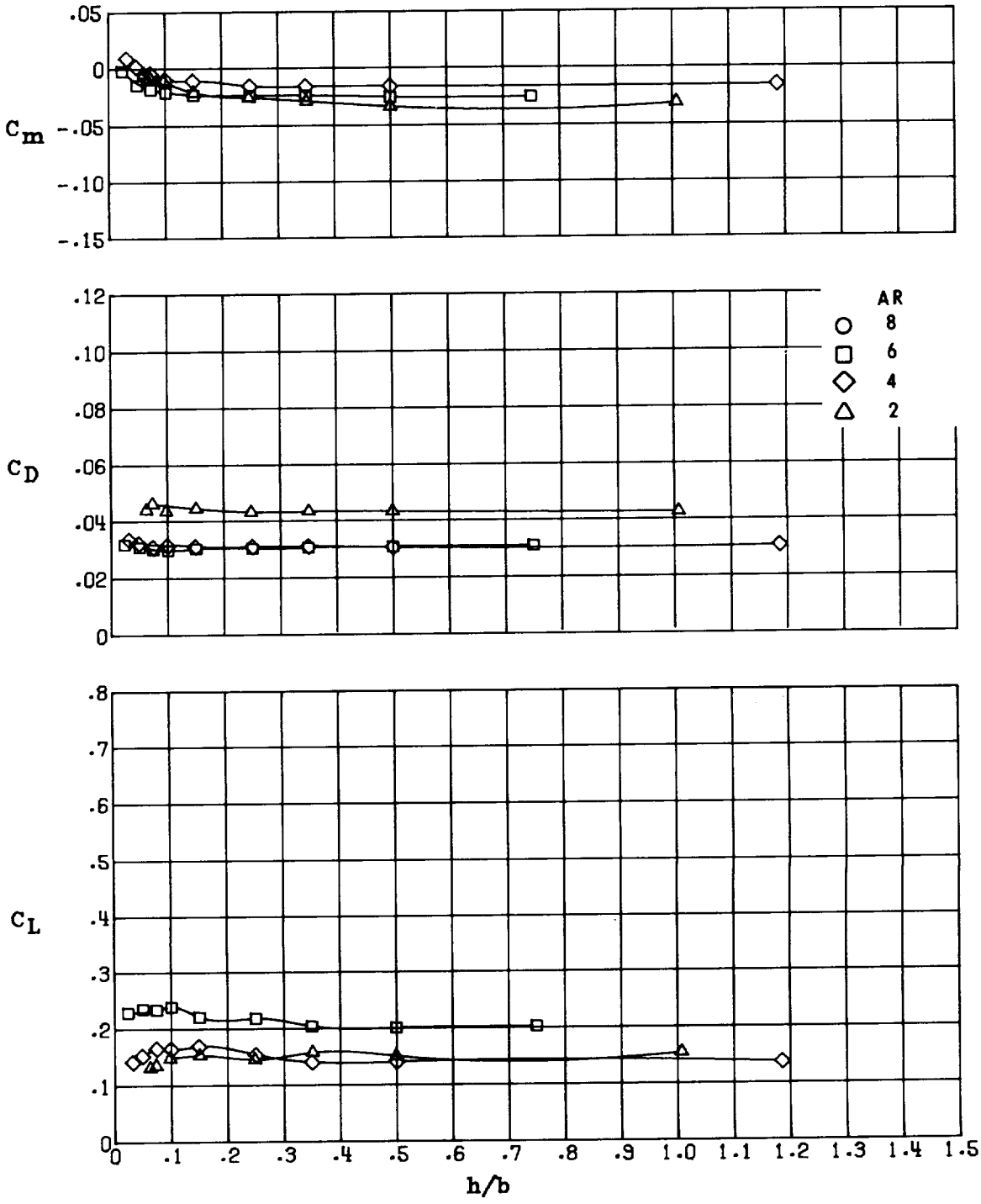

(b) $\delta_f = 5°$.

Figure 27.- Continued.

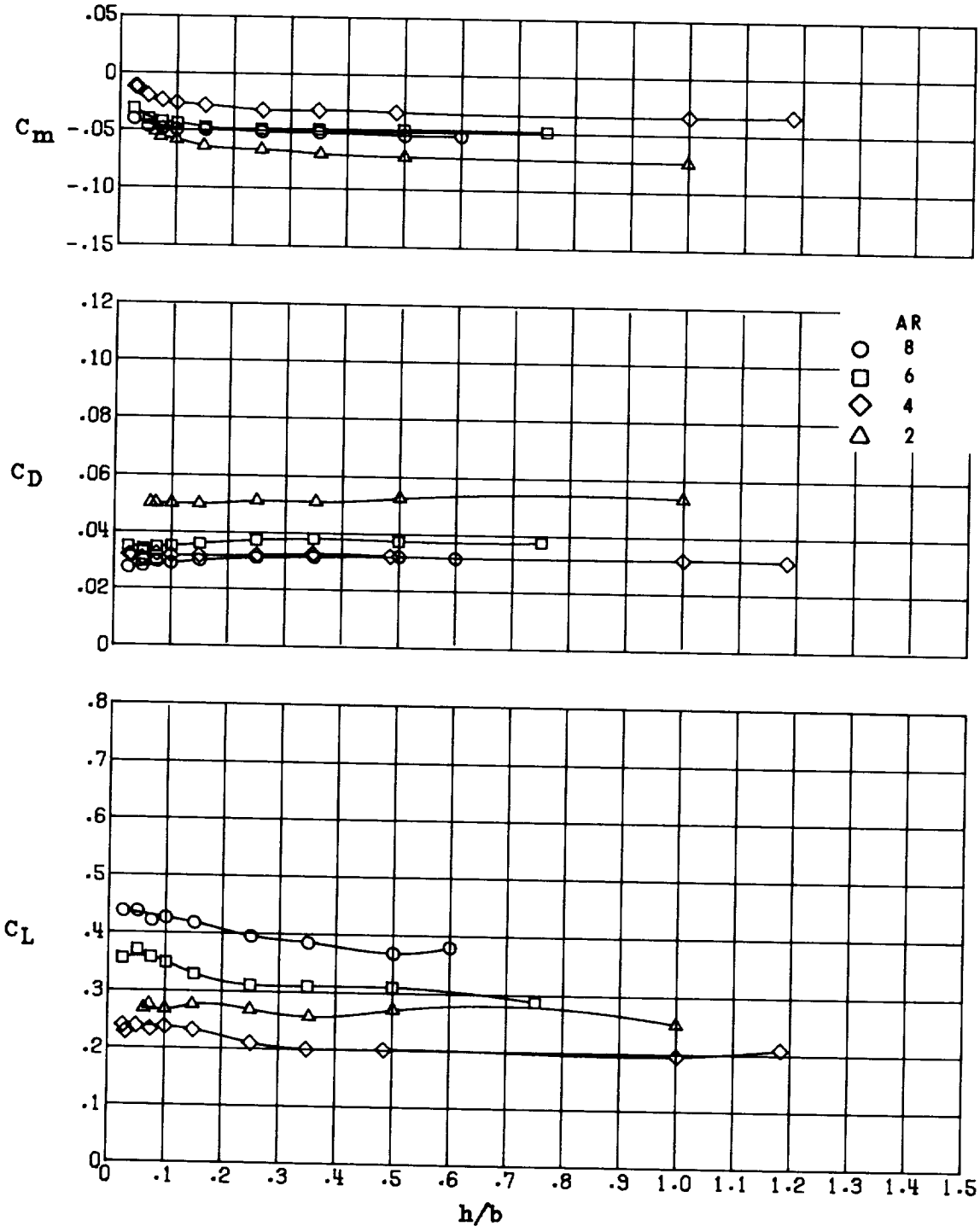

(c) δ_f = 10°.

Figure 27.- Continued.

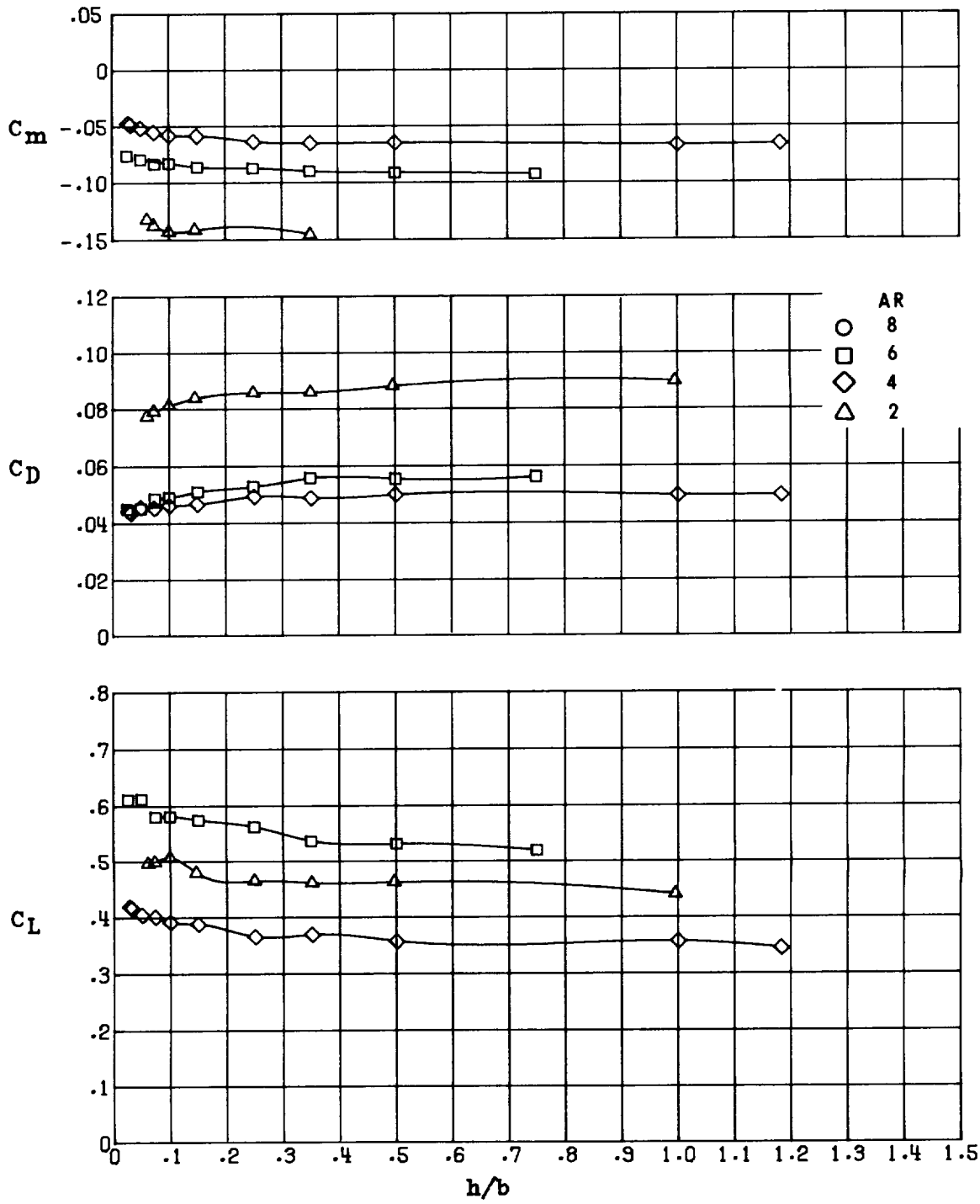

(d) $\delta_f = 20°$.

Figure 27.- Concluded.

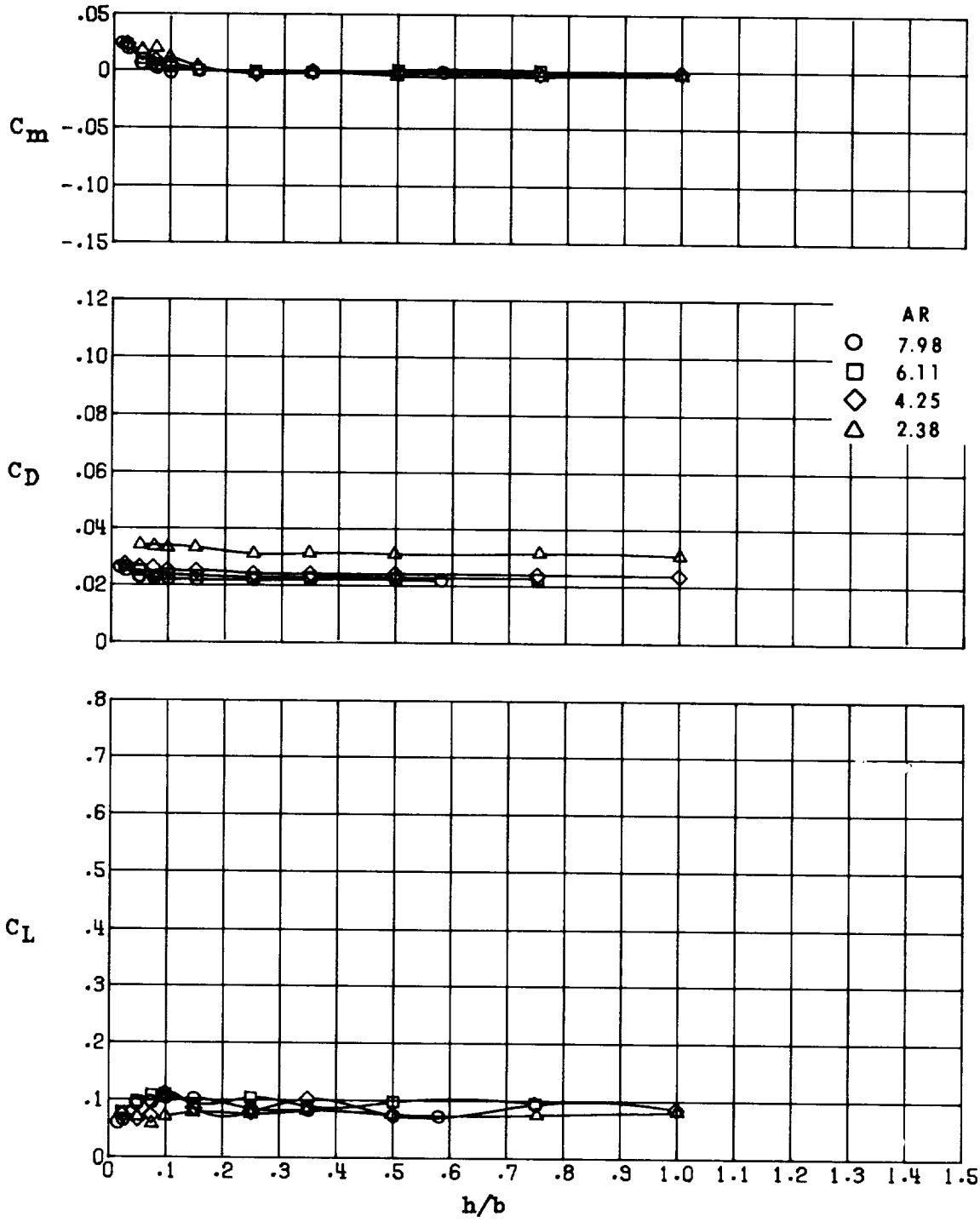

(a) $\delta_f = 0°$.

Figure 28.- Effect of aspect ratio on the longitudinal aerodynamics in ground effect of configuration II ($\Lambda = 15°$) at several flap deflections. $\delta_e = 0°$; $\alpha = 0.78°$.

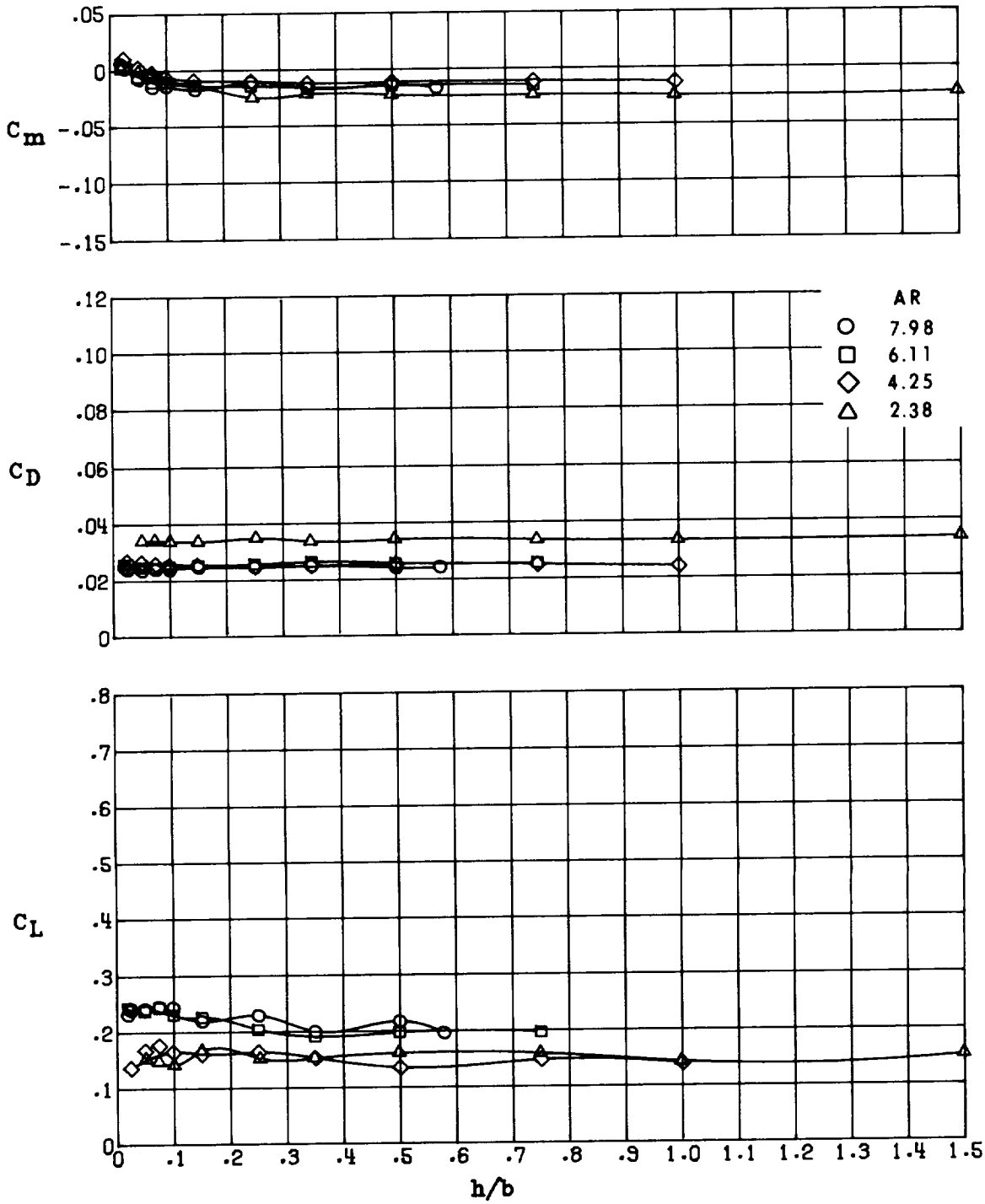

(b) $\delta_f = 5°$.

Figure 28.- Continued.

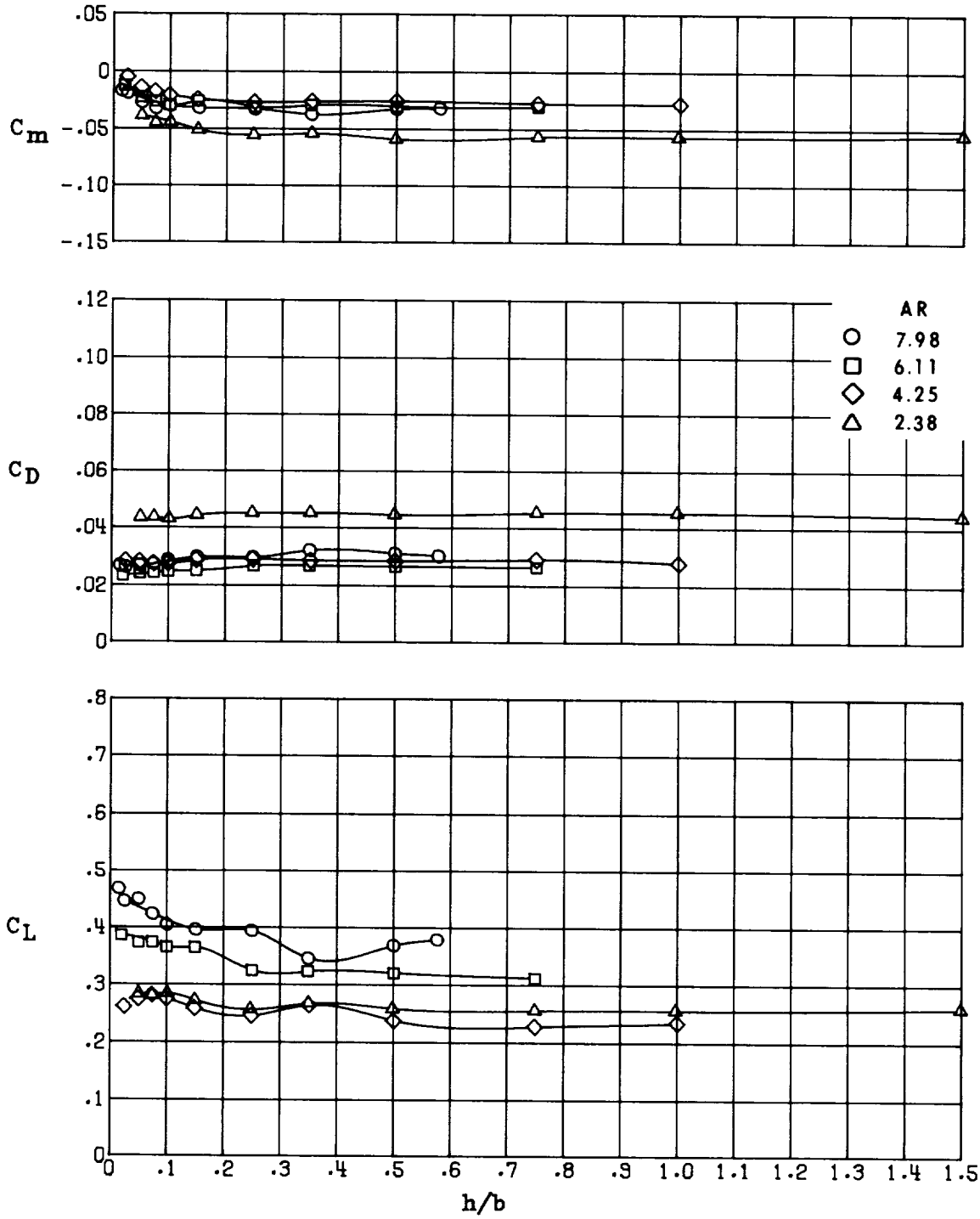

(c) $\delta_f = 10°$.

Figure 28.- Continued.

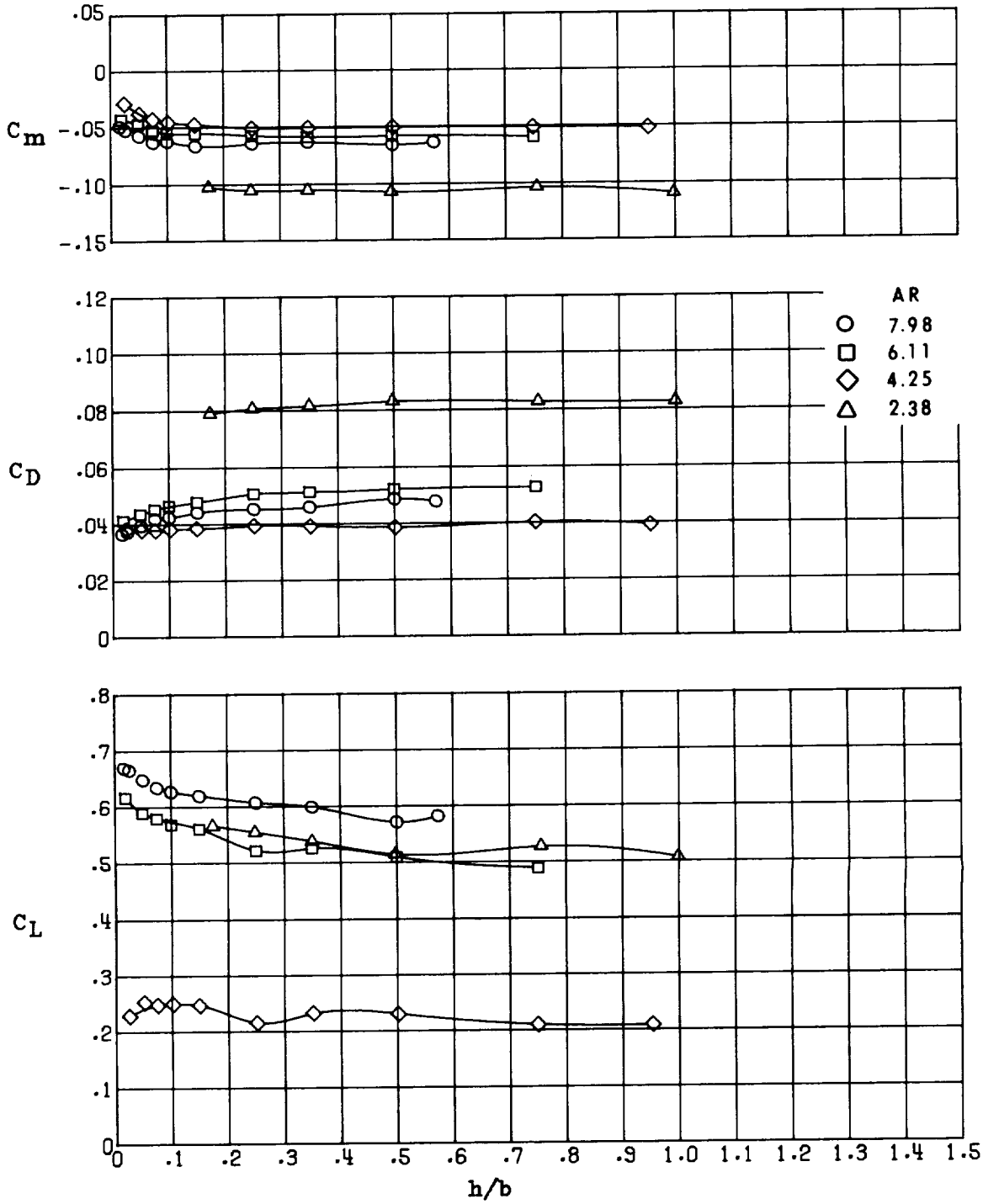

(d) $\delta_f = 20°$.

Figure 28.- Concluded.

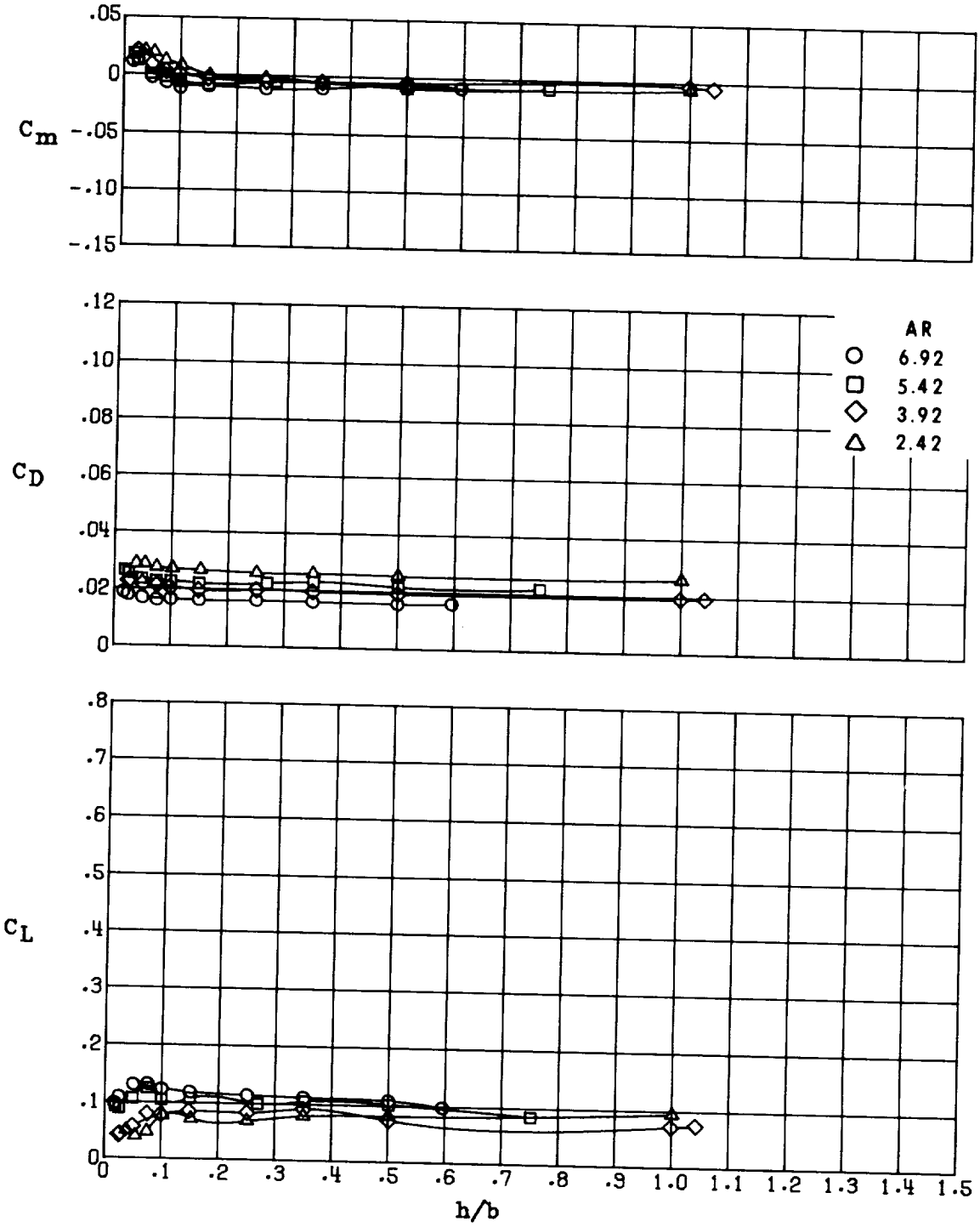

(a) $\delta_f = 0°$.

Figure 29.- Effect of aspect ratio on the longitudinal aerodynamics in ground effect of configuration III ($\Lambda = 30°$) at several flap deflections. $\delta_e = 0°$; $\alpha = 0.78°$.

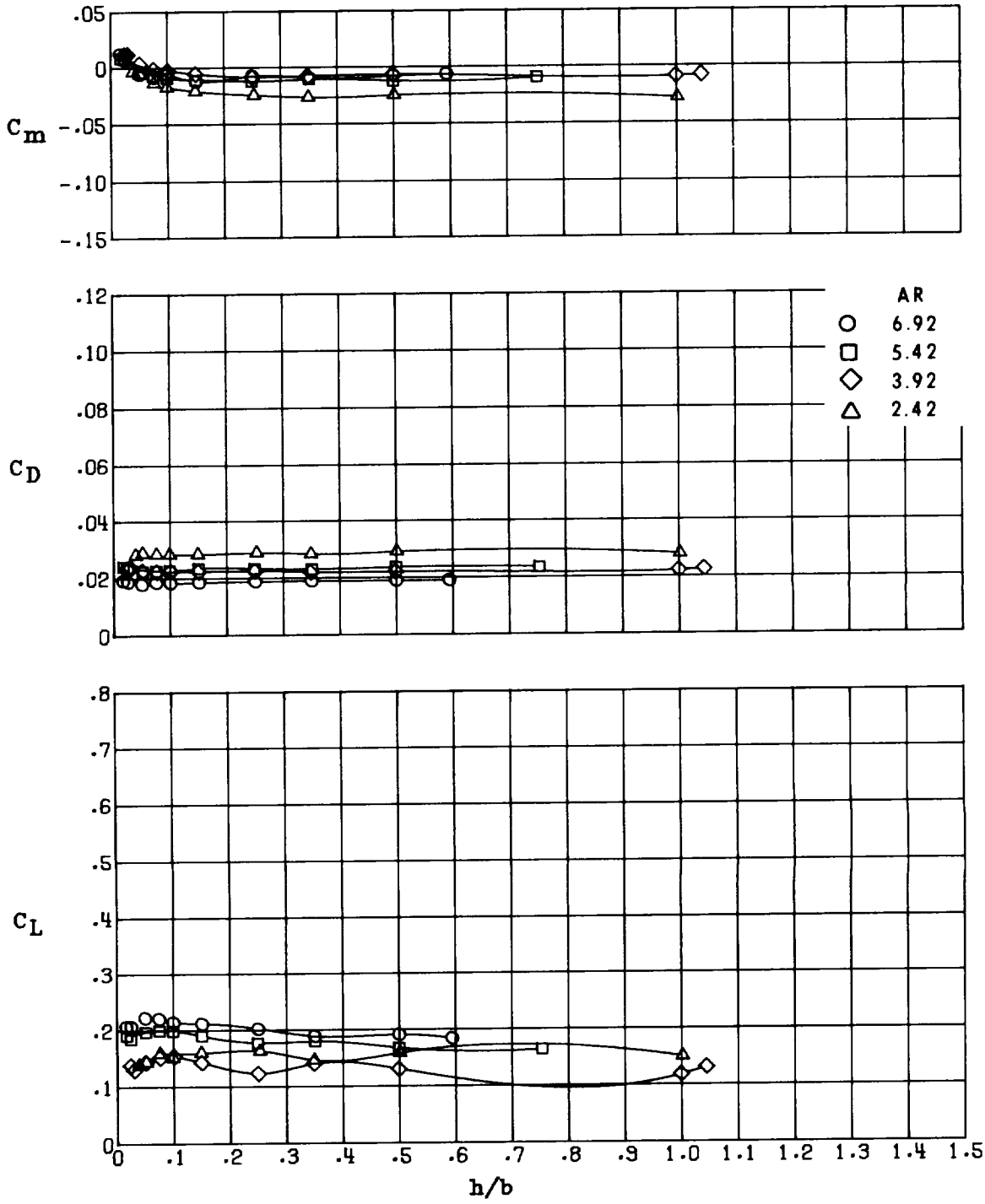

(b) $\delta_f = 5°$.

Figure 29.- Continued.

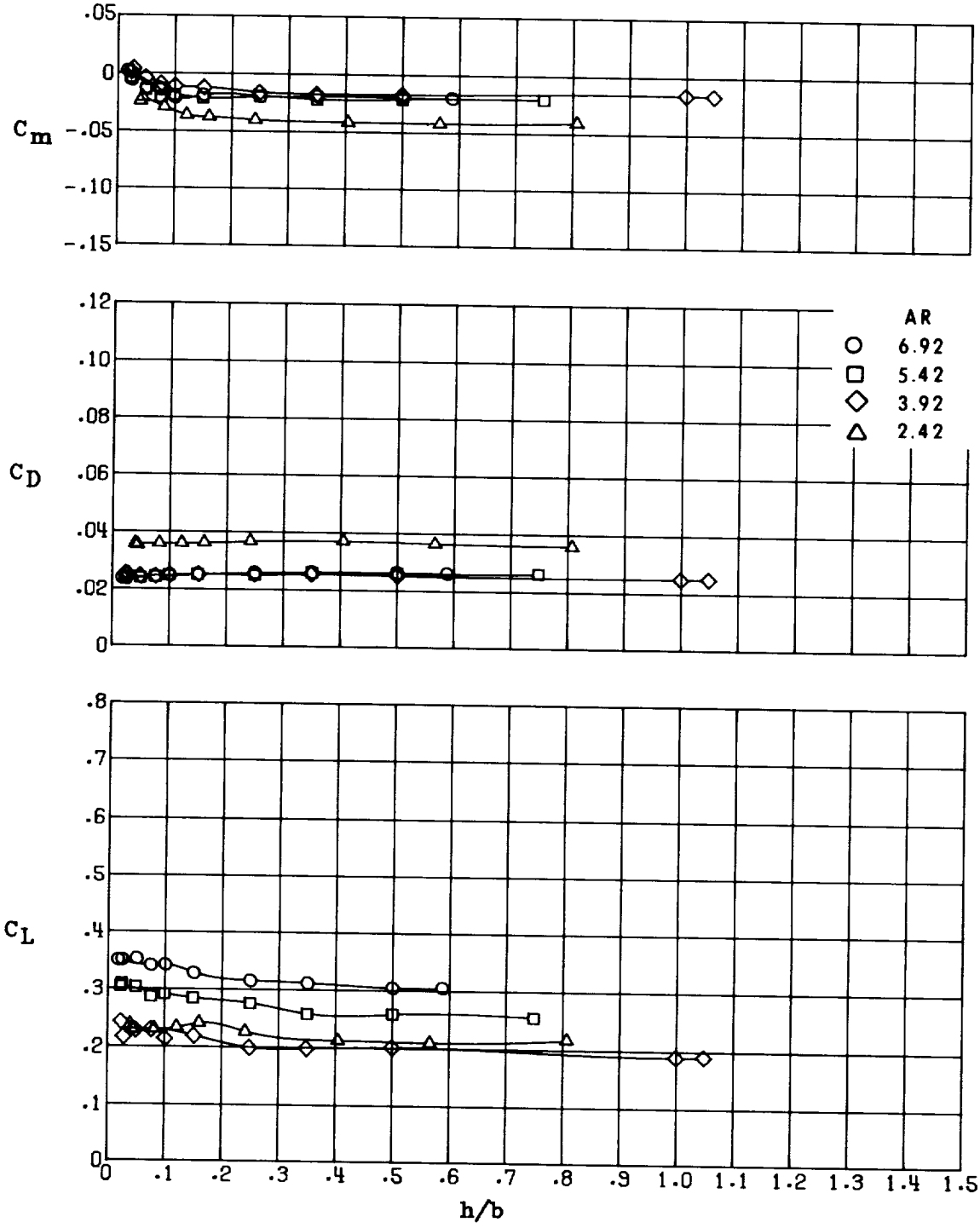

(c) $\delta_f = 10°$.

Figure 29.- Continued.

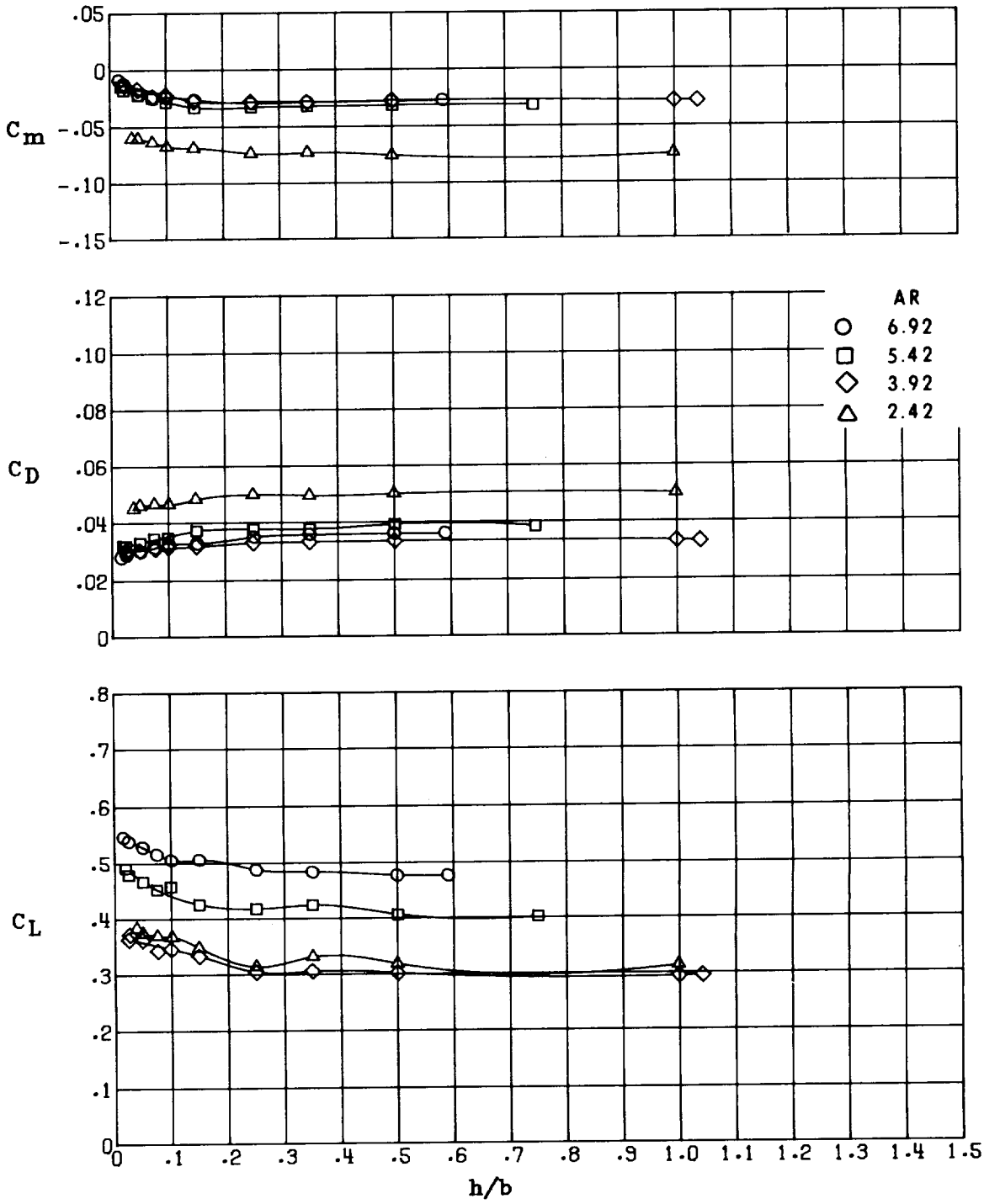

(d) $\delta_f = 20°$.

Figure 29.- Concluded.

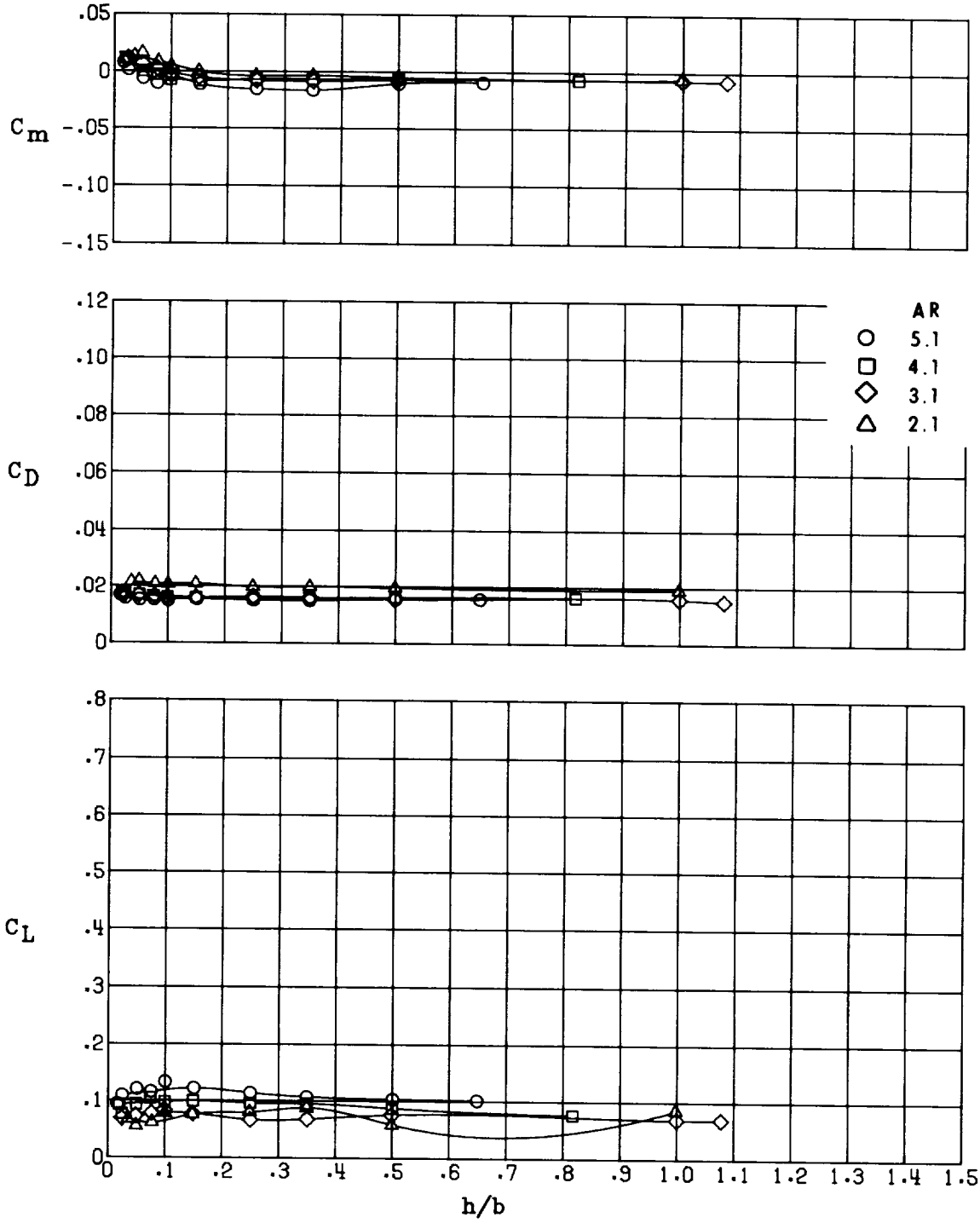

(a) $\delta_f = 0°$.

Figure 30.- Effect of aspect ratio on the longitudinal aerodynamics in ground effect of configuration IV ($\Lambda = 45°$) at several flap deflections. $\delta_e = 0°$; $\alpha = 0.78°$.

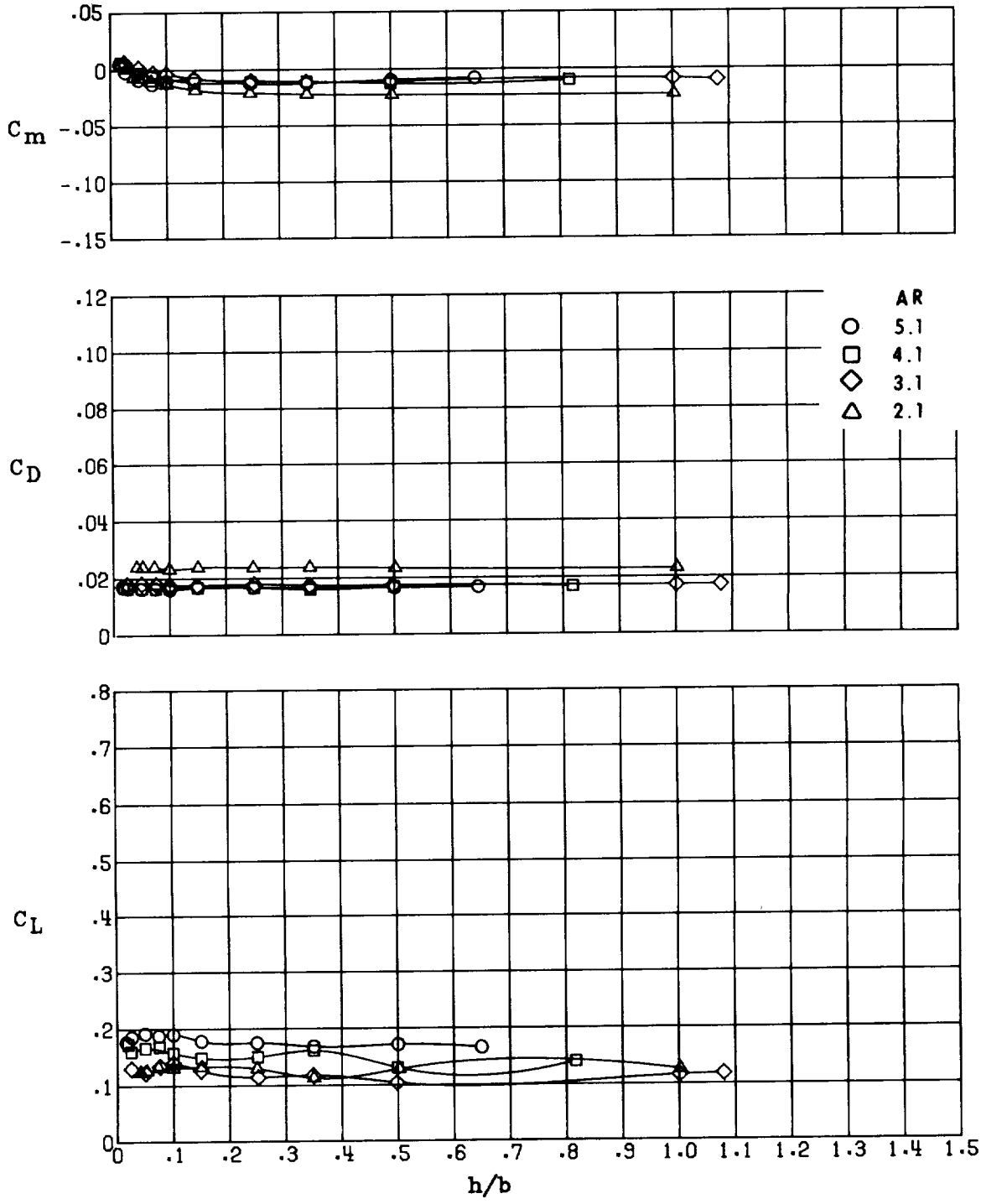

(b) $\delta_f = 5°$.

Figure 30.- Continued.

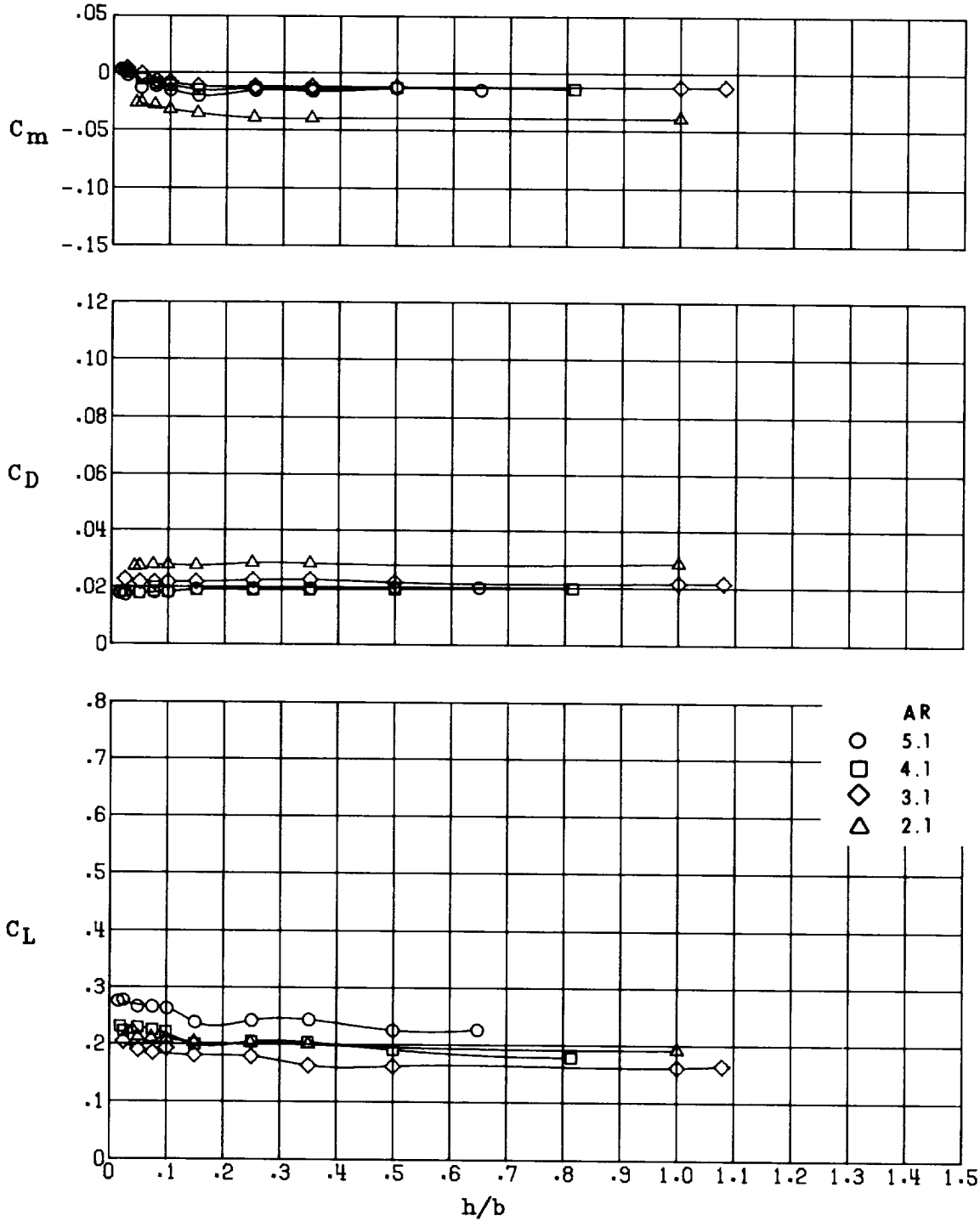

(c) δ_f = 10°.

Figure 30.- Continued.

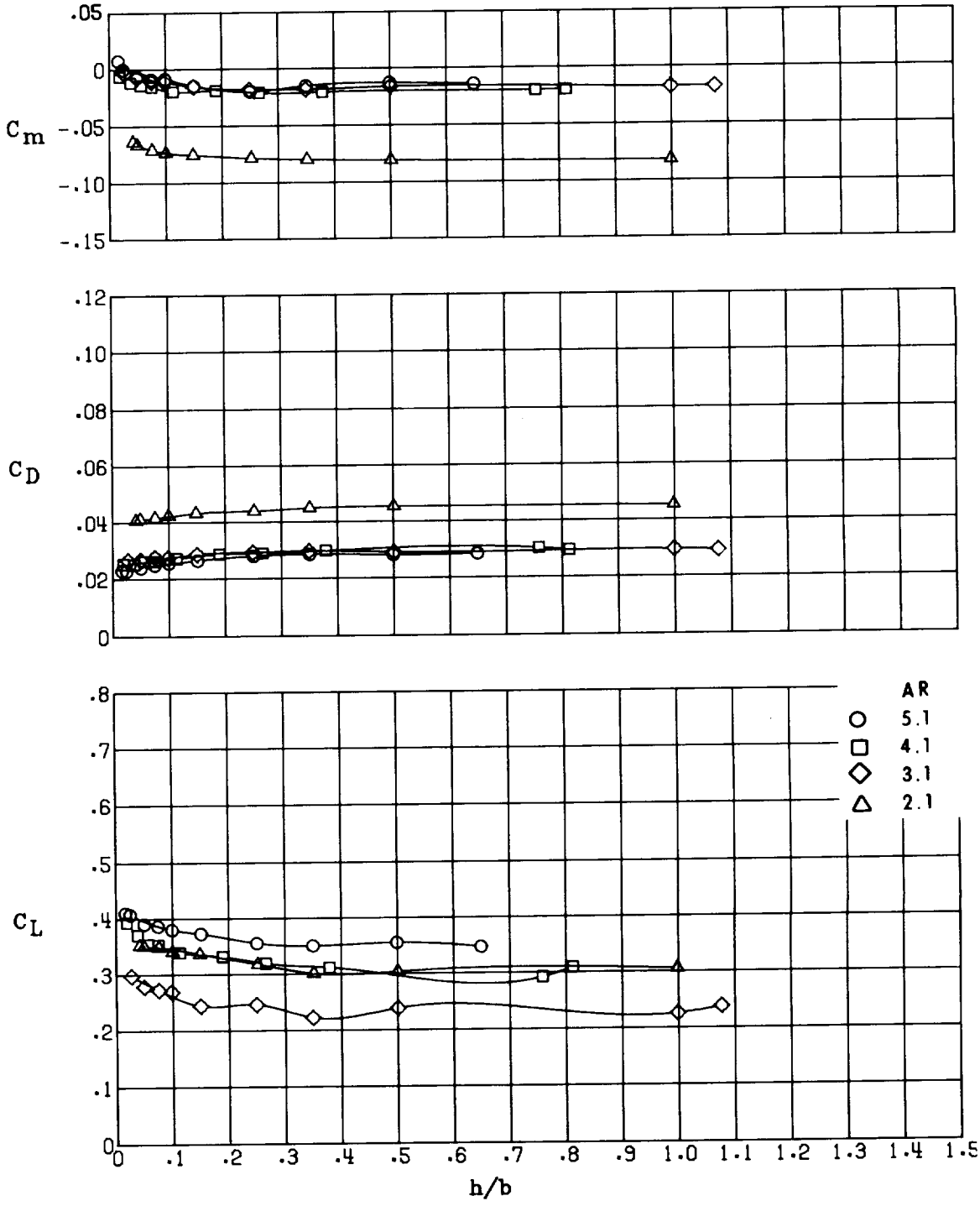

(d) $\delta_f = 20°$.

Figure 30.- Concluded.

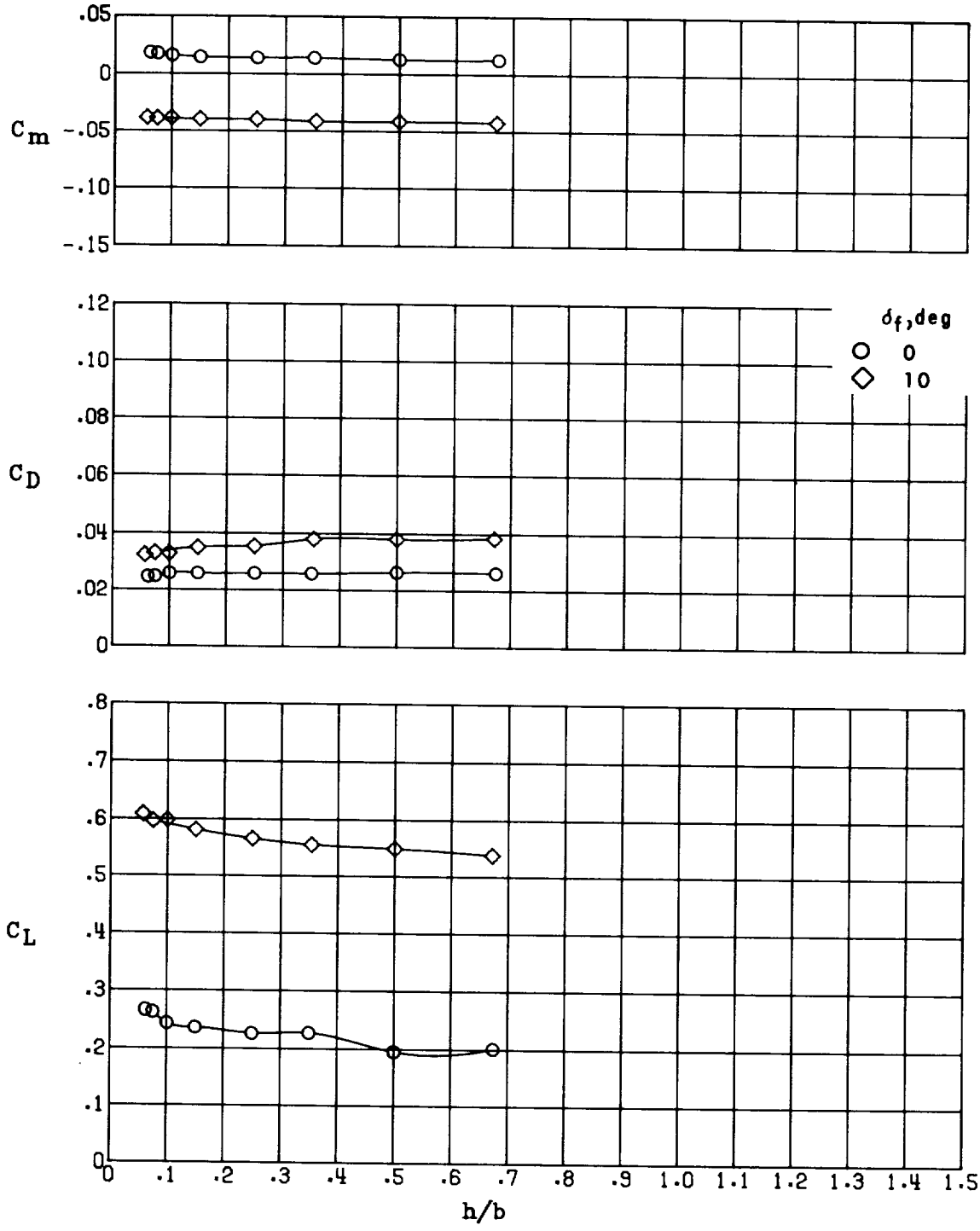

(a) AR = 8.

Figure 31.- Effect of flap deflection on the longitudinal aerodynamics in ground effect of configuration I (Λ = 0°) at several aspect ratios. δ_e = 0°; α = 2.78°.

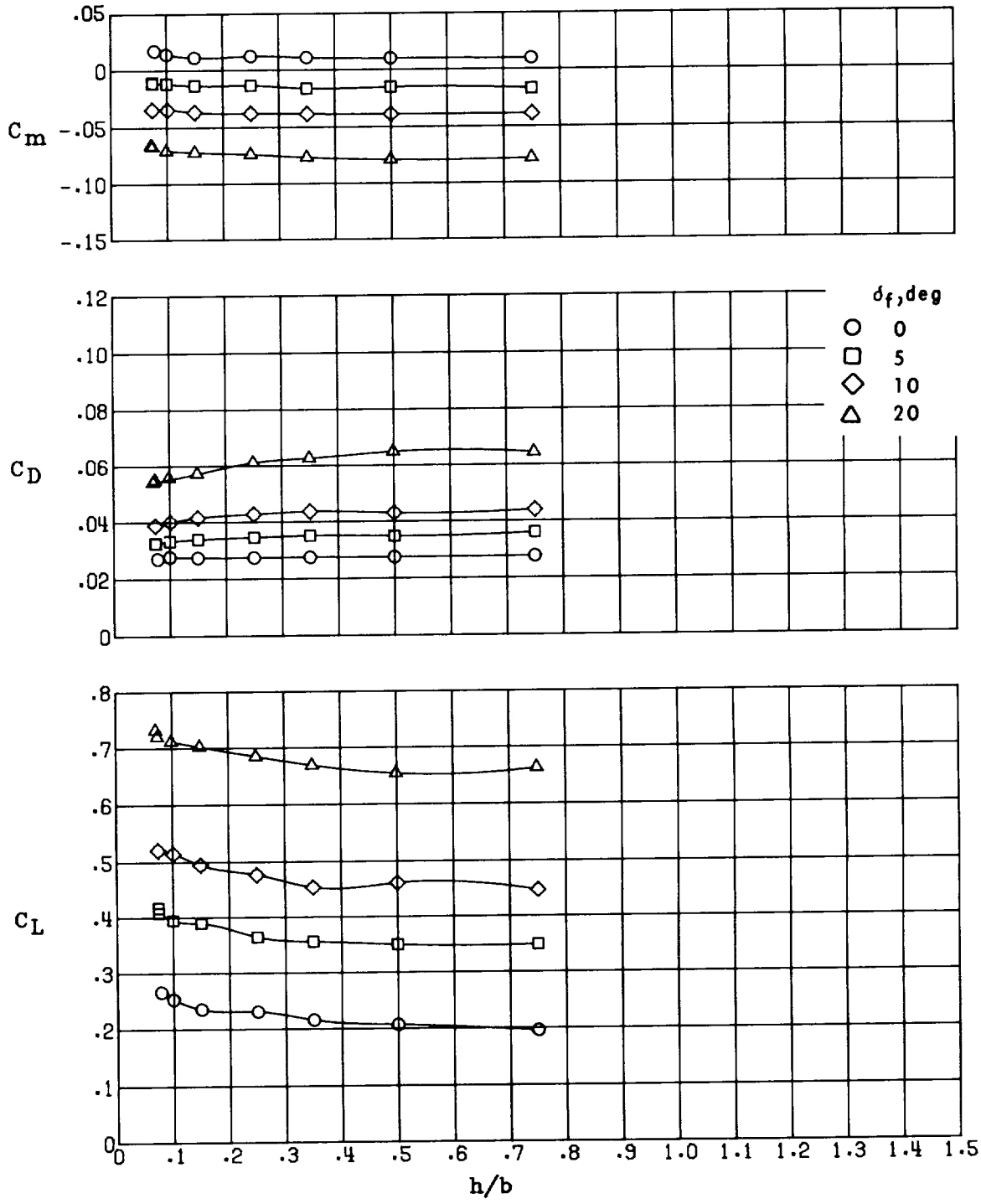

(b) AR = 6.

Figure 31.- Continued.

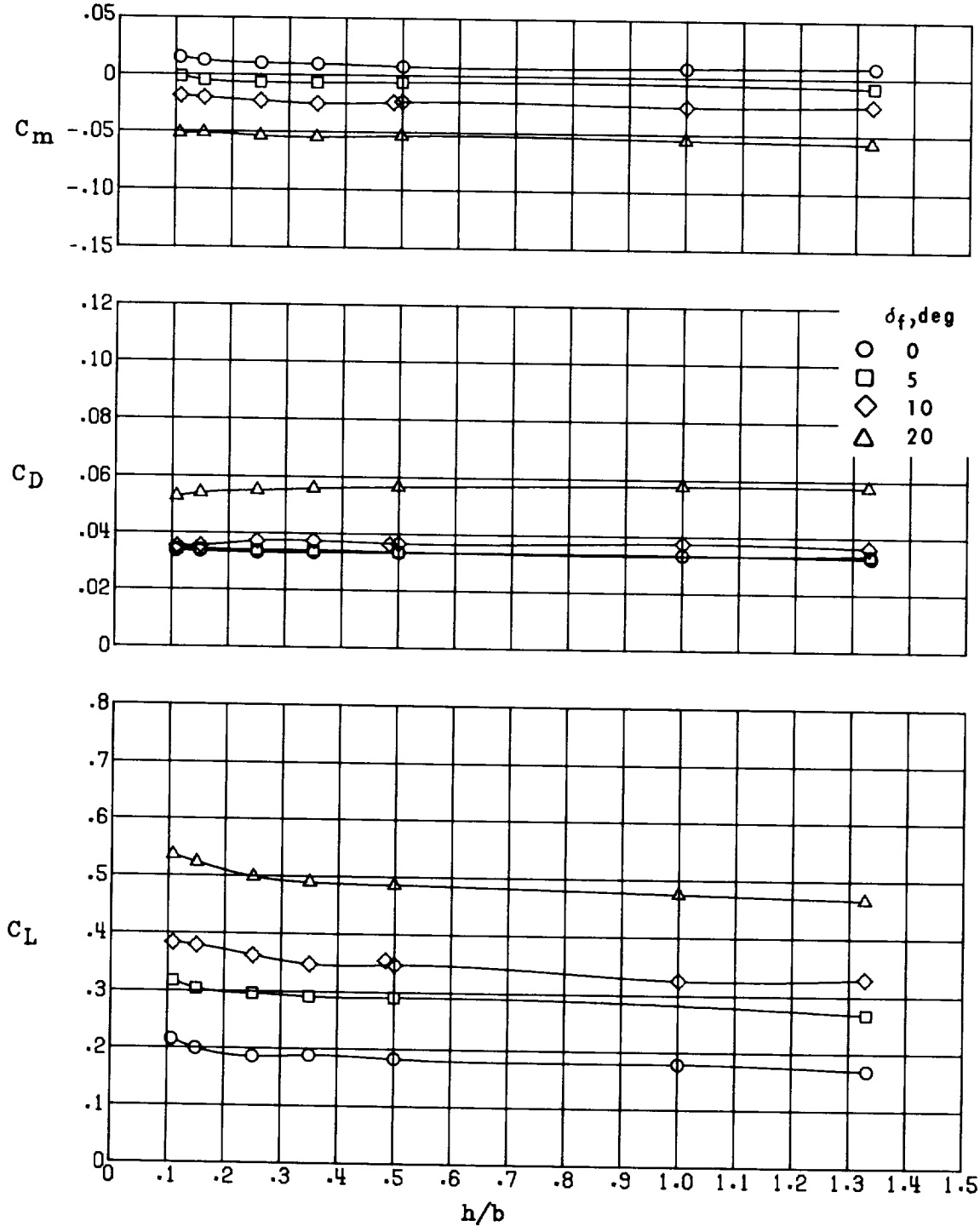

(c) AR = 4.

Figure 31.- Continued.

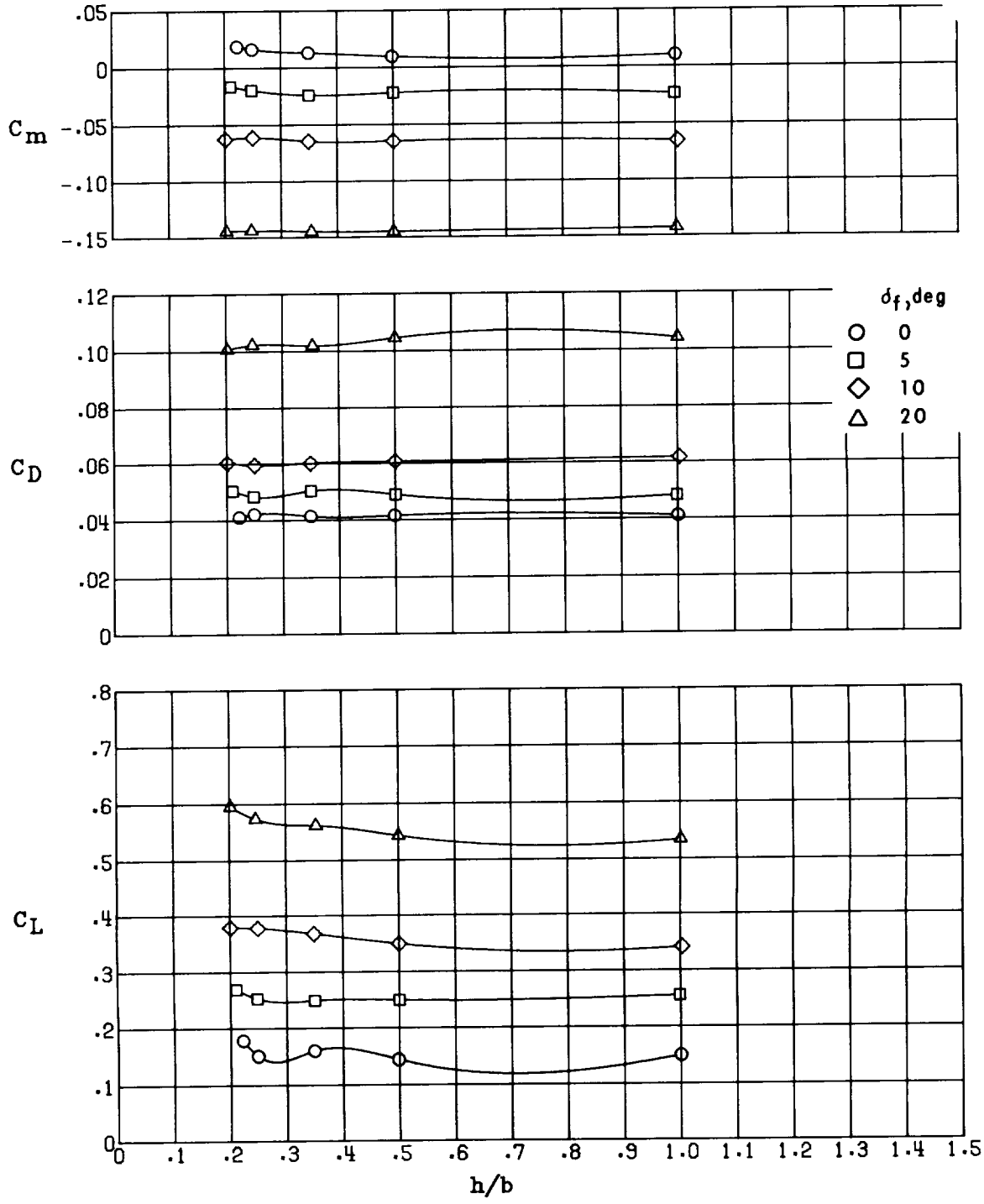

(d) AR = 2.

Figure 31.- Concluded.

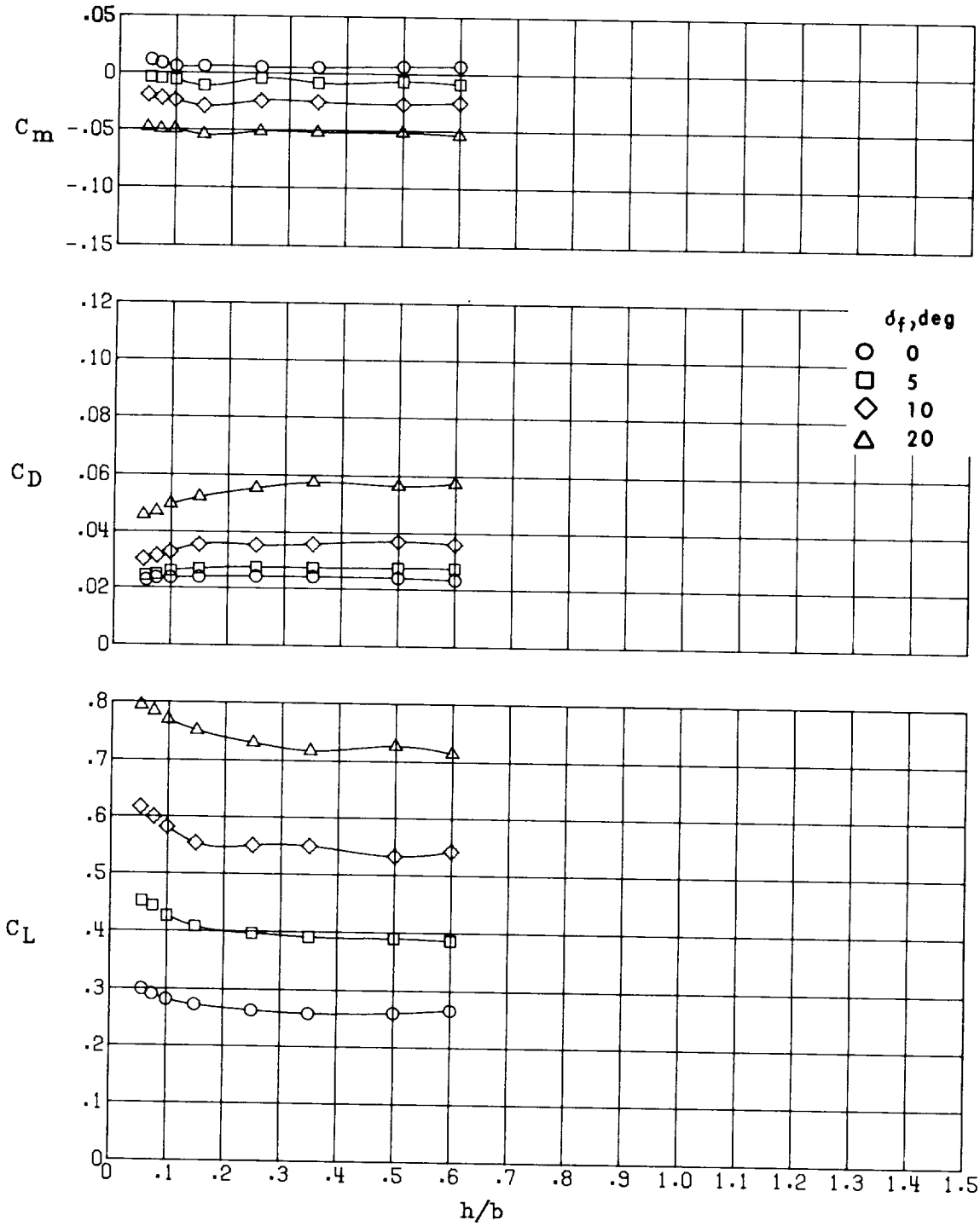

(a) AR = 7.98.

Figure 32.- Effect of flap deflection on the longitudinal aerodynamics in ground effect of configuration II (Λ = 15°) at several aspect ratios. δ_e = 0°; α = 2.78°.

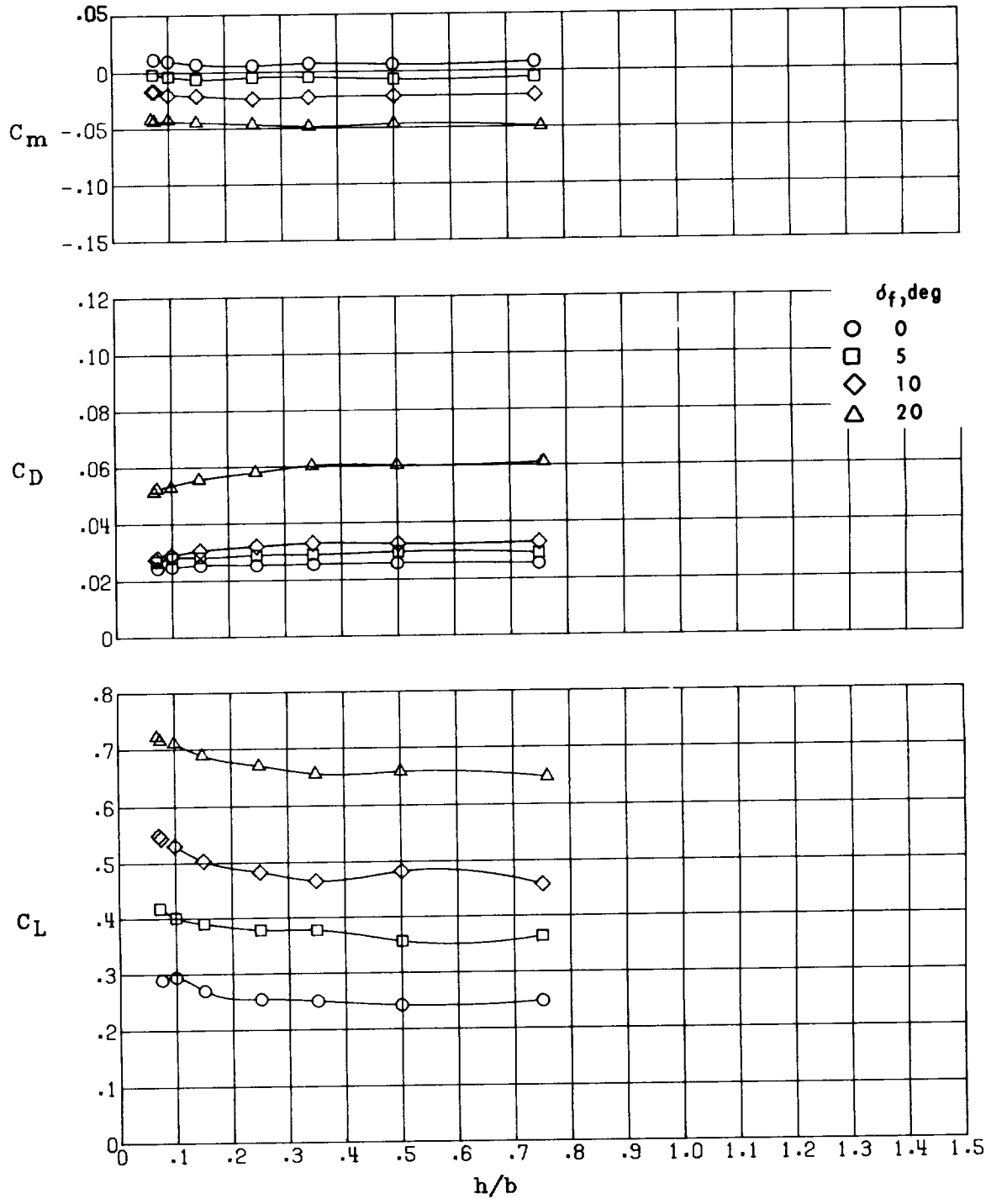

(b) AR = 6.11.

Figure 32.- Continued.

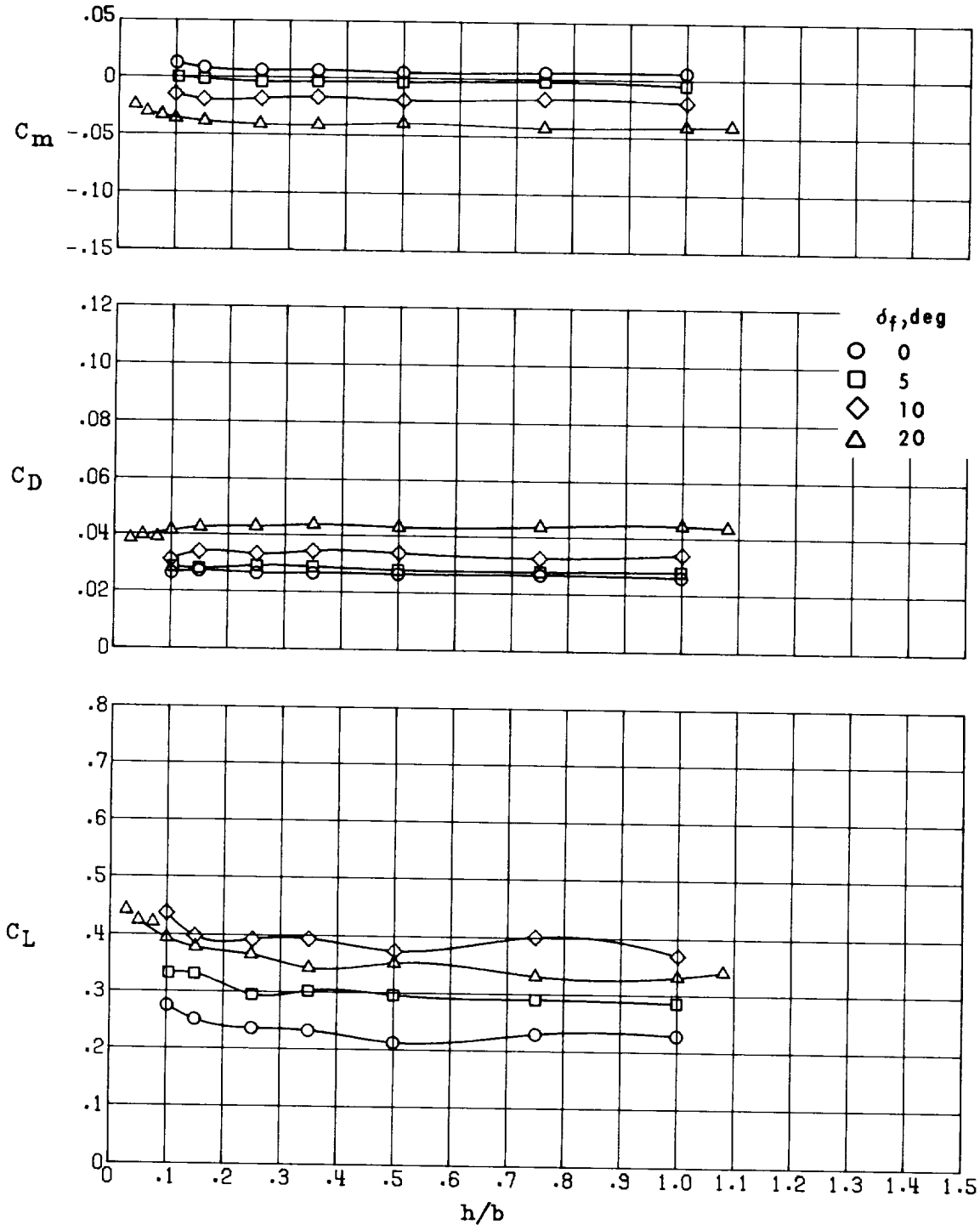

(c) AR = 4.25.

Figure 32.- Continued.

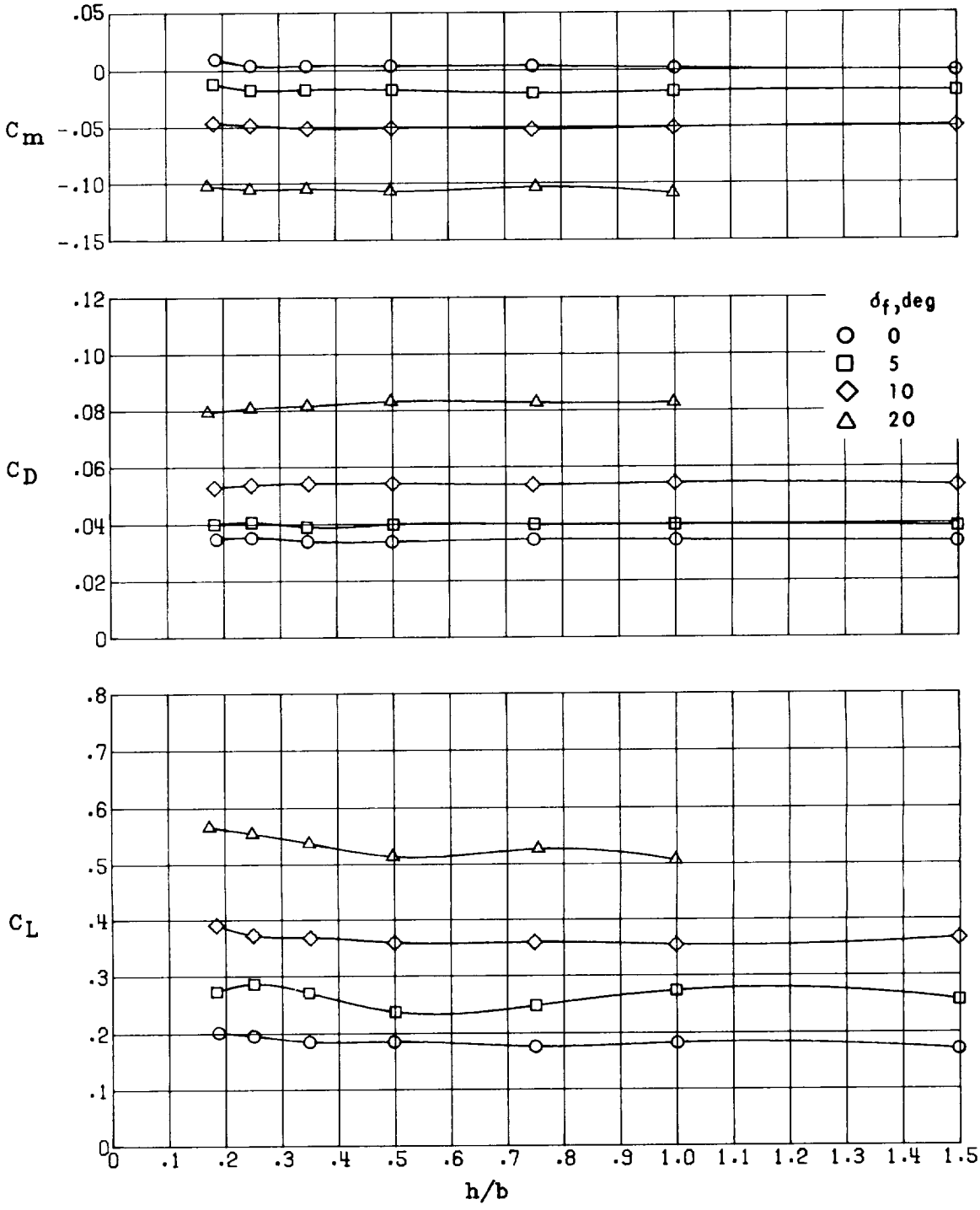

(d) AR = 2.38.

Figure 32.- Concluded.

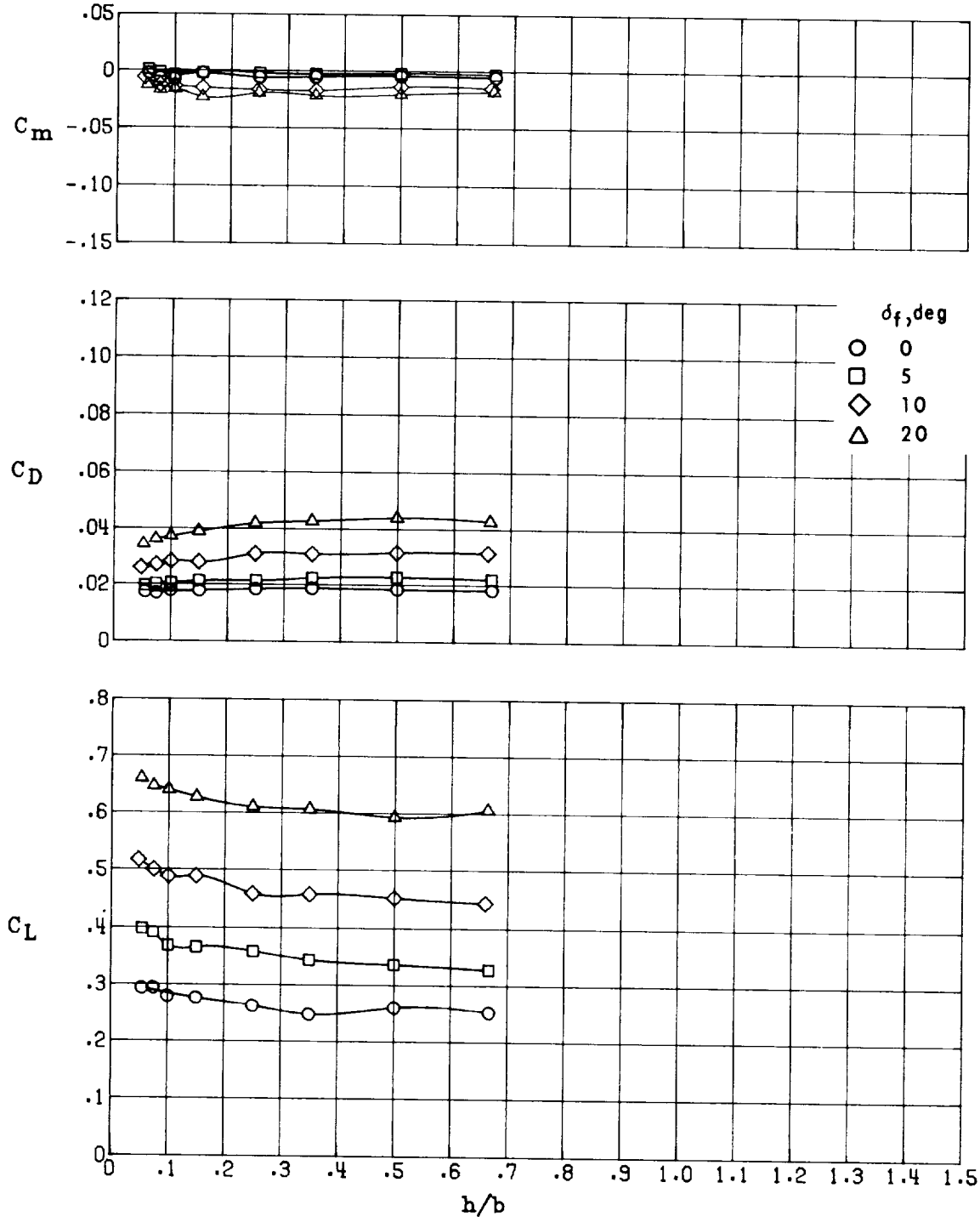

(a) AR = 6.92.

Figure 33.- Effect of flap deflection on the longitudinal aerodynamics in ground effect of configuration III (Λ = 30°) at several aspect ratios. δ_e = 0°; α = 2.78°.

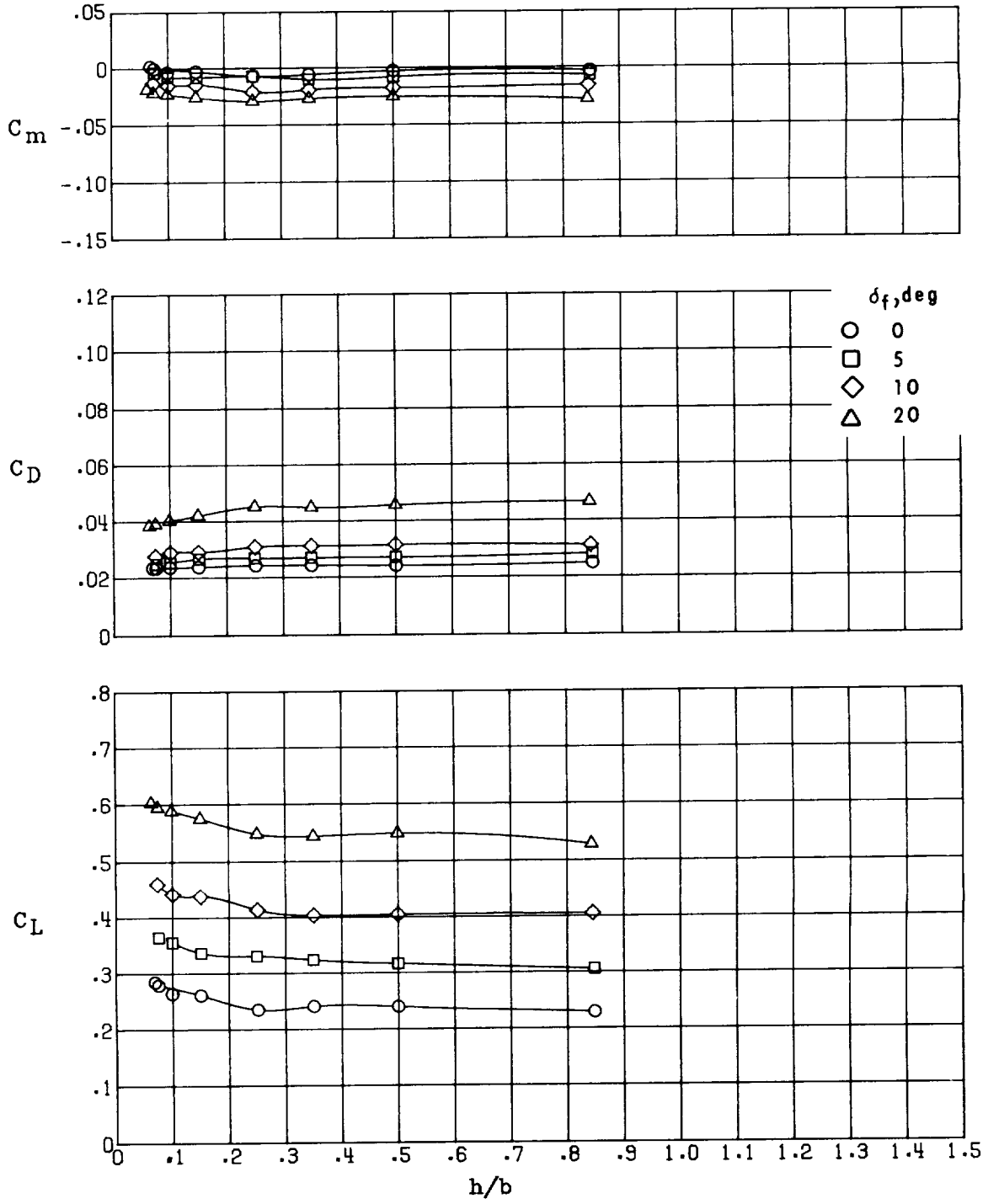

(b) AR = 5.42.

Figure 33.- Continued.

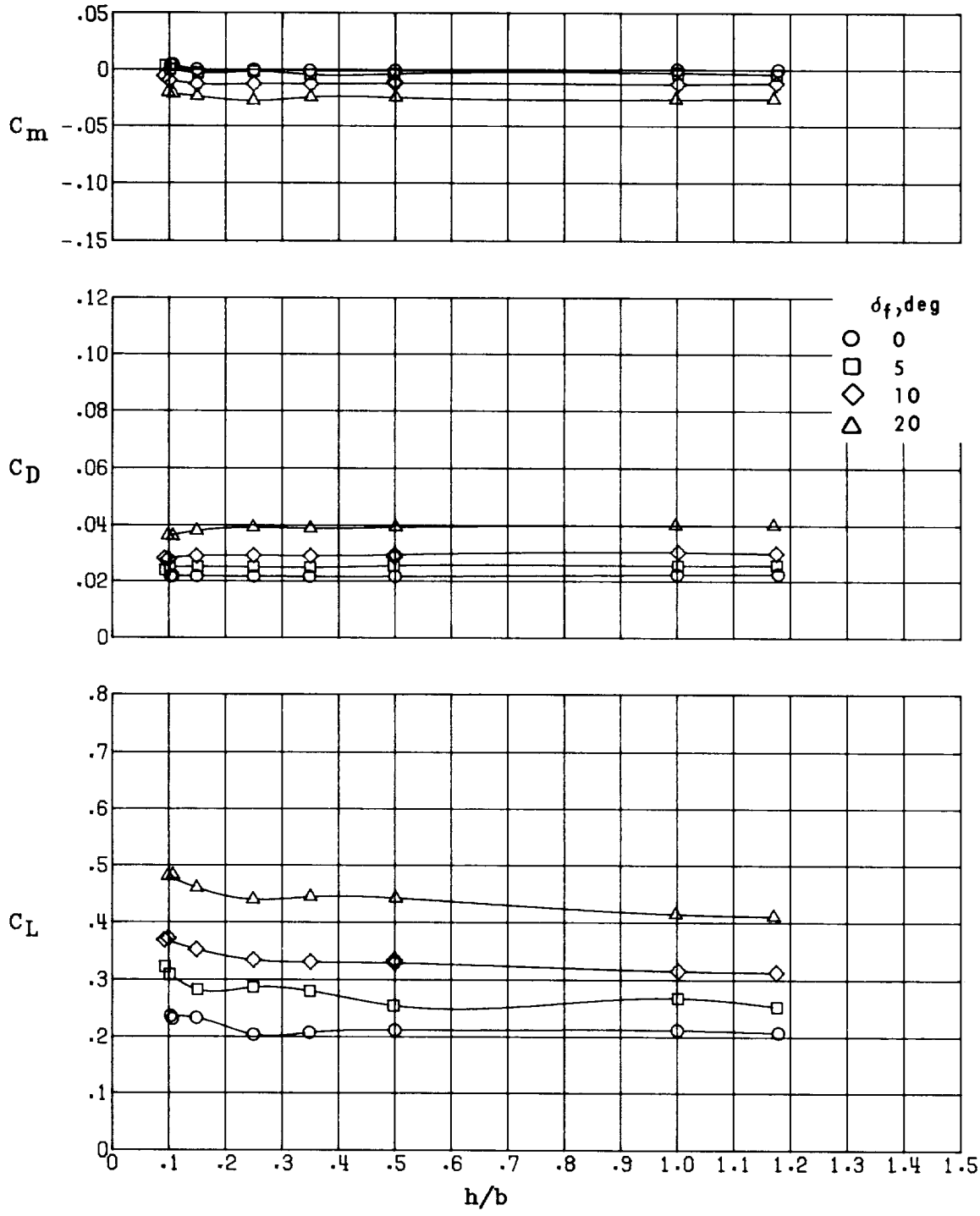

(c) AR = 3.92.

Figure 33.- Continued.

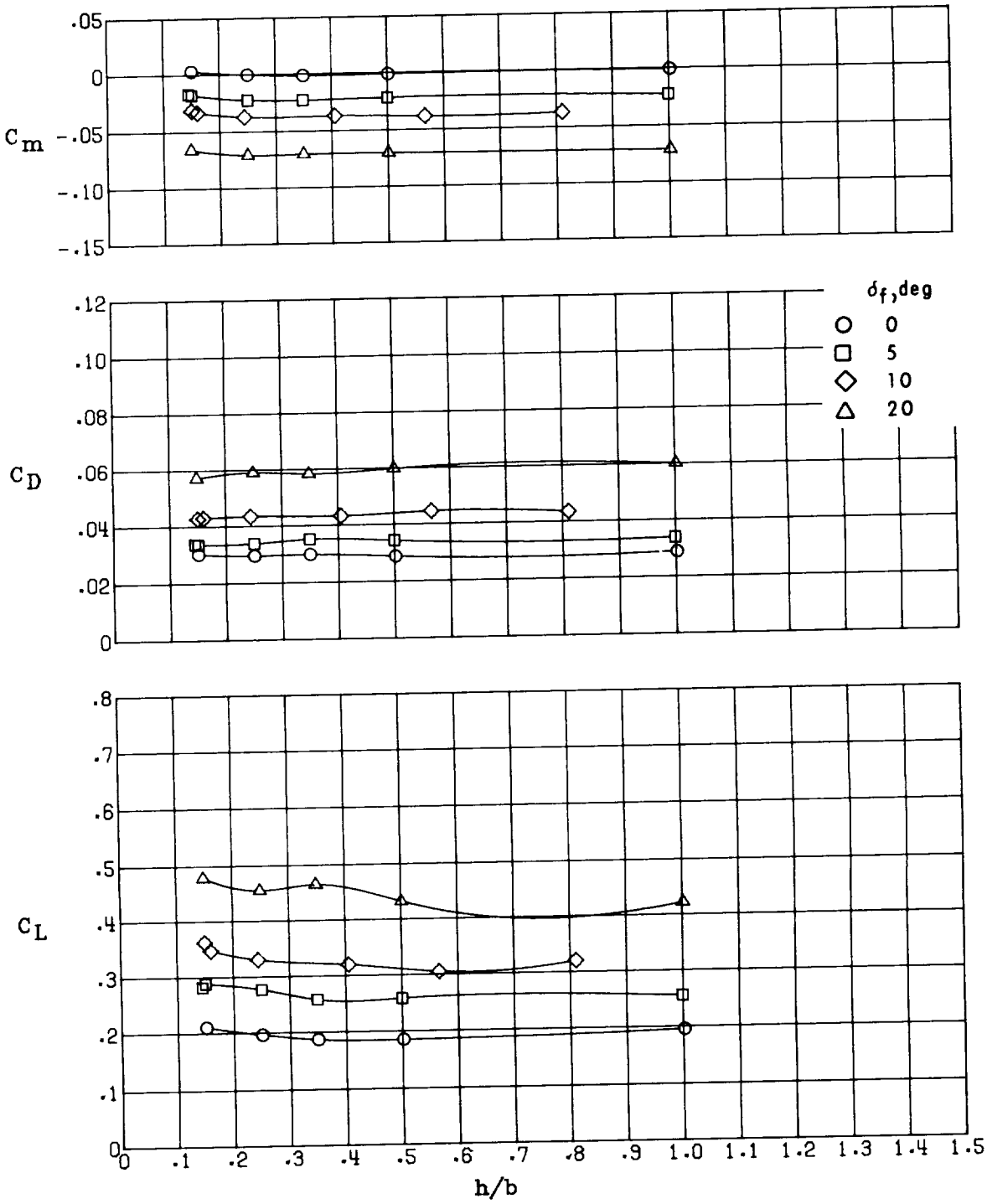

(d) AR = 2.42.

Figure 33.- Concluded.

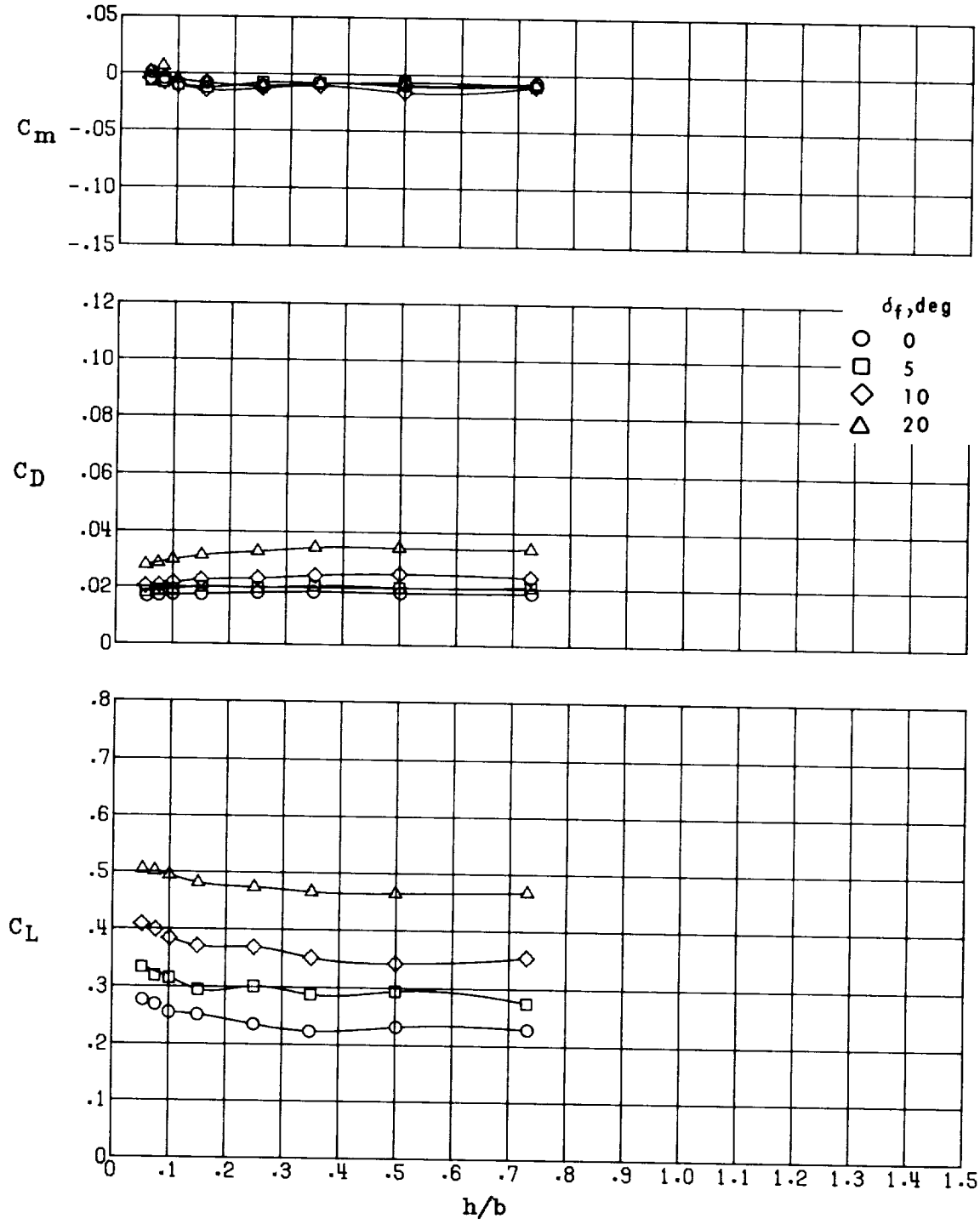

(a) AR = 5.1.

Figure 34.- Effect of flap deflection on the longitudinal aerodynamics in ground effect of configuration IV (Λ = 45°) at several aspect ratios. δ_e = 0°; α = 2.78°.

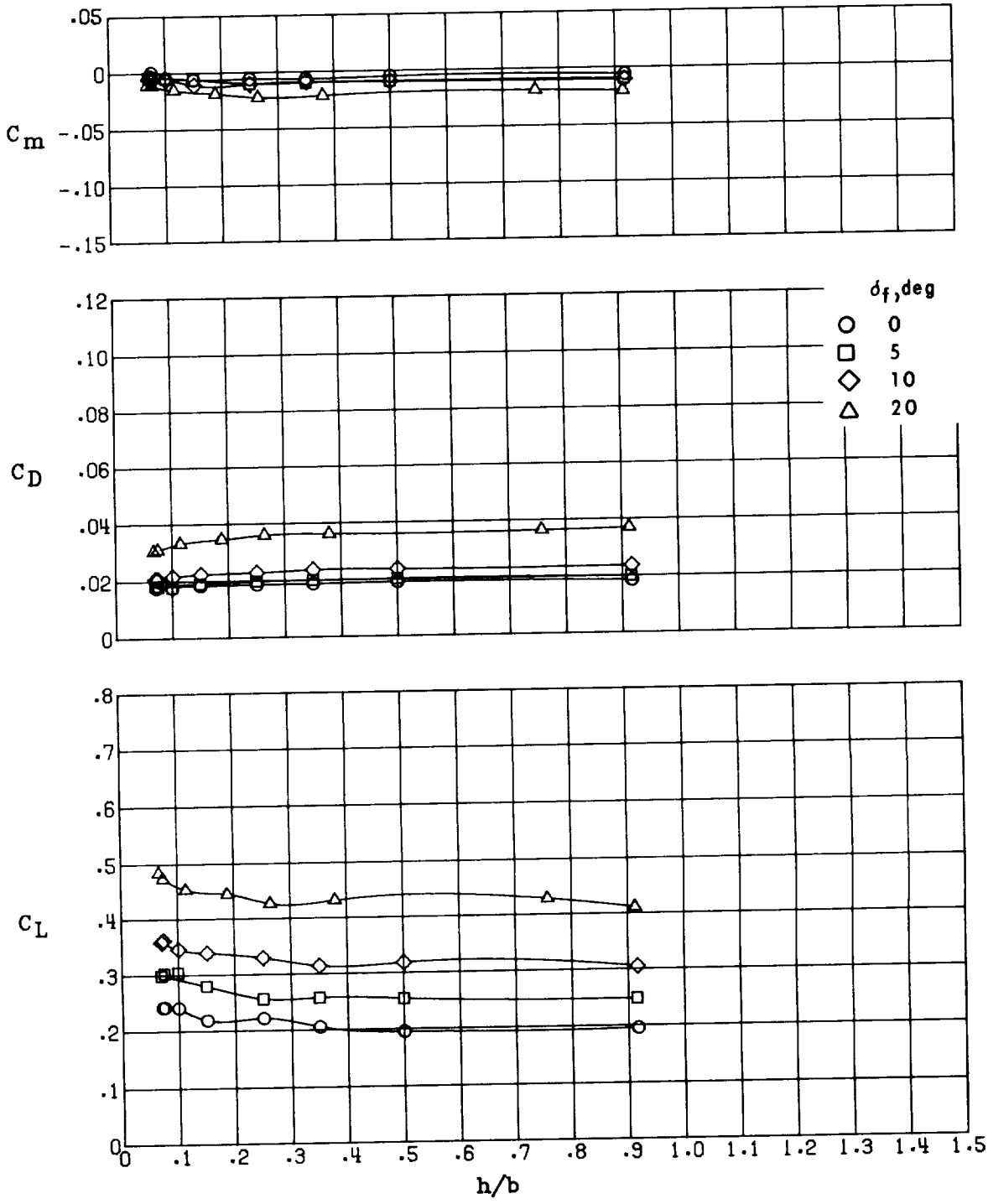

(b) AR = 4.1.

Figure 34.- Continued.

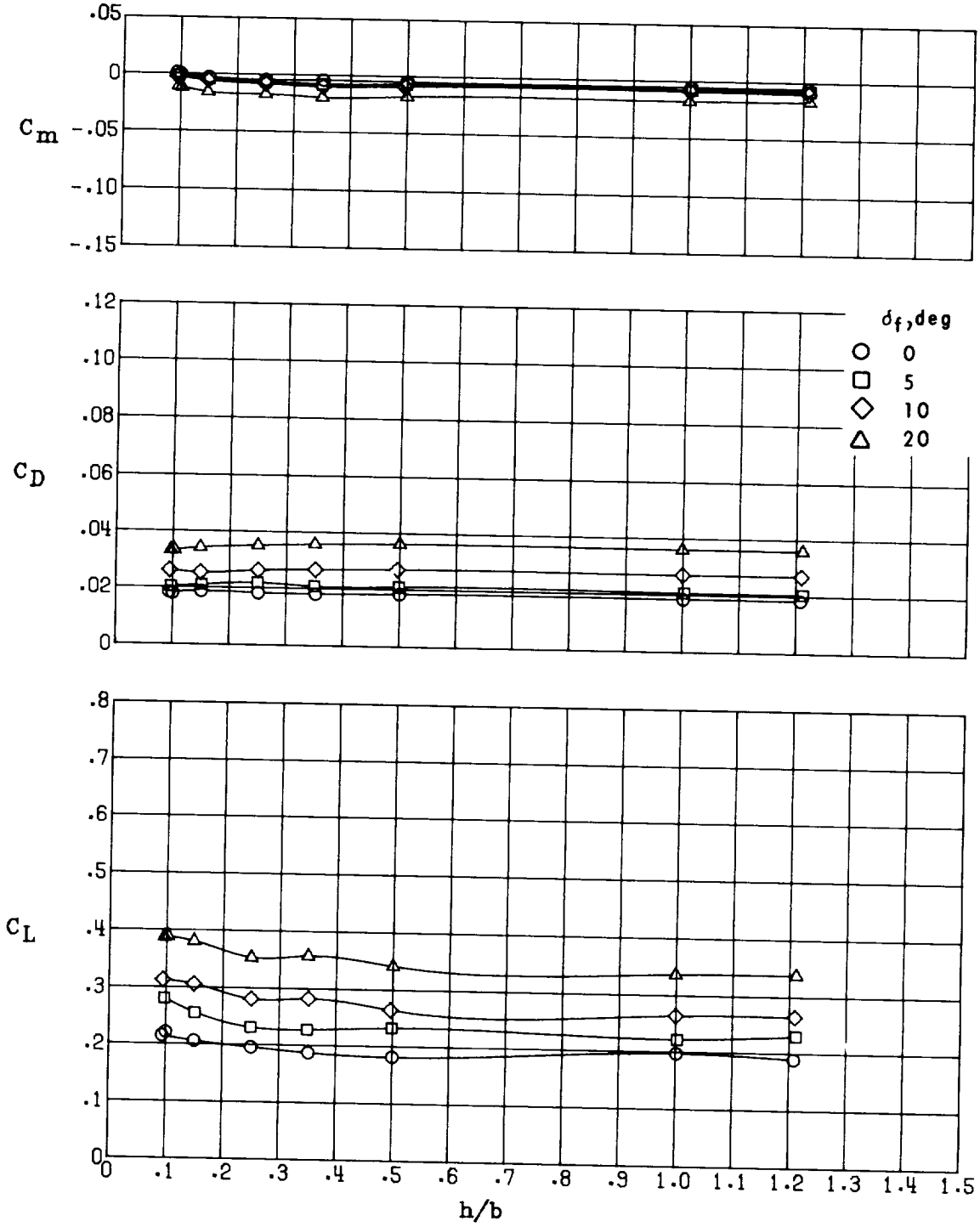

(c) AR = 3.1.

Figure 34.- Continued.

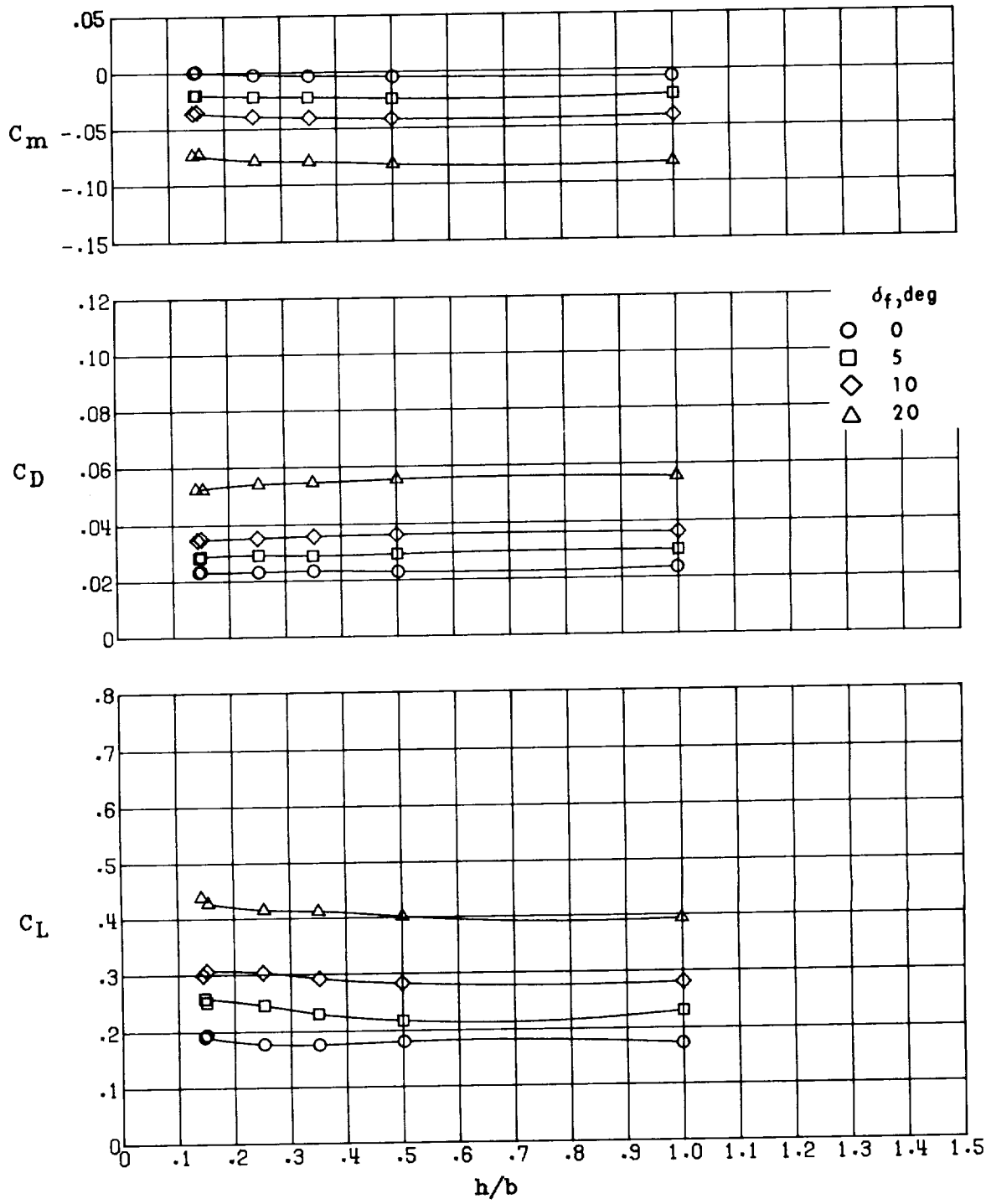

(d) AR = 2.1.

Figure 34.- Concluded.

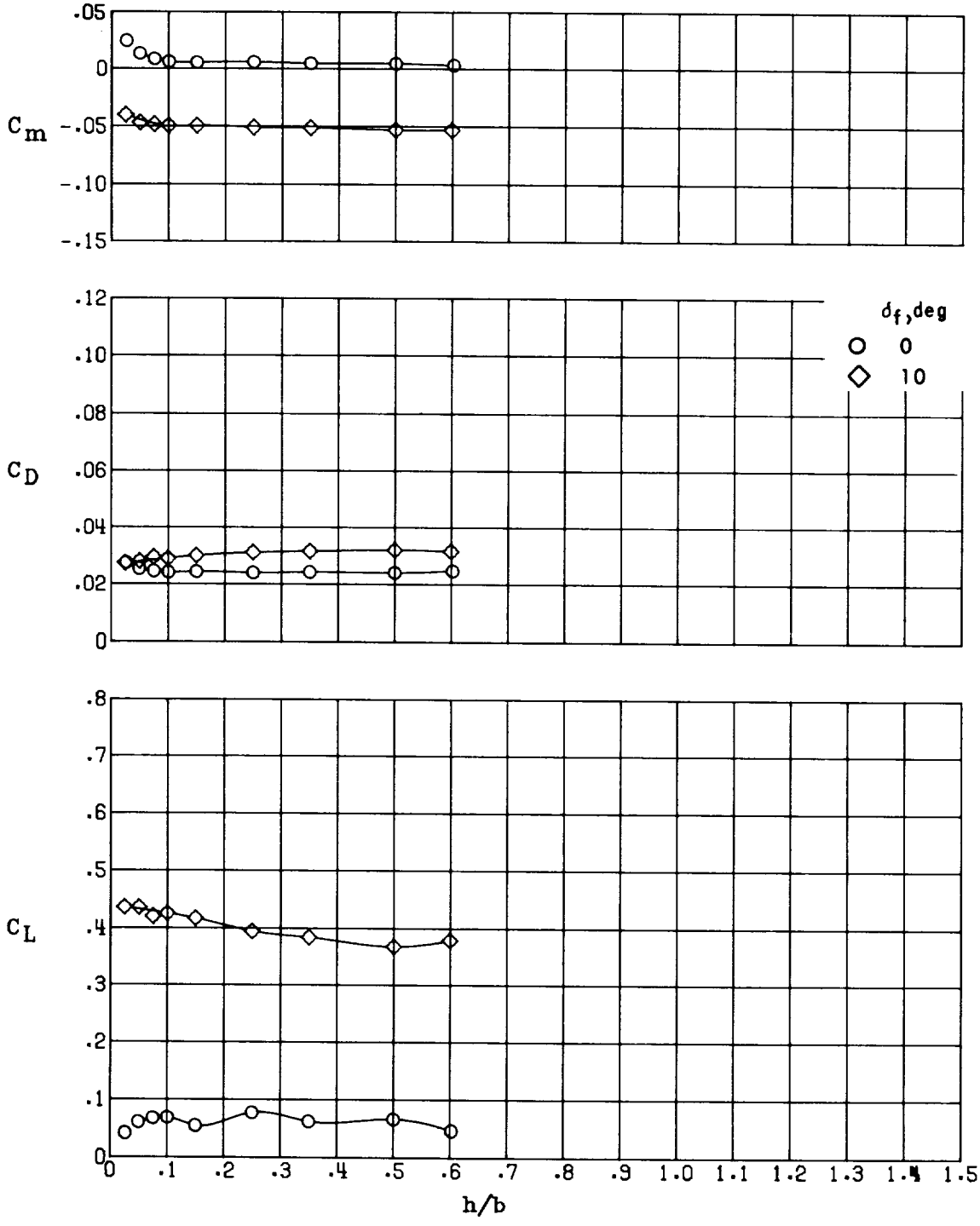

(a) AR = 8.

Figure 35.- Effect of flap deflection on the longitudinal aerodynamics in ground effect of configuration I ($\Lambda = 0°$) at several aspect ratios. $\delta_e = 0°$; $\alpha = 0.78°$.

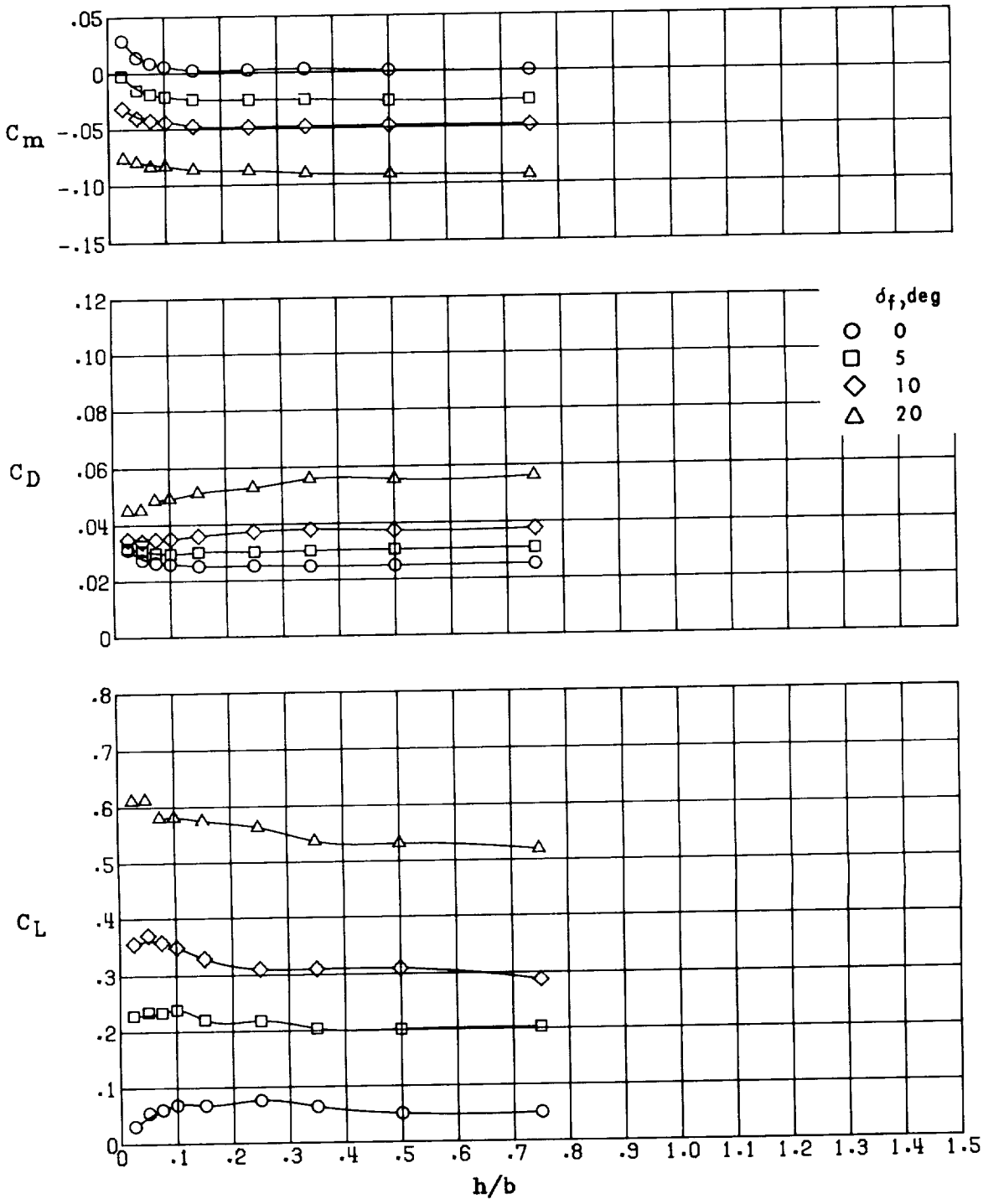

(b) AR = 6.

Figure 35.- Continued.

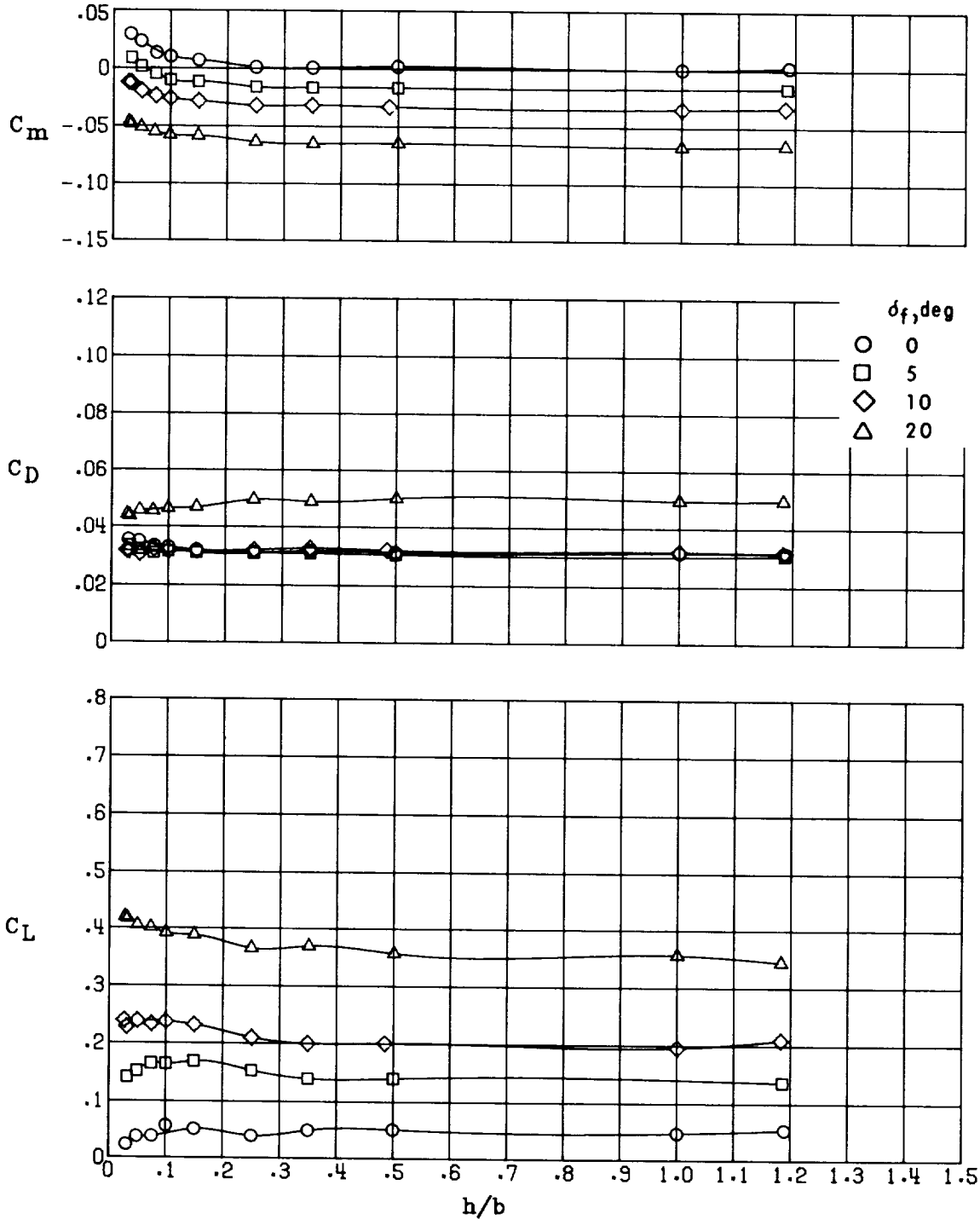

(c) AR = 4.

Figure 35.- Continued.

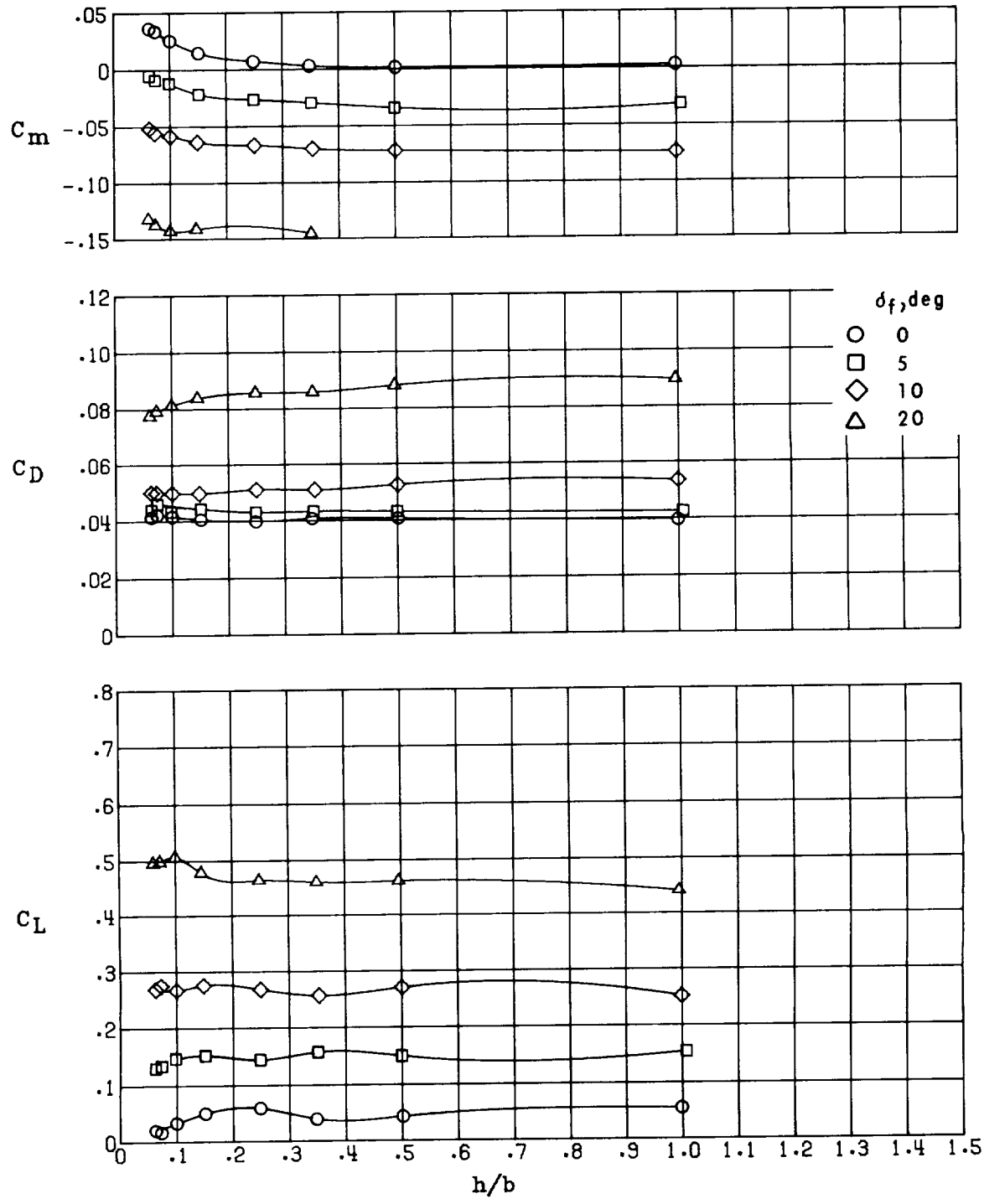

(d) AR = 2.

Figure 35.- Concluded.

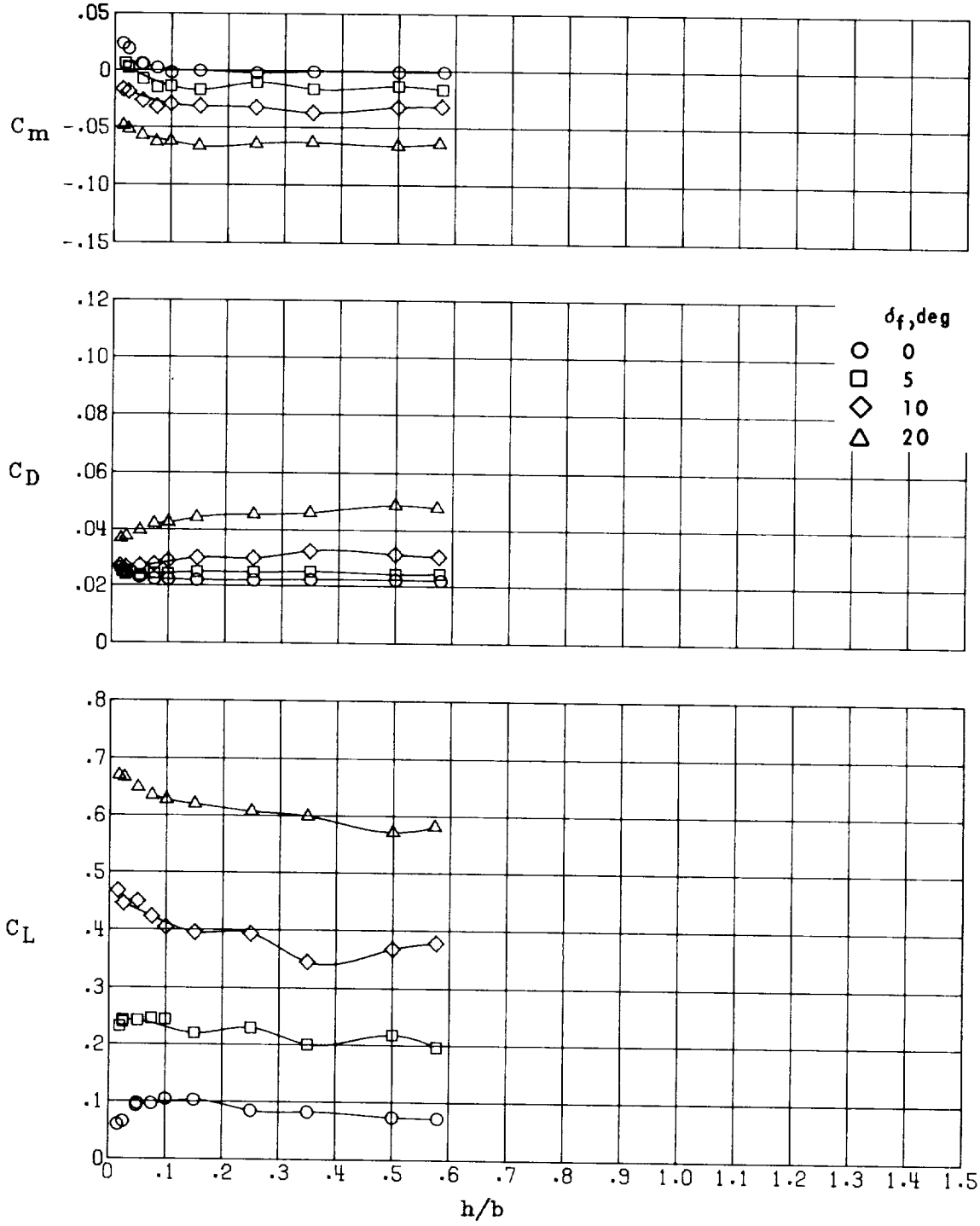

(a) AR = 7.98.

Figure 36.- Effect of flap deflection on the longitudinal aerodynamics in ground effect of configuration II (Λ = 15°) at several aspect ratios. δ_e = 0°; α = 0.78°.

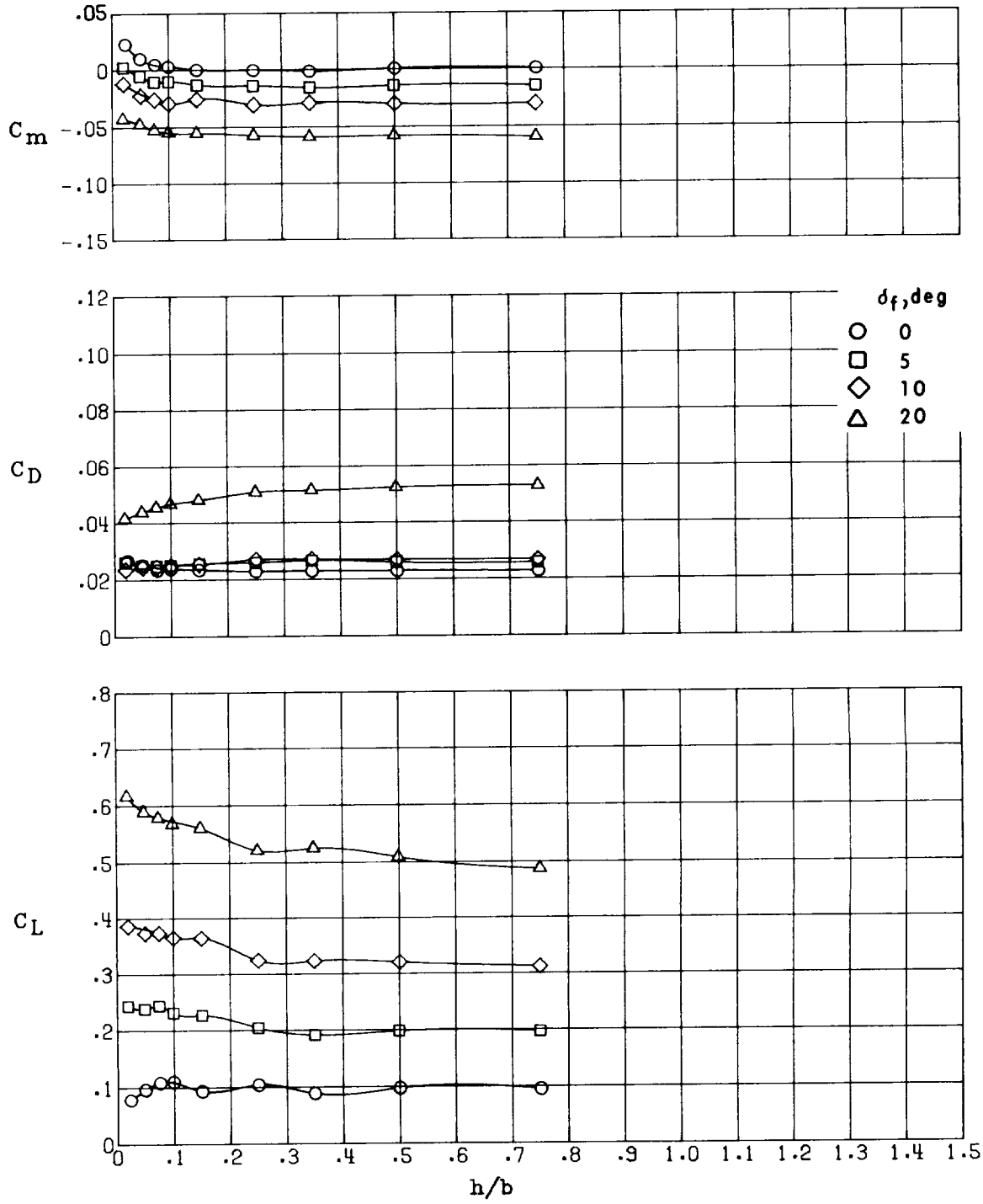

(b) AR = 6.11.

Figure 36.- Continued.

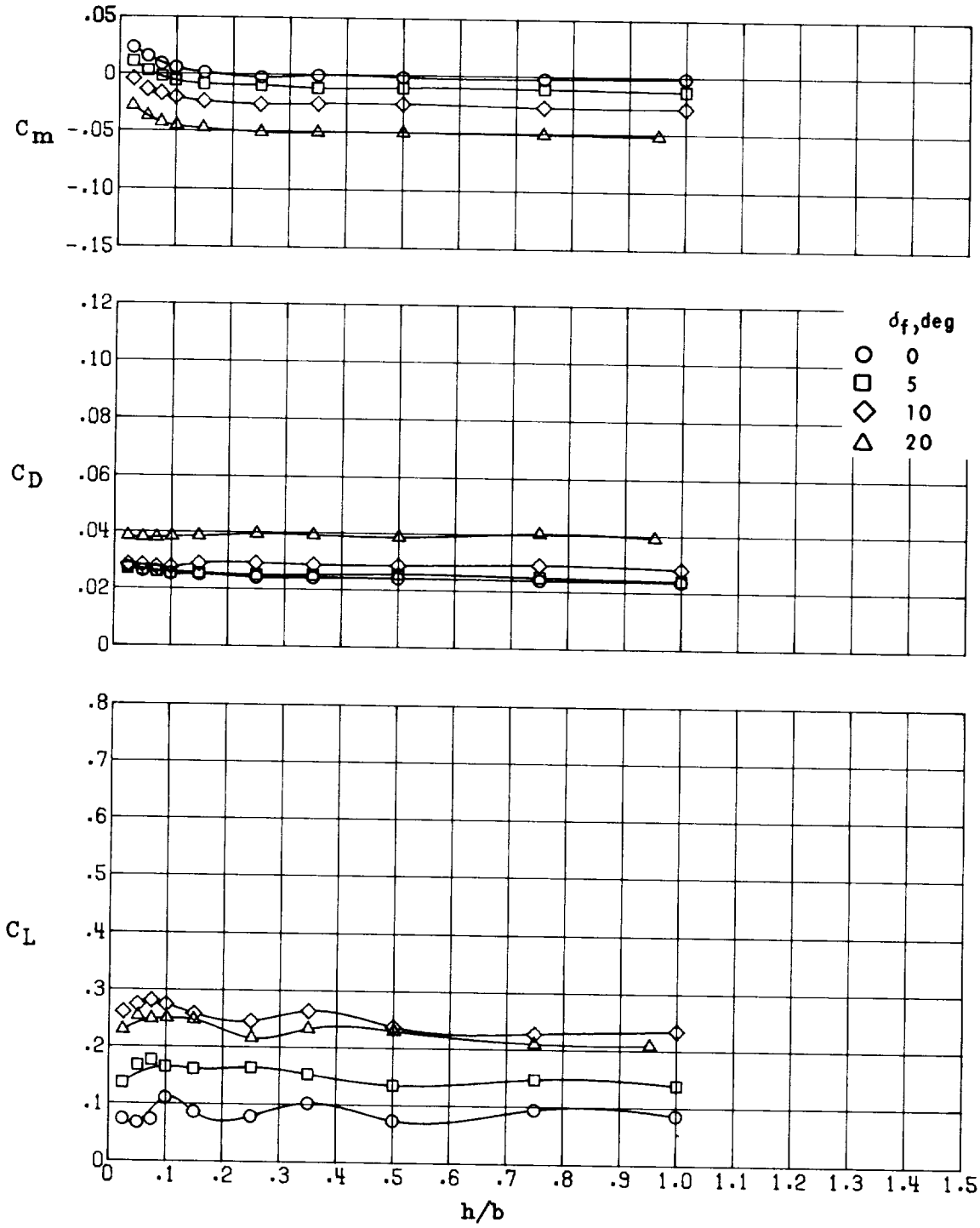

(c) AR = 4.28.

Figure 36.- Continued.

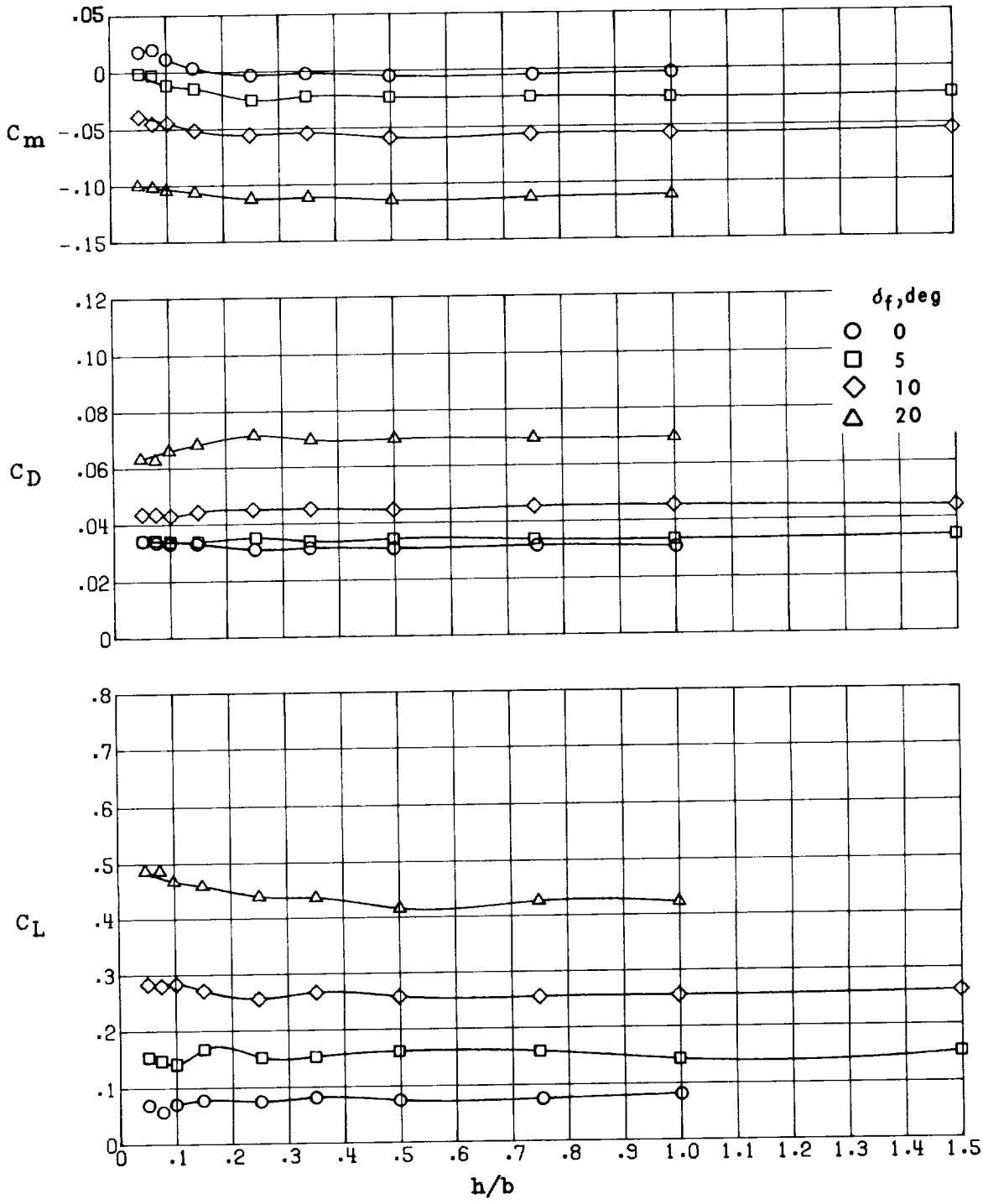

(d) AR = 2.42.

Figure 36.- Concluded.

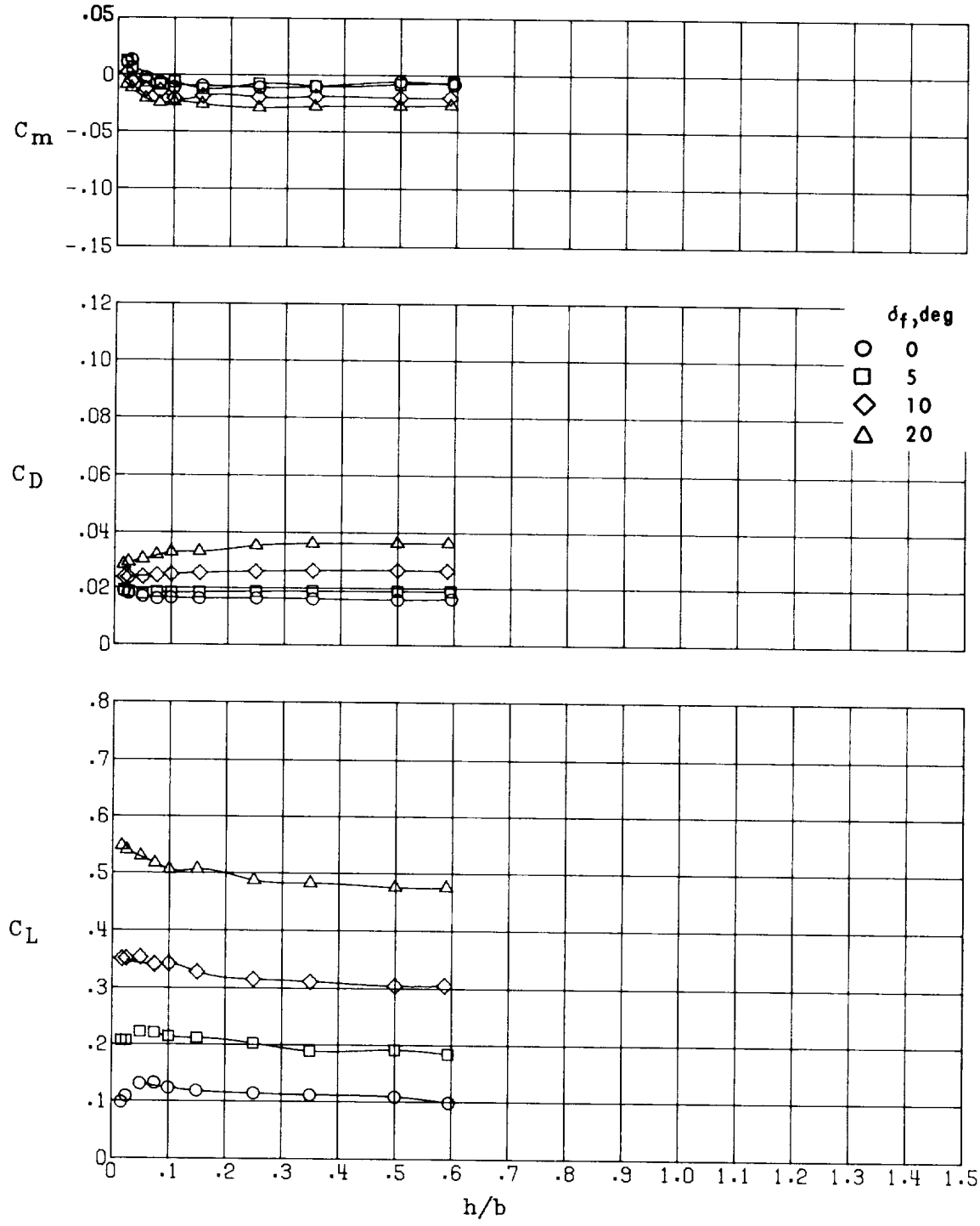

(a) AR = 6.92.

Figure 37.- Effect of flap deflection on the longitudinal aerodynamics in ground effect of configuration III (Λ = 30°) at several aspect ratios. δ_e = 0°; α = 0.78°.

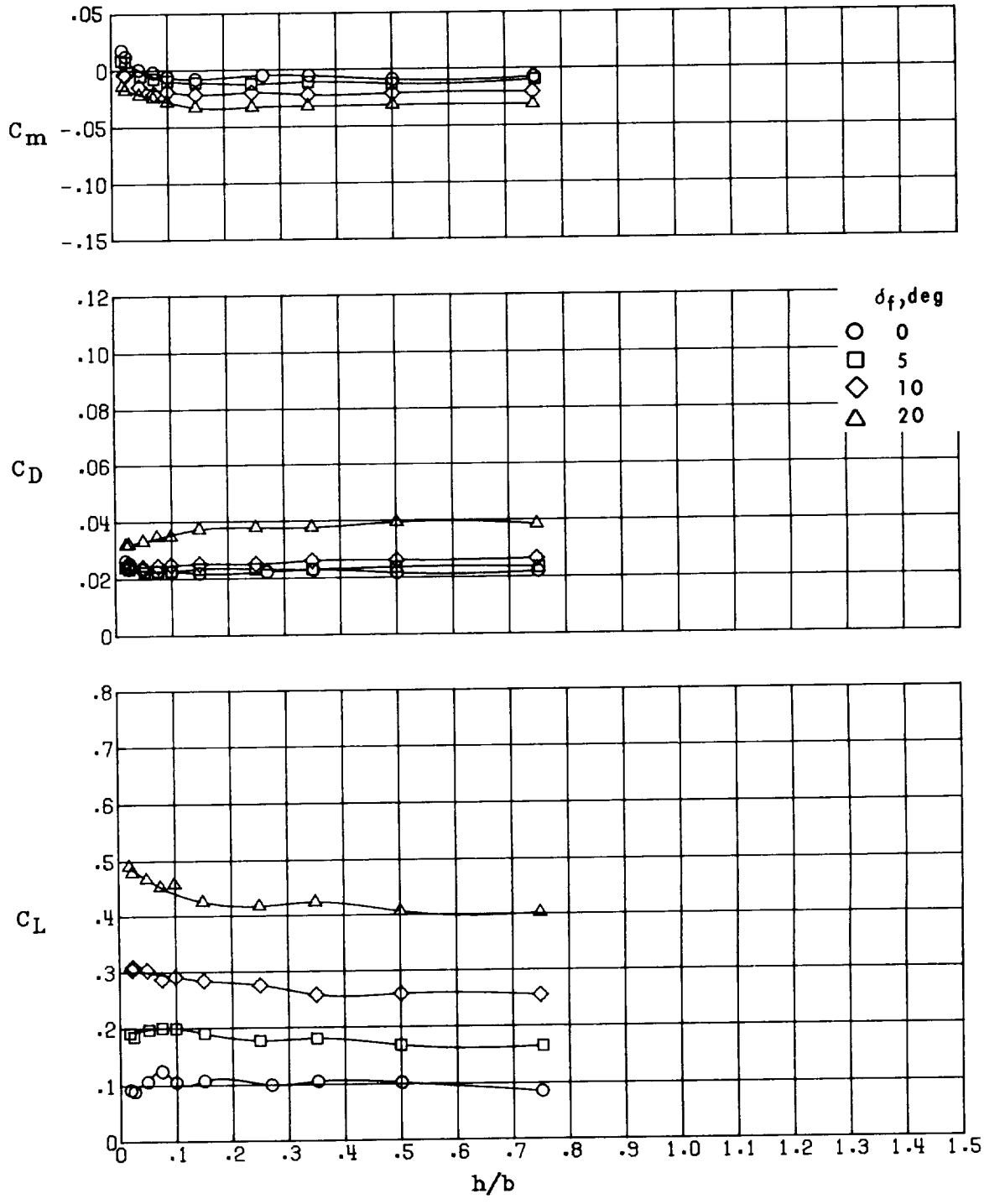

(b) AR = 5.42.

Figure 37.- Continued.

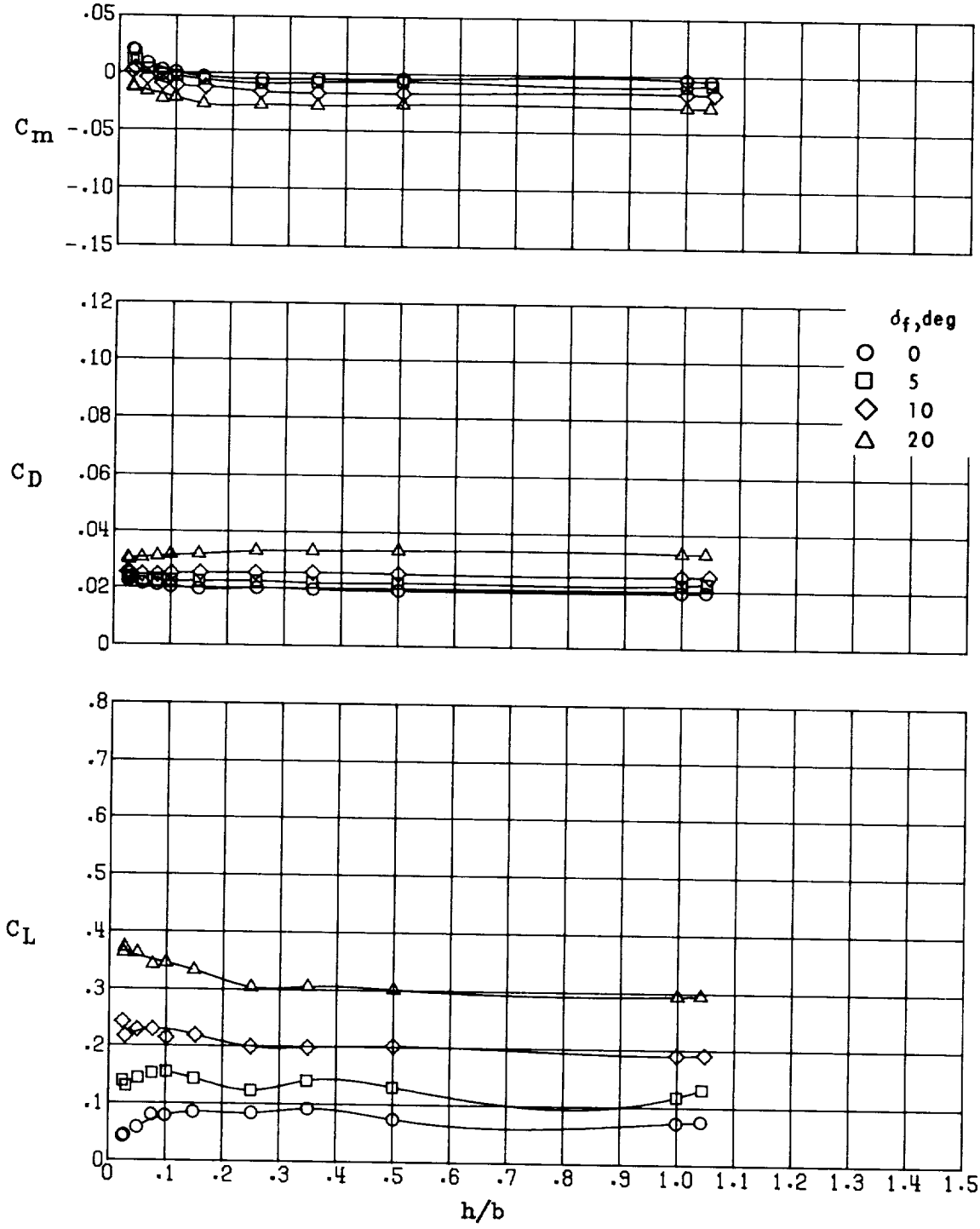

(c) AR = 3.92.

Figure 37.- Continued.

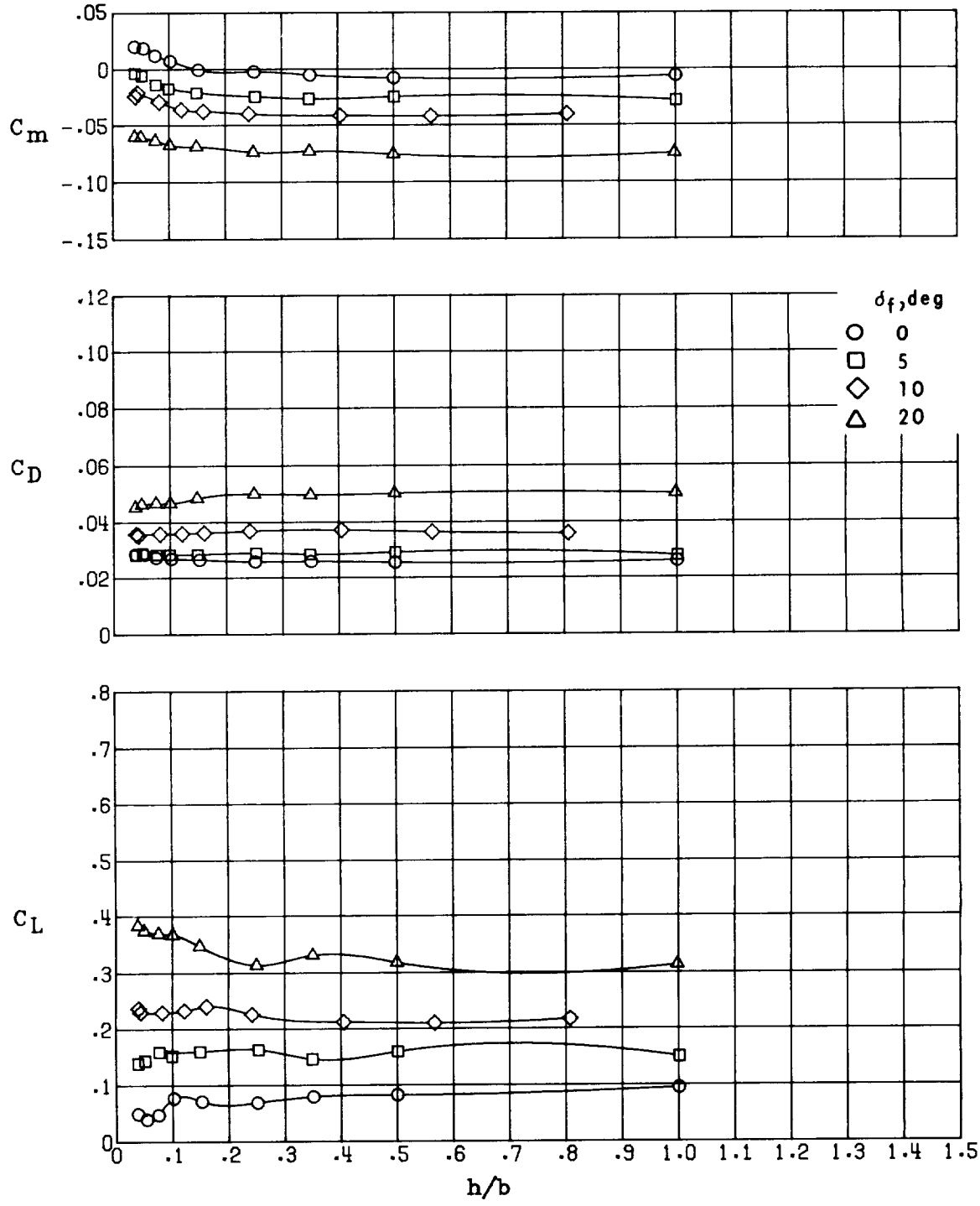

(d) AR = 2.42.

Figure 37.- Concluded.

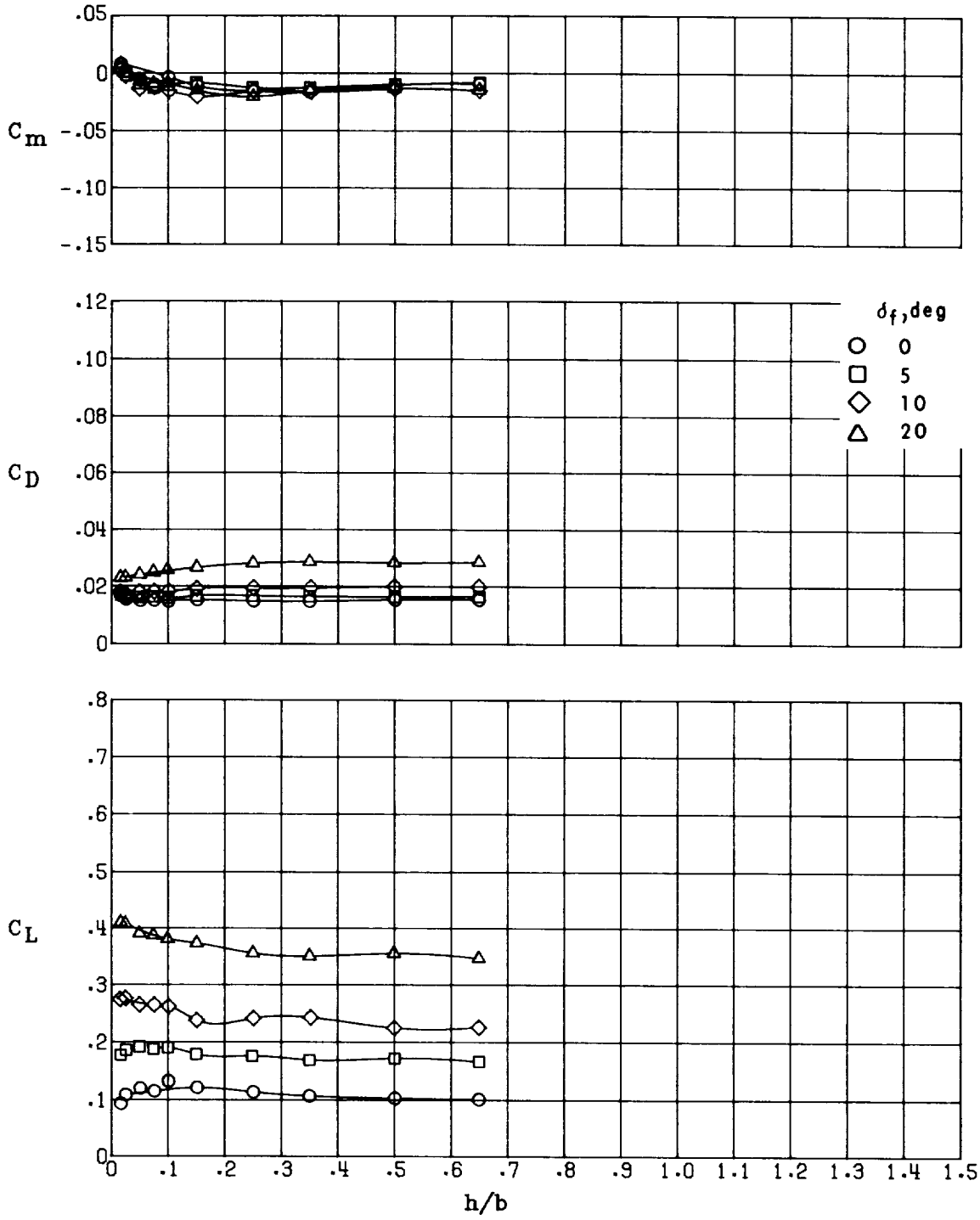

(a) AR = 5.1.

Figure 38.- Effect of flap deflection on the longitudinal aerodynamics in ground effect of configuration IV (Λ = 45°) at several aspect ratios. δ_e = 0°; α = 0.78°.

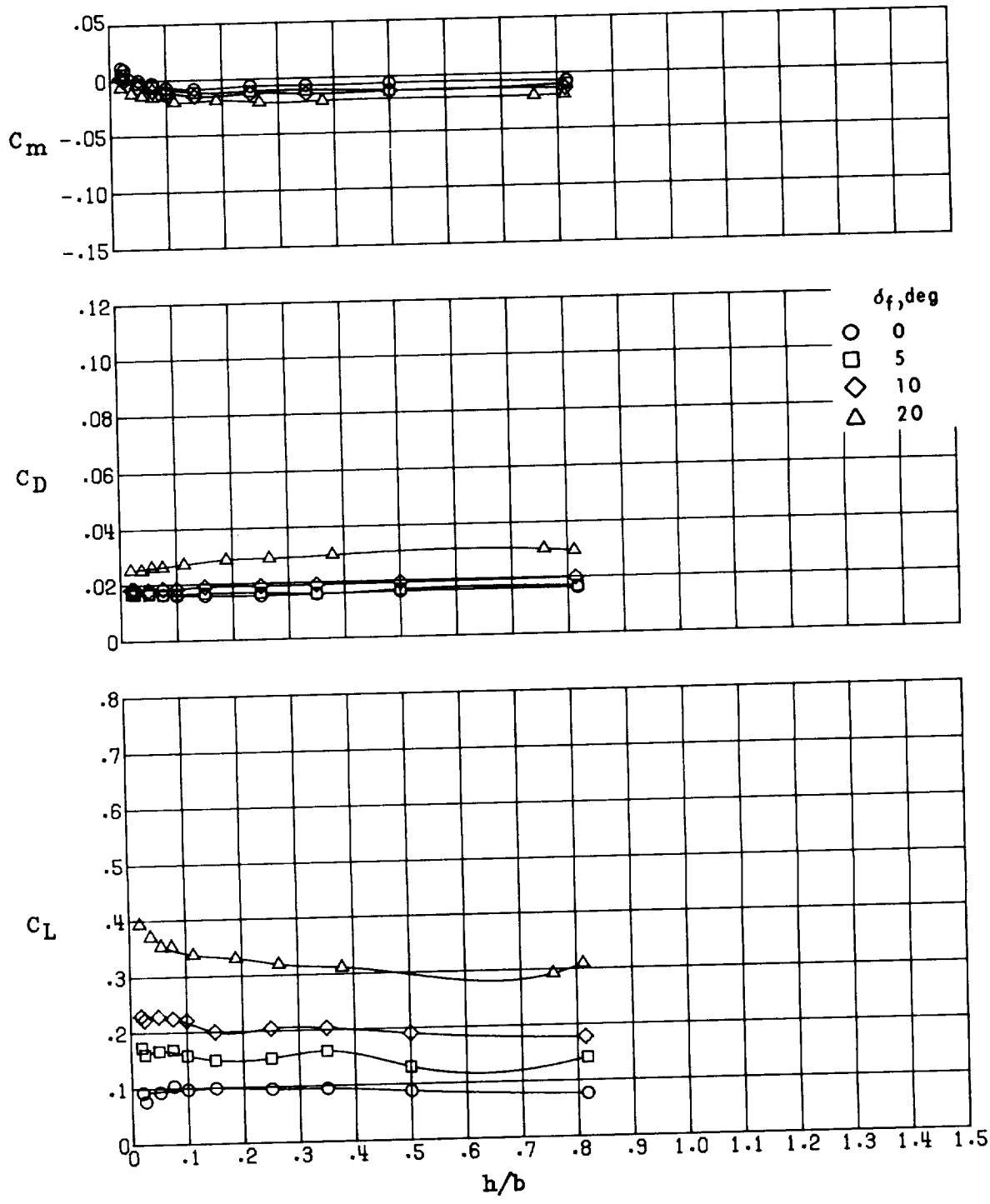

(b) AR = 4.1.

Figure 38.- Continued.

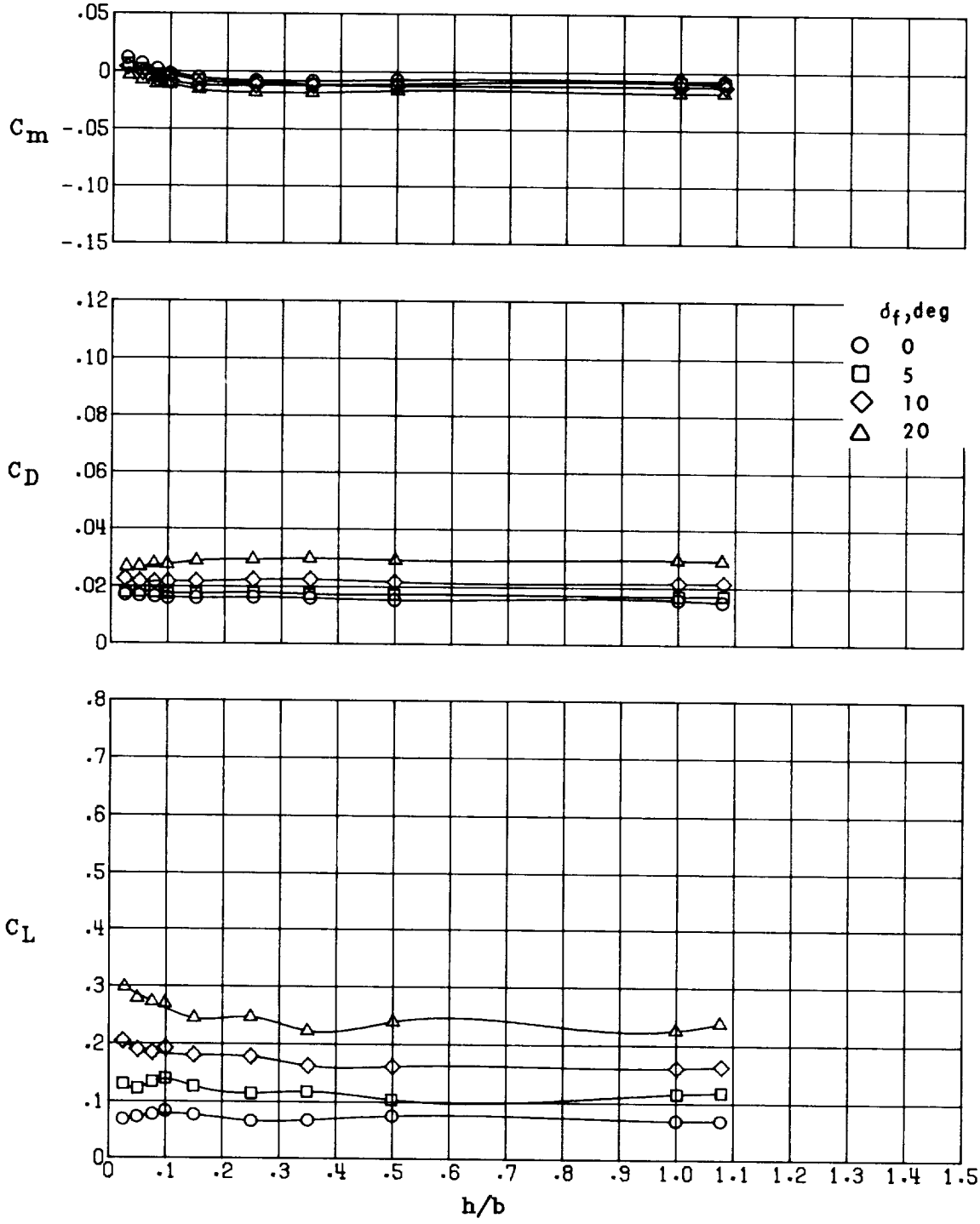

(c) AR = 3.1.

Figure 38.- Continued.

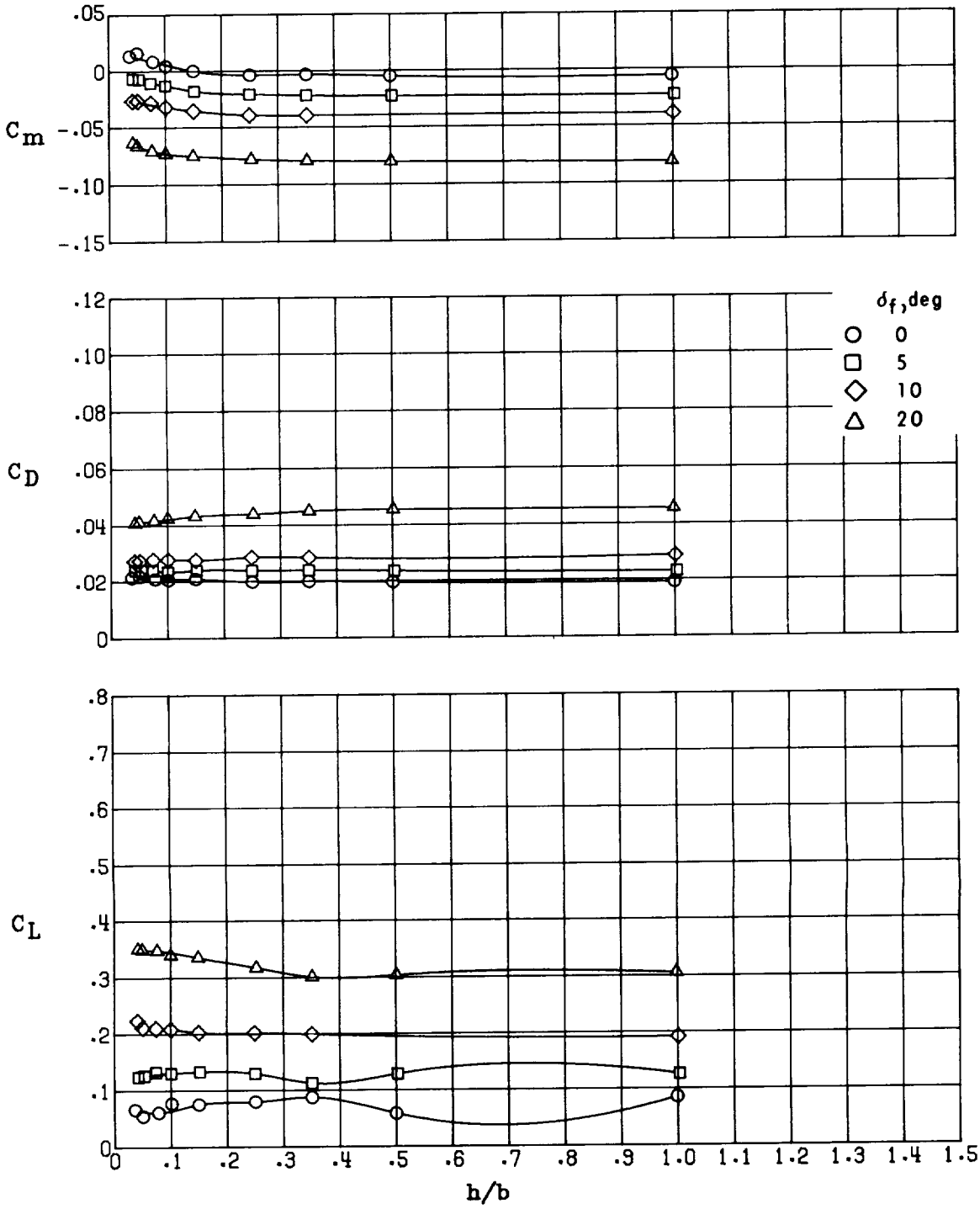

(d) AR = 2.1.

Figure 38.- Concluded.

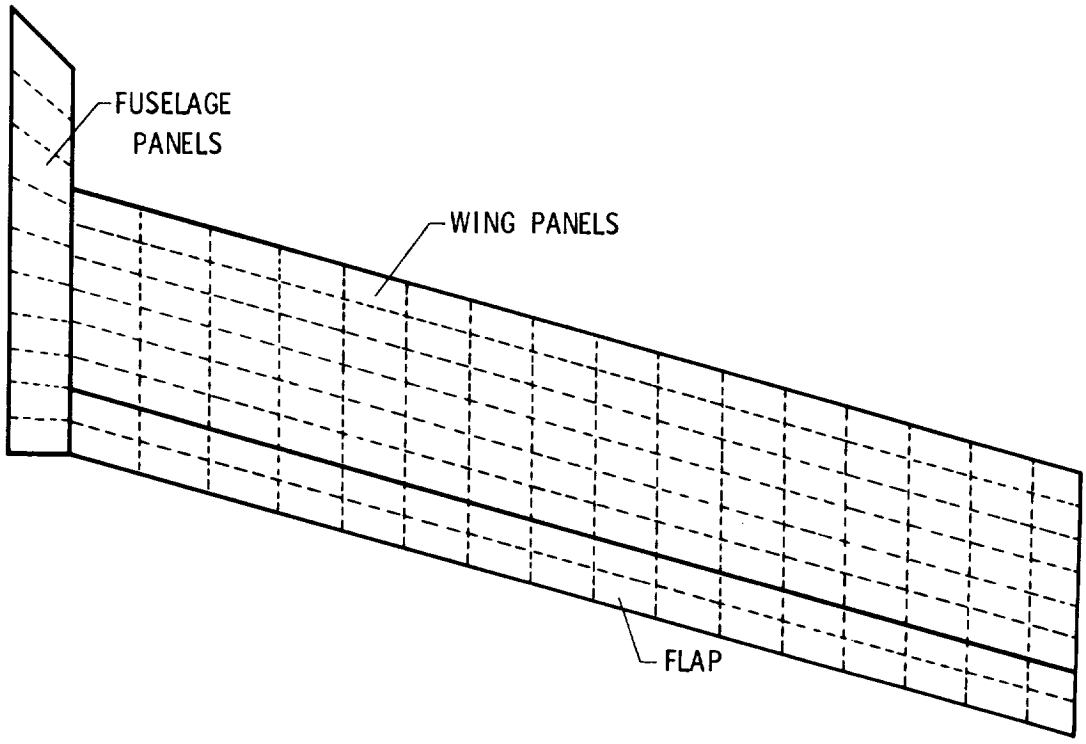

Figure 39.- Vortex-lattice panel representation of configuration II-A.

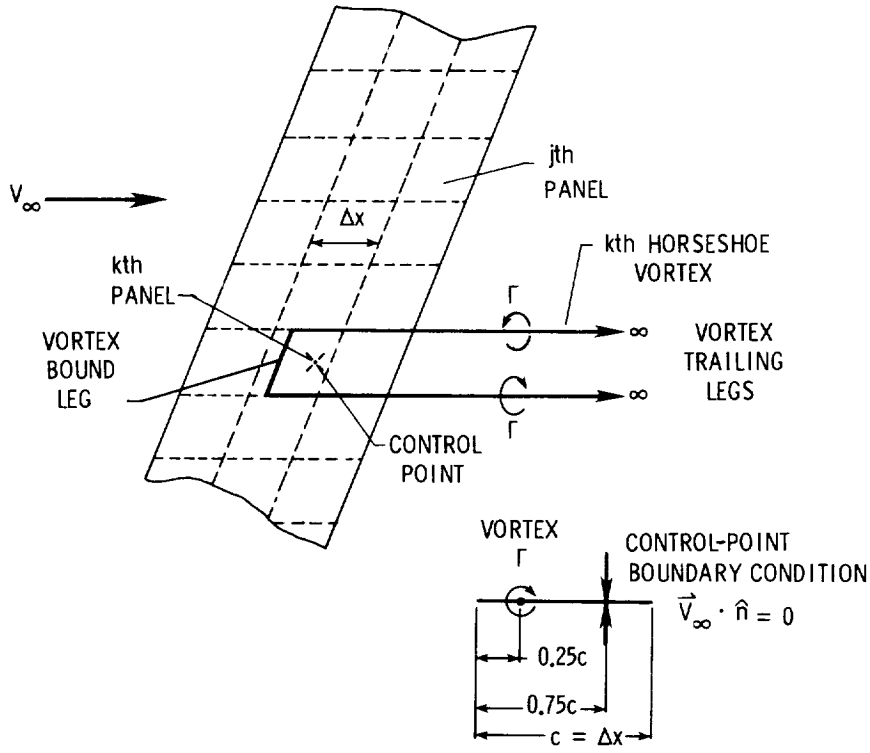

Figure 40.- Location of vortex and control point on individual vortex-lattice panel.

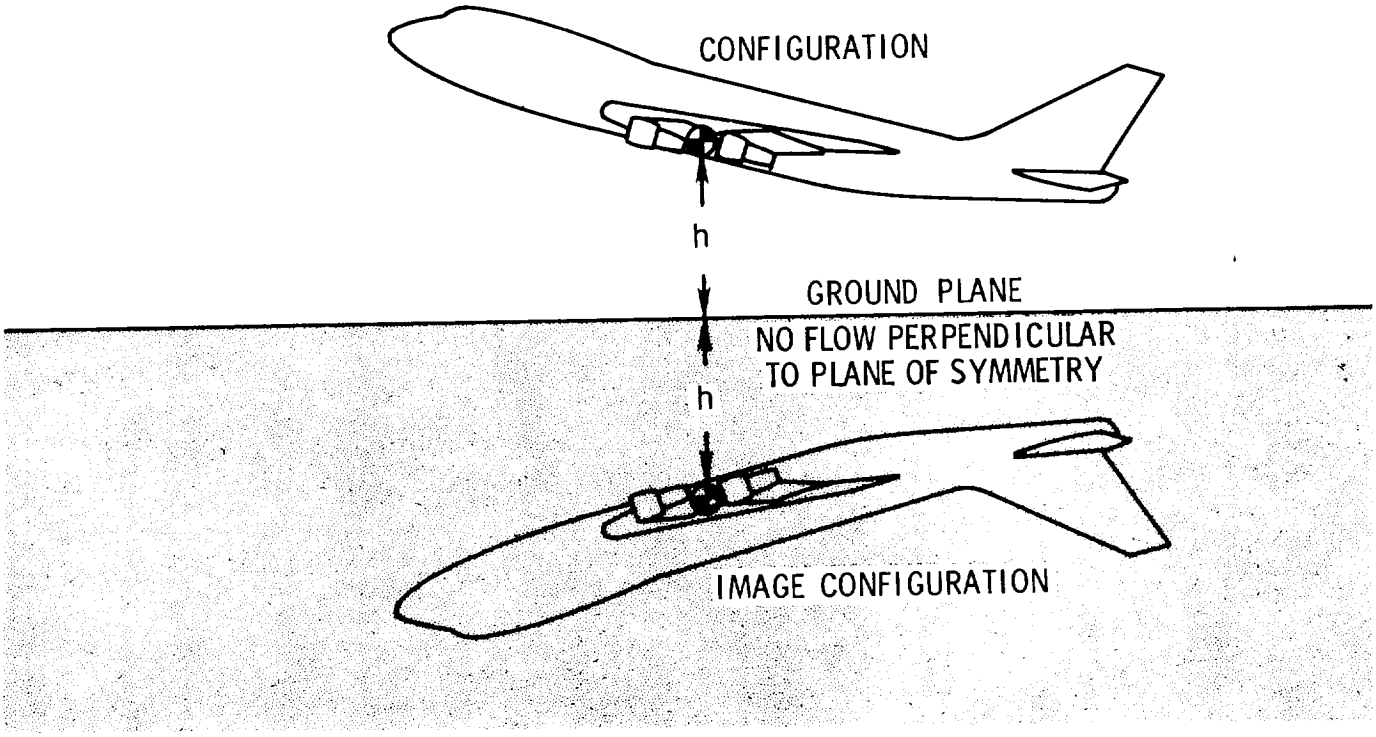

Figure 41.- Ground-plane image concept for vortex-lattice method.

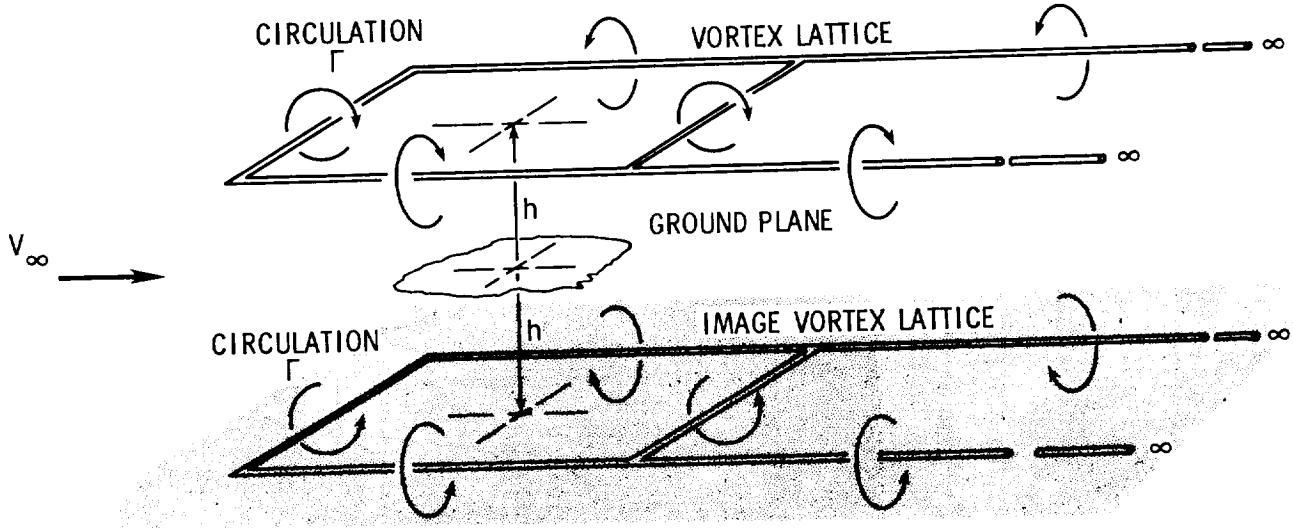

Figure 42.- Fundamental ground-induced vortex-lattice image system.

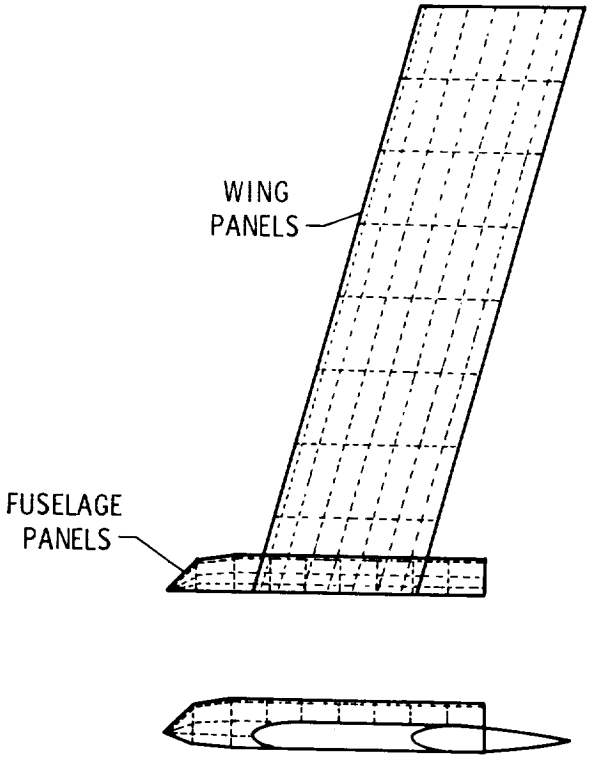

Figure 43.- The Hess surface-panel representation of configuration II-A.

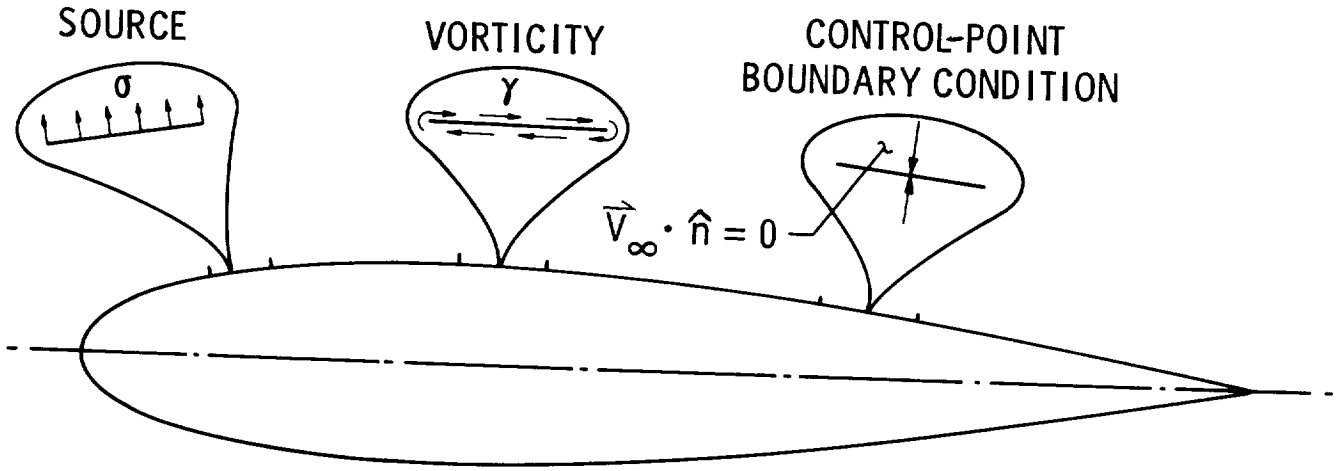

Figure 44.- Distribution of source, vorticity, and control-point locations for Hess surface panels.

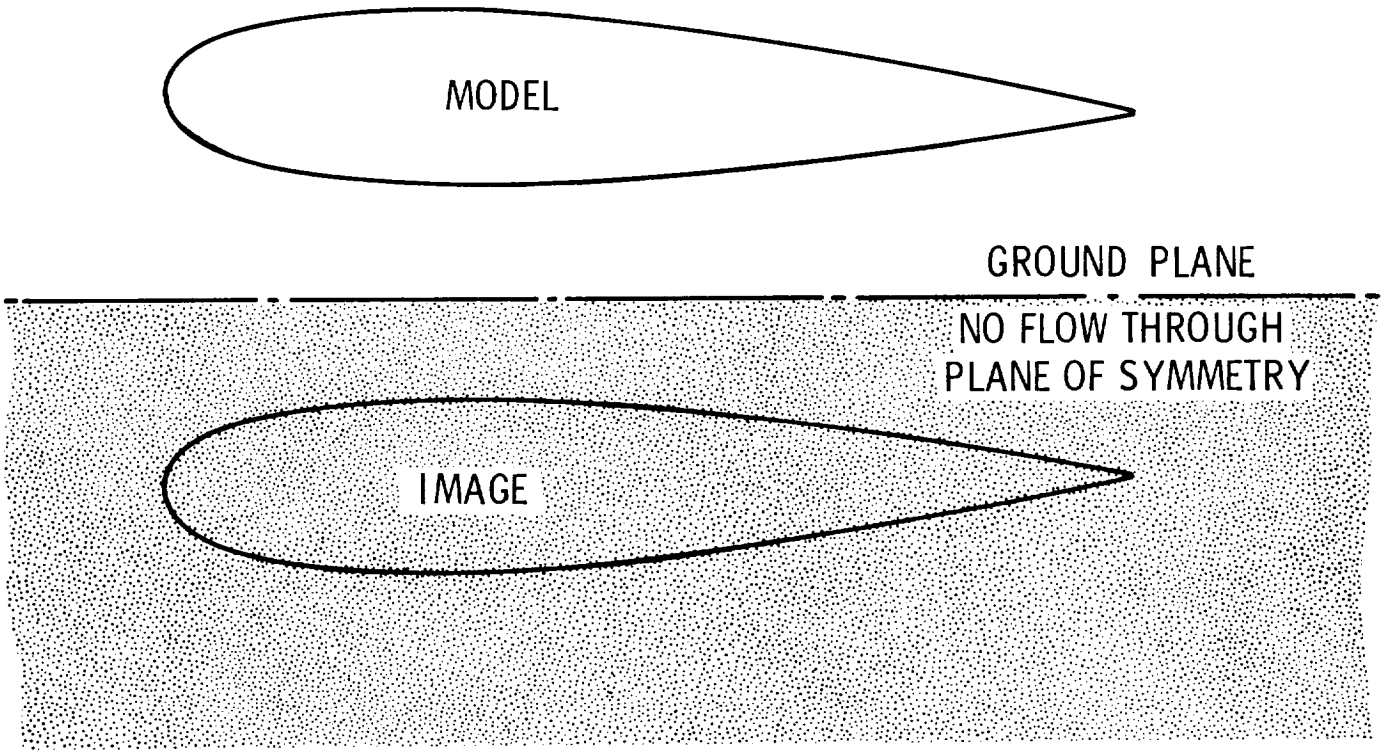

Figure 45.- Ground-plane image system for Hess surface-panel method.

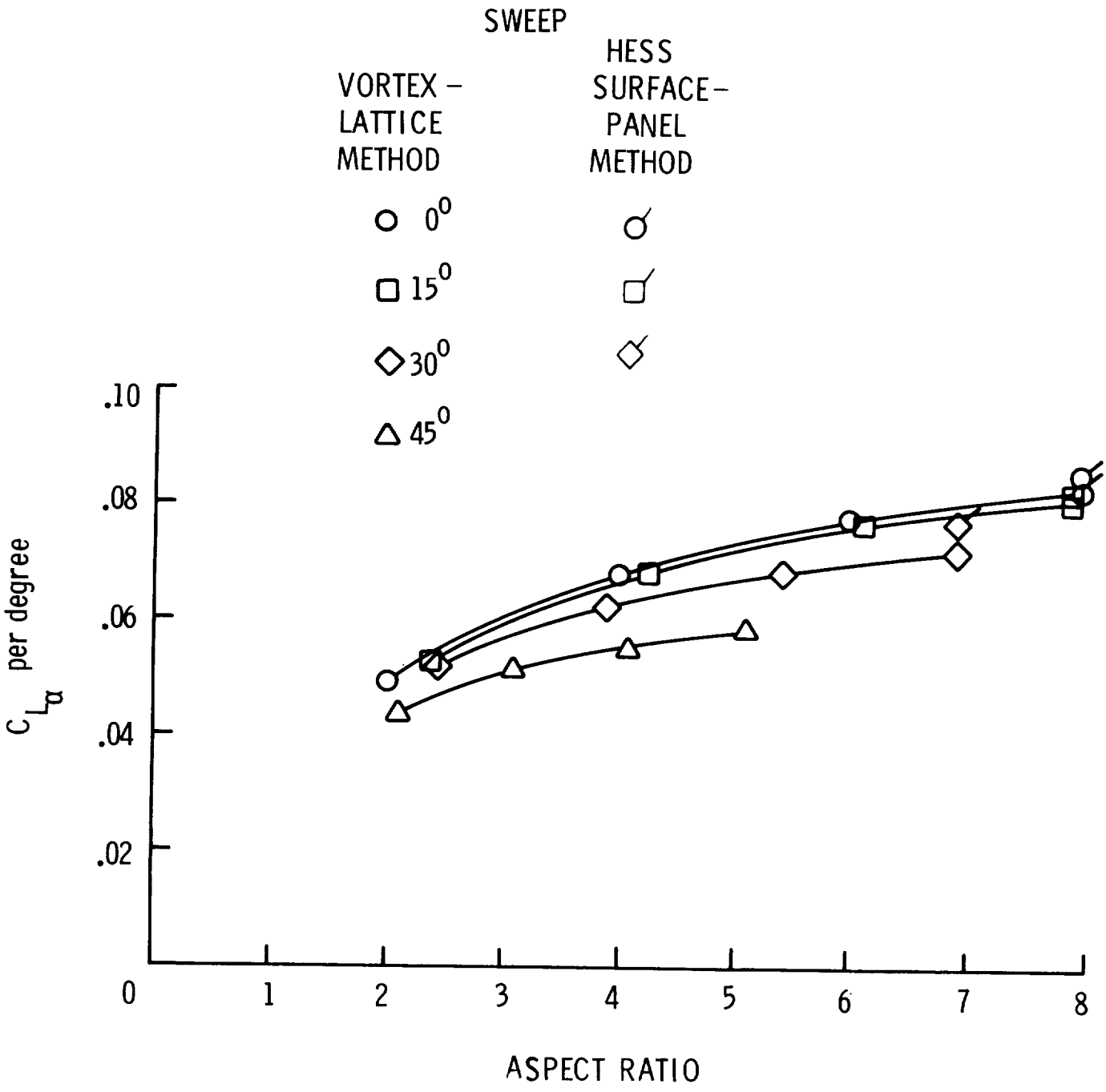

Figure 46.- Theoretical effect of aspect ratio on lift-curve slope for configurations I to IV.

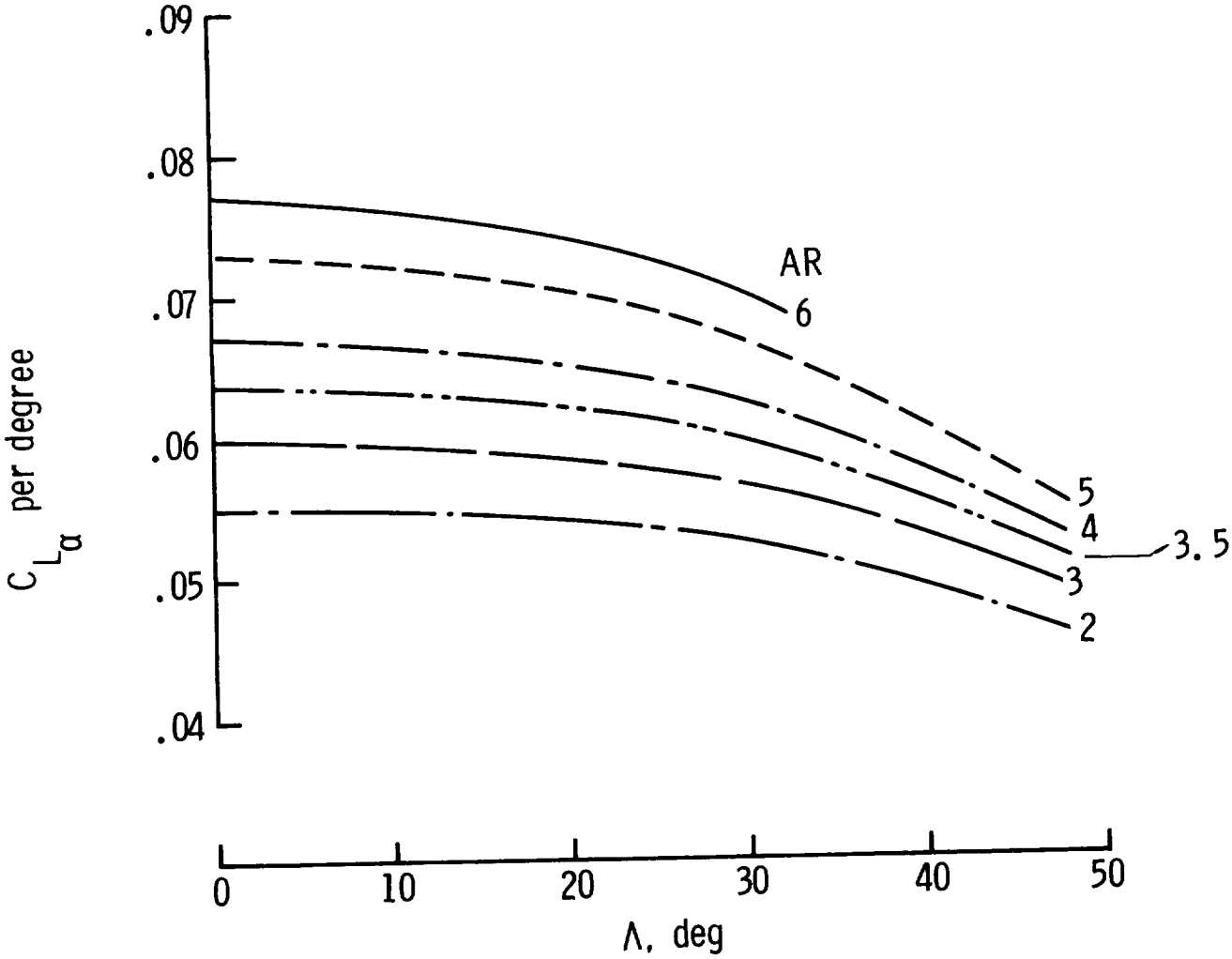

Figure 47.- Theoretical effect of wing sweep angle on lift-curve slope at constant aspect ratio.

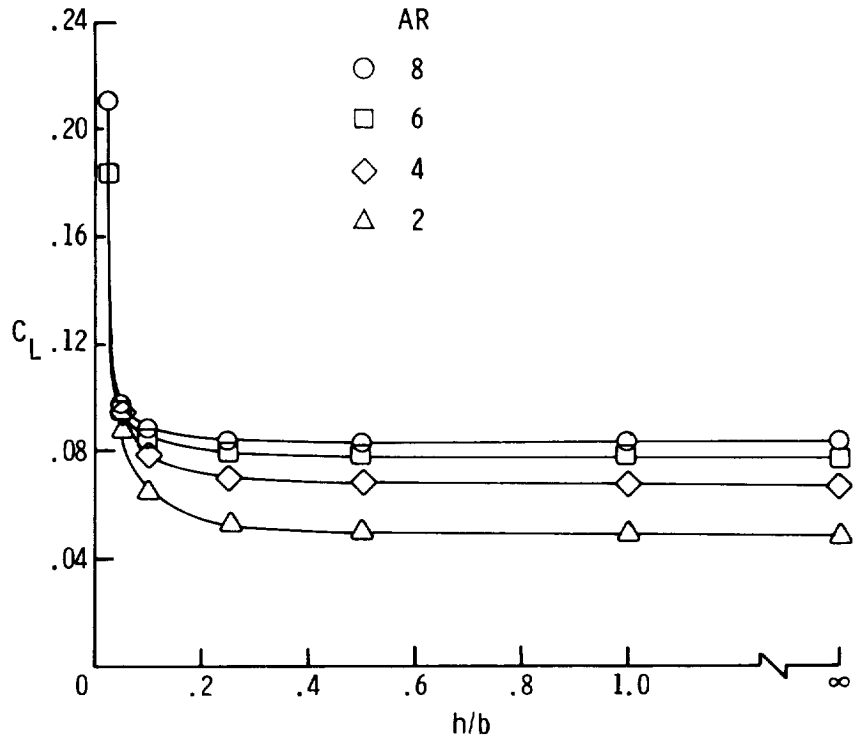

(a) Configuration I. $\Lambda = 0°$.

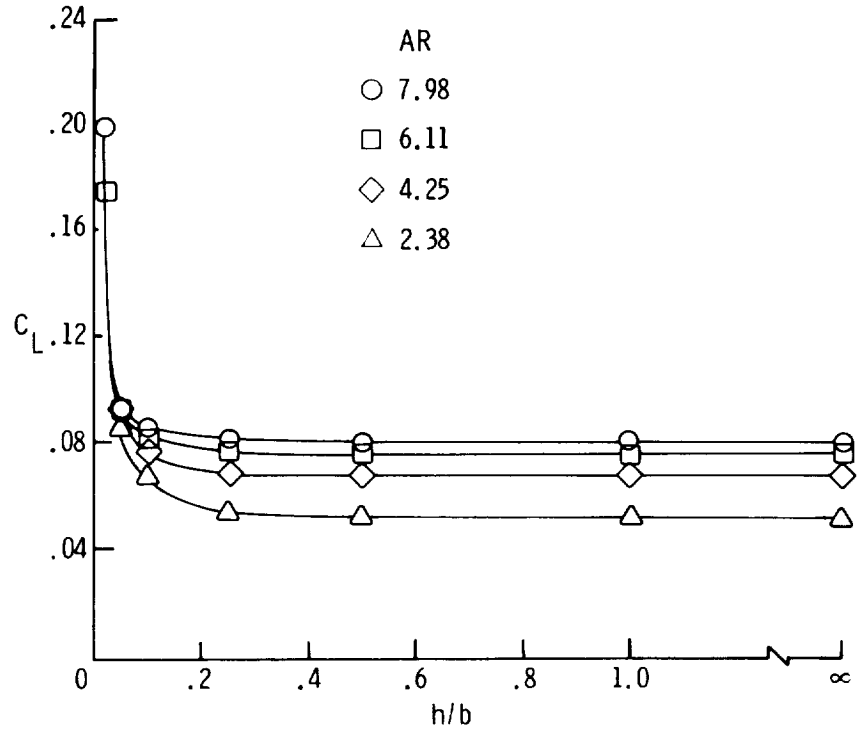

(b) Configuration II. $\Lambda = 15°$.

Figure 48.- Theoretical vortex-lattice results of the effect of ground proximity on lift coefficient at $\alpha = 1°$ for various configurations.

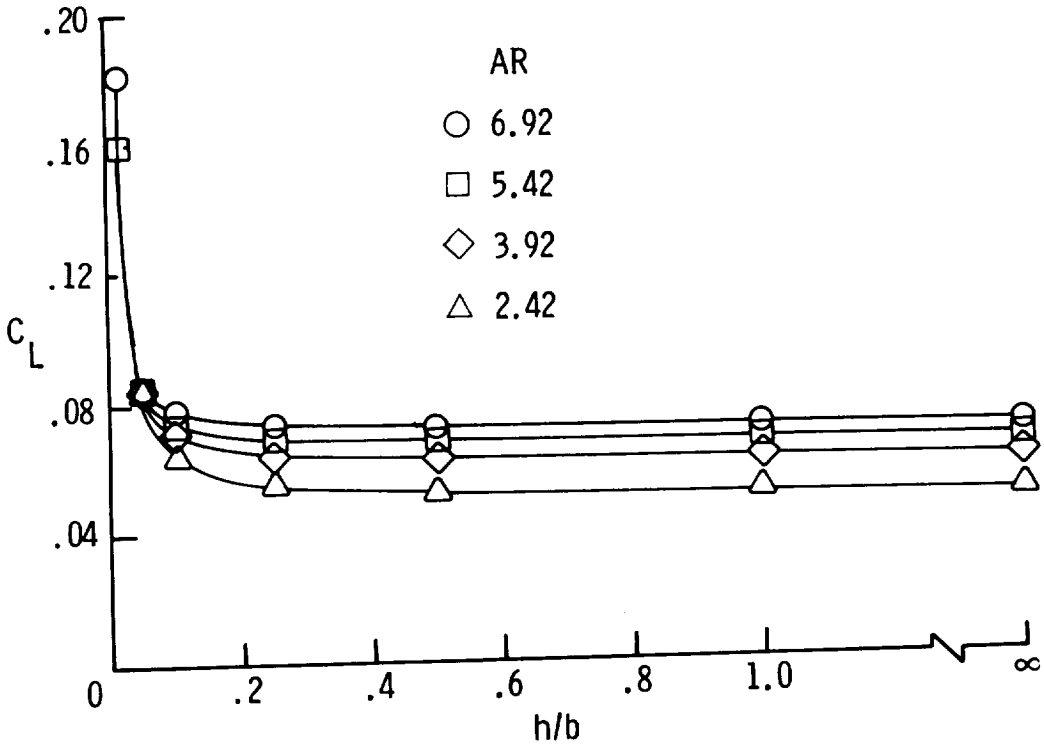

(c) Configuration III. $\Lambda = 30°$.

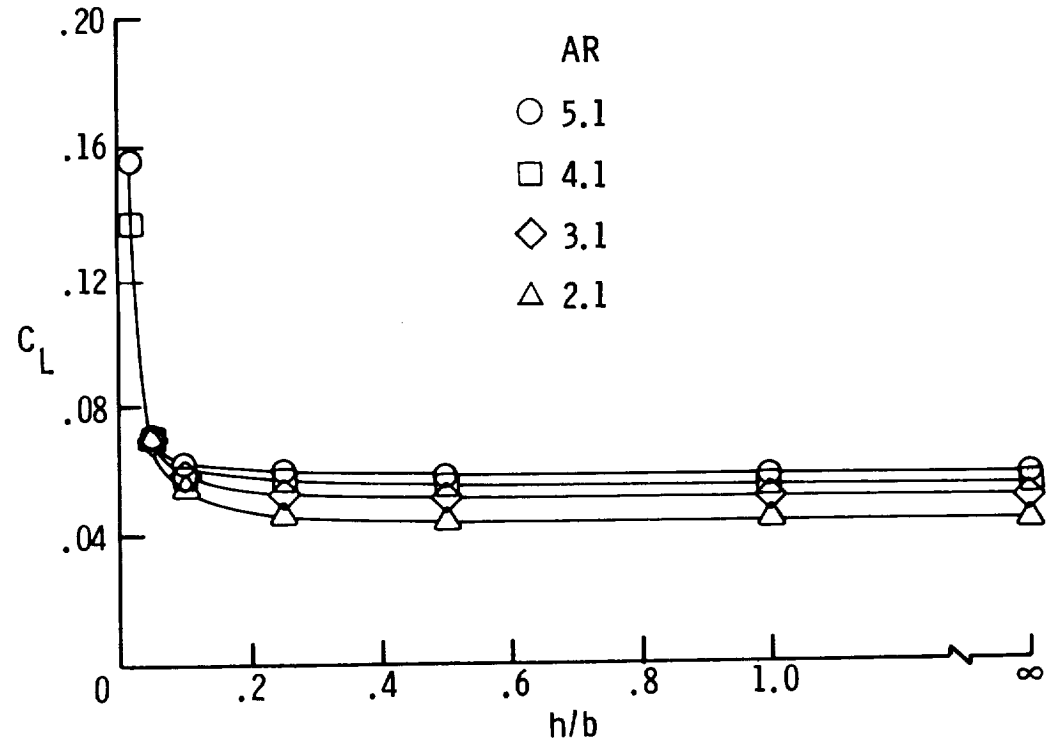

(d) Configuration IV. $\Lambda = 45°$.

Figure 48.- Concluded.

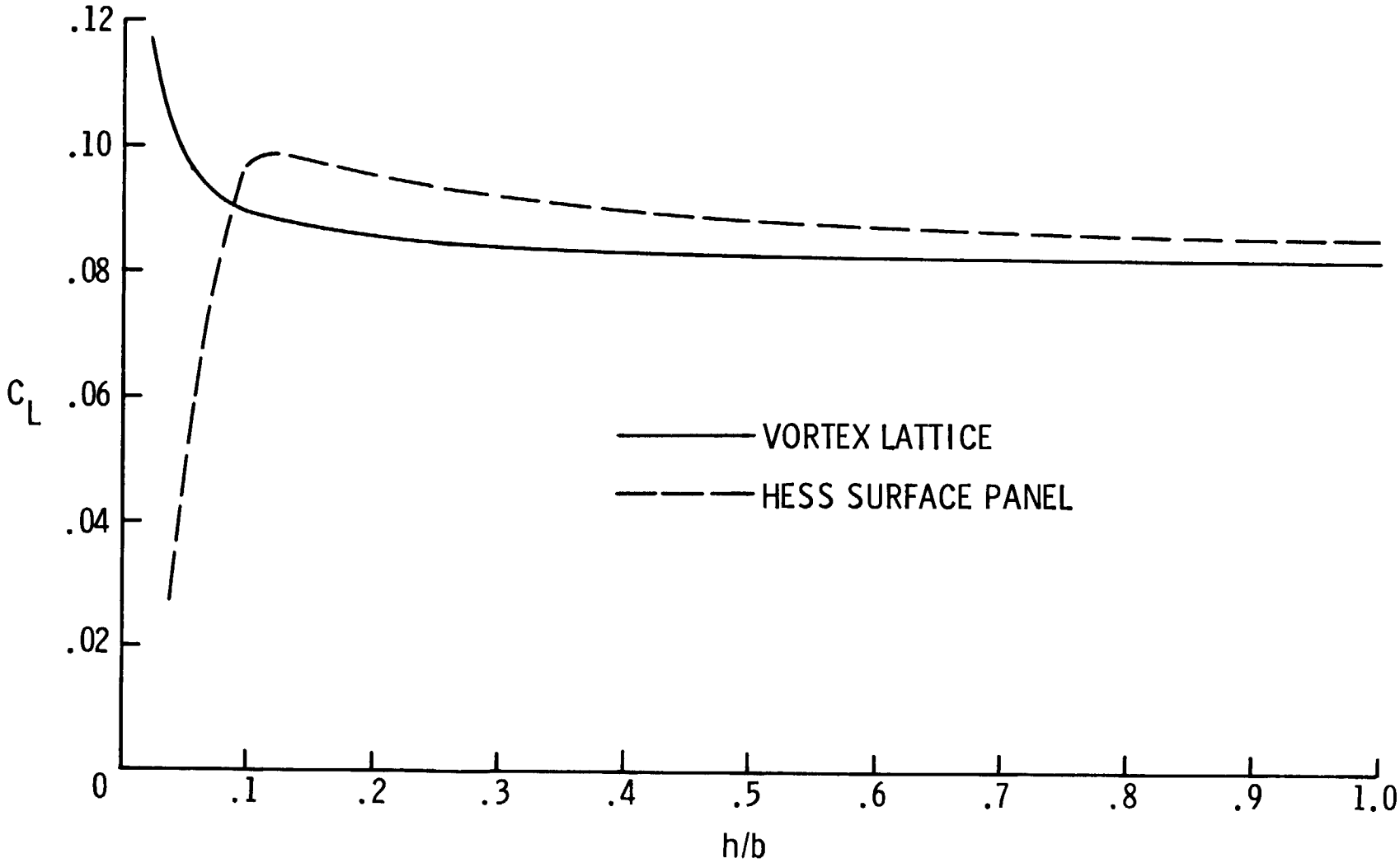

(a) Configuration I-A.

Figure 49.- Comparison of ground effects predicted by vortex-lattice and Hess surface-panel methods.

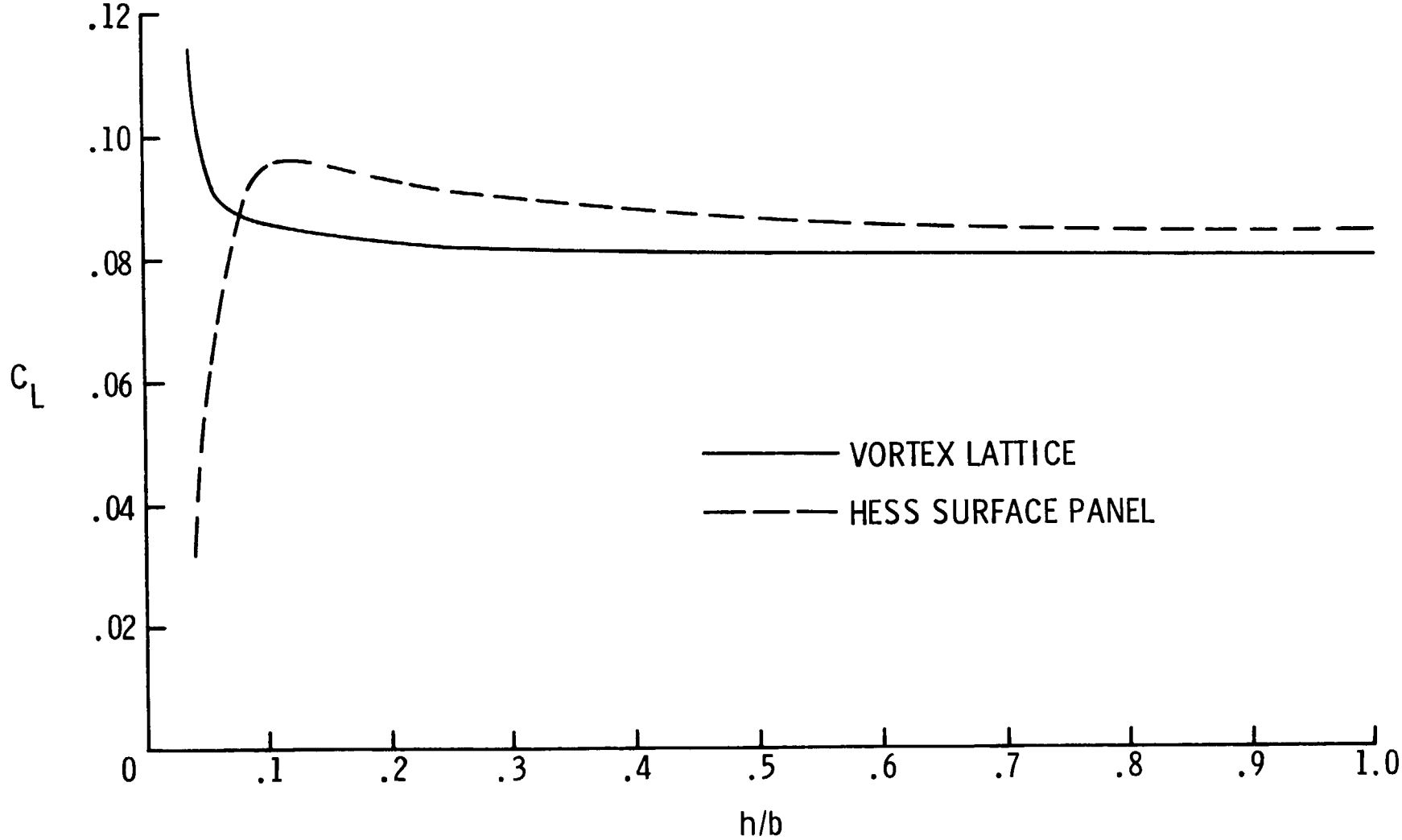

(b) Configuration II-A.

Figure 49.- Continued.

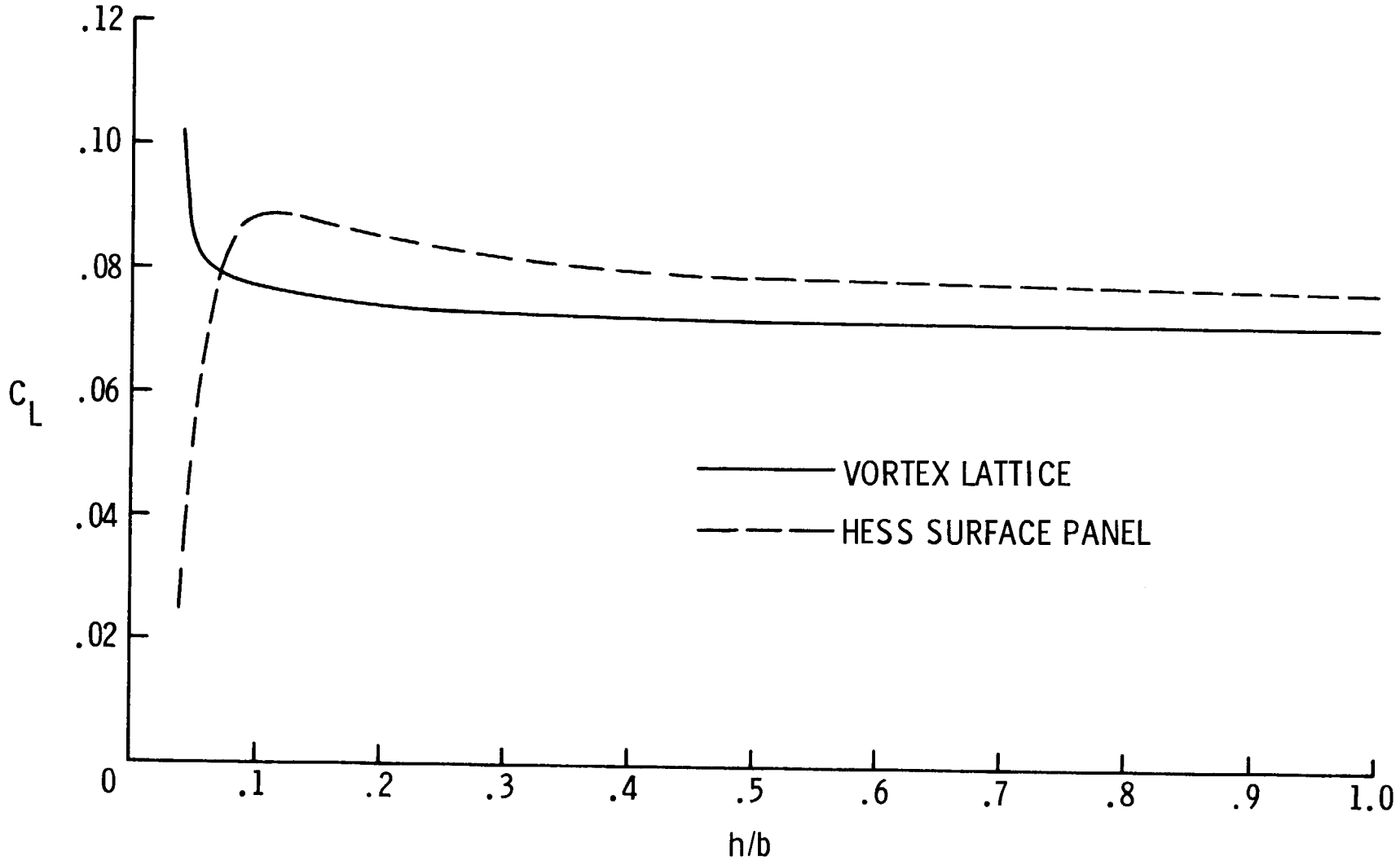

(c) Configuration III-A.

Figure 49.- Concluded.

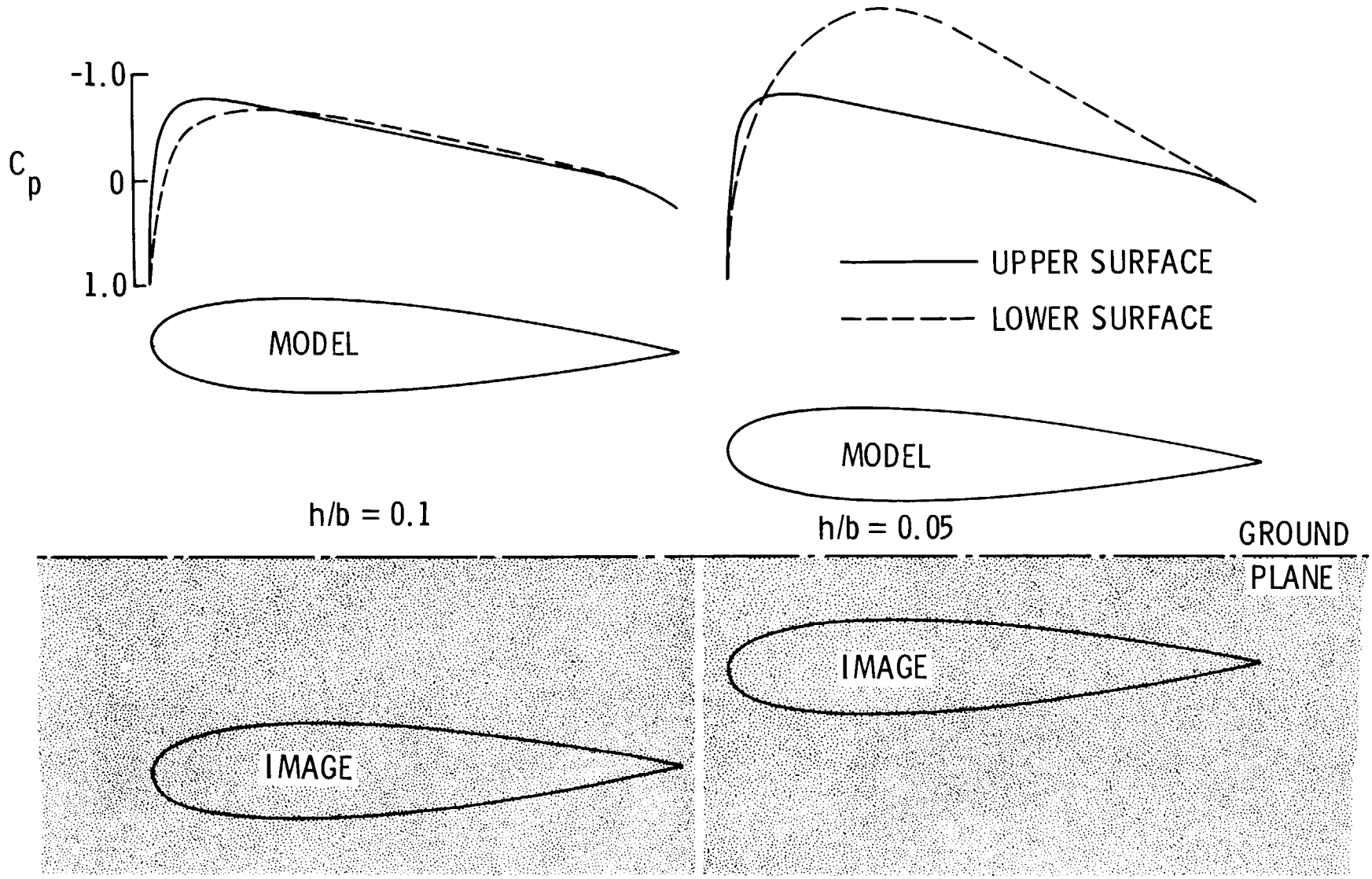

Figure 50.- Theoretical pressure distribution due to venturi effect caused by ground-image system of configuration I-A at $\alpha = 1°$.

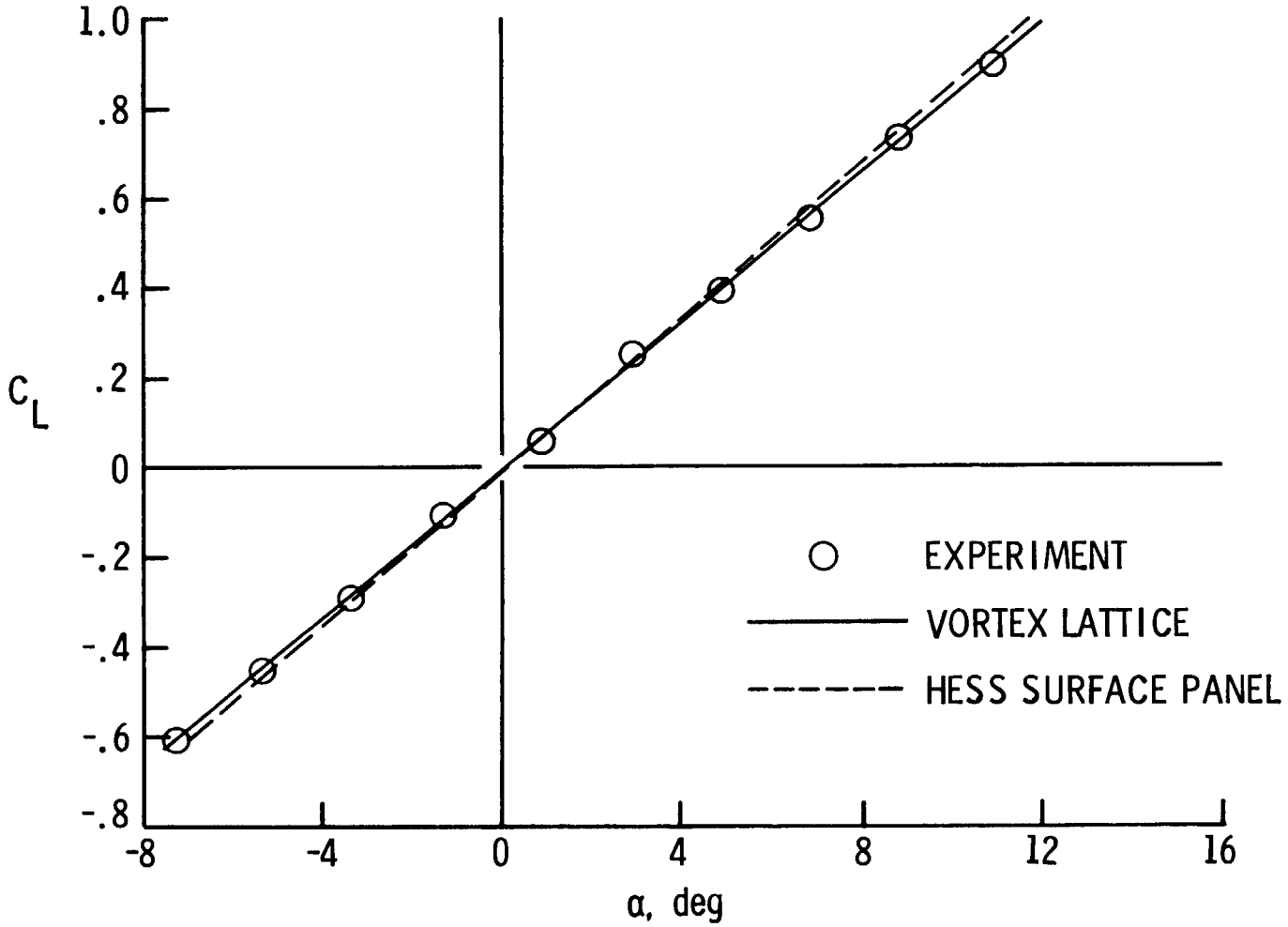

(a) Configuration I-A.

Figure 51.- Comparison with experimental data of lift coefficients predicted by vortex-lattice and Hess surface-panel methods.

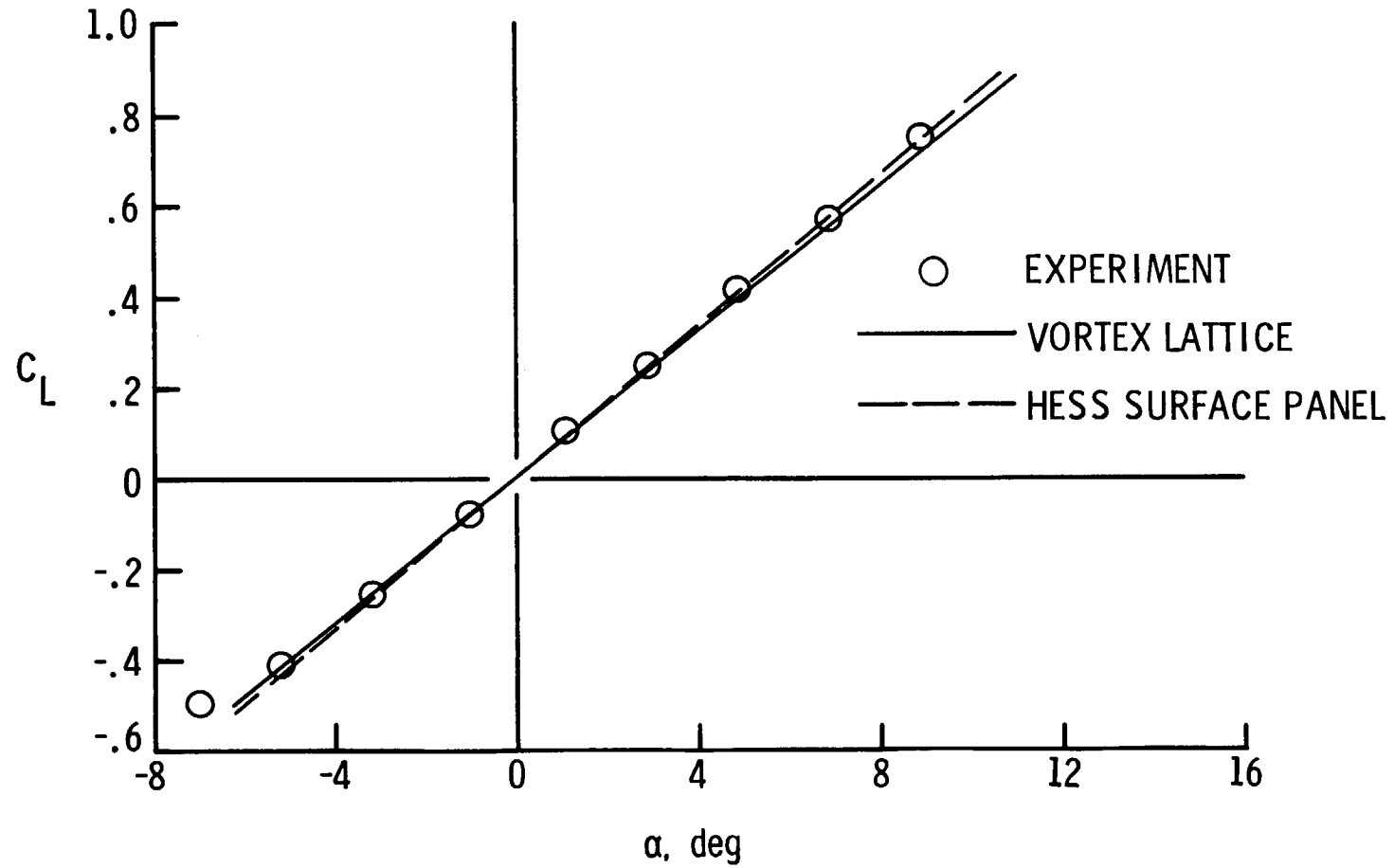

(b) Configuration II-A.

Figure 51.- Continued.

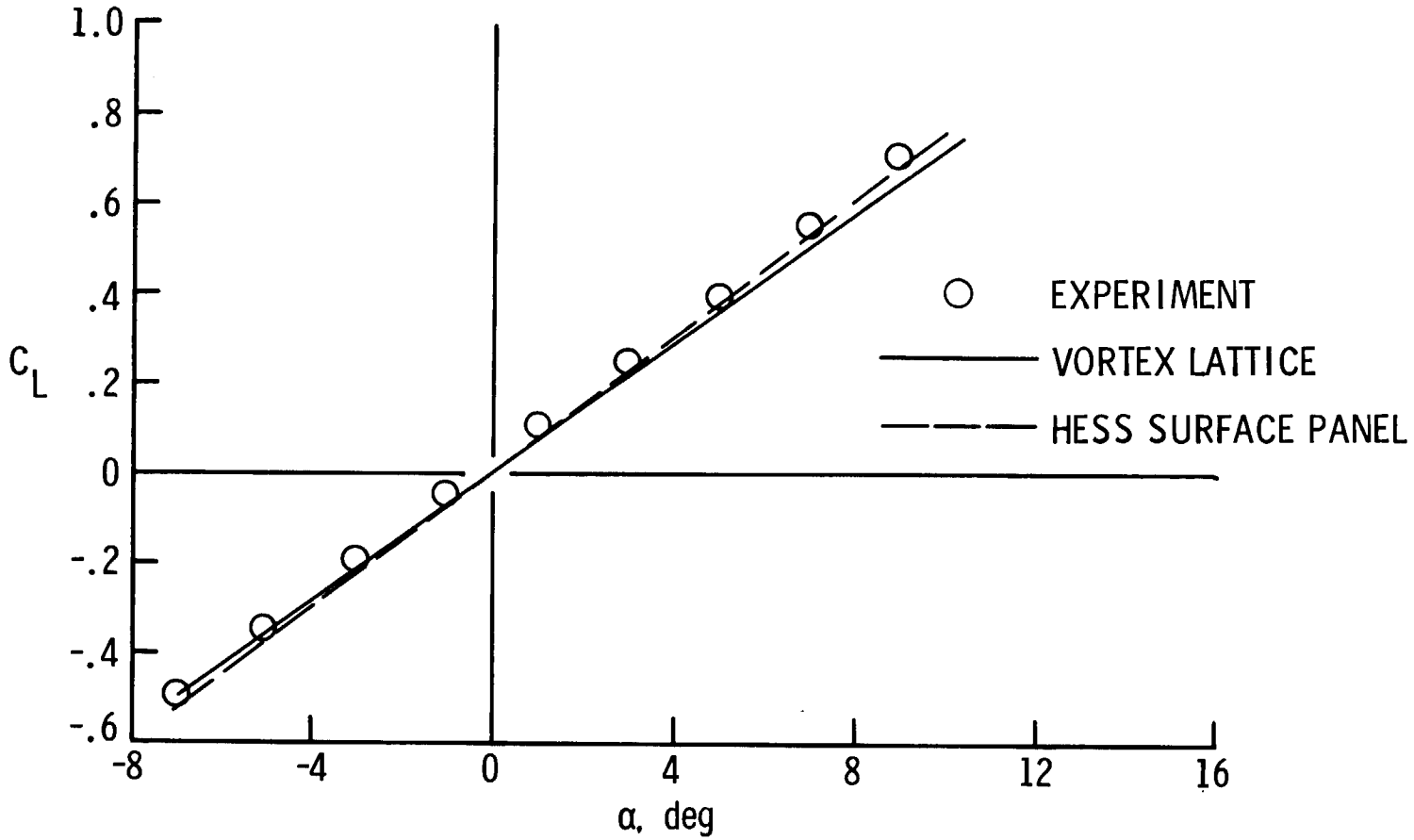

(c) Configuration III-A.

Figure 51.- Concluded.

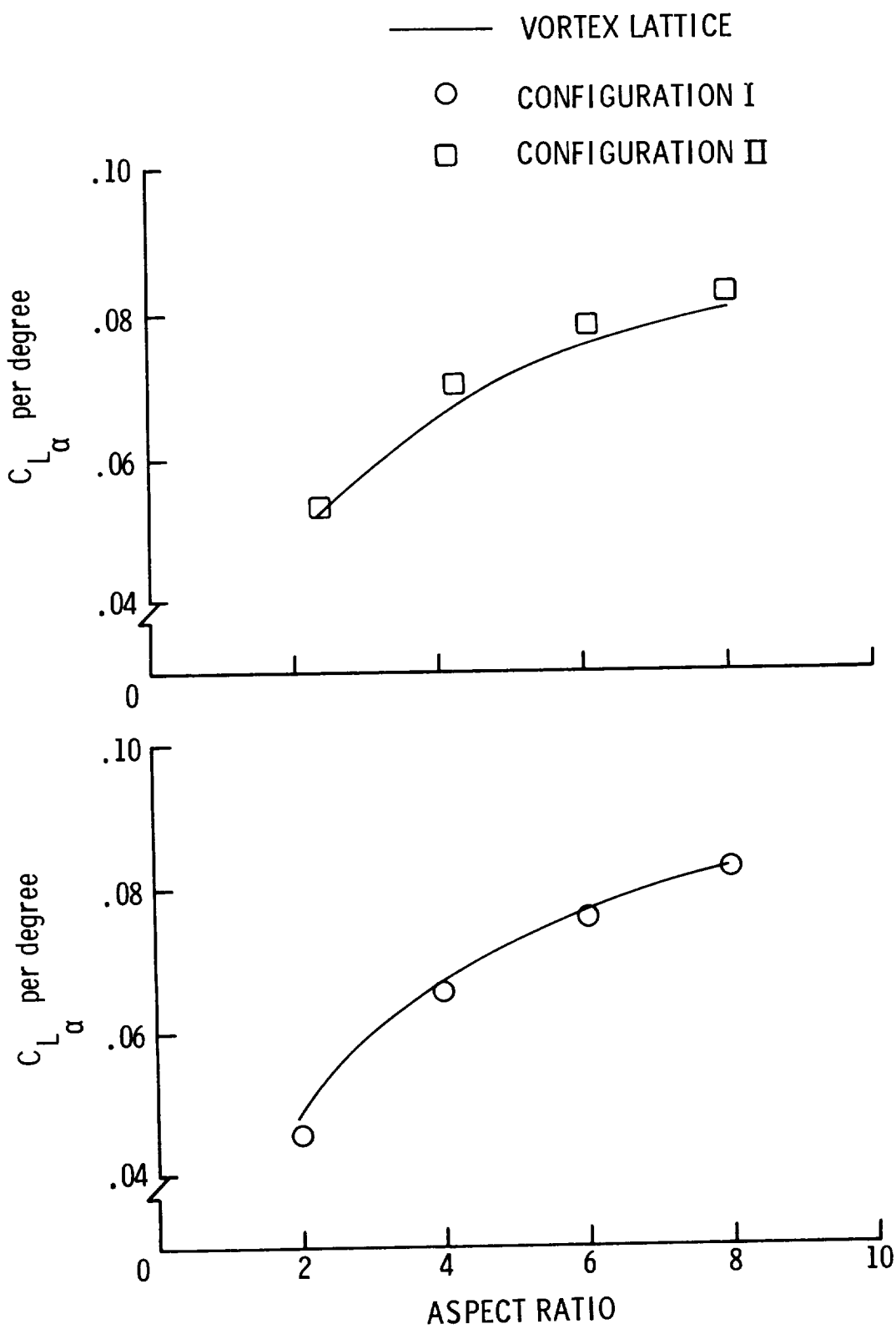

(a) Configurations I and II.

Figure 52.- Comparison of lift-curve slope C_{L_α} predicted by vortex-lattice method and experimentally determined C_{L_α} at several aspect ratios.

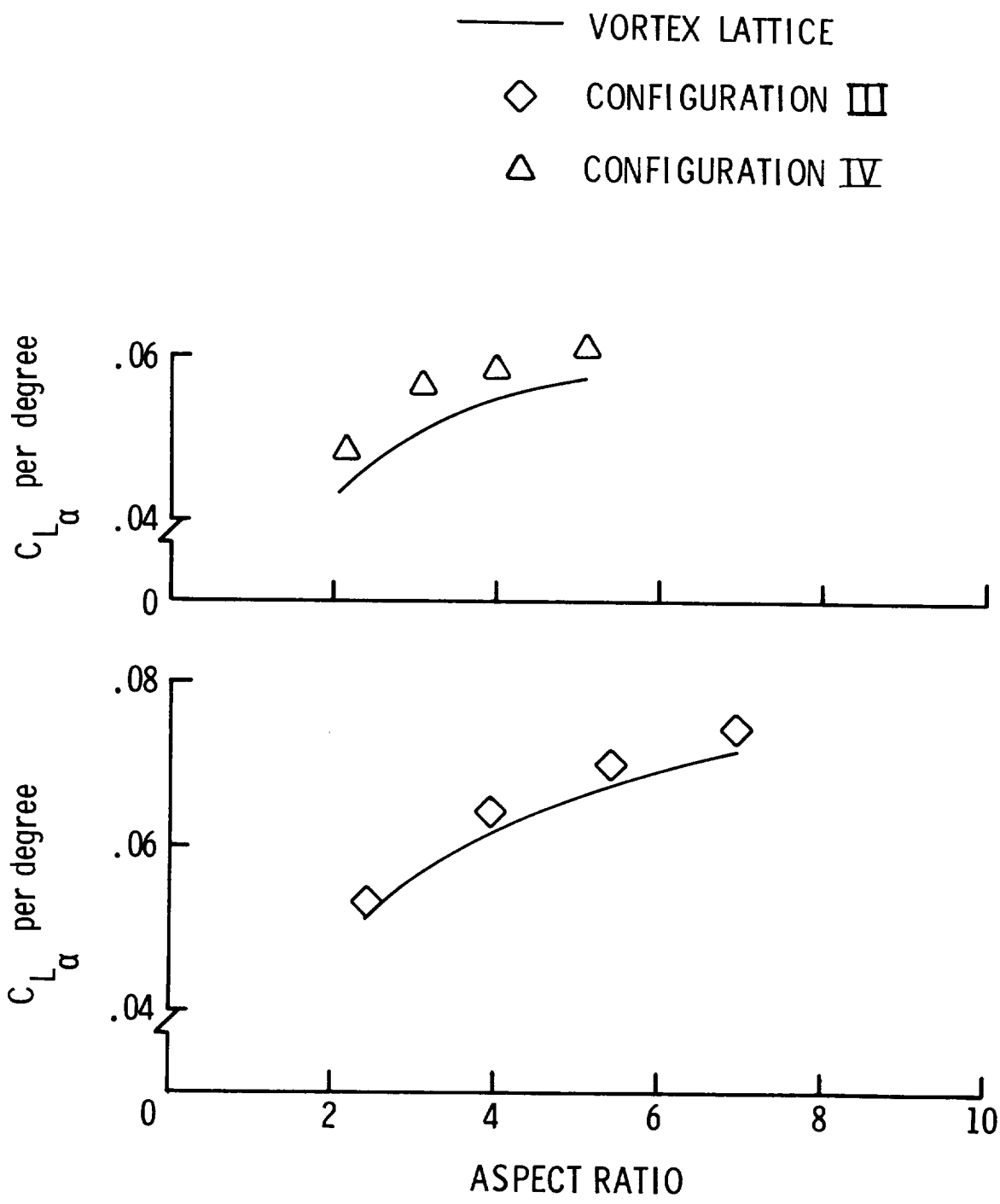

(b) Configurations III and IV.

Figure 52.- Concluded.

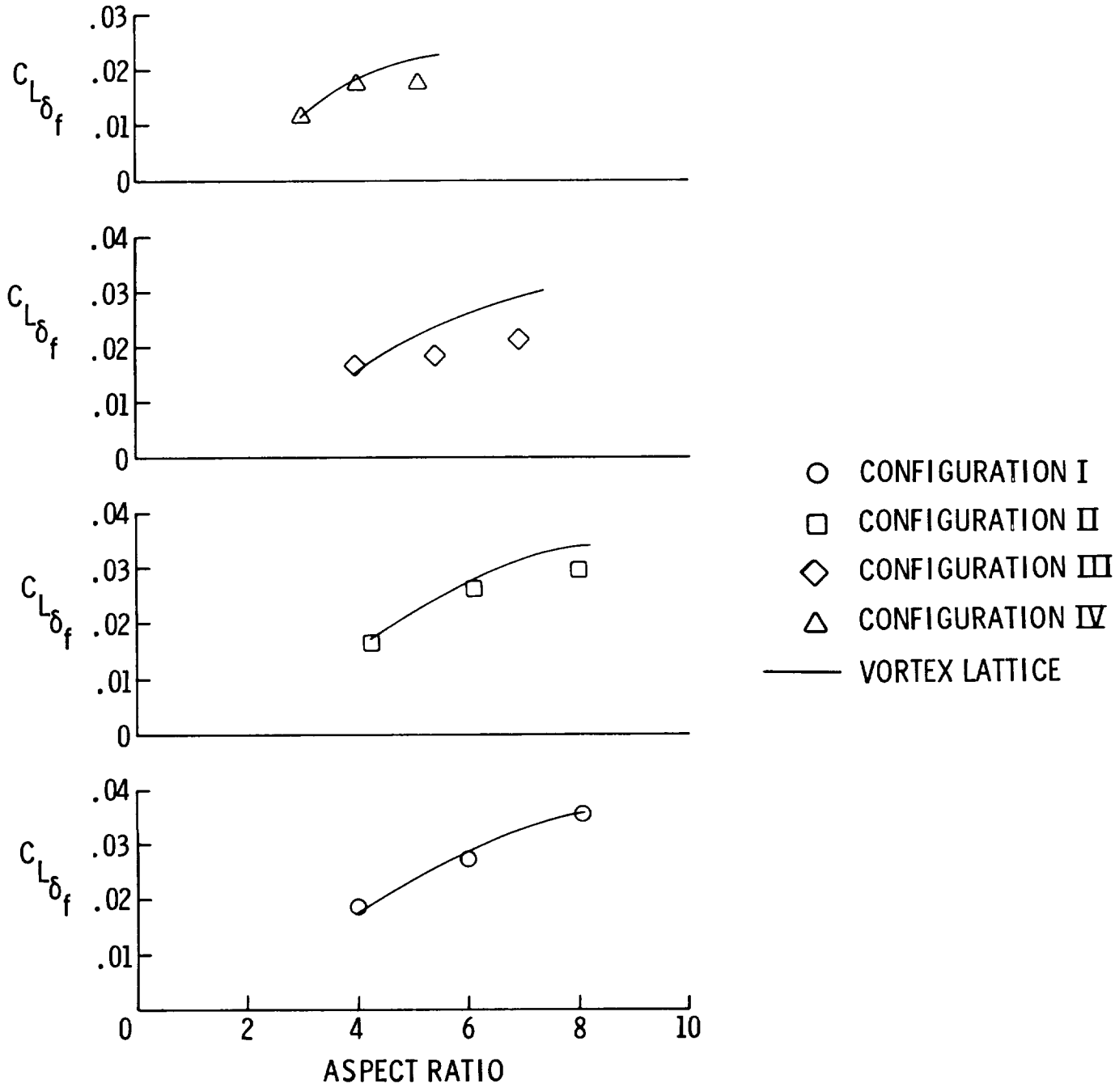

Figure 53.- Comparison of flap effectiveness $C_{L_{\delta_f}}$ predicted by vortex-lattice method with experimentally determined $C_{L_{\delta_f}}$.

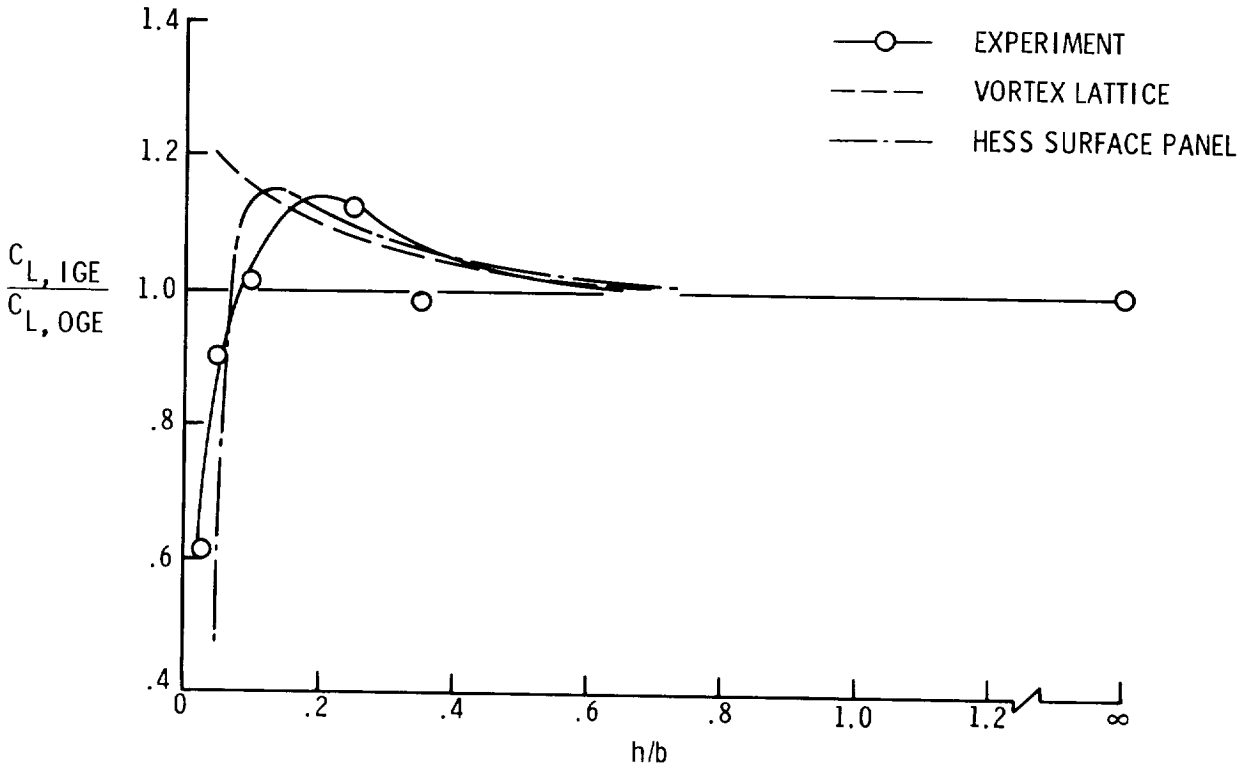

(a) Configuration I-A.

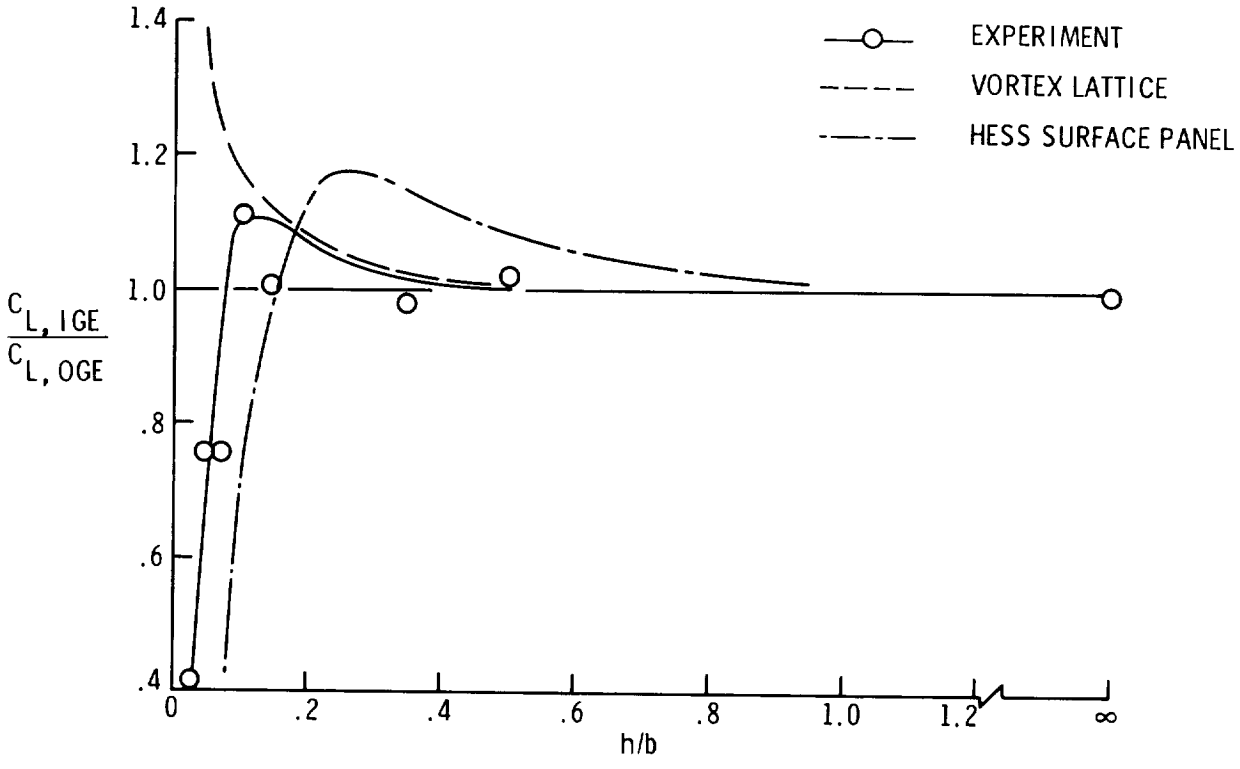

(b) Configuration I-C.

Figure 54.- Comparison of experimentally determined ground effects with ground effects on lift coefficient predicted by vortex-lattice and Hess surface-panel methods.

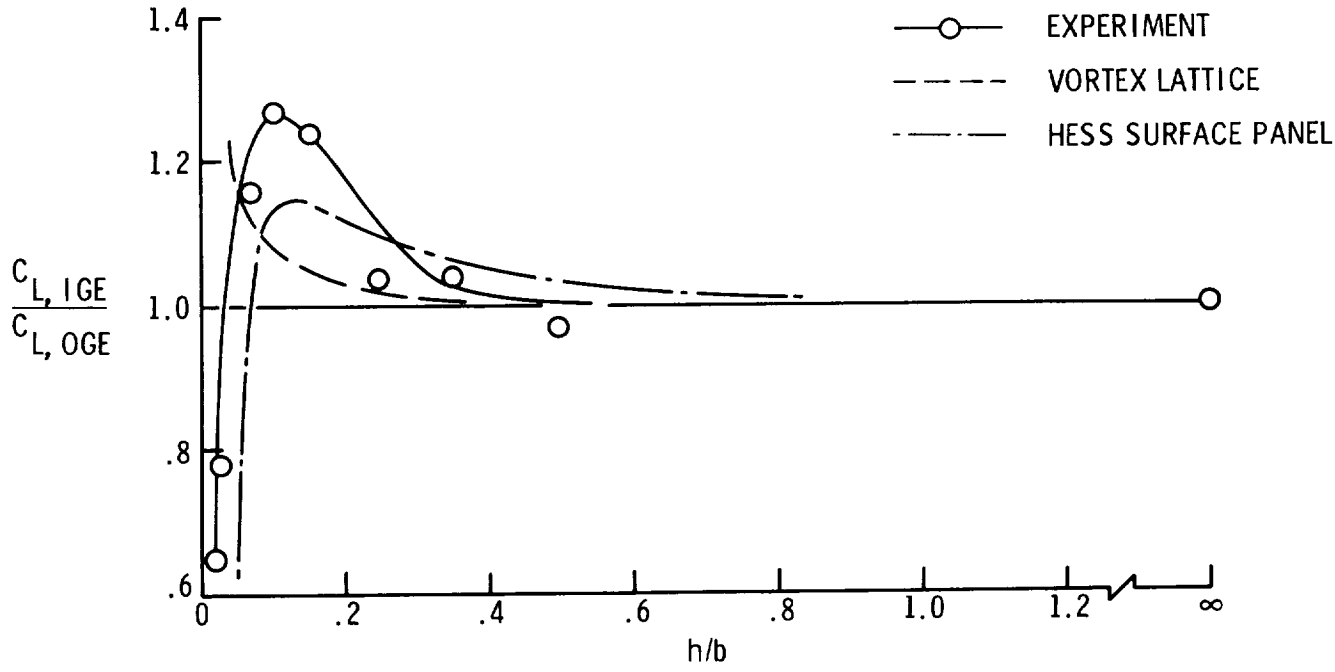

(c) Configuration II-A.

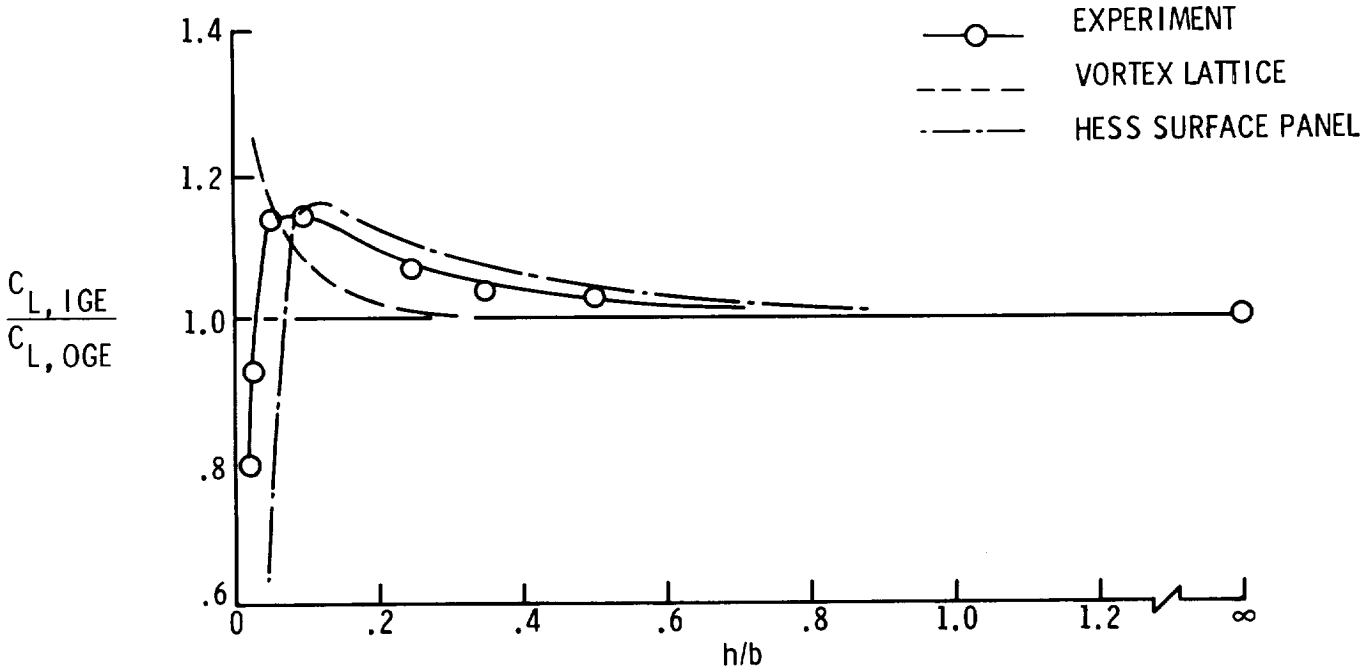

(d) Configuration III-A.

Figure 54.- Concluded.

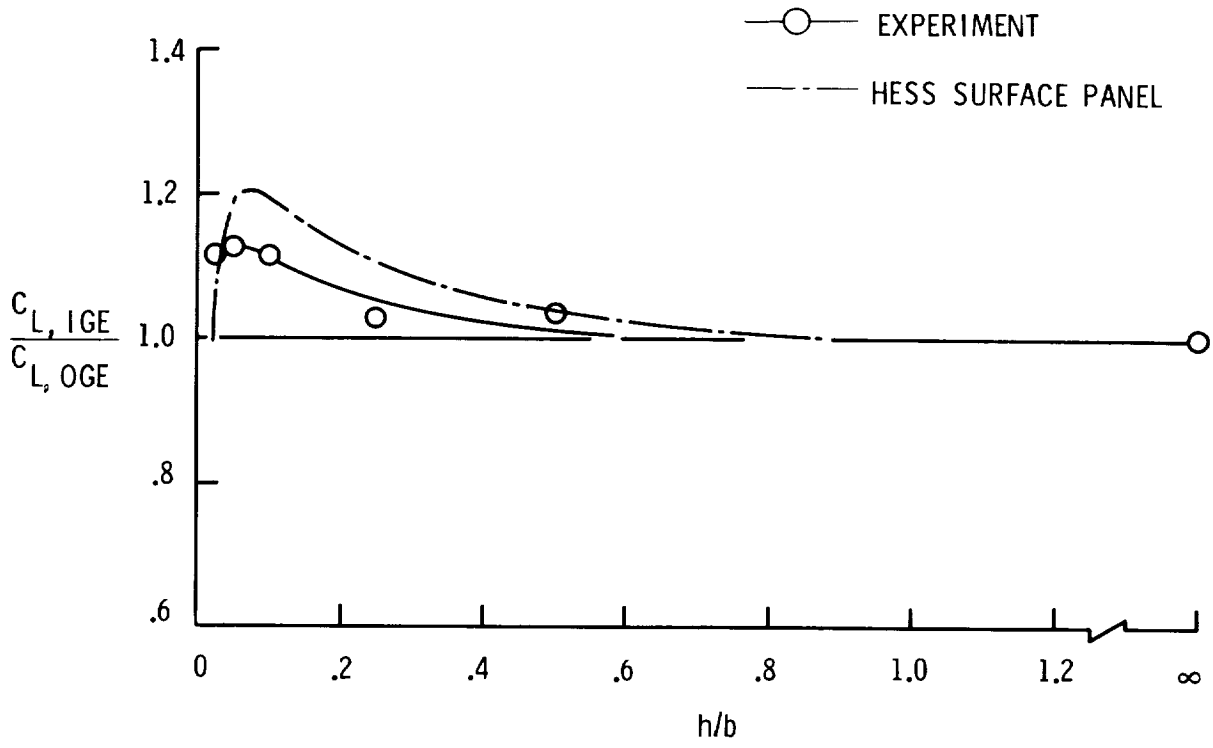

(a) Configuration I-C.

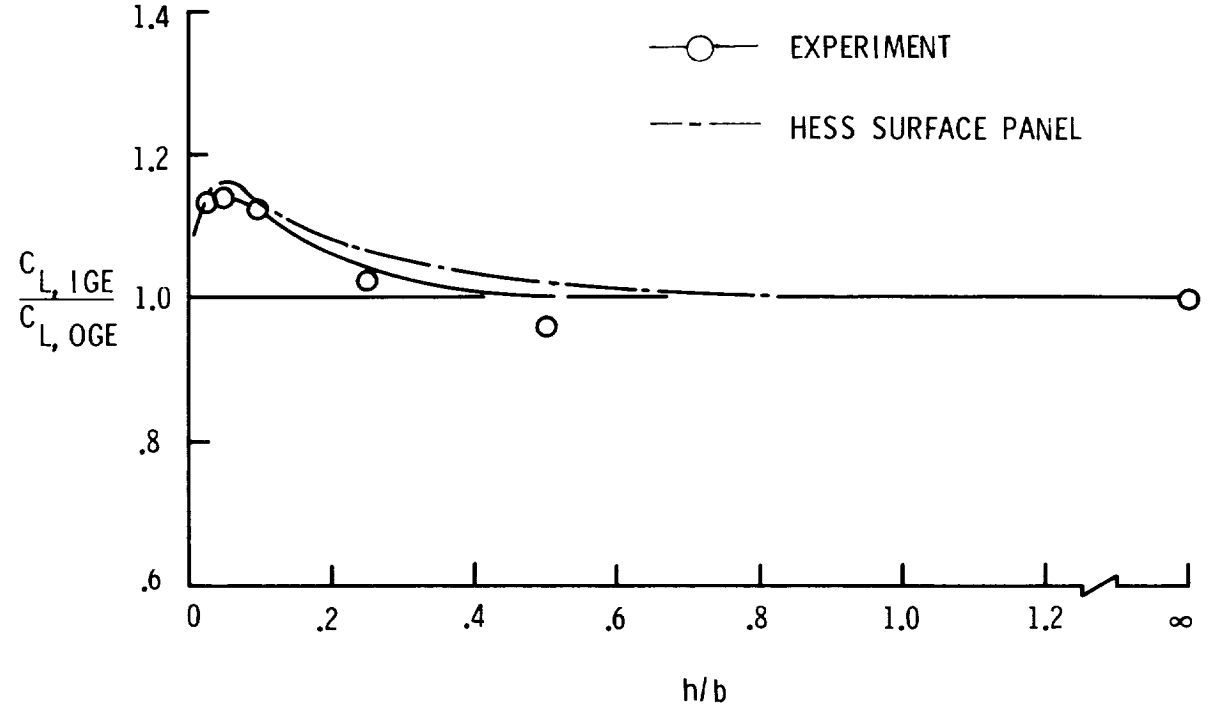

(b) Configuration III-B.

Figure 55.- Comparison of experimentally determined ground effects with ground effects on lift coefficient predicted by Hess surface-panel method. $\delta_f = 10°$.

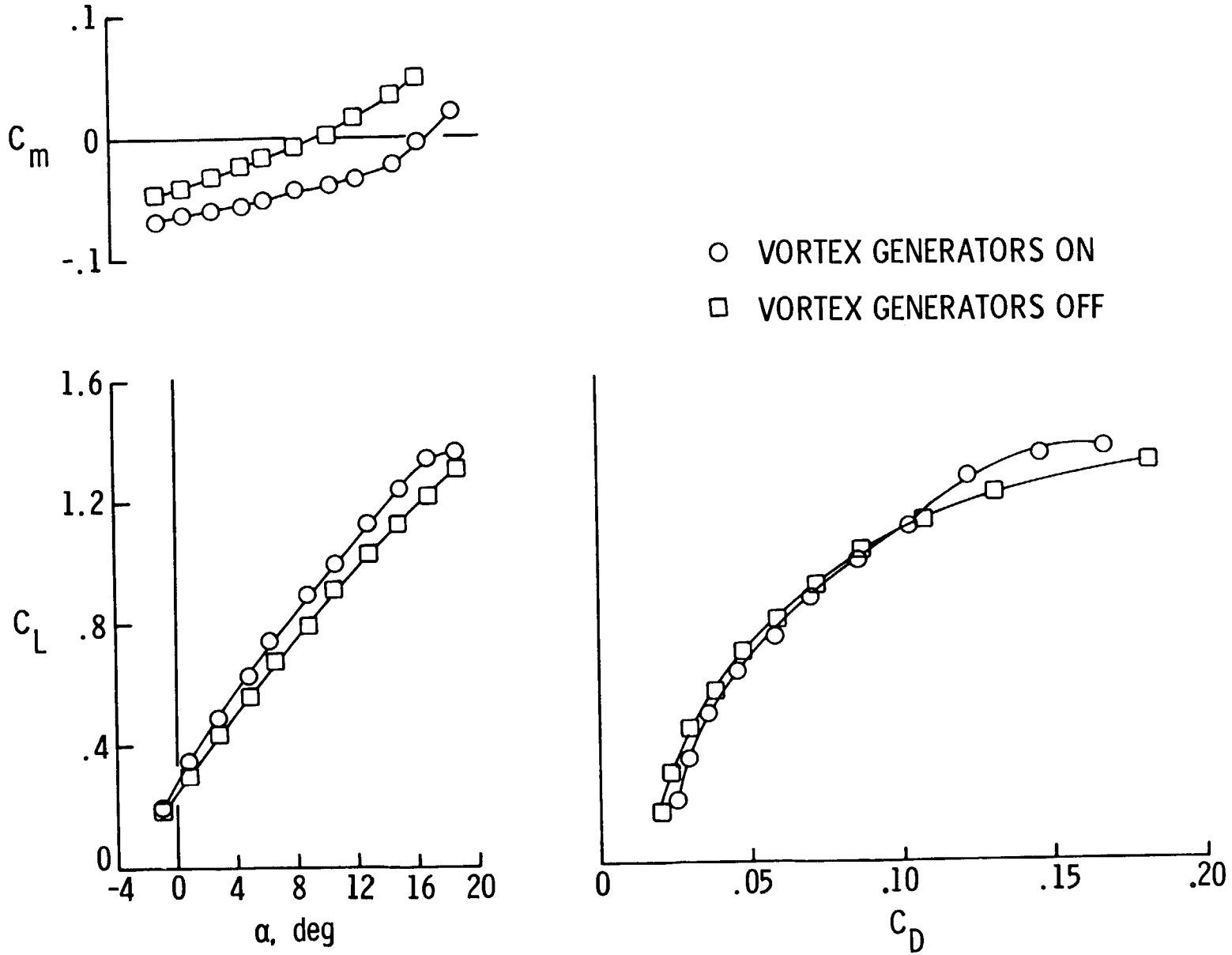

Figure 56.- Effect of vortex generators on the longitudinal aerodynamics of configuration III-B. $\delta_f = 10°$; $\delta_e = 10°$.

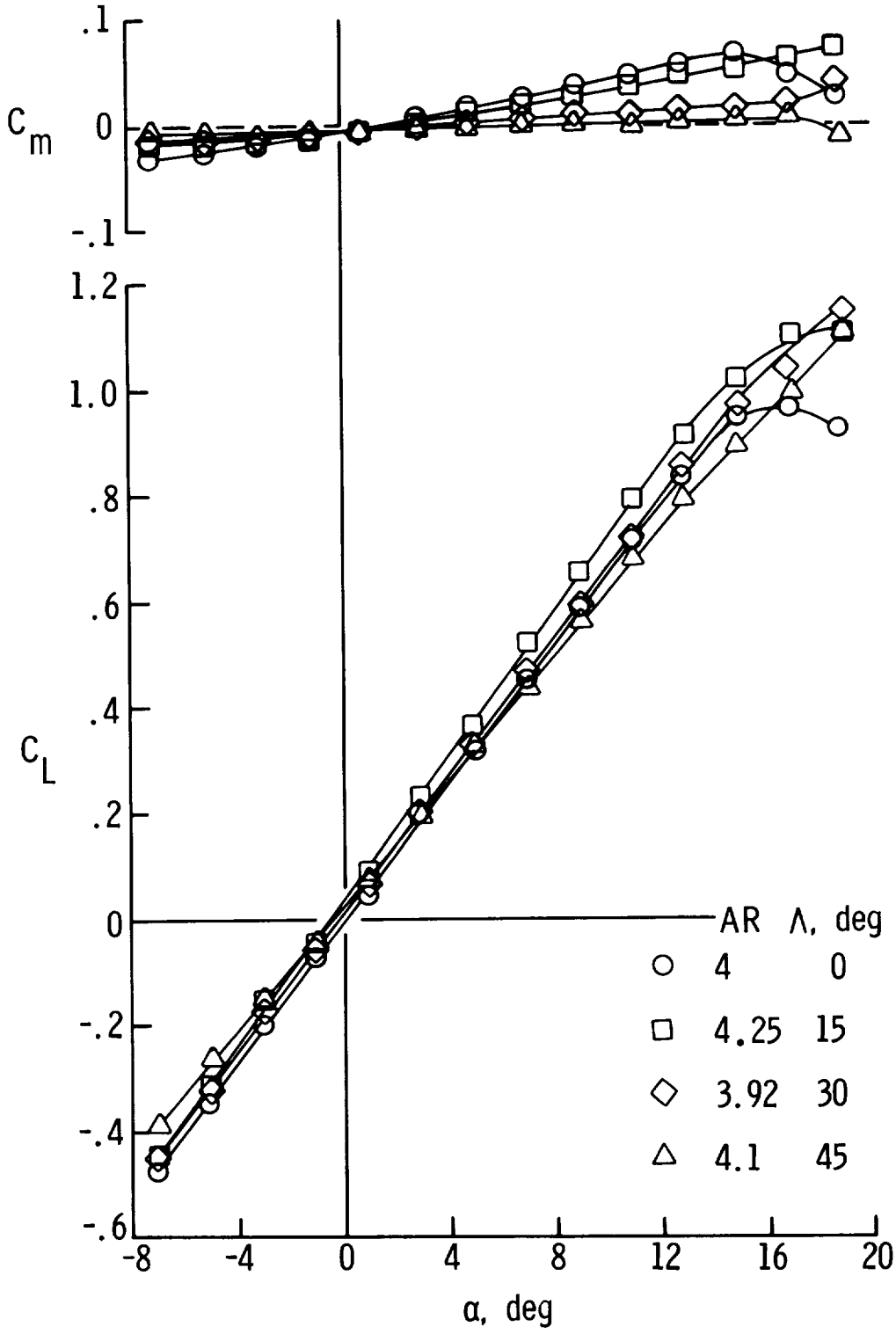

Figure 57.- Effect of sweep on lift and pitching-moment coefficients at approximately constant aspect ratio with vortex generators in place. $\delta_f = 0°$; $\delta_e = 0°$.

1. Report No.	2. Government Accession No.	3. Recipient's Catalog No.
NASA TP-2068		

4. Title and Subtitle	5. Report Date
AN EXPERIMENTAL AND THEORETICAL INVESTIGATION OF THICK WINGS AT VARIOUS SWEEP ANGLES IN AND OUT OF GROUND EFFECT	October 1982
	6. Performing Organization Code 505-43-23-04
7. Author(s) John W. Paulson, Jr., and Scott O. Kjelgaard	8. Performing Organization Report No. L-15314
9. Performing Organization Name and Address NASA Langley Research Center Hampton, VA 23665	10. Work Unit No.
	11. Contract or Grant No.
12. Sponsoring Agency Name and Address National Aeronautics and Space Administration Washington, DC 20546	13. Type of Report and Period Covered Technical Paper
	14. Sponsoring Agency Code

15. Supplementary Notes

16. Abstract

An analysis of the effects of sweep and aspect ratio on the longitudinal aerodynamics of a wing in and out of ground effect has been made. Experimental data were obtained in the Langley 4- by 7-Meter Tunnel for a wing with various sweep angles, aspect ratios, and flap deflections both in and out of ground effect. Theoretical predictions of the out-of-ground-effect lift coefficients and flap effectiveness and the in-ground-effect lift coefficients are compared with the experimental results.

17. Key Words (Suggested by Author(s))	18. Distribution Statement
Ground effects Aspect ratio Wing sweep Spanloader	Unclassified - Unlimited Subject Category 02

19. Security Classif. (of this report)	20. Security Classif. (of this page)	21. No. of Pages	22. Price
Unclassified	Unclassified	163	A08

For sale by the National Technical Information Service, Springfield, Virginia 22161

NASA-Langley, 1982